CHEMICAL REVIEWS

Review

Cite This: *Chem. Rev.* 2018, 118, 4981−5079

pubs.acs.org/CR

Metal Catalysts for Heterogeneous Catalysis: From Single Atoms to Nanoclusters and Nanoparticles

Lichen Liu and Avelino Corma*

Instituto de Tecnología Química, Universitat Politécnica de València-Consejo Superior de Investigaciones Científicas (UPV-CSIC), Avenida de los Naranjos s/n, 46022 Valencia, España

ABSTRACT: Metal species with different size (single atoms, nanoclusters, and nanoparticles) show different catalytic behavior for various heterogeneous catalytic reactions. It has been shown in the literature that many factors including the particle size, shape, chemical composition, metal−support interaction, and metal−reactant/solvent interaction can have significant influences on the catalytic properties of metal catalysts. The recent developments of well-controlled synthesis methodologies and advanced characterization tools allow one to correlate the relationships at the molecular level. In this Review, the electronic and geometric structures of single atoms, nanoclusters, and nanoparticles will be discussed. Furthermore, we will summarize the catalytic applications of single atoms, nanoclusters, and nanoparticles for different types of reactions, including CO oxidation, selective oxidation, selective hydrogenation, organic reactions, electrocatalytic, and photocatalytic reactions. We will compare the results obtained from different systems and try to give a picture on how different types of metal species work in different reactions and give perspectives on the future directions toward better understanding of the catalytic behavior of different metal entities (single atoms, nanoclusters, and nanoparticles) in a unifying manner.

CONTENTS

Received: January 3, 2018
Published: April 16, 2018

DOI: 10.1021/acs.chemrev.7b00776
Chem. Rev. 2018, 118, 4981−5079

1. INTRODUCTION

With the actual explosion of work on nanoscience and especially on nanomaterials, one cannot avoid to look back in time and to see that nanomaterials were already prepared and regularly used for heterogeneous catalysis more than 60 years ago.[1−3] Indeed, supported metal catalysts were based on metal crystallites close to the nanometer size, and catalytic reactions with zeolitic materials occurred in nanopores with a dimension below 1 nm, where strong confinement effects impacted the reactivity.[4,5]

In the first case, that is, metal catalysts, previous researchers were already able to establish structure−reactivity correlations with the techniques available, such as transmission electron microscopy and chemisorption of gases. They discovered the different relative activity shown by metal atoms located at crystal edges, corners, and facets during different catalytic reactions, and they classified reactions on metal catalysts as structure-sensitive and nonstructure-sensitive reactions.[6] As a consequence of those studies, it was possible to rationalize the impact of the size of supported metal nanoparticles on their catalytic reactivity.[7]

It is obvious that, with the resolution of the characterization techniques available at that time, it was not possible to visualize metal particles below 1 nm. Nevertheless, one could already infer that the electronic properties of metal particles should strongly change when going below 1 nm (see Figure 1). So, it could be expected that the subnanometric metal particles would interact differently with reactants, showing distinct reactivity with respect to larger nanoparticles.[8]

Today, it is possible to see single metal atoms and subnanometric metal clusters formed by a few atoms, by means of the aberration-corrected electron microscopy.[9,10] Moreover, new materials synthesis techniques allow one to prepare metal entities with a very narrow size distribution. These

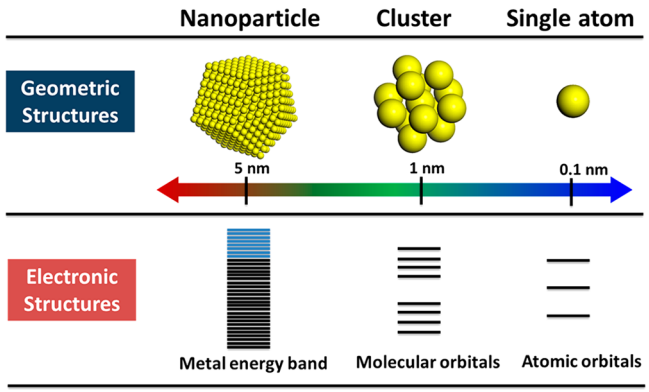

Figure 1. Geometric and electronic structures of single atom, clusters, and nanoparticles.

achievements can now be not only visualized by electron microscopy but also can be studied by X-ray absorption spectroscopy (XAS) on their coordination environment of those metal species under reaction conditions.[11] The next step, as will be shown in this Review, is to directly see the evolution of the subnanometric metal species under reaction conditions. While it is true that much knowledge has been achieved on metal catalysts and the experimental work accumulated is very large, we do not have a unified theory that can explain and predict the behavior of different metal catalysts with different particle sizes for different reactions.

Here, we have attempted to go from supported single atoms to metal clusters and to metal nanoparticles above 1 nm, showing how the differences in electronic structures, due to particle size and interactions with the support, reactants, and potential evolution during the catalytic reactions, affect the catalytic process and, therefore, their activity and selectivity. First, we will discuss the geometric and electronic properties of three types of metal species: single atoms, nanoclusters, and nanoparticles, discussing the interaction between different metal species and the support and reactants. In the following sections of this Review, we will summarize the catalytic applications of single atoms, nanoclusters, and nanoparticles for different types of reactions, including CO oxidation, deNO_x reactions, selective oxidation, selective hydrogenation, organic reactions, electrocatalytic, and photocatalytic reactions. Furthermore, we will compare the catalytic results obtained from single atoms, clusters, and nanoparticles in an attempt to explain their difference in reactions studied, and what can be expected to occur on still nonstudied systems.[12] We hope that such a critical review can be helpful in achieving a better understanding of metal-catalyzed heterogeneous reactions.

2. ELECTRONIC AND GEOMETRIC STRUCTURES OF DIFFERENT METAL SPECIES

Before starting the discussion on the catalytic properties of different types of metal species, the size effects on the electronic and geometric structures of metal species will be briefly discussed. For mononuclear metal complex, their electronic structures are strongly related to their coordination environment, being especially dependent on the ligands and solvent, and they have already been intensively studied and clearly defined.[13,14] However, in the case of metal clusters and nanoparticles, the situation becomes much more complicated due to the orbital overlapping between metal atoms. Taking Au as an example (see Figure 2), the work function of Au species with different

DOI: 10.1021/acs.chemrev.7b00776
Chem. Rev. 2018, 118, 4981−5079

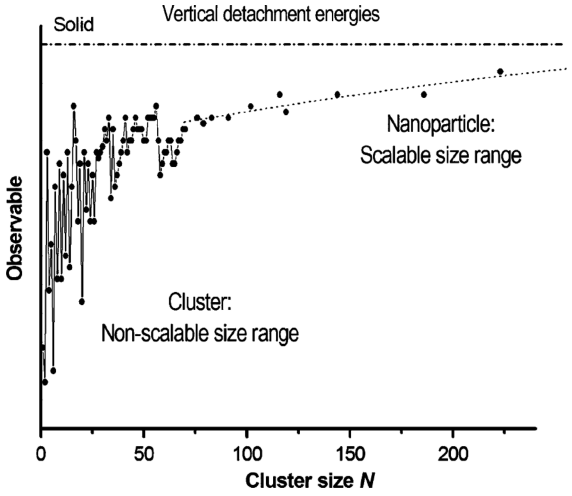

Figure 2. Work function obtained from ultraviolet photoelectron spectroscopy (UPS) of Au clusters with different atomicty. Adapted with permission from ref 15. Copyright 1992 AIP Publishing LLC.

atomicity is strongly dependent on the particle size.[15] For Au clusters with less than 30 atoms, the work function varies greatly with the atomicity, while when the atomicity increases above 70 atoms (>1.5 nm), the work function almost remains constant and slowly increases with the growth of particle size. If one considers the orbital structures of Au nanoclusters with less than 40 atoms, the size-dependent electronic structures are more significant.[16] As shown in Figure 3, the frontier orbitals of planar Au_n clusters ($n \leq 7$) consist of several lobes localized on the Au atoms with unsaturated coordination environment. Moreover, those frontier orbitals are fully accessible for the interaction with molecules through the overlap of electronic orbitals. However, when the atomicity increases above 8, the geometric structure of the Au nanocluster will change from planar to 3D.[17] In that case, the coordination number of the surface atoms increases and the contribution of the atoms inside the particle to the composition of the frontier orbitals becomes more important. As a consequence, orbital overlap with substrate molecules would be less efficient if compared to smaller clusters with fully accessible orbital structures.

When the atomicity of metal particles increases to >40 (with particle size >1 nm), the bandgap between HOMO and LUMO becomes smaller than those in subnanometric metal clusters. For larger metal nanoparticles (>2 nm), a continuous energy level will form.[18] Especially, for metal nanoparticles like Au, Ag, and Cu, their size-dependent electronic structures will be reflected on their plasmonic properties.[19] As a result, their optical properties will also vary with the particle size, which will further affect their catalytic behavior in photocatalysis.

In the case of supported single atoms, they can be stabilized by the support by chemical bonding, especially when single atoms are anchored on inorganic supports like transition metal oxides and zeolites. Thus, those single atoms may show limited geometric transformation under reaction conditions. However, when single atoms are supported on organic polymers with functional groups (like amine, carbonyl groups, thiol, etc.), they may adapt their coordination environment under reaction conditions due to the interaction between single atoms with substrate molecules. On the other hand, when the particle size reaches the cluster region (less than 20 atoms), the geometric structures of those clusters are quite flexible and can be strongly affected by the environment. One metal cluster with specific atomicity can have several possible geometric configurations, which depends on the support, reactant, and reaction conditions. The geometric structure of a metal cluster is also related to its charge. For instance, theoretical calculations show that the geometric configuration of Au_3 cluster can change from linear to triangular when the charge changes from Au_3^- to Au_3^+.[20] During redox reactions, the charge of metal clusters then may change

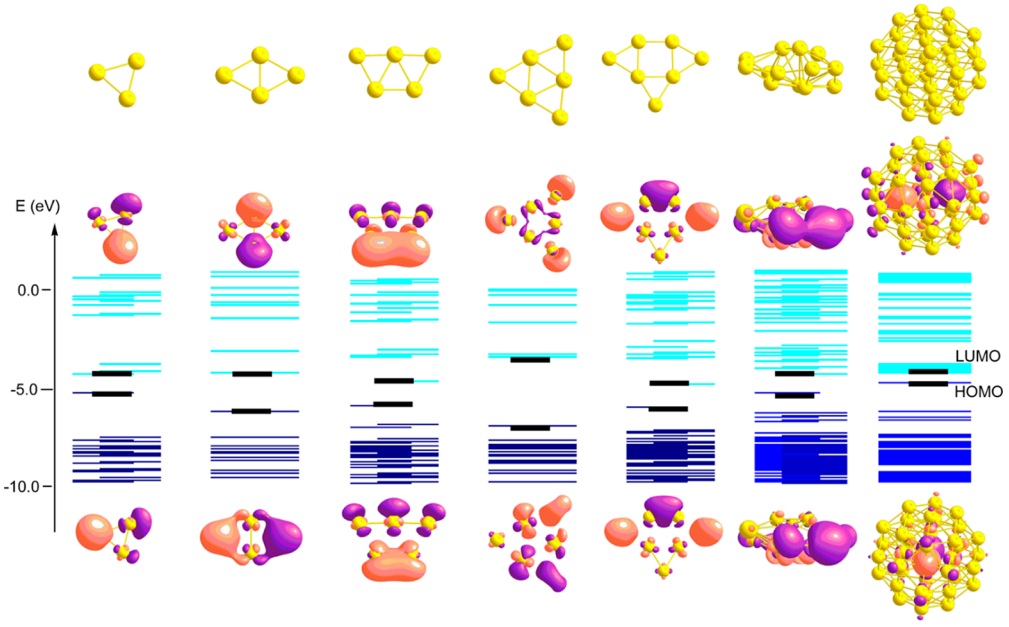

Figure 3. Electronic structures of Au clusters according to theoretical calculations. Optimized structure (top) and calculated isosurfaces of the lowest unoccupied molecular orbital (LUMO, center) and highest occupied molecular orbital (HOMO, bottom) of Au_3, Au_4, Au_5, Au_6, Au_7, Au_{13}, and Au_{38} clusters, together with molecular orbital energy levels in blue. Obtained at the B3LYP/LANL2DZ level using the Gaussian 09 program. Adapted with permission from ref 16. Copyright 2014 American Chemical Society.

DOI: 10.1021/acs.chemrev.7b00776
Chem. Rev. 2018, 118, 4981−5079

during the catalytic cycles, implying that the geometric configuration may also show a dynamic transformation under reaction conditions. That complexity will be reflected on their catalytic behavior, as will be shown in the following section when discussing the catalytic applications of metal clusters.

In the case of metal nanoparticles (>1 nm, usually with more than 40 atoms), their geometric structures are less sensitive, and usually the geometric structure of one metal nanoparticle is relatively stable, although the geometric configuration of exposed surface atoms (facet, corner, edge, metal−support interface, etc.) may change due to the environment.[21,22] Furthermore, the strain effects and lattice defects in metal nanoparticles are also important factors when considering the influences of geometric structures on catalytic properties.[23]

3. INFLUENCE OF PARTICLE SIZE ON THE METAL−SUPPORT AND METAL−REACTANT INTERACTIONS

3.1. Metal−Support Interaction on Different Types of Metal Species

The importance of the interaction between metal species and the support has been recognized since the 1970s through the concept of strong metal−support interaction (SMSI).[24] The realistic situation in practical supported metal catalysts is too complicated to elucidate the fundamental mechanism behind. Therefore, the metal−support interaction has been studied by surface science techniques to understand the structures and properties of supported metal species at atomic level. When metal species are deposited on a solid carrier, it can be expected that their locations are related to the local surface structure of the carrier. As a model surface, rutile(110) surface can provide three types of anchoring sites for single Pt atoms, including the Ti rows, O rows, and O-vacancy sites. It has been observed that only Pt atoms located at the O-vacancy sites are stabilized while Pt atoms on the other sites are mobile at room temperature. Electron transfer from Pt to TiO_2 has also been observed because Pt atoms located at the O-vacancies are in contact with Ti atoms.[25] In some more complicated systems, different types of O-vacancy sites may exist on one surface. It has been shown that Au single atoms are exclusively stabilized in the "narrow" hollow sites instead of the "wide" hollow sites on $Fe_3O_4(001)$ surface (Figure 4), which is caused by the electronic difference between the two types of surface hollow sites.[26] It should also be mentioned that, for a given support, different metals may show distinct behavior. When Au is deposited on anatase $TiO_2(101)$ surface, Au clusters are preferentially formed on the edge sites while Pt clusters are formed both on terrace and edge sites.[27] The electronic interaction between Au−TiO_2 and Pt−TiO_2 may cause their different stability and mobility on the anatase surface, which further influence their spatial distributions. These results from surface science studies indicate that the structures and electronic properties of the support have a significant influence on the spatial location and stability of metal species. It can also be speculated that they will further influence the catalytic behavior of metal species.

In supported metal catalysts, one of the important roles of the support is to stabilize the metal species from sintering, being a quite common phenomenon during the preparation and application of metal catalysts. However, it is difficult to model the sintering process in a quantitative way. In past years, on the basis of concepts from surface chemistry, Campbell et al. have studied the influence of particle size on the stability of supported

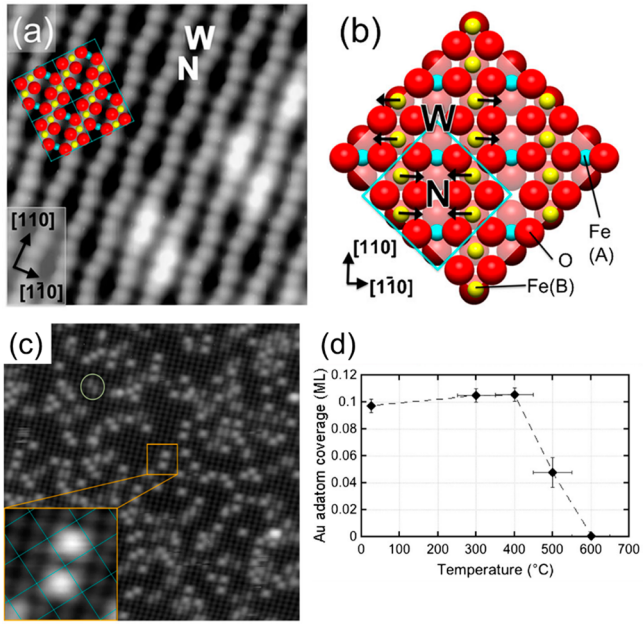

Figure 4. (a) STM image (6 nm × 6 nm) of the clean $Fe_3O_4(001)$ surface. The bright double protrusions located on the Fe(B) rows correspond to hydroxyl species. (b) Top view of the $Fe_3O_4(001)$ surface. Alternate pairs of surface Fe(B) cations (yellow) relax perpendicular to the Fe(B) row (relaxation indicated by blue arrows), creating two types of hollow sites within the reconstructed surface cell: wide (W) and narrow (N). (c) STM image (30 nm × 30 nm) of 0.12 ML Au deposited on $Fe_3O_4(001)$ surface at room temperature. Au adatoms are located between the surface Fe(B) rows, in the center of the cell, that is, at the narrow sites. (d) Coverage of single Au adatoms after annealing 0.1 ML Au to various temperatures. The decrease of surface coverage of Au adatoms is caused by the sintering of single Au atoms into clusters. Adapted with permission from ref 26. Copyright 2012 American Physical Society.

metal species.[28,29] Considering the physical models for sintering, the adsorption heat of metal atoms onto a metal particle is used as a parameter to describe the size effect on thermal stability of metal species. According to their work, the thermal stability of metal species will dramatically increase when increasing the particle size in the range from 1 to 6 nm. When the particle size is as large as 6 nm, metal nanoparticles become relatively stable toward sintering. Using similar concepts, Campell et al. have also studied the effects of supports on the thermal stability of metal species.[30] As shown in Figure 5, regardless of the support, the thermal stability of metal species also increases when increasing the particle size. However, if there are oxygen vacancies in the metal oxide support (for instance, CeO_{2-x}), Ag nanoparticles with sizes of 2−3 nm can show excellent stability.

Basically, the sintering of metal species can be described by the Ostwald ripening and particle migration and coalescence models. As illustrated in Figure 6, the sintering of small metal nanoparticles can be divided into three stages.[31] In the first stage, rapid loss of activity and agglomeration of small metal particles will occur through an Ostwald ripening mechanism, as has been investigated by in situ transition electron microscopy.[32,33] For that process, the driving force is the different surface diffusion energy of metal particles with different sizes. Therefore, the Ostwald ripening process can be significantly suppressed if the size of metal particles can be controlled in a narrow range. Indeed, in a recent work, Wettergren et al. have produced highly stable size-selected Pt nanoclusters by precisely

DOI: 10.1021/acs.chemrev.7b00776
Chem. Rev. 2018, 118, 4981−5079

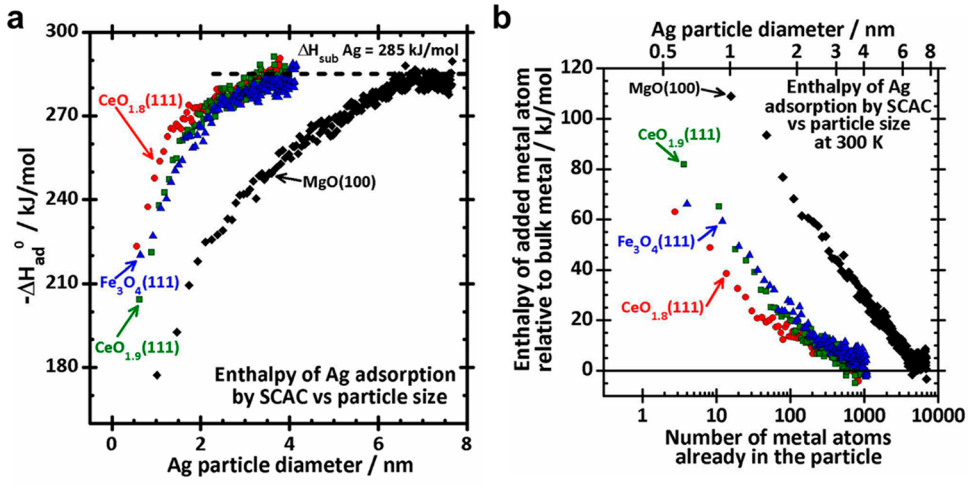

Figure 5. (a) Size-dependent adsorption heat of Ag atom when Ag is vapor deposited onto different metal oxide surfaces at 300 K for growing Ag nanoparticles on the surface. (b) Size-dependent partial molar enthalpy of Ag atoms in Ag nanoparticles on different oxide surfaces. Adapted with permission from ref 27. Copyright 2013 American Chemical Society.

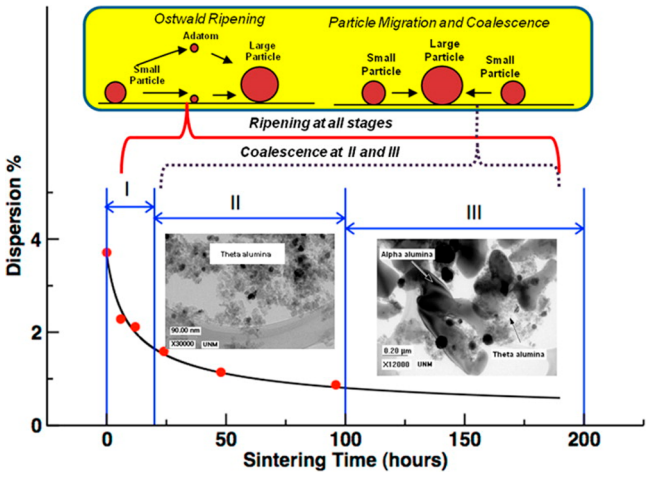

Figure 6. Schematic illustration of Ostwald ripening and particle migration and coalescence during the sintering process. Adapted with permission from ref 31. Copyright 2013 American Chemical Society.

controlling the particle size distribution in a narrow range.[34] Pt nanoclusters with a broad size distribution will show significant Ostwald ripening during thermal treatment, while if the size of Pt nanoclusters has been well controlled, both Pt_{22} and Pt_{68} clusters will show good stability against sintering through Ostwald ripening.

The size-dependent properties on the metal−support interaction can also be reflected on the evolution of geometric structures of metal species during thermal treatments. Frenkel et al. have found an unusual contraction of surface Pt−Pt bonds in Pt nanoclusters supported on γ-Al_2O_3 (ca. 0.9 nm) during in situ X-ray absorption measurements.[35] As shown in Figure 7, the lattice distance of Pt−Pt bonds decreases when increasing the temperature, which is contrary to conventional supported Pt nanoparticles (like the Pt/C sample). Furthermore, the size effects on the Pt−Pt bond dynamics have also been investigated by in situ EXAFS. When the size of Pt particles supported on γ-Al_2O_3 increases from ca. 0.9 to ca. 2.9 nm, such abnormal negative thermal expansion will disappear, and Pt particles will show positive thermal expansion coefficient, indicating that only

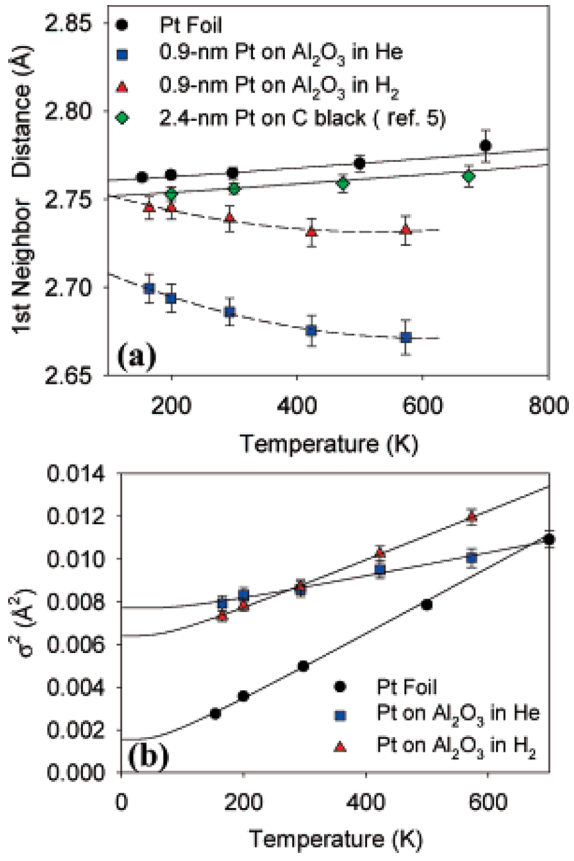

Figure 7. Evolution of Pt−Pt coordination parameters in supported Pt/γ-Al_2O_3 catalyst with 1 wt % of Pt and a Pt foil reference. (a) Temperature-dependent Pt−Pt first-neighbor distances of the Pt nanoclusters supported on γ-Al_2O_3 (ca. 0.9 nm), Pt nanoparticles (ca. 2.4 nm) supported on carbon black, and a Pt foil reference. (b) The mean-square relative displacement of the supported Pt clusters and Pt foil standard as a function of temperature. Adapted with permission from ref 35. Copyright 2006 American Chemical Society.

Pt particles with very small sizes can show the non-bulk-like properties.[36]

DOI: 10.1021/acs.chemrev.7b00776
Chem. Rev. 2018, 118, 4981−5079

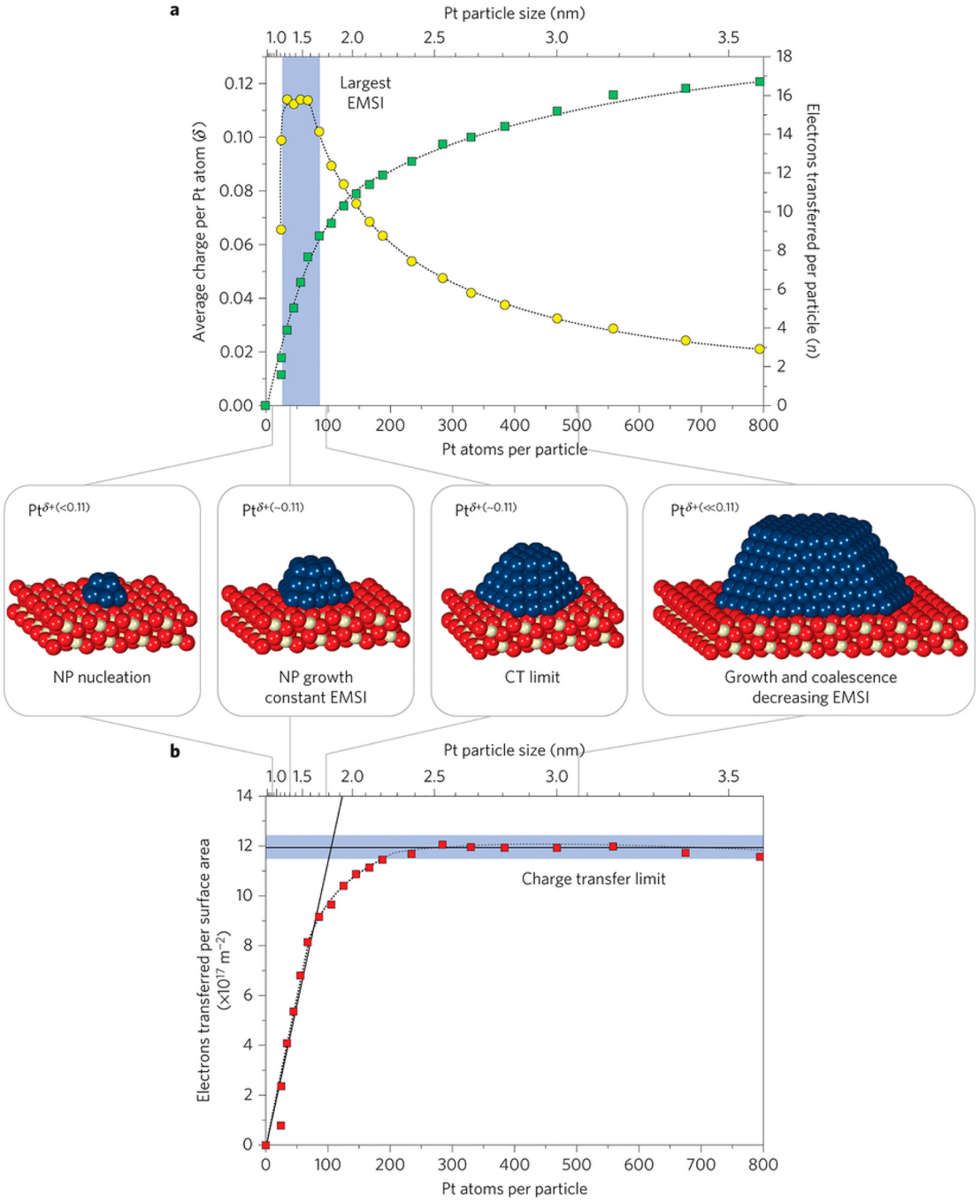

Figure 8. (a) The average charge on each Pt atom in Pt particles with different sizes measured by resonant photoemission spectroscopy. The partial charge on each Pt atom reaches a maximum for Pt nanoparticles with 30−70 atoms. (b) The relationship between electrons transferred per surface area and the size of Pt deposited on CeO_2. At higher Pt coverage, the total amount of transferred electrons approaches a charge-transfer limit. Schematic models of Pt/CeO_2 samples with different size of Pt species are also shown in this figure. Adapted with permission from ref 40. Copyright 2016 Macmillan Publishers Limited, part of Springer Nature.

3.2. Electronic Interaction between Metal Species and the Support

Electron transfer between the support and metal species is a result of the balancing between the Fermi energy level of the metal species and the support. The electron transfer will affect the charge density and distribution of metal species, which will further affect the catalytic properties.[37] Considering that the electronic structures will be dependent on the particle size, the metal−support interaction by electron-transfer process will also be dependent on the particle size.

In 2008, the electronic transfer between subnanometric Au clusters and alumina film has been studied by STM imaging and theoretical modeling. Nilius et al. have shown that three electrons are transferred from the alumina support to Au_5 and Au_7 clusters, respectively.[38] When the atomicity of Au clusters increases to 18, four electrons transferred from MgO to Au clusters were observed. It should be noted that the number of transferred electrons between Au clusters and the support is less on 2D Au clusters than on 1D Au clusters, which should be related to their different electronic structures.[39]

DOI: 10.1021/acs.chemrev.7b00776
Chem. Rev. 2018, 118, 4981−5079

In a recent work, Libuda et al. have measured the size effects of metal species, ranging from subnanometric clusters to nanoparticles, on the electronic metal−support interaction (EMSI) between Pt and CeO_2.[40] As shown in Figure 8, the electronic states of Pt species measured by resonant photoemission spectroscopy are strongly dependent on the particle size. Pt nanoparticles with about 30−70 atoms show the highest positive charge on each Pt atom, which indicates the strongest electronic metal−support interaction. To explain the size effects on the charge-transfer process between Pt and CeO_2, density functional calculations have been performed. According to the DFT calculations, the particle size of Pt, the density of Pt species on CeO_2 surface, and the concentration of surface Ce^{3+} on the CeO_2 surface can be the reasons accounting for the experimental results. Looking into those results from another viewpoint, in many experimental works, the sizes of supported Pt species (the supports vary from metal oxides to carbon or other materials) in the high-performance catalysts are usually in the range of 1−3 nm, which is consistent with the above work.[41−43] Such coincidence implies that the electronic interaction between the metal and support and the catalytic performances of metal particles can be correlated.

Nevertheless, the electron transfer between metal and the support is also affected by the geometric location of the metal species on the support. As a typical example, Au atoms are found to be negatively charged when deposited on thin MgO(100) film with 3-layer thickness.[44] In the case of Pd atoms, they remain neutral on the same support, which is in line with theoretical calculations.[45] Interestingly, when the support is FeO(111)/Pt(111) surface, it has been found that Au atoms are positively charged while Pd atoms remain neutral. Au atoms show preferential binding to the hcp hollow positions of FeO(111)/Pt(111) surface, while Pd atoms show a random distribution on the same surface and still remain neutral.[46] By comparing the results obtained from different systems, it is proposed that the charge states of Au atoms are related to the positions occupied by Au atoms on different surface.[47]

In a recent work, Vajda et al. have investigated the structural evolution of subnanometric Co clusters under oxidation conditions.[48] Size-selected Co_n clusters (n = 4, 7, and 27) were first deposited on amorphous alumina and ultrananocrystalline diamond (UNCD) surfaces before being oxidized by exposure to ambient atmosphere. Grazing incidence X-ray absorption near-edge spectroscopy (GIXANES) and near-edge X-ray absorption fine structure (NEXAFS) were used to characterize the clusters to get information about their structural evolution by oxidative treatment. Most of the Co^0 species were oxidized to Co^{2+} in all samples regardless of the size and the support. However, XANES analysis of Co clusters on UNCD showed that ∼10% fraction of a Co^0 phase remained and resisted the oxidative conditions for all three Co clusters. Moreover, about 30%, 27%, and 12% fraction sof a Co^{3+} phase in Co_4, Co_7, and Co_{27} clusters were detected, respectively. In the alumina-supported clusters, metallic Co^0 species were not observed, and it was proposed that the dominating Co^{2+} species could be attributed to the formation of cobalt aluminate due to the strong binding of Co^{2+} to the support. NEXAFS showed that their structures also follow the tetrahedral morphology of the support.[49]

For simplicity, the electronic interaction between metal species and the support can be modeled as a metal−semiconductor junction.[50,51] Therefore, the electronic energy level will reach an equilibrium state at the metal−support interface, with the equilibrium energy level structure being dependent on both the metal species and the support. For metal species supported on a specific solid carrier, the electronic structure of the metal−support junction is related to the atomicity of metal species. Basically, for supported large metal nanoparticles, they prefer to be in the metallic state, especially for noble metal nanoparticles (such as Au, Ag, Pt, etc.). It has been observed in many systems that metal clusters prefer to be positively charged, which is a medium state between metallic nanoparticles and isolated atoms. Besides, for electron-donor support, metal species may prefer to be in the electron-rich state as compared to those supported on electron-acceptor support. For instance, when Ru nanoparticles are supported on electride compound, the electron density in Ru nanoparticles is higher than those supported on conventional supports, and the Ru/electride catalysts show higher activity for ammonia synthesis.[52,53]

Moreover, the charge-transfer process between metal and support also plays an important role with working catalysts. A typical example is the separation of photogenerated electrons and holes at the interface of the metal−semiconductor.[54] An electronic equilibrium will be established once the contact of metal and semiconductor is formed. Because the electronic structures of the semiconductor support are usually constant, the electronic structures of metal species have significant influence on the electronic structures of the metal−semiconductor junction. When photogenerated electrons are produced in the semiconductor, they will probably be transferred to the metal particles through a Schottky barrier.[55] As shown in Figure 9, the charge-transfer rates between ZnO nanoparticles and Au particles with different sizes have been measured by ultrafast spectroscopy. When the particle size increases from ca. < 1 nm

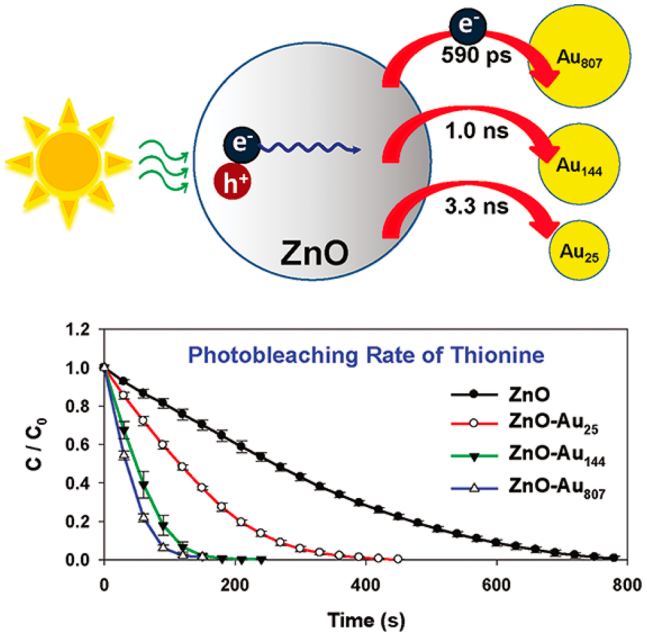

Figure 9. Schematic illustration of charge transfer between ZnO nanoparticle and Au particles with different sizes. The kinetic curves of photocatalytic degradation of thionine (a model dye molecule) are also presented to show the kinetics of the recombination of photogenerated electrons and holes in ZnO nanoparticles. With a faster charge-transfer process between Au particles and ZnO nanoparticles, the photocatalytic degradation of thionine will be faster. Adapted with permission from ref 56. Copyright 2011 American Chemical Society.

DOI: 10.1021/acs.chemrev.7b00776
Chem. Rev. 2018, 118, 4981−5079

(Au_{25}) to ca. 3.5 nm (Au_{807}), the charge-transfer rate also increases, leading to higher photocatalytic activity for thionine degradation.[56]

3.3. Metal–Reactants Interaction on Different Types of Metal Species

When molecules are absorbed by metal species, orbital hybridization between metal and the adsorbed molecules will occur. Because CO is usually used as a probe molecule to study the electronic and geometric structures of metal species, Sitja et al. have measured the CO adsorption energy on Pd particles with different sizes ranging from 0.6 to 6 nm, as shown in Figure 10.[57]

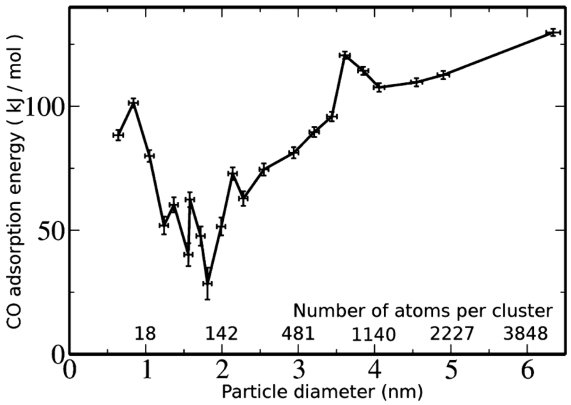

Figure 10. Size-dependent CO adsorption energy on Pd species from subnanometric clusters to nanoparticles. Adapted with permission from ref 57. Copyright 2013 American Chemical Society.

When the size of Pd particles is larger than 1.8 nm, the CO adsorption energy shows a gradual increase when increasing the particle size. However, for Pd particles below 2 nm, the CO adsorption energy shows irregular oscillation, because according to DFT calculations, electronic and geometric structures of metal clusters strongly depend on the atomicity.[58] The variations in the CO adsorption energy indicate the transition of metal species from nonmetallic to metallic when changing the particle size from molecule-like state (below 1 nm) to bulk-like state (nanoparticles larger than 2 nm). The same tendency was observed when CO molecules are adsorbed on Au particles with different sizes. Lowest adsorption energy was observed on Au nanoparticles of ~2 nm, which corresponds to the transition of nonmetallic to metallic properties.[59]

When small molecules are adsorbed on metal species, the geometric deformation will also be dependent on the particle size. Lei et al. have studied the structural changes in Pt nanoparticles of 1–3 nm when interacting with small molecules. Thus, significant relaxation of Pt–Pt bonds can be observed in Pt nanoparticles of ~1 nm when H_2 and CO are adsorbed on the surface, as a consequence of orbital hybridization between the metal species and molecules. When the size increases to 2–3 nm, the adsorbate-induced lattice relaxation of Pt nanoparticles is much smaller, which can be ascribed to its lower fraction of surface unsaturated-coordinated Pt atoms.[60]

Because of the interaction between metal species and molecules, different types of metal species can suffer dynamic transformations under various treatments. It has been found that, by consecutive treatment with CO and NO, Pd nanoparticles can show dynamic size and shape transformations under different atmospheres.[61,62] In oxidative atmosphere (such as O_2, NO), Pd nanoparticles will disintegrate into smaller particles or even subnanometric species. After reductive treatment with CO or H_2, Pd species will agglomerate into larger particles. Tracking by in situ EXAFS, it has been demonstrated that the dynamics for the above redispersion–agglomeration behavior is strongly related to the particle size of metal species. In this sense, we have recently reported the reversible transformation of Pt nanoclusters (~1 nm) into single Pt atoms in high-silica CHA zeolite.[63] As shown in Figure 11, the size of Pt species in the chabazite can go from single atoms to small Pt nanoparticles (1–2 nm) by controlling the temperature and atmosphere.

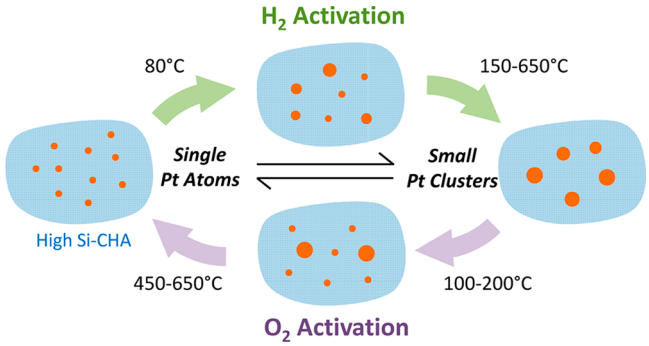

Figure 11. Reversible transformation between single Pt atoms and Pt nanoclusters (~1 nm) confined in CHA zeolite under reduction–oxidation treatments. Adapted with permission from ref 53. Copyright 2017 American Chemical Society.

Such dynamic structural transformation of supported metal species has also been found on other metals like Au and Cu when the metal species interact with molecules.[64,65] Understanding such dynamic processes can help to control the size of metal species at a precise level and provide an alternative approach for generation of supported metal catalysts or can serve as a strategy for the regeneration of deactivated catalyst.[66,67] In the above discussion, we have presented some factors that can affect the size, shape, and electronic characteristics of metal catalysts. They will be useful to explain the reactivity of the supported metal catalysts.

4. CATALYTIC APPLICATIONS OF SUPPORTED SINGLE ATOMS

4.1. CO Oxidation

4.1.1. Au Single Atoms for CO Oxidation. Since the pioneering work from Haruta, the application of Au catalysts for low-temperature CO oxidation has attracted plenty of attention, and great effort has been made to develop Au catalysts with new structures and to identify the active sites.[68] Although it has been well demonstrated that Au nanoparticles (~2 nm) can be very active for low-temperature CO oxidation, there is still debate on the catalytic role of subnanometric Au species, including Au clusters and single Au atoms. Zhang et al. have reported two examples of supported single Au atoms for CO oxidation. In one report, Au/FeO_x catalysts with very low Au loading (0.03 wt % to 0.09 wt %) exhibited high activity and excellent stability for CO oxidation. From high-resolution STEM images, the presence of highly dispersed Au single atoms in the Au/FeO_x sample with 0.03 wt % of Au was confirmed. Nevertheless, in the Au/FeO_x sample with Au loading of 0.09 wt %, a small amount of Au clusters and nanoparticles could also be observed.[69,70] In another work, Au/CeO_2 with low Au loading amount (0.05 wt %, containing singly dispersed Au atoms) was prepared and used for

DOI: 10.1021/acs.chemrev.7b00776
Chem. Rev. 2018, 118, 4981–5079

Table 1. Catalytic Performance of Pt/FeO_x Catalysts (Samples A and B) in Comparison with Au/Fe_2O_3 from the World Gold Council[a]

	metal loading (wt %)	reaction	temperature (°C)	specific rate × 10^2 (mol_{CO} h^{-1} g_{metal}^{-1})	TOF × 10^2[c]
sample A	0.17	CO oxidation	27	43.5	13.6
sample B	2.5	CO oxidation	27	17.7	8.01
Au/Fe_2O_3[b]	4.4	CO oxidation	27	21.7	4.76
sample A	0.17	CO-PROX	27	67.6	21.2
sample B	2.5	CO-PROX	27	20.3	9.15
Au/Fe_2O_3[b]	4.4	CO-PROX	27	39.3	8.60
sample A	0.17	CO-PROX	80	99.2	31.1
sample B	2.5	CO-PROX	80	35.8	16.2
Au/Fe_2O_3[b]	4.4	CO-PROX	80	80.3	17.6

[a]Sample A with low Pt loading contains Pt single atoms, while sample B with high Pt loading mainly contains Pt clusters and nanoparticles. Adapted with permission from ref 72. Copyright 2014 Macmillan Publishers Limited, part of Springer Nature. [b]The Au/Fe_2O_3 sample was provided by the World Gold Council. [c]TOFs were calculated on the basis of the metal dispersion in the catalysts. For Pt/FeO_x samples, the metal dispersion was measured by CO chemisorption. For Au/Fe_2O_3 sample, the dispersion was estimated by the average particle size.

oxidation of CO in the presence of H_2 (CO-PROX).[71] It was reported that the Au single atoms supported on CeO_2 show higher selectivity to oxidation of CO, with very low selectivity to oxidation of H_2 at 80 °C, than Au/CeO_2 samples containing Au clusters and nanoparticles, making the single-atom Au/CeO_2 an excellent catalyst for CO-PROX reaction. Unfortunately, no information about how CO and O_2 are activated and how they react on supported single Au atoms was reported. This could be an interesting research to investigate if it is the cooperative effect between Au and CeO_2 that should be responsible for the observed activity. If this is so, then the catalytic active site would not be a single atom, but an association of Au and Ce/O.

4.1.2. Pt Single Atoms for CO Oxidation. In the case of Pt, Zhang et al. reported that it was possible to prepare single Pt atoms dispersed on FeO_x by a coprecipitation method, and the catalytic properties of Pt single atoms were studied for the CO oxidation reaction.[72] As shown in Table 1, the Pt_1/FeO_x (sample A) with Pt single atoms show a higher specific rate and higher TOF than Pt/FeO_x catalyst containing Pt clusters and nanoparticles (sample B), indicating that singly dispersed Pt atoms supported on FeO_x can be an efficient catalyst for both CO oxidation and CO-PROX under mild conditions. DFT calculations show that O_2 is activated at the neighboring O-vacancy site of the Pt atom in FeO_x support. The partially vacant 5d orbitals of the positively charged Pt atoms can adsorb and activate CO with lower barrier energy than Pt clusters, which makes Pt single atoms more active for CO oxidation.

According to theoretical calculations, it appears that the FeO_x support in the Pt_1/FeO_x catalyst participates in the catalytic pathways for CO oxidation. It should be then interesting to study the behavior of single Pt atoms dispersed on inert supports (like Al_2O_3, SiO_2, TiO_2, etc.). Following that, Narula et al. studied the catalytic properties of Pt single atoms supported on an inert support (θ-Al_2O_3) for CO oxidation, and the results were compared to those obtained with Pt nanoparticles (~1 nm) supported on θ-Al_2O_3.[73] It was found that singly dispersed Pt atoms can catalyzed the CO oxidation reaction. However, the TOF at 200 °C for Pt nanoparticles was nearly 4-fold higher than that for Pt/θ-Al_2O_3 with singly dispersed Pt atoms, indicating that Pt nanoparticles were intrinsically more active than Pt single atoms for CO oxidation when supported on θ-Al_2O_3.

In the case of TiO_2, Christopher et al. reported the generation of stable single Pt atoms on TiO_2 by strong electrostatic adsorption of a very low amount of Pt on TiO_2 (0.025−0.05 wt %). The activity was compared to a Pt/TiO_2 sample (1.0 wt % of Pt) containing Pt nanoparticles (~1 nm). Kinetic studies showed that both Pt single atoms and nanoparticles followed the same reaction mechanism, and the rate-limiting step was related to O_2 activation. The catalytic results indicated that single Pt atoms were 4−6-fold more active than Pt nanoparticles (~1 nm) on the basis of activity normalized to Pt mass. It is suggested by the authors that the Pt−TiO_2 interface is the active site for CO oxidation and the rate-limiting step involves the migration of atomic oxygen from TiO_2 to isolated Pt atoms or interfacial Pt species in the Pt/TiO_2 sample containing Pt nanoparticles.[74] However, the catalytic behavior of subnanometric Pt clusters was not studied, and it seems that part of the isolated Pt atoms sintered into Pt clusters according to the IR spectra during the CO oxidation test in a fixed-bed reactor.

Furthermore, it has been reported that Pt single atoms within a zeolite can catalyze CO oxidation at 150 °C with moderate activity.[75] Unfortunately, no direct activity comparison between single Pt atoms and Pt clusters or nanoparticles was performed in that work.

Because water plays a critical role in the activity and selectivity of Au nanoparticles for CO oxidation reaction and CO-PROX,[76,77] its potential role in catalytic properties of Pt single atoms has been recently studied. Single Pt atoms were generated on CeO_2 by atomic layer deposition (ALD), and the role of water in CO oxidation was studied.[78] By kinetic and isotopic studies together with theoretical calculations, it was proposed that CO oxidation can be significantly improved by a water-mediated Mars−van Krevelen mechanism instead of the previously reported Langmuir−Hinshelwood mechanism on Au catalysts. Notably, transformation of part of the single Pt atoms into Pt clusters after the CO oxidation reaction at 90−100 °C was observed by high-resolution STEM. Therefore, it can still be discussed if the active species are the single Pt atoms or the Pt clusters and Pt nanoparticles formed under reaction conditions.

The stability of single atoms is a critical issue due to their strong trend to agglomerate into clusters or nanoparticles, especially in the presence of CO. Recently, it has been found that Pt atoms can evaporate from Pt nanoparticles during a high-temperature treatment of $Pt/La-Al_2O_3$ catalyst in air at 800 °C and be trapped by CeO_2 nanocrystals.[79] Those trapped Pt atoms on CeO_2 were stable up to 800 °C in air, and the addition of CeO_2 can significantly improve the stability of $Pt/La-Al_2O_3$ catalyst during the high-temperature aging treatment. However, the activity of those Pt single atoms for CO oxidation reaction is much lower than for other reported Pt/CeO_2 catalysts

DOI: 10.1021/acs.chemrev.7b00776
Chem. Rev. 2018, 118, 4981−5079

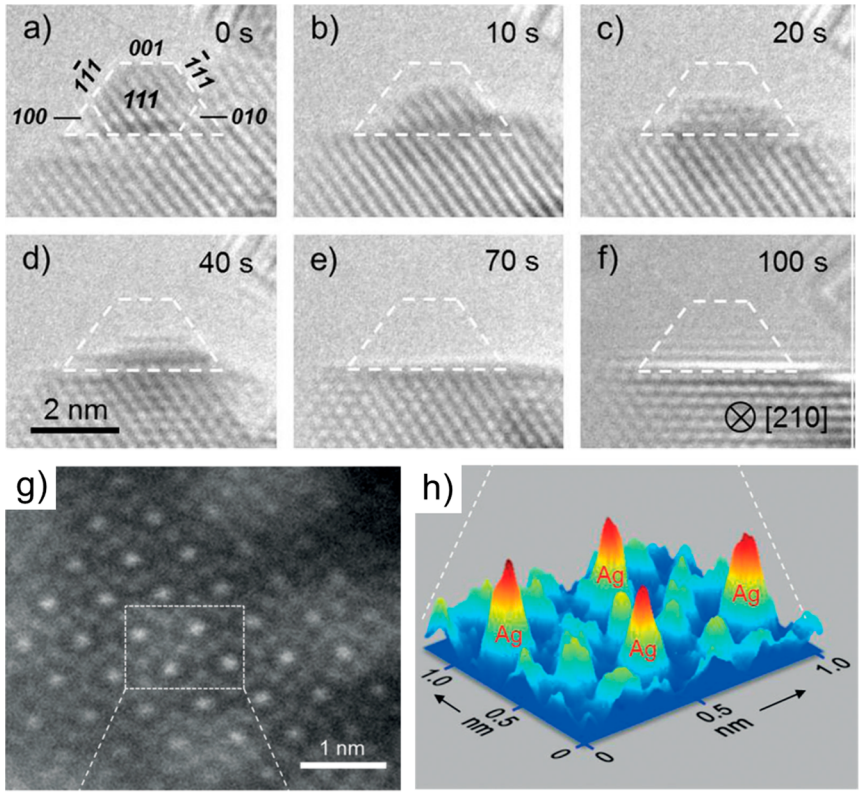

Figure 12. (a–f) High-resolution TEM images on the disintegration of Ag nanoparticles on hollandite manganese oxide during the calcination in air. (g,h) High-resolution STEM image of the singly dispersed Ag atoms in the lattice of hollandite manganese oxide after the disintegration of Ag nanoparticles. Adapted with permission from ref 83. Copyright 2015 Wiley-VCH Verlag GmbH & Co. KGaA, Weinheim.

containing Pt nanoparticles. Besides, it has also been reported that mesoporous Al_2O_3 can serve as the support to stabilize Pt single atoms, even after H_2 reduction treatment at 400 °C.[80] It is claimed that those Pt single atoms are highly stable during the CO oxidation reaction up to 400 °C.

4.1.3. Other Supported Single Metal Atoms for CO Oxidation. Besides Au and Pt, other heterogeneous catalysts containing single metal atoms have also been reported as active species for CO oxidation. Atomically dispersed Pd on La-modified Al_2O_3 then showed enhanced activity in CO oxidation. However, it should be taken into account that the Pd single atoms were partially reduced and sinter into metallic Pd nanoparticles under reaction conditions, especially when the temperature was above 100 °C. Neverthelss, those sintered Pd nanoparticles could be redispersed into single Pd atoms after high temperature calcination (700 °C) in air.[81]

In another example, Ag nanoparticles supported on hollandite manganese oxide could be redispersed into singly dispersed Ag atoms by calcination in air at 400 °C as confirmed by in situ TEM and in situ small X-ray diffraction (see Figure 12).[82,83] Structural characterizations show that the redispersed Ag atoms enter the tunnels of hollandite manganese oxide crystallites. These atomically dispersed Ag species are positively charged and show 4–5 times higher activity than pristine catalyst containing Ag nanoparticles for low-temperature CO oxidation reaction. However, Ag nanoparticles and single Ag atoms showed very similar apparent activation energy, indicating the redispersion of Ag nanoparticles into Ag atoms mainly improve the numbers of active sites for CO oxidation.

Supported single Pd and Ir atoms have also been reported as catalysts for CO oxidation, although their catalytic performances were not as impressive as Au and Pt atoms.[84,85] In a recent work, it is reported that singly dispersed Pd atoms supported on CeO_2 are active for CO oxidation.[86,87] Theoretical calculations indicate the cooperative effect between isolated PdO_x species and CeO_2 during the catalytic cycle for CO oxidation.

4.2. Water–Gas Shift

Like CO oxidation, water–gas shift (WGS) is also a widely used model reaction. In 2003, Flytzani-Stephanopoulos et al. pointed out the important role of nonmetallic Au and Pt species on CeO_2-based catalysts for WGS reaction.[88] After chemical leaching of the metallic nanoparticles in conventional Au/CeO_2 and Pt/CeO_2 catalysts containing a large number of metallic nanoparticles, their activity is almost not affected, implying that those residual nonmetallic Au and Pt are the active species. In following work, the authors have further demonstrated that atomically dispersed Pt stabilized by alkali ions are the active sites for WGS reactions.[89] The introduction of alkali ions can generate partially oxidized Pt-alkali-$O_x(OH)_y$ sites, which are able to catalyze the WGS reaction at low temperature range (200–300 °C). According to their latest works, not only single Au and Pt atoms supported on CeO_2, but also single atoms supported on other oxides (like TiO_2, FeOx, SiO_2, zeolites, etc.) are proposed to be the active sites in WGS reaction.[90,91] It is also found that atomically dispersed metal species (both Pt and Au) supported on various supports show almost the same apparent activation energy (see Figure 13b and d), implying that a common single-site species exists in different catalysts for the WGS reaction.[92]

In the above works, alkali ions are required to stabilize Au and Pt single atoms. In a recent work, Zhang et al. reported the utilization of single Ir atoms for WGS reaction without the

DOI: 10.1021/acs.chemrev.7b00776
Chem. Rev. 2018, 118, 4981–5079

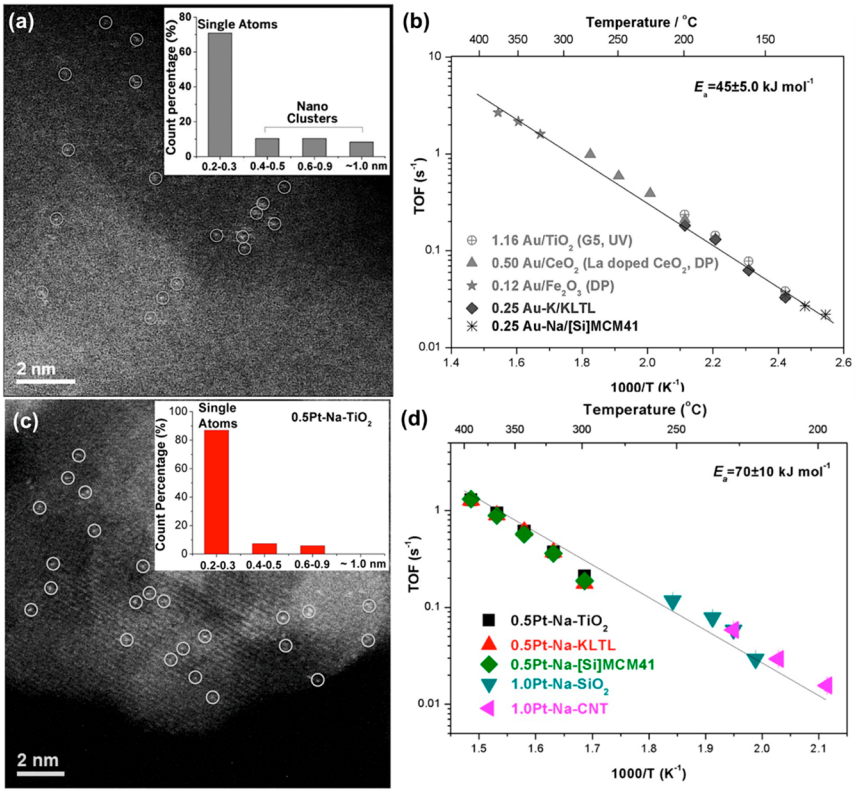

Figure 13. (a) High-resolution STEM image and the corresponding size distribution of Au species in Au−Na/[Si]MCM41 catalyst with 0.25 wt % of Au. (b) TOF values of atomically dispersed Au species on different supports. The TOF values are obtained under the same reaction conditions. Adapted with permission from ref 90. Copyright 2014 Association for the Advancement of Science. (c) High-resolution STEM image and the corresponding size distribution of Pt species in Pt−Na/TiO_2 catalyst with 0.5 wt % of Pt. (d) TOF values of atomically dispersed Pt species on different supports. The TOF values are obtained under the same reaction conditions. Adapted with permission from ref 91. Copyright 2015 American Chemical Society.

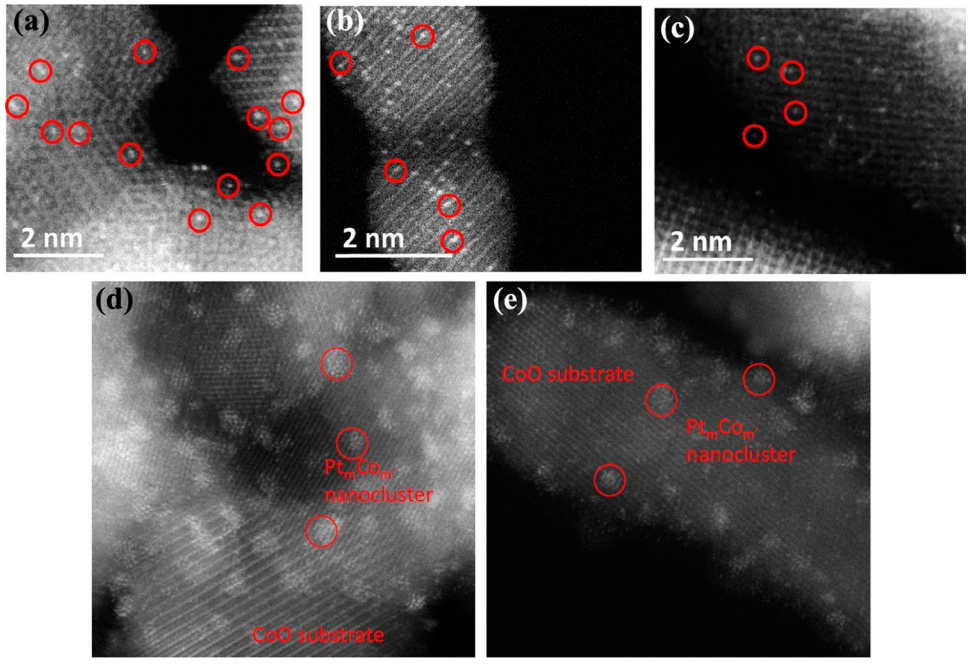

Figure 14. (a−c) High-resolution STEM images of singly dispersed Pt atoms on Co_3O_4 nanorods. Pt atoms are indicated by red circles. (d,e) High-resolution STEM images of Pt_mCo_n/CoO sample after WGS reaction at 350 °C. Pt_mCo_m clusters are indicated by red circles. Adapted with permission from ref 95. Copyright 2013 American Chemical Society.

addition of alkali ions.[93] By decreasing the Ir loading to 0.01 wt %, it was possible to generate isolated Ir sites on FeO_x, and those Ir single atoms show higher TOFs for WGS reaction at 300 °C as compared to Ir clusters and nanoparticles.

DOI: 10.1021/acs.chemrev.7b00776
Chem. Rev. 2018, 118, 4981−5079

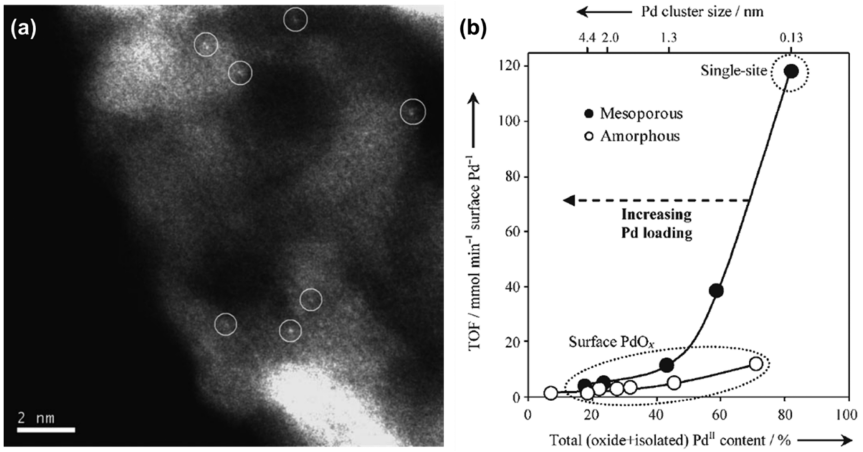

Figure 15. (a) High-resolution STEM image of Pd/Al_2O_3 sample containing 0.03 wt % of Pd. (b) Relationships between the TOFs of surface Pd species for aerobic oxidation of crotyl alcohol and the particle size and chemical states of Pd in various Pd/Al_2O_3 catalysts. Adapted with permission from ref 100. Copyright 2007 Wiley-VCH Verlag GmbH & Co. KGaA, Weinheim.

The size of the metal species will also affect the product distributions in WGS reaction. The high activity and suppressed selectivity to methanation product (CH_4) has been reported on atomically Rh species supported on TiO_2 during WGS reaction.[94] At 300 °C, the selectivity to CH_4 was almost zero on Rh/TiO_2 catalysts containing Rh single atoms as the dominant species, while Rh nanoparticles gave ~50% selectivity to CH_4. On the basis of spectroscopic characterizations, it is proposed that H_2 dissociation is not favorable on isolated Rh atoms, and this leads to low CO_2 methanation activity.

Nevertheless, it should be taken into consideration that when working with single atoms, metal clusters and nanoparticles can also be present, and metal species may undergo dynamic structural transformation (including morphological and chemical transformation) under reaction conditions. It is then crucial when studying the catalytic behavior of single atoms to investigate their state under reaction conditions. Along this line, in a recent work, Pt single atoms supported on Co_3O_4 nanorods were used as catalyst for WGS reaction.[95] It was observed that in the fresh catalyst, single Pt atoms were dispersed on Co_3O_4 nanorods, and they were stable after calcination in air. However, after catalyzing WGS reaction at 350 °C, single Pt atoms aggregated and formed Pt_mCo_n bimetallic clusters, as determined by STEM images (Figure 14). Interestingly, the activation energy of Pt_mCo_n clusters for WGS reaction was lower than that of single Pt atoms. This work illustrates that metal atoms or clusters may have strong interaction with the supports, and they can show dynamic structural transformations during the reactions.

Such transformation of metal species under reaction conditions was also confirmed by in situ TEM techniques.[96] It was observed that subnanometric Au clusters were generated from singly dispersed Au atoms under WGS reaction conditions. However, the whole evolution process of Au species was not clearly demonstrated, probably due to the instrument limitation. The contrast between Au species and the CeO_2 support is not high enough for studying such a process when working under bright-field transmission mode. Similar agglomeration of subnanometric Au species into Au nanoparticles has also been observed on $Au/CeZrO_4$ catalyst by in situ TEM.[97] This is an interesting phenomenon, and we believe that the dynamic evolution of subnanometric metal species could be studied with high-resolution HAADF-STEM and XANES-EXAFS spectroscopy to detect the potential structural transformation under reaction conditions.

4.3. Oxidation of Alcohols

Selective oxidation of alcohols has wide applications in transformation of biomass platform molecules and fine chemicals. It has been presented that metal nanoparticles (such as Pt, Au, Pd, etc.) show excellent activity and selectivity for selective oxidation of alcohols under mild conditions.[98,99] In recent years, it has been reported that single atoms can also serve as the active sites for oxidation of alcohols. In 2007, Hackett et al. reported the generation and application of single Pd atoms supported on mesoporous alumina for selective oxidation of allylic alcohols.[100] As shown in Figure 15, Pd species (from single Pd atoms to clusters to nanoparticles) showed strong size effects on the TOFs in oxidation of crotyl alcohol. With smaller Pd species, the TOF value became higher and reached the maximum with Pd single atoms while the high selectivity was also preserved. The selective oxidation of allylic alcohols can also be catalyzed by supported Au nanoparticles, giving very high selectivity (99%) to α,β-unsaturated carbonyl compounds.[101] As compared to the state-of-art supported Au catalysts (538 h^{-1} at 120 °C), Pd single atoms supported on mesoporous alumina show even higher TOF (4400 h^{-1} at 60 °C), although the selectivity to α,β-unsaturated carbonyl compound is lower (~90%). The lifetime of the nanoparticulate Au catalysts for selective oxidation of allylic alcohols were very long; however, the lifetime of the Pd single atoms during the oxidation of alcohols was not mentioned.

In the past few years, the development of non-noble metal catalysts as a substitute for noble metals is emerging in heterogeneous catalysis. Recently, it has been widely reported that single transition metal atoms (such as Co, Fe, etc.) can be stabilized by N-doped carbon. Beller et al. reported the application of Co−N−C and Fe−N−C catalysts for oxidative esterification of alcohols and oxidative dehydrogenation of N-heterocycles.[102,103] With the help of high-resolution STEM, it was revealed that the active sites for these selective oxidation reactions may be associated with the atomically dispersed metal species embedded in the carbon support while the residual nanoparticles are not active.[104] A series of catalysts containing transition metal atoms stabilized by N-doped carbon have been studied for selective oxidation of alcohols.[105] It was found that beside Co−N−C and Fe−N−C, Cu−N−C, Ni−N−C, and Cr−

DOI: 10.1021/acs.chemrev.7b00776
Chem. Rev. 2018, 118, 4981−5079

N−C are also active for the oxidation of benzyl alcohol to benzyl aldehyde. Among them, Cu−N−C sample shows the best performance, which is only 1 order of magnitude lower than Pt-based catalyst. However, these atomically dispersed metal species show poor activity for oxidation of aliphatic alcohols. Isotopic studies show that the β-H elimination is a key step in oxidation of benzyl alcohol. Deeper understanding of the catalytic mechanism in these systems is necessary to further improve the performance and stability of those catalysts for substituting noble metal catalysts.

4.4. Selective Hydrogenation

4.4.1. Pt-Group Single-Atom Catalysts for Hydrogenation Reactions. Pt-group metals are widely used industrially for hydrogenation reactions. In those industrial catalysts, Pt-group metals mainly exist as nanoparticles. In recent years, new methodologies have been developed to generate single-site Pt-group metals, and these single-atom catalysts have shown promising catalytic performances for hydrogenation reactions.

A series of Pt/FeO_x catalysts were prepared by a coprecipitation method, and Pt species with different particle sizes ranging from single atoms to nanoparticles were generated by tuning the loading of Pt (see Figure 16).[106] The catalytic performances of various Pt/FeO_x catalysts are exhibited in Table 2. Interestingly, all of the Pt/FeO_x catalysts show excellent selectivity for the chemoselective hydrogenation of 3-nitrostyene, and the TOFs based on all of the Pt atoms in the catalyst almost keep constant when the Pt loading increases from 0.08 to 0.75 wt %, although the size distribution of Pt species varies with the loading amount of Pt. The Pt single atoms in the 0.08%Pt/FeO_x-R200 sample show a remarkable TOF of 1494 h^{-1}, which is nearly 20 times higher than that of Pt/TiO_2 (containing Pt nanoparticles). Notably, subnanometric Pt clusters can also be observed in the 0.08%Pt/FeO_x-R250 sample, which exhibits the highest TOF, implying that Pt clusters may also play a role in the hydrogenation of nitroarenes.

As compared to conventional Pt nanoparticles, Pt single atoms may show different selectivity in hydrogenation of different molecules.[107] Stabilized on phosphomolybdic acid, Pt single atoms show higher TOFs in hydrogenation of polar groups like $-NO_2$ and C═O as compared toPt nanoparticles supported on carbon. However, in the case of hydrogenation of C═C and C≡C groups, Pt single atoms are less active, indicating that the reactivity of different types of Pt species is dependent on the substrate molecules.

Different reactivity of single atoms will cause unique selectivity in hydrogenation reactions. For instance, Pd single atoms supported on graphene showed high selectivity to 1-butene during selective hydrogenation of 1,3-butadiene, while Pd nanoparticles gave higher selectivity to *cis*-2-butene and *trans*-2-butene and slightly more full hydrogenation products, as shown in Figure 17.[108] Moreover, when the hydrogenation of 1,3-butadiene is performed in the presence of 70% propene in the feed gas, Pd single atoms show negligible propene conversion while Pd nanoparticles will react much more with propene. Unique selectivity of Pd single atoms has also been reported for hydrogenation of alkynes.[109] Pd atoms stabilized by C_3N_4 show excellent selectivity (~90%) in hydrogenation of 1-hexyne to 1-hexene. However, there are still some arguments on the catalytic properties of single Pd atoms. For instance, Rossell et al. have reported that single Pd atoms supported on Fe_3O_4 show no activity in hydrogenation of alkenes, while Pd clusters and nanoparticles are active.[110]

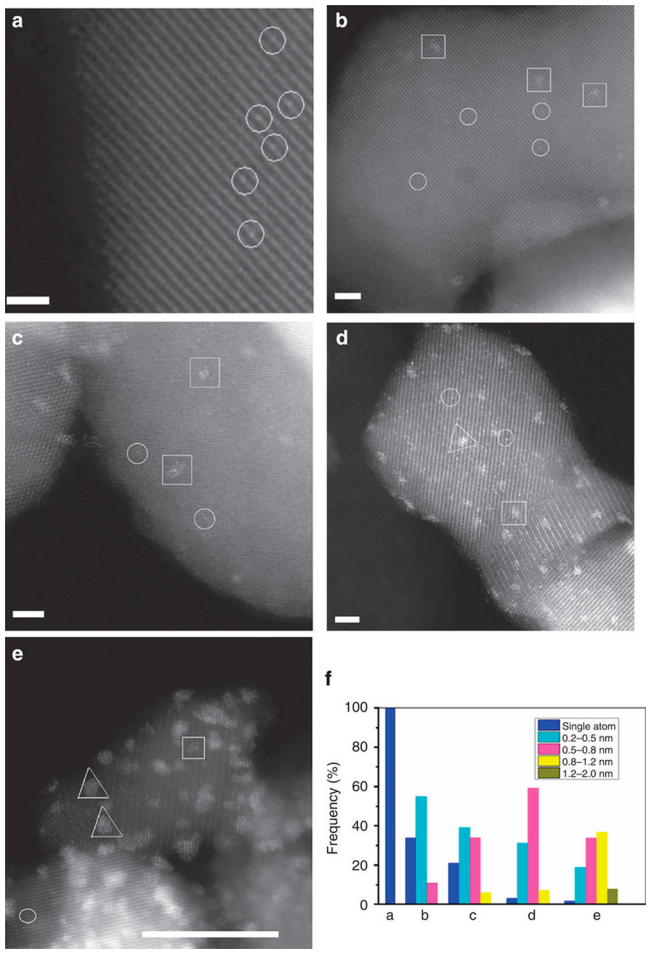

Figure 16. STEM images of various Pt/FeO_x catalysts with different Pt loading. (a) Pt/FeO_x with 0.08 wt % of Pt and reduced by H_2 at 200 °C. (b) Pt/FeO_x with 0.08 wt % of Pt and reduced by H_2 at 250 °C. (c) Pt/FeO_x with 0.31 wt % of Pt and reduced by H_2 at 250 °C. (d) Pt/FeO_x with 0.75 wt % of Pt and reduced by H_2 at 250 °C. (e) Pt/FeO_x with 4.30 wt % of Pt and reduced by H_2 at 250 °C. The circles, squares, and triangles in the above images correspond to single Pt atoms, two-dimensional Pt clusters, and three-dimensional Pt nanoparticles, respectively. Adapted with permission from ref 106. Copyright 2014 Macmillan Publishers Limited, part of Springer Nature.

In another example, it is shown that singly dispersed Ru and Ru nanoparticles supported on Al_2O_3 or TiO_2 give different catalytic behavior during CO_2 hydrogenation.[111] In the case of Ru/Al_2O_3 catalysts with low loading of Ru (0.1 wt %), Ru mainly exists as singly dispersed atoms (see Figure 18c). These single Ru atoms will agglomerate into Ru clusters and nanoparticles after CO_2 hydrogenation reaction at 350 °C, with a gradually increased activity for CO_2 conversion and change of the product distribution as a function of time on stream (see Figure 18a). After the transformation from singly dispersed Ru into Ru clusters and nanoparticles (see Figure 18d), the activity of Ru species will increase greatly, and CH_4 becomes the major product instead of CO for the fresh catalyst (see Figure 18b). Similar phenomenon and catalytic behavior have also been observed with Ru species supported on TiO_2, suggesting that the CO_2 hydrogenation reaction undergoes different mechanisms on single Ru atoms and Ru clusters or nanoparticles. These results again show the dynamic behavior of metal catalysts under

DOI: 10.1021/acs.chemrev.7b00776
Chem. Rev. 2018, 118, 4981−5079

Table 2. Chemoselective Hydrogenation of 3-Nitrostyrene on Different Pt/FeO_x Catalysts[a]

entry	catalyst	time (min)	conv. (%)	sel. (%)	TOF (h^{-1})[d]
1	0.08%Pt/FeO_x-R200	49	95.6	98.4	1494
2	0.08%Pt/FeO_x-R250	50	96.5	98.6	1514
3[b]	0.08%Pt/FeO_x-R250	7	88.8	91.1	11064
4	0.31%Pt/FeO_x-R250	67	95.8	94.4	1506
5	0.75%Pt/FeO_x-R250	73	96.7	92.6	1324
6	2.73%Pt/FeO_x-R250	110	97.8	92.9	933
7[c]	4.30%Pt/FeO_x-R250	34	94.2	92.7	762
8	0.2%Pt/TiO_2-R450	840	96.8	94.0	88
9	0.08%Pt/SiO_2	65	87.9	46.9	
10	0.08%Pt/Al_2O_3	158	87.3	27.8	
11	Fe_3O_4	210			
12	Fe_2O_3	240			

[a]Adapted with permission from ref 106. Copyright 2014 Macmillan Publishers Limited, part of Springer Nature. Reaction conditions: Pt/substrate = 0.08%, 40 °C, and 3 bar of H_2; 5 mL of reaction mixture, 0.5 mmol of 3-nitrostyrene, toluene as solvent, and *o*-xylene as internal standard. [b]Reaction performed at 80 °C with 10 bar of H_2. [c]Pt/substrate = 0.45%. [d]The TOFs were calculated on the basis of the total amount of Pt species in the catalysts.

reaction conditions.[112] Interestingly, Matsubu et al. have found that Ru nanoparticles were disintegrated into isolated Ru sites under H_2-lean conditions (CO_2:H_2 = 10:1) at 200 °C, implying that the dynamic behavior (agglomeration−disintegration) depends on the reaction conditions. Consequently, the selectivity to CO increases and selectivity to CH_4 decreased gradually with time on stream.

The hydrogenation of CO_2 can also be performed in the liquid phase. In a recent work, Mori et al. have demonstrated the application of Ru-based heterogeneous catalysts (with Ru loading of ∼0.4 wt %) for hydrogenation of CO_2 into formic acid in H_2O in the presence of $NaHCO_3$ as base.[113] On the basis of structural characterization, it was proposed that mononuclear Ru centers supported on layered double hydroxides (LDHs) were the active sites for the above process. The catalytic performances of supported Ru species could be modulated by the chemical composition of LDHs, which were affected by the surface hydroxyl groups.

As could be expected from electronic considerations, the coordination environments of the supported single atoms have a significant impact on the catalytic properties. The interaction between small molecules (CO and C_2H_4) and mononuclear Ir complex is different on MgO and zeolite supports, resulting in a support-dependent behavior for H_2 dissociation.[114] When

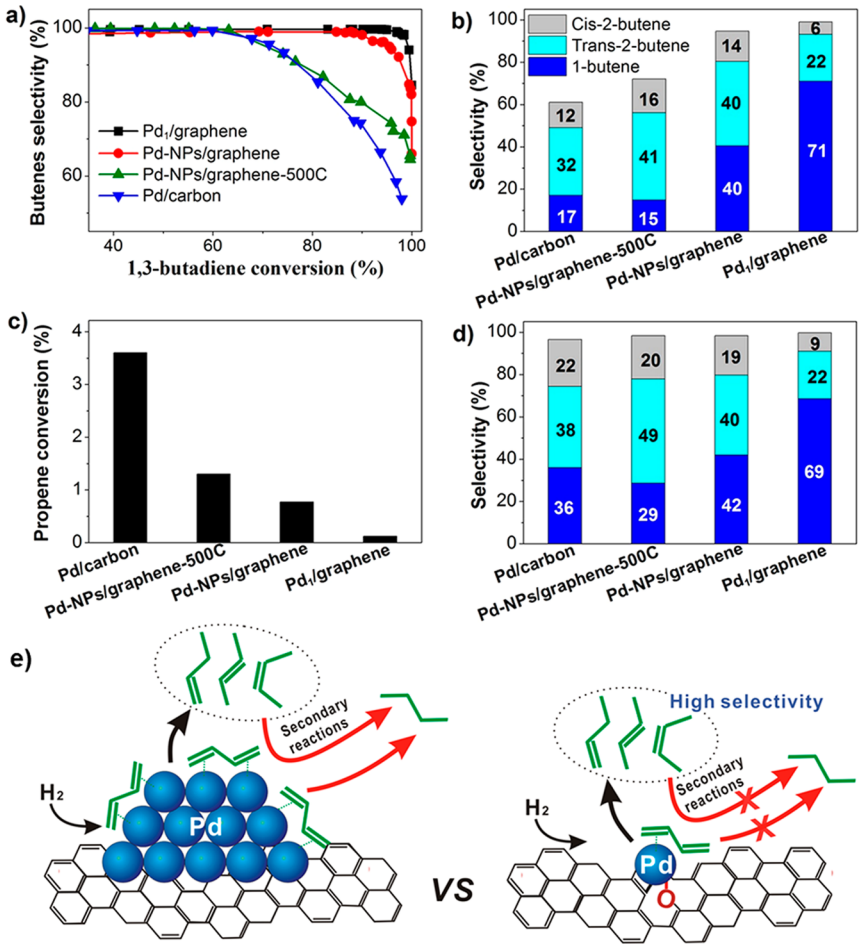

Figure 17. Catalytic performances of Pd_1/graphene, Pd-NPs/graphene, Pd-NPs/graphene-500C, and Pd/carbon samples for selective hydrogenation of 1,3-butadiene. (a) Selectivity to butenes as a function of butadiene conversion by changing the reaction temperatures. (b) Distribution of butene products at 95% conversion of butadiene. Conversion of propene (c) and the distribution of butene products (d) at 98% conversion of butadiene in the presence of 70% of propene in the feed gas. (e) Schematic illustration of the reactivity of 1,3-butadiene on Pd nanoparticles and Pd single atoms, showing different chemoselectivity. Adapted with permission from ref 108. Copyright 2015 American Chemical Society.

DOI: 10.1021/acs.chemrev.7b00776
Chem. Rev. 2018, 118, 4981−5079

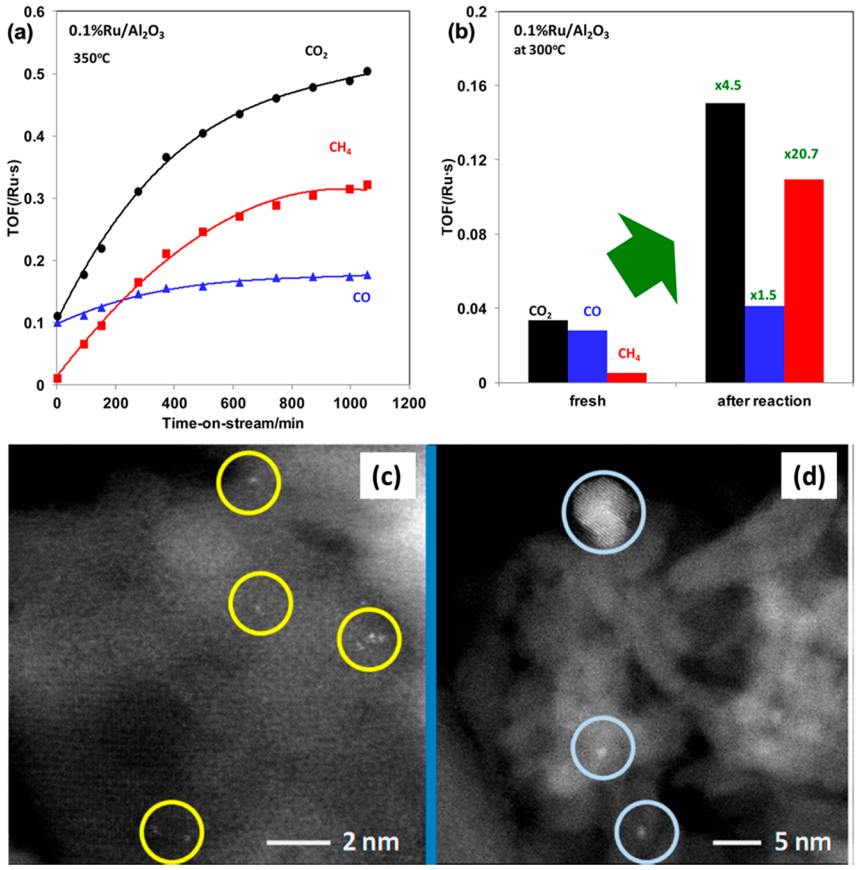

Figure 18. (a) TOFs of CO_2, CO, and CH_4 as a function of time-on-stream at 350 °C over Ru/Al_2O_3 catalyst (with 0.1% of Ru). (b) TOFs for CO_2 conversion and CO/CH_4 production at steady state over a fresh and used (after CO_2 hydrogenation reaction at 350 °C) Ru/Al_2O_3 catalyst at 300 °C. (c) STEM image of the fresh Ru/Al_2O_3 catalyst, showing the presence of single Ru atoms in the catalyst. (d) STEM image of the Ru/Al_2O_3 catalyst after CO_2 hydrogenation reaction at 350 °C, showing the presence of Ru clusters and nanoparticles. Adapted with permission from ref 111. Copyright 2013 American Chemical Society.

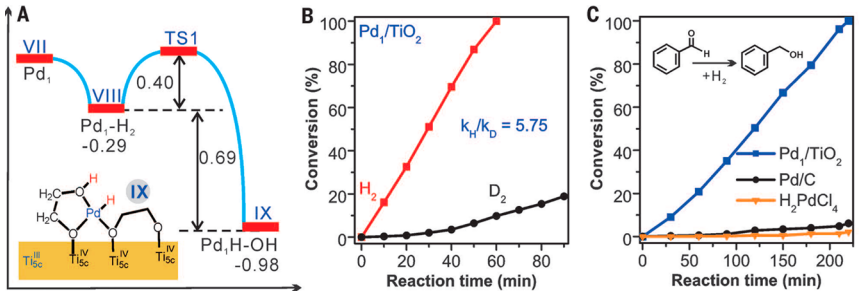

Figure 19. (A) Catalytic mechanism of heterolytic activation of H_2 on Pd single atom stabilized by ethylene glycolate ligands in Pd_1/TiO_2 catalyst. (B) Primary isotope effect on Pd_1/TiO_2 catalyst in hydrogenation of styrene. (C) Catalytic performances of Pd_1/TiO_2, Pd/C, and H_2PdCl_4 for hydrogenation of benzaldehyde. Adapted with permission from ref 118. Copyright 2016 The American Association for the Advancement of Science.

mononuclear Ir complexes are supported on electron-withdrawing HY zeolite support, single Ir atoms can activate C_2H_4 and H_2 simultaneously. With a basic support such as MgO as electron-donor support, mononuclear Ir complexes are electron-rich and bonded by CO, and this situation is not favorable for the hydrogenation of ethene due to its low activity for H_2 dissociation.[115]

Metal−organic frameworks (MOFs), as hybrid porous materials with well-define structures, can also serve as the support for mononuclear complexes to generate single-atom catalyst.[116] As compared to conventional solid supports, the electron-donor ability of MOFs (UiO-66 and UiO-67) falls between those of HY zeolite and MgO. The catalytic activity for mononuclear Ir catalyst supported on MOFs also falls between those on MgO and HY zeolite, which is in line with electron-donor properties of the Ir centers. The bonding interaction between mononuclear Ir complex with MOFs is affected by the framework structure. When tuning the structure of MOFs, the bonding site of the mononuclear Ir complex will vary, leading to different catalytic behaviors.[117]

Single metal atoms can also be stabilized on solid supports together with some organic ligands.[118] In a recent work, Zheng and his co-workers developed a photochemical method to generate atomically dispersed Pd catalysts on TiO_2 nanosheets.

DOI: 10.1021/acs.chemrev.7b00776
Chem. Rev. 2018, 118, 4981−5079

As shown in Figure 19A, these Pd atoms were stabilized by ethylene glycolate ligands, and it was proposed on the basis of theoretical calculations that H_2 could be activated by a synergistic effect of Pd and the ethylene glycolate ligand. The Pd_1/TiO_2 catalyst containing a high amount of atomically dispersed Pd species (1.5 wt %) showed excellent performance for hydrogenation of C═C. On the basis of isotopic studies (Figure 19B), heterolytic activation of H_2 on those single-site Pd species rather than homolytic dissociation mechanism on conventional Pd nanoparticles was proposed, and it was reflected by the excellent activity of Pd_1/TiO_2 catalyst for hydrogenation of C═O groups (Figure 19C).

4.4.2. Single-Atom Au Catalysts for Hydrogenation Reactions. In 1973, Bond et al. reported the application of supported Au catalyst for hydrogenation of olefins. The activity increased by a factor of 7000 when decreasing the Au loading from 1% to 0.01%, implying that hydrogenation on Au catalysts is a structure-sensitive reaction and Au species with very small size are the active sites.[119] With the development of characterization tools, together with more robust catalyst preparation methodologies, further insights on the nature of the Au active sites for hydrogenation reactions have been achieved.

In 2003, Gates et al. reported the reactivity of mononuclear Au complex supported on MgO for hydrogenation of ethene.[120] In this work, they found that Au single-atom catalyst could readily catalyze the hydrogenation of ethene at 80 °C and the TOFs of Au species would decrease when increasing the particle size (see Figure 20). Furthermore, combining the catalytic results with

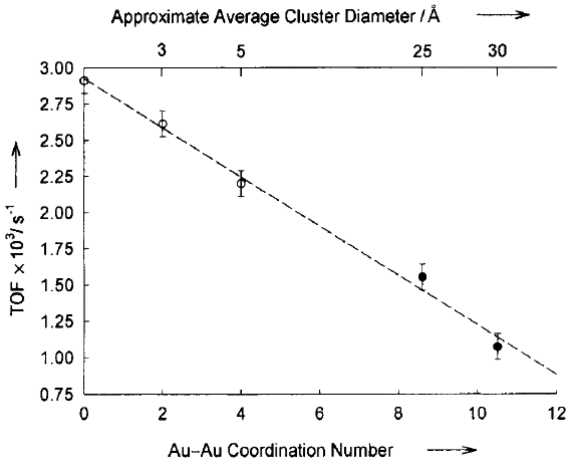

Figure 20. Activities of MgO-supported Au catalysts with different sizes (from mononuclear Au complex to Au clusters and nanoparticles) for hydrogenation of ethene. Adapted with permission from ref 120. Copyright 2003 Wiley-VCH Verlag GmbH & Co. KGaA, Weinheim.

XAS characterization results, the authors have proposed that only mononuclear $Au^{\delta+}$ species were active for hydrogenation of ethene, while metallic Au particles were not active. When working with Au/ZrO_2 catalysts for selective hydrogenation of 1,3-butadiene, it was found that the TOFs for hydrogenation of 1,3-butadiene remained almost constant when the Au loading was low (from 0.01 wt % to 0.08 wt %).[121] By correlating the catalytic and characterization results from XPS, it then was proposed that only highly dispersed $Au^{\delta+}$ species were the active sites while metallic Au nanoparticles were not active.[122] Furthermore, in the case of Au/ZrO_2 containing only $Au^{\delta+}$ species, only semihydrogenation products (butenes) can be obtained with 1-butene as the major product (ca. 64%). However, the fully hydrogenated product (butane) appeared on Au/ZrO_2 catalysts containing metallic Au nanoparticles, and an increasing amount of *trans*-2-butene was observed. The role of the cationic Au species in hydrogenation of olefins has also been demonstrated in Au(III)-MOF hybrid material.[123] Because of the bonding interaction between Au(III) Schiff base complex and the linker in MOFs, single-atom Au species can be stabilized and show excellent activity and high selectivity in hydrogenation of 1,3-butadiene to butenes.

The unique catalytic properties of Au single atoms in hydrogenation have also been reflected in *para*-hydrogen-induced polarization.[124,125] To achieve *para*-hydrogen-induced polarization, two H atoms in the *para*-hydrogen molecule must end up in the same product molecule, which is the so-called pairwise hydrogen addition. Therefore, to achieve that goal, isolated well-defined sites are required to avoid the H-transfer reactions on metal catalysts. It has been shown that single Au atoms supported on carbon nanotubes show at least 1 order of magnitude higher activity in hydrogenation of olefins and alkynes than conventional nanoparticulate Au catalysts.

4.4.3. Non-noble Single-Atom Metal Catalysts for Hydrogenation Reactions. In recent years, non-noble metal catalysts have attracted great attention and shown promising catalytic performances for substituting noble metal catalysts for selective hydrogenation reactions. For instance, Co nanoparticles covered by thin carbon layers have been reported as active and selective catalyst for chemoselective hydrogenation of nitroarenes to corresponding anilines.[126] The active sites are proved to be the surface of metallic Co nanoparticles, and the role of the thin carbon layers is to protect Co nanoparticles from deep oxidation.[127,128] Recently, a facile method to generate a Co−N−C catalyst containing singly dispersed Co atoms on N-doped carbon matrix has been presented.[129] As shown in Figure 21, Co atoms were clearly observed by high-resolution STEM, and their local coordination structure has also been clarified by EXAFS and XANES. The Co−N−C catalyst showed excellent activity and selectivity in hydrogenation of nitroarenes to corresponding azo products in the presence of strong base (NaOH), but the activity of Co−N−C catalysts was also lower than that of supported Au nanoparticles.[130,131] In another work, using MOF as precursor, Co−N−C catalyst containing atomically dispersed CoN_x species was prepared and tested for selective hydrogenation of nitroarenes to corresponding anilines.[132] However, there is no direct comparison study on the catalytic performance of single-site Co catalysts and nanoparticulate Co catalysts.

MOFs, as a versatile family of porous materials, can serve as tunable support for single-site non-noble metals. Taking advantage of the coordination interaction between the framework nodes and mononuclear metal complex, single-site Co catalyst can be generated and stabilized in MOFs. Single-site Co catalyst in MOFs can be applied for hydrogenation of unsaturated bonds, such as alkenes, imines, carbonyls, and heterocycles (see Figure 22).[133] High turnover numbers and stability can be achieved in those reactions, due to the open structure of MOFs and stabilization effects of single-site Co on the nodes. Besides, single-site Ni catalyst can also be prepared and shows promising catalytic performances for hydrogenation of alkenes.[134] It can be expected that the preparation and reactivity of single-site metal species in MOFs will expand the scope of single-site metal catalysts.[135]

DOI: 10.1021/acs.chemrev.7b00776
Chem. Rev. 2018, 118, 4981−5079

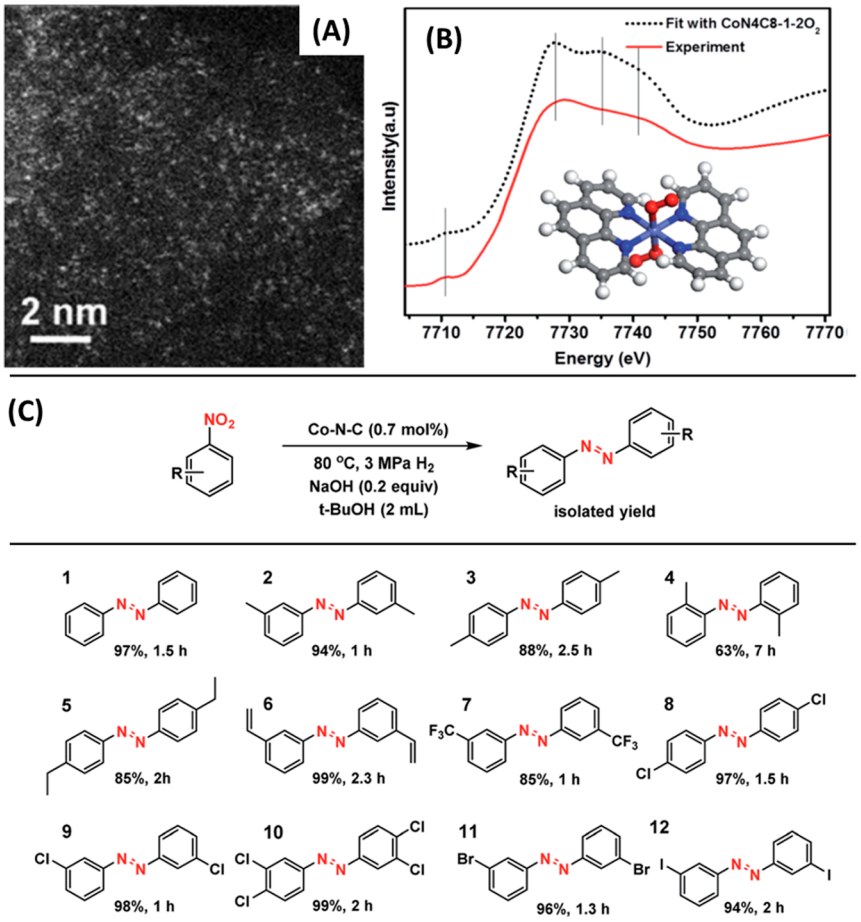

Figure 21. (A) High-resolution STEM image of singly dispersed Co atoms stabilized by N-doped carbon matrix (Co−N−C catalyst). (B) Determination of the coordination structure of Co−N−C catalyst according to the fitting and simulation of XANES spectrum. (C) Hydrogenation of nitroarenes to corresponding azo products using Co−N−C catalyst. Adapted with permission from ref 129. Copyright 2016 The Royal Society of Chemistry.

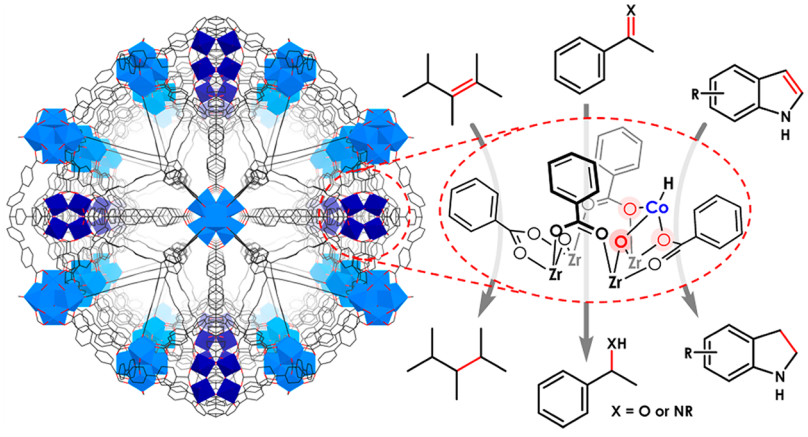

Figure 22. Schematic illustration of immobilization of single-site Co catalyst in porous metal−organic framework and its catalytic applications for hydrogenation reactions. The metal center in MOF is Zr or Hf, and the organic linker is *p*-biphenylcarboxylate. The single-site Co catalyst is stabilized by the secondary building unites. Adapted with permission from ref 133. Copyright 2016 American Chemical Society.

4.5. Dehydrogenation and Reforming Reactions

For hydrogenation reactions, activation of H_2 molecules is usually a key step. In dehydrogenation and some reforming reactions, the cleavage of X−H bonds and the recombination of H into H_2 molecules become key steps.

Using grafted organometallic complexes as model catalyst, Hu et al. have investigated the evolution of metal species under reaction conditions by in situ spectroscopic techniques. For instance, mononuclear Fe complex can transform into FeO_x nanoparticles when reduced by H_2 at 400 °C. Interestingly, these agglomerated Fe species disintegrated into isolated Fe^{II} species according to the XANES and EXAFS spectra.[136] The evolution of Fe species is presented in Figure 23. The authors have also studied supported Ga catalysts. Similarly, by studying the XAS

DOI: 10.1021/acs.chemrev.7b00776
Chem. Rev. 2018, 118, 4981−5079

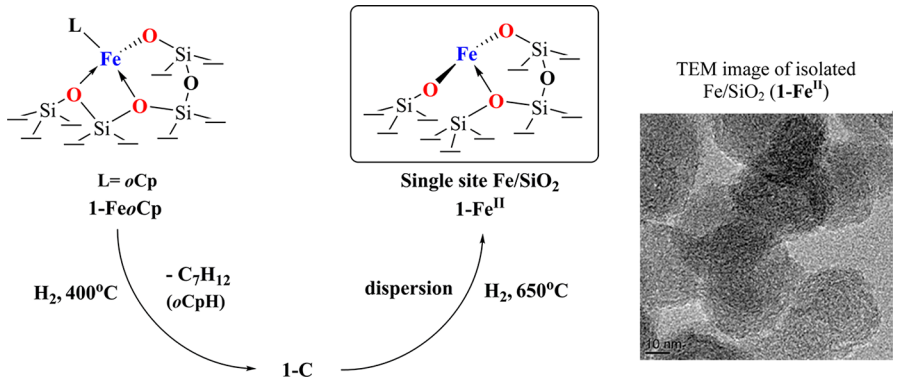

Figure 23. Transformation of surface Fe species in the presence of H_2 at evaluated temperature to form isolated Fe^{II} sites (1-Fe^{II}). Mononuclear Fe complex (1-Fe*o*Cp) was reduced by H_2 at 400 °C and formed nanosized FeO_x (1-C). These nanosized FeO_x were disintegrated into highly dispersed Fe^{II} species when the temperature reached 650 °C in H_2. A TEM image of the Fe/SiO_2 catalyst containing isolated Fe^{II} sites is also presented. Adapted with permission from ref 136. Copyright 2015 American Chemical Society.

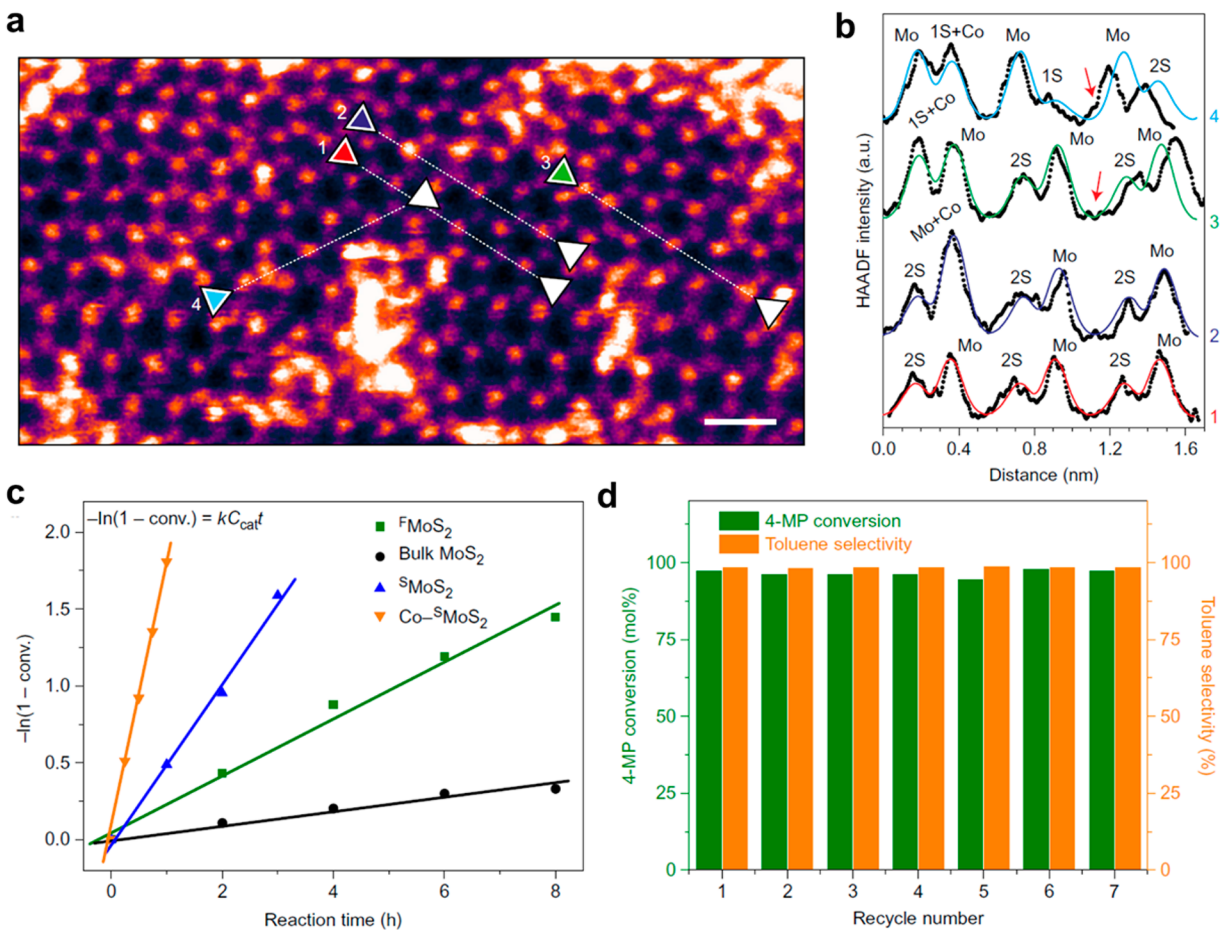

Figure 24. (a) Atomic-resolution STEM image of single-layer Co−MoS_2 catalyst. (b) Intensity profiles of four different lines and corresponding simulation results in the high-resolution STEM image. The location of Co atoms is determined according to the contrast. The dots with higher contrast intensity are ascribed to Co atoms. (c) Kinetic comparison between different types of catalysts for the hydrodeoxygenation of 4-methylphenol to toluene. (d) Stability test of single-layer Co−MoS_2 catalyst for hydrodeoxygenation of 4-methylphenol to toluene. Adapted with permission from ref 130. Copyright 2017 Macmillan Publishers Limited, part of Springer Nature.

results under reducing conditions, single-site Ga species are proposed to be the active sites for dehydrogenation of propane to propene.[137] Wang et al. have reported that atomically dispersed Au supported on $ZnZrO_x$ can be an efficient catalyst for low-temperature dehydrogenation of ethanol to acetaldehyde.[138] After NaCN-leaching treatment, Au nanoparticles in the fresh $Au/ZnZr_{10}O_x$ catalyst were removed while the activity for ethanol dehydrogenation was almost not affected, implying that cationic Au atoms dispersed on $ZnZr_{10}O_x$ were the active species.

The conversion of oxygen-rich biomass through hydrodeoxygenation is an important process for making biofuels and biomass-derived chemicals.[139] Recently, Liu et al. reported the

DOI: 10.1021/acs.chemrev.7b00776
Chem. Rev. 2018, 118, 4981−5079

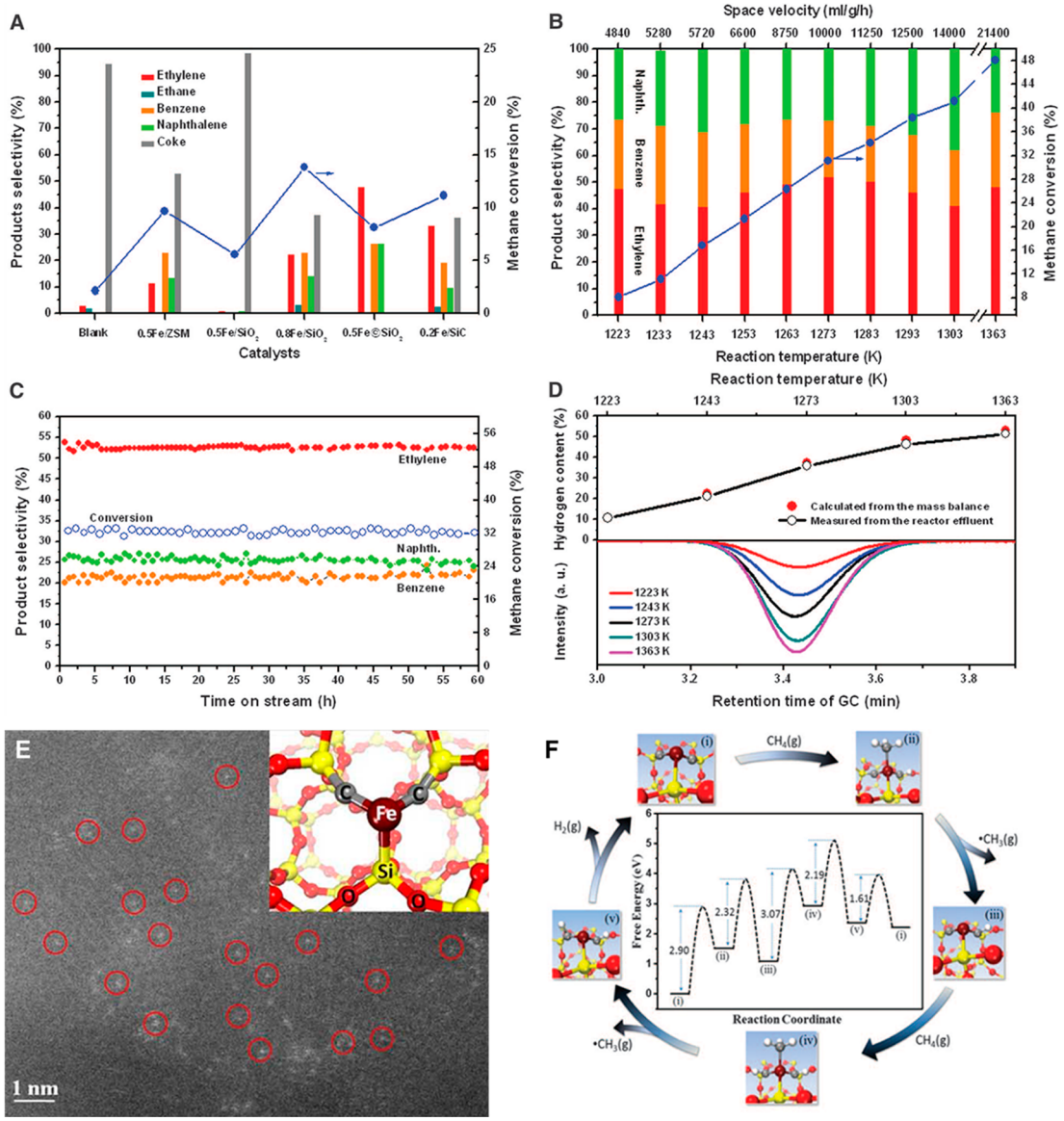

Figure 25. (A) Product distributions on various Fe-based catalysts. (B) Activity and distributions of the products on Fe@SiO_2 (with 0.5% of Fe) at different reaction conditions and space velocities. (C) Long-term stability test of Fe@SiO_2 (with 0.5% of Fe) at 1293 K. (D) Amount of H_2 produced at different temperature on Fe@SiO_2 (with 0.5% of Fe) catalyst. (E) High-resolution STEM image of Fe@SiO_2 (with 0.5% of Fe) catalyst after the reaction. (F) Schematic illustration of the catalytic mechanism of CH_4 activation on single-site Fe species confined in the SiO_2 matrix according to theoretical calculations. Adapted with permission from ref 144. Copyright 2014 The American Association for the Advancement of Science.

superior activity of Co-modified single-layer MoS_2 for hydrodeoxygenation reaction.[140] As shown in Figure 24, isolated Co atoms doped on the basal planes of the matrix of MoS_2 monolayers can be seen by high-resolution STEM. Further structural analysis according to high-resolution STEM images and DFT calculations reveals that the sulfur vacancy sites are generated from the Co−S−Mo interfacial sites after reduction by H_2 at 300 °C, which allow one to catalyze the hydrodeoxygenation of 4-methylphenol at low 180 °C instead of 300 °C with conventional catalysts to avoid the loss of sulfur during the hydrodeoxygenation process. As shown in Figure 24c, single-layer Co−MoS_2 catalysts showed about 34 times higher activity than nonpromoted single-layer MoS_2 and also significantly higher activity than other reference samples. Excellent stability and selectivity were also achieved on single-layer Co−MoS_2 catalysts when working at 180 °C. However, it should also be noted that, although singly dispersed Co atoms can be observed in the single-layer Co−MoS_2 sample, there are also some agglomerated Co−S−Mo species that can be observed in the STEM images. However, the catalytic properties of those agglomerated Co−S−Mo sites are not discussed in this work. Another point to be considered is the long-term stability of the catalysts under the HDS conditions due to the loss of sulfur and the resulting structural deformation.

Ni− and Co−MoS_2 catalysts are classic and widely used hydrodesulfurization catalysts.[141] On the basis of mechanistic and structural studies, it has been well established that the active sites for hydrodesulfurization reaction are Co−S−Mo sites (not single Co−S−Mo site, but continuous Co−S−Mo sites) on the edges of MoS_2 crystallites.[142] Although there are some differences between hydrodeoxygenation and hydrodesulfurization reactions, the generation of sulfur vacancies seems to be common in both systems.

DOI: 10.1021/acs.chemrev.7b00776
Chem. Rev. 2018, 118, 4981−5079

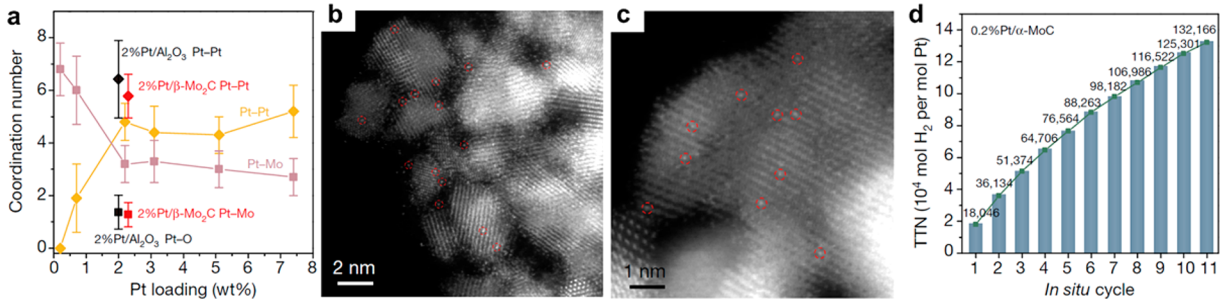

Figure 26. (a) Coordination number of Pt−Pt bonding and Pt−Mo bonding in different supported Pt catalysts. It is clearly shown that the Pt−Pt contribution in Pt/α-MoC catalysts will increase with the Pt loading. (b) High-resolution STEM image of Pt/α-MoC with 2.0 wt % of Pt. Singly dispersed Pt atoms can be observed as bright dots in this image. (c) High-resolution STEM image of Pt/α-MoC with 0.2 wt % of Pt. Singly dispersed Pt atoms can be observed as bright dots in this image. (d) Aqueous reforming of methanol for H_2 production on 0.2%Pt/α-MoC under practical conditions. Adapted with permission from ref 151. Copyright 2017 Macmillan Publishers Limited, part of Springer Nature.

Nonoxidative activation of CH_4 and selective transformation into olefins and aromatics are desired for utilization of natural gas resource. However, traditional Mo-based catalysts are limited by a fast catalyst deactivation under nonoxidative reaction conditions.[143] Bao and his co-workers have developed a supported Fe@SiO_2 catalyst, showing remarkable activity and selectivity for direct nonoxidative conversion of methane to ethylene, aromatics, and H_2.[144] In the Fe@SiO_2 catalyst after activation in CH_4/N_2 at 1173 K, atomically dispersed Fe species are confined in the matrix of SiO_2 through Fe−Si and Fe−C bonding, according to the in situ XAS analysis and high-resolution STEM (see Figure 25E). As shown in Figure 25, only Fe@SiO_2 catalyst containing atomically Fe sites can selectively transform CH_4 into desired products without the formation of coke, and give high selectivity to ethylene (~52.7% at 1293 K). Excellent stability has also been achieved at 1293 K with no obvious changes in conversion and selectivity. By in situ spectroscopic characterizations and theoretical calculations, the activation of CH_4 on single-site Fe catalyst is proposed as described in Figure 25F. CH_4 is activated on Fe atoms and gives $CH_3^{\bullet}$ radicals and H_2. Next, $CH_3^{\bullet}$ radicals in the gas phase will form ethylene and aromatics. In this work, the unique geometric and electronic structures of single-site Fe catalysts can efficiently break the C−H bonds in CH_4 without formation of coke. The concept of Fe@SiO_2 catalyst has further been applied for nonoxidative activation of CH_4 in hydrogen-permeable tubular membrane reactor.[145] By adding H_2 in the feed gas into the membrane reactor, 30% conversion of CH_4 and 99% selectivity to C2 products (acetylene and ethylene) can be achieved with good stability at 1303 K.

It has been reported that single-atom catalysts can also work in some reforming reactions. For instance, single Pt and Au atoms supported on ZnO (the loading of Au and Pt is kept as low as 0.0125 wt % to ensure the full dispersion of single atoms) showed much higher activity than pristine ZnO sample for methanol steam reforming to H_2 and CO_2. It was proposed that Pt/Au atoms play a synergistic role together with ZnO for the activation of methanol and water.[146] Moreover, atomically dispersed Pt species stabilized on MgSnAl-LDH (layered double hydroxides) were reported as active species for cyclization of *n*-heptane.[147] As compared to catalysts containing Pt nanoparticles, catalyst with Pt single atoms as the dominating species showed lower selectivity toward C1−C4 products and higher selectivity toward iso-C7 and cyclo-C7 products. It should be noticed that an industrial naphtha reforming catalyst is based on very highly dispersed Pt in alkaline L-zeolites.[148] This process converts *n*-C_6, *n*-C_7, and *n*-C_8 alkanes into the corresponding aromatic products.

Reforming of methanol with water for production of H_2 is an attractive alternative to provide H_2 for polymer electrolyte membrane fuel cells. It has been reported that homogeneous Ru-based catalyst can catalyze the reforming of methanol into H_2 and CO_2 in the presence of a strong base, at low temperature (95 °C).[149] From a practical point of view, it will be more desirable to develop heterogeneous catalysts for reforming of methanol with H_2O for H_2 production.[150] Recently, Lin et al. have developed a new series of supported Pt catalysts on α-MoC as efficient heterogeneous catalysts for methanol reforming with water.[151] Only Pt species supported on α-MoC showed excellent activity and very low CO selectivity for methanol reforming with water. When compared to Pt species supported on other solid carriers (such as β-Mo_2C, Al_2O_3, TiO_2), the activities were much lower. The size of Pt species supported on α-MoC could be tuned by modulation of the Pt loading, which were quantified by EXAFS (see Figure 26a). Notably, singly dispersed Pt atoms on α-MoC were observed by high-resolution STEM (see Figure 26b and c) in a series of Pt/α-MoC catalysts, even when the Pt loading was as high as 2 wt %. When the Pt loading decreased to 0.2 wt %, it was claimed that only Pt single atoms were observed and all of the Pt atoms were bonded with α-MoC through strong interaction, according to DFT calculations. Those single Pt atoms dispersed on α-MoC showed the highest TOF and superior stability for methanol reforming reaction. The critical role of Pt single atoms was emphasized in this work, while the catalytic properties of Pt clusters and Pt nanoparticles were not fully discussed. According to the EXAFS results, it was clearly shown that Pt clusters and nanoparticles were the dominating species when the Pt loading was higher than 0.2 wt % and those Pt catalysts were also active for this reaction, even though the TOF values based on single Pt atoms were lower.

4.6. Hydroformylation

Hydroformylation of olefins is an important industrial process for the production of aldehydes and alcohols. So far, the industrial hydroformylation reactions are performed under homogeneous conditions, using molecular Rh-based and Co-based complexes as catalysts.[152] In the last two decades, great efforts have been devoted to transform the conventional homogeneous into heterogeneous systems for convenient separation and recyclability of the catalysts.[153,154] Generally, the active sites for hydroformylation are thought to be mononuclear metal centers. Therefore, it could be possible to achieve immobilized single-atom catalyst for heterogeneous

DOI: 10.1021/acs.chemrev.7b00776
Chem. Rev. 2018, 118, 4981−5079

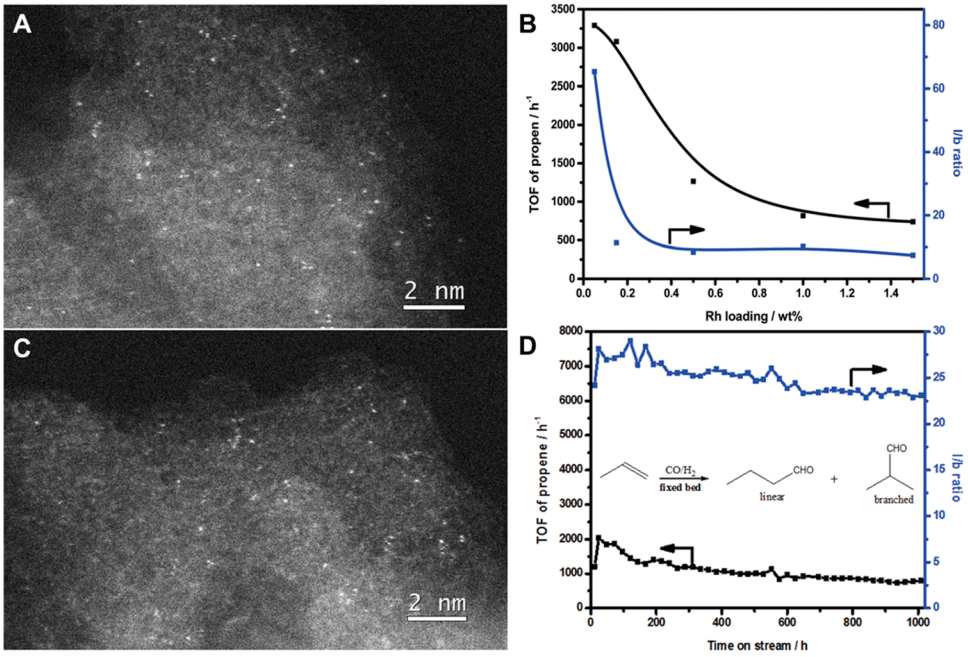

Figure 27. (A) High-resolution STEM image of the catalyst containing singly dispersed Rh atoms in porous organic copolymers. (B) TOF values for hydroformylation of propene catalyzed by various Rh-biphephos&PPh3@copolymers catalysts with different loading of Rh. The catalyst with the lowest Rh loading shows the highest TOF values and higher linear/branched ratio in the products. (C) High-resolution STEM image of the same catalyst after 1008 h of time-on-stream for propene hydroformylation, showing the presence of singly dispersed Rh atoms. (D) Long-term stability test of the Rh-biphephos&PPh3@copolymers containing singly dispersed Rh atoms for hydroformylation of propene. Adapted with permission from ref 156. Copyright 2016 The Royal Society of Chemistry.

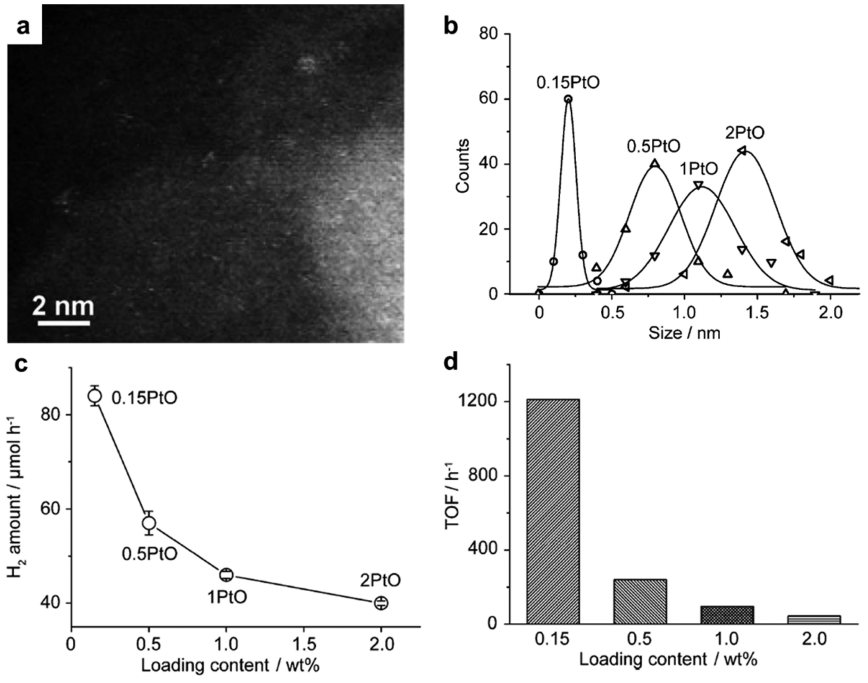

Figure 28. (a) High-resolution STEM image of PtO/TiO_2 catalyst, showing the presence of single Pt atoms as well as Pt clusters. (b) Size distributions of PtO species in various PtO/TiO_2 catalysts. (c) H_2 evolution rates on PtO/TiO_2 catalysts with different Pt loading. (d) H_2 evolution rates normalized to the amount of Pt species in various PtO/TiO_2 catalysts. Adapted with permission from ref 159. Copyright 2014 Wiley-VCH Verlag GmbH & Co. KGaA, Weinheim.

hydroformylation reactions if the metal centers can be stabilized by the solid support and their reactivity is not suppressed. Recently, singly dispersed Rh atoms have been successfully anchored on porous organic polymer from the copolymerization of vinyl functionalized phosphorus ligands, and these single-atom Rh catalysts showed excellent activity and reusability for hydroformylation of olefins.[155,156] As shown in Figure 27, singly dispersed Rh atoms in organic support containing vinyl biphephos ligands can be clearly observed by high-resolution STEM. These Rh atoms showed high TOFs in hydroformylation

DOI: 10.1021/acs.chemrev.7b00776
Chem. Rev. 2018, 118, 4981−5079

of propene and high selectivity to linear butaldehyde. Even after reaction for more than 1000 h, the fine dispersion of single Rh atoms was still preserved in the catalyst.

Other than organic polymers, inorganic solids can also serve as the supports for single Rh atoms for hydroformylation reactions. For instance, single Rh atoms supported ZnO nanowires showed comparable performances (in terms of turnover numbers) like state-of-art $RhCl(PPh_3)_3$ complex for hydroformylation of styrene.[157] In another work, single Rh atoms supported on CoO also showed excellent TOFs for hydroformylation of propene.[158] It was also found that the distributions of aldehyde products were related to the size of Rh species. Single Rh atoms gave the highest selectivity toward linear butaldehyde (~94%), while Rh nanoparticles gave much more isobutyraldehyde, which might come from the different adsorption geometry of propene molecules on different Rh sites. Considering the influences of metal−support interaction, comprehensive studies on the support effects on Rh single-atom catalysts will bring more information and mechanistic insights for developing more efficient and selective heterogeneous catalysts for hydroformylation reactions.

4.7. Photocatalytic Reactions

In recent works, Yang et al. have prepared isolated Pt atoms and Pt clusters with different sizes through a ligand-assisted method, and their activity for photocatalytic H_2 evolution from methanol has been reported.[159,160] In their samples, Pt mainly existed as PtO, as determined by XPS. The TOF of Pt species decreased when increasing the particle size (see Figure 28). Pt single atoms showed the highest activity among the as-prepared catalysts, with about 30 times higher activity than Pt NPs (ca. 2 nm). In that work, only the chemical states of Pt in the pristine photocatalysts have been characterized by XPS. However, considering the transfer of photogenerated electrons to PtO sites, PtO species would probably be reduced. If this occurs, it should also be considered.

In another case, Pt single atoms deposited on C_3N_4 can catalyze the photocatalytic H_2 generation from triethanolamine aqueous solution.[161] As shown in Figure 29, Pt/C_3N_4 catalysts containing Pt single atoms show almost the same H_2 evolution rate normalized to Pt loading, when the Pt loading varied from 0.075 to 0.16 wt %. When the size of Pt species increases into cluster or even nanoparticle regime, the normalized H_2 evolution rate drops with the particle size.

In a recent work, single-atom catalyst was reported as photocatalyst for CO_2 reduction using triethanolamine as electron donor under visible light irradiation.[162] Single-site Co species were incorporated to MOF-525 and stabilized by the porphyrin units. The introduction of Co showed a much higher production rate of CO and CH_4 than the pristine MOF, although the production of CO and CH_4 is still quite low (less than 3 μmol after 6 h).

4.8. Electrocatalytic Reactions

Electrocatalytic water splitting for production of H_2 is an alternative approach for the conversion of solar energy into chemical fuels.[163] In conventional systems, Pt nanoparticles supported on carbon is the state-of-art catalyst for H_2 evolution. To reduce the amount of precious metal, singly dispersed Pt atoms supported on N-doped carbon by atomic layer deposition have been developed as electrocatalyst for H_2 evolution reaction.[164] As compared to conventional Pt/C catalyst with Pt nanoparticles, the single-atom Pt catalyst showed ca. 37 times higher mass activity and higher stability in acid medium. It is

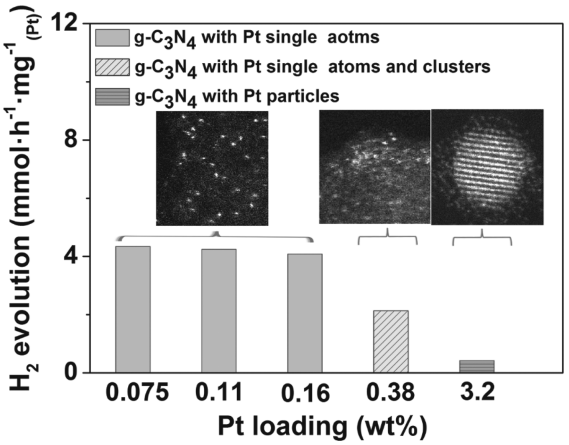

Figure 29. Photocatalytic hydrogen evolution rates from triethanolamine aqueous solution on various Pt/C_3N_4 catalysts with different loading of Pt. When the Pt loading is lower than 0.16 wt %, Pt mainly exist as singly dispersed atoms. When it increases to 0.38 wt %, Pt clusters will appear and Pt continues to grow into Pt nanoparticles in the Pt/C_3N_4 sample with 3.2 wt % of Pt. The H_2 evolution rates have been normalized to the mass of Pt cocatalyst in various catalysts. Adapted with permission from ref 161. Copyright 2016 Wiley-VCH Verlag GmbH & Co. KGaA, Weinheim.

proposed that the partially occupied 5d orbitals of Pt atoms supported on the nitrogen-doped graphene are responsible for the remarkable high activity. Besides, Pt single-atom species supported on covalent triazine framework (CTF) also showed excellent performance for electrocatalytic H_2 oxidation without the requirement of overpotential.[165] Interestingly, the authors have also found that the activity of Pt single atoms for oxygen reduction reaction (ORR) is quite low as compared to conventional Pt/C catalyst, which is favorable for protecting the cathode in fuel cells from corrosive degradation.

Catalysts based on non-noble single metal atoms have also been prepared for electrocatalytic H_2 evolution reaction. For instance, single Co atoms supported on N-doped graphene (named as Co-NG) showed promising activity and high stability in both acid and basic media for H_2 evolution, even in comparison with other non-noble metal catalysts (see Figure 30).[166] It has also been proved that atomically dispersed Co species in N-doped carbon are the active sites for hydrogen evolution reaction, while Co nanoparticles encapsulated in carbon layers are not active.[167] In another work, single Ni atoms supported on porous N-doped graphene also showed excellent activity and stability for hydrogenation evolution in acid medium.[168] According to theoretical studies, it was proposed that the coordination between Co and N atoms could stabilize those single Co atoms and also tune their electronic properties.

Polymer electrolyte membrane fuel cells (PEMFCs) are promising choice for green energy conversion process. So far, the oxygen reduction reaction (ORR) is still the bottleneck half reaction in PEMFCs, which is usually catalyzed by noble metal catalysts, such as Pt. To lower the cost and achieve sustainable energy conversion devices, the development of non-noble metal catalysts as substitutes for Pt-based catalysts has become a hot topic in the past 10 years.[169,170] Since the breakthrough achieved by Dodelet and his co-workers, Fe-based and Co-based catalysts with comparable electrocatalytic performance to Pt-based electrocatalysts have attracted great attention, and progress has been made on identification of the active sites and on the methodologies for catalysts synthesis.[171] Usually, Fe-based

DOI: 10.1021/acs.chemrev.7b00776
Chem. Rev. 2018, 118, 4981−5079

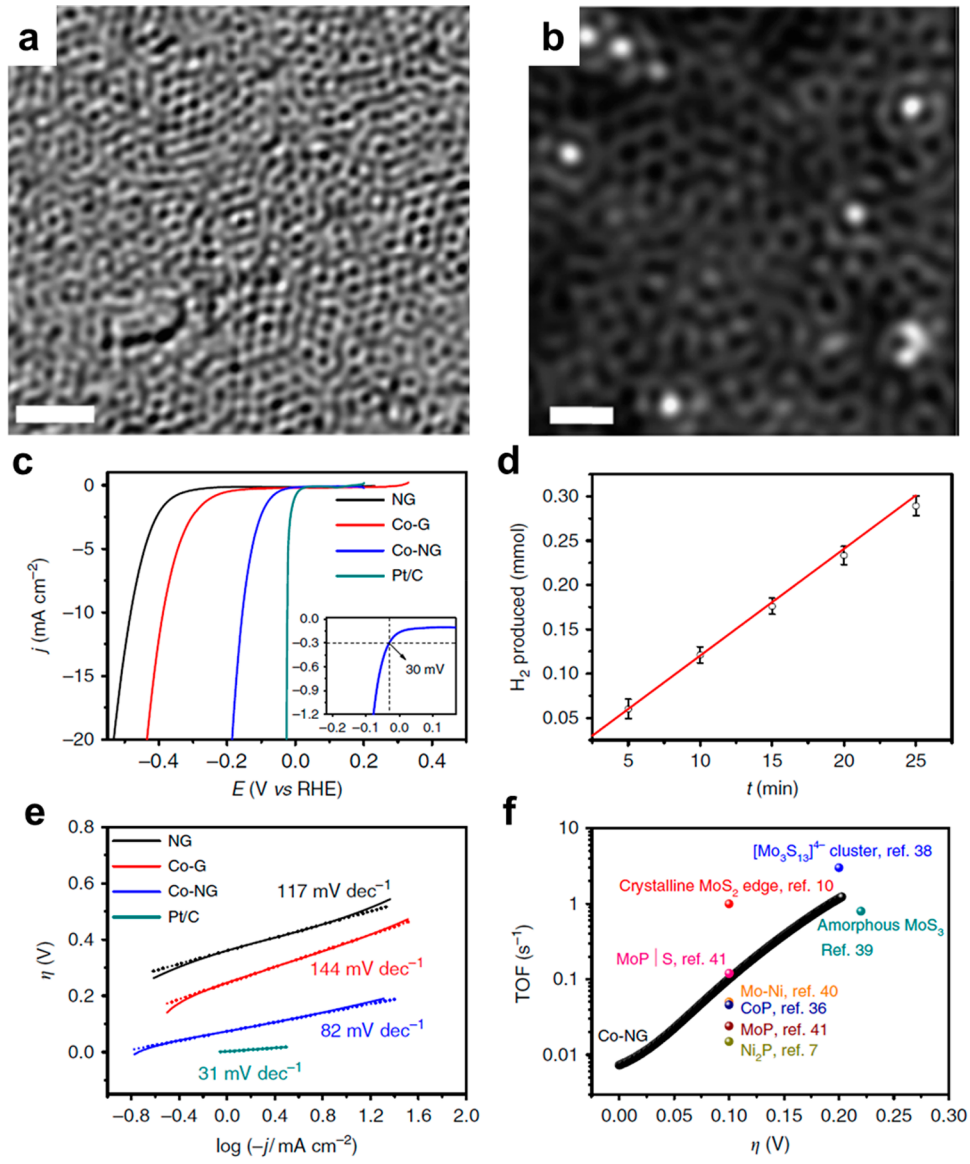

Figure 30. (a) TEM image and (b) high-resolution STEM image of single Co atoms dispersed on N-doped graphene (named as Co-NG). (c) Electrocatalytic hydrogenation evolution performances of different catalysts in 0.5 M H_2SO_4 at scan rate of 2 mV s^{-1}. (d) The amount of evolved H_2 gas measured by gas chromatograph (black plots) and the theoretical values by assuming 100% Faradaic efficiency (red line). (e) Tafel plots of the polarization curves. (f) Comparison between the Co-NG catalyst and reported non-noble metal catalysts for hydrogenation evolution reaction. Adapted with permission from ref 166. Copyright 2015 Macmillan Publishers Limited, part of Springer Nature.

catalysts for ORR were prepared by the pyrolysis from Fe-containing metal−organic complex. After the high-temperature pyrolysis, complicated solid catalyst containing different types of Fe species (including metallic Fe nanoparticles, FeO_x nanoparticles, FeC_x nanoparticles, and highly disersed FeN_x species) would be obtained. Acid-leaching treatments could remove most of the nanoparticles in the sample, while those nanoparticles encapsulated in carbon layers still remained, making it extremely difficult to identify the active sites in Fe-based catalysts for ORR. It has been demonstrated that the presence of N in the carbon support plays a key role for the generation of highly active Fe-based ORR catalysts, which are often called Fe−N−C catalysts.[172] However, there are still several possible structures on the Fe−N_x centers according to different coordination configurations. In a recent work, Zitolo et al. have employed multiple techniques to clarify the atomic structure of the active sites in Fe−N−C catalyst.[173] With the help of ^{57}Fe Mössbauer spectroscopy, EXAFS, and XANES, it is proposed that porphyrin-like FeN_4C_{12} moieties located in strongly disordered graphene sheets or between zigzag graphene edges are the active sites for ORR, while nanoparticulate Fe or FeC_x species are inert for ORR. However, there are still some arguments on the elucidation of the active sites in Fe−N−C catalyst. Jiang et al. have compared the ORR activity of three Fe−N−C catalysts containing different types of Fe species. As shown in Figure 31, the copresence of atomically dispersed Fe−N_x species and encapsulated Fe/FeC_x nanoparticles showed higher ORR activity than the catalyst with only Fe−N_x species.[174] It is then proposed that synergistic interactions may exist between atomically dispersed Fe−N_x species and nanoparticulate Fe/FeC_x species. It is clear that further work is required to clarify those synergistic interactions and to explain the results obtained on different catalysts.

DOI: 10.1021/acs.chemrev.7b00776
Chem. Rev. 2018, 118, 4981−5079

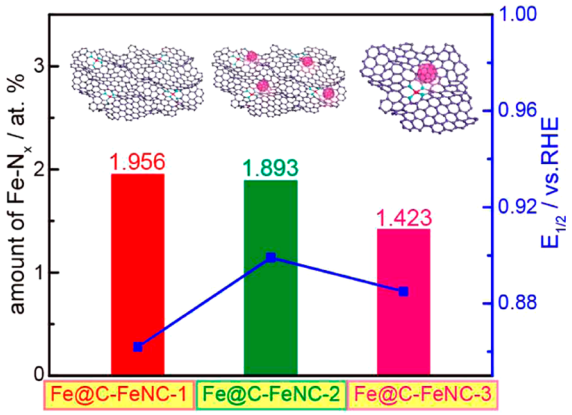

Figure 31. Correlation between the amount of Fe−N_x species and ORR activity in terms of $E_{1/2}$ values in three Fe−N−C catalysts with different compositions of atomically dispersed Fe−N_x and nanoparticulate Fe/FeC_x species. Adapted with permission from ref 174. Copyright 2016 American Chemical Society.

In an analogous way as it occurs with Fe, Co−N−C catalysts containing atomically dispersed Co−N_x species have also been prepared, and promising results as potential candidates to substitute Pt-based catalysts just start to be presented. For instance, by tuning the chemical compositions (the ratio of Co and Zn) in Co/Zn-MOF precursor, singly dispersed Co atoms in N-doped carbon can be prepared.[175] According to the characterization results from EXAFS, the coordination environment of single Co atoms in N-doped carbon support can also be tuned by the preparation parameters, which is further reflected on the activity for electrocatalytic oxygen reduction.

The influence of atomicity on the selectivity for electrocatalytic CO_2 reduction has also been reported on non-noble Fe−N−C catalysts.[176] In the case of Fe−N−C catalyst containing mainly isolated Fe sites, CO_2 can be reduced to CO with over 90% Faradaic yield at low overpotential, while Fe−N−C catalysts containing metallic Fe nanoparticles covered by carbon layers mainly catalyze the reduction of H_2O to H_2 instead of CO_2 reduction. This work indicates that, by tuning the contributions of active sites in the Fe−N−C catalyst, it might be possible to generate a mixture of CO and H_2 with the desired ratio. If this is achieved, it should be a key advancement for the new economy based on renewable energy.

4.9. Single-Atom Catalysts for Other Reactions

Heterogeneous catalysts containing single-site metal species have also been reported as efficient catalysts for reactions other than those described above, and some examples will be discussed here. For instance, Pd complex with N-containing or P-containing ligands are efficient catalysts for a variety of cross-coupling reactions. Inspired by the catalytic mechanism in homogeneous systems for hydrocarbonylation of terminal alkynes (see Figure 32A and B), Ding and co-workers have synthesized a porous organic copolymer material containing acid sites (−SO_3H groups) and phosphine ligands for the stabilization of singly

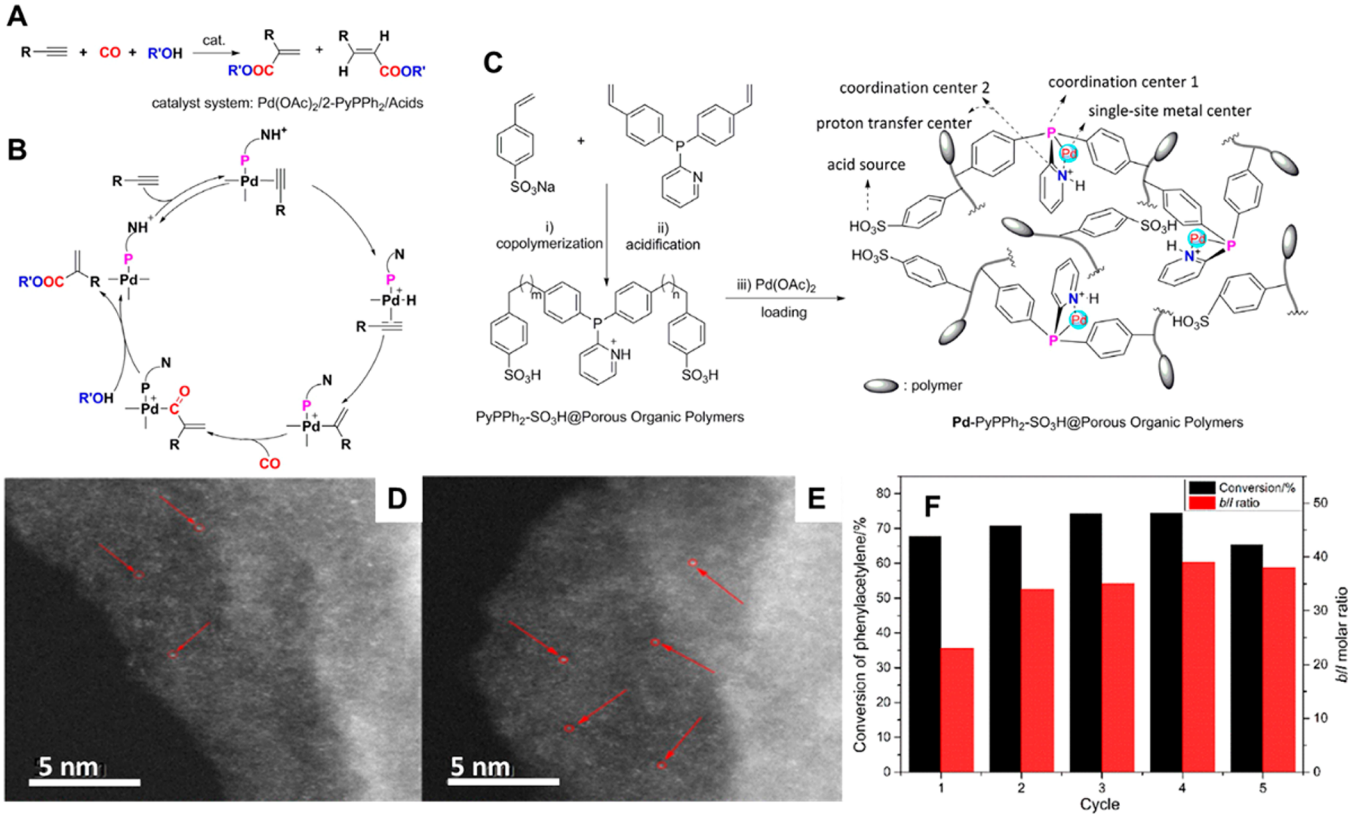

Figure 32. (A) Hydrocarbonylation of terminal alkynes catalyzed by Pd catalyst. (B) Mechanism of the alkoxycarbonylation of alkynes in the presence of the Pd$(OAc)_2$/2-$PyPPh_2$/acidic promoters. (C) Synthesis of porous organic copolymers containing acid sites and phosphine ligands. (D) High-resolution STEM images of the as-prepared Pd-$PyPPh_2$-SO_3H@POPs catalyst, showing the presence of isolated Pd atoms. (E) High-resolution STEM image of the used Pd-$PyPPh_2$-SO_3H@POPs catalyst, showing the preservation of isolated Pd atoms. (F) Stability tests of Pd-$PyPPh_2$-SO_3H@POPs catalyst in the methoxycarbonylation of phenylacetylene for five cycles. Adapted with permission from ref 177. Copyright 2016 Wiley-VCH Verlag GmbH & Co. KGaA, Weinheim.

DOI: 10.1021/acs.chemrev.7b00776
Chem. Rev. 2018, 118, 4981−5079

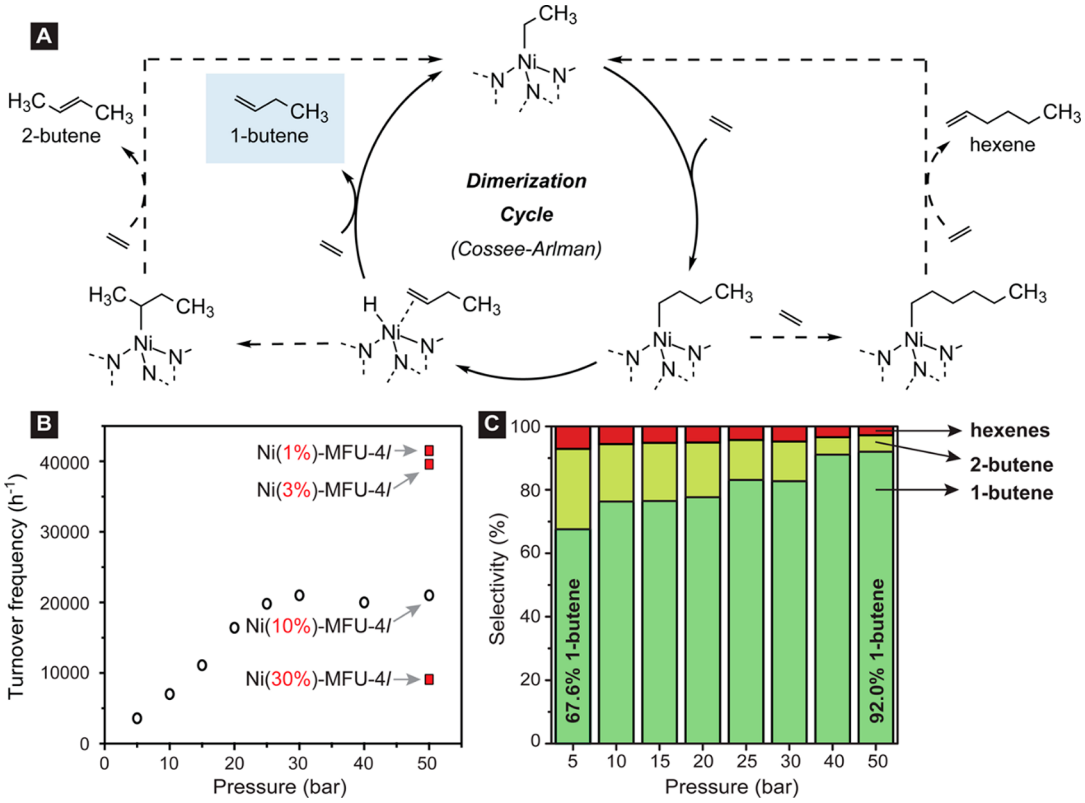

Figure 33. (A) Proposed catalytic cycle via Cossee−Arlman pathway for ethylene dimerization in Ni-MFU-4*l*. (B) The influences of reaction pressure and Ni contents in Ni-MFU-4*l* on the activity for ethylene dimerization reaction. (C) Selectivity to 1-butene, 2-butene, and hexenes at various ethylene pressures for Ni(10%)-MFU-4*l* at 25 °C with 100 equiv of methylaluminoxane. Adapted with permission from ref 179. Copyright 2016 American Chemical Society.

dispersed Pd atoms (see Figure 32C).[177] According to high-resolution STEM images, this hybrid material (named as Pd-PyPPh$_2$-SO$_3$H@POPs) contained singly dispersed Pd atoms and showed excellent catalytic performance for the methoxycarbonylation of phenylacetylene and acetylene. Furthermore, those singly dispersed Pd atoms were still preserved after the reaction, and a hot filtration experiment also confirmed that the reaction was catalyzed by a heterogeneous catalyst. In another work, single-site Pd species were immobilized in 2,2′-bipyridine-functionalized periodic mesoporous organosilica for oxidative Heck reaction.[178] According to characterization by XAS (XANES and EXAFS), the singly dispersed nature of Pd species was confirmed, and it was claimed that those singly dispersed Pd species were an active and stable catalyst for the oxidative Heck reaction.

The ethylene dimerization reaction produces almost one-half of the world's 1-butene, which is used as the raw material for linear low-density polyethylene. So far, this process is catalyzed by homogeneous Ni or Ti catalysts in liquid phase. Although there are some reports on the applications of Ni-based heterogeneous catalysts for ethylene dimerization, the selectivity is not satisfactory. Recently, Dincă et al. have reported the application of Ni-substituted Zn-MOF (Ni-MFU-4*l*) as a highly selective (~96% selectivity to 1-butene) catalyst for dimerization of ethylene in batch reactor.[179] As shown in Figure 33, single-site Ni species can be generated by substituting Zn in the secondary-building unit of Zn-MOF, and they can catalyze the ethylene dimerization reaction via a Cossee−Arlman mechanism with high activity and selectivity.[180] Nevertheless, single-site Ni species can also be generated in covalent-organic framework (COF) through the bonding between Ni cations and N-containing ligands in the COF.[181,182] The Ni-COF catalysts showed activity comparable to those classic homogeneous counterparts and a much higher selectivity to C6+ olefins (>40%).

In 1998, Periana et al. reported the application of Pt complex for oxidation of methane to methanol in concentrated H_2SO_4.[183] Mechanistic studies show that mononuclear Pt(II) species are the active sites for activation of C−H in CH_4. Following the work in homogeneous systems, Schuth et al. prepared a covalent triazine-based framework (CTF) as the solid host for mononuclear Pt complex.[184] As shown in Figure 34, the coordination environment of Pt species in the heterogeneous Pt/CTF catalyst is similar to that of the homogeneous Periana catalyst, which was also confirmed by EXAFS and high-resolution STEM images (see Figure 34).[185] The catalytic performance of Pt/CTF catalyst showed slightly higher activity than the homogeneous analogue (Periana catalyst) under the same conditions and excellent recyclability, indicating that by mimicking the structure of the homogeneous catalyst, it is possible to generate similar active sites in heterogeneous catalysts.

Vinyl chloride monomer is a major chemical as raw material for production of polyvinyl chloride. In the traditional industrial process, mercuric chloride supported on carbon is used as the catalyst for acetylene hydrochlorination, which causes environmental concerns due to the high toxicity of mercury. In 1980s, Hutchings et al. reported the application of supported Au complex as catalyst for acetylene hydrochlorination.[186] After research and development for more than two decades, the first

DOI: 10.1021/acs.chemrev.7b00776
Chem. Rev. 2018, 118, 4981−5079

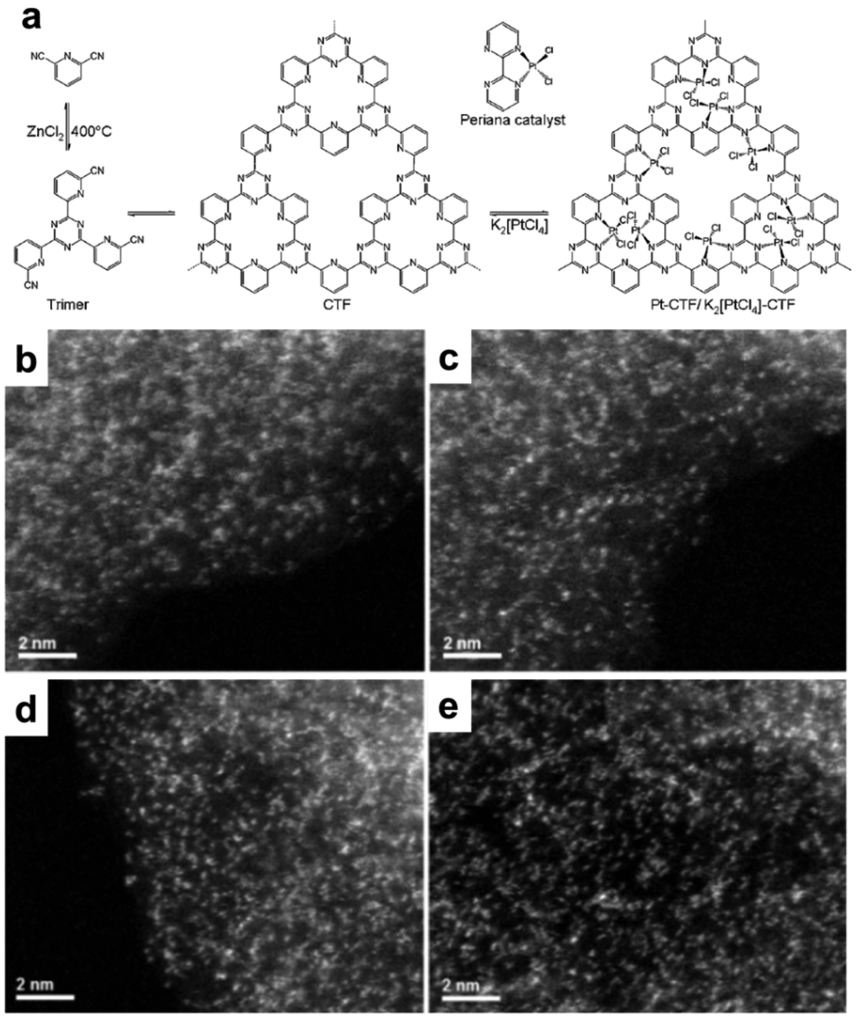

Figure 34. (a) Preparation of covalent triazine-based framework (CTF) as the solid support for mononuclear Pt complex, with coordination environment similar to that of its homogeneous analogue. Adapted with permission from ref 184. Copyright 2009 Wiley-VCH Verlag GmbH & Co. KGaA, Weinheim. (b,c) High-resolution STEM images of the as-prepared Pt/CTF catalyst before the reaction. (d,e) High-resolution STEM images of the as-prepared Pt/CTF catalyst after oxidation of methane in concentrated H_2SO_4. The bright dots in the above STEM images correspond to highly dispersed single Pt atoms. Adapted with permission from ref 185. Copyright 2016 American Chemical Society.

application of Au-based catalyst for large-scale industrial process has been completed in China for acetylene hydrochlorination reaction in 2015.[187] In previous works, it was speculated that single-site Au species are the active sites for acetylene hydrochlorination. However, there is little information on their atomic structures and chemical states. The application of high-resolution electron microcopy and XAS techniques (EXAFS and XANES) has allowed one to determine the active sites in Au-catalyzed acetylene hydrochlorination reaction.[188] According to that work, singly dispersed Au species are the active sites, and the redox cycles between Au(I) and Au(III) are observed under in situ conditions by XANES.

4.10. Single-Atom Sites in Bimetallic Particles

In the above examples, singly dispersed metal atoms were supported on solid supports (such as zeolites, metal oxides, polymers, etc.), and it has been usually proposed that those metal centers act as the active sites without synergistic effects from neighboring metal atoms. Actually, single-atom sites can also be generated in bimetallic particles. In that case, the electronic structures of single-atom sites can be affected by the neighboring metal atoms, which could lead to different catalytic behaviors as compared to single-atom sites on nonmetallic support.

Because of the weak interaction between H and Cu surface and the suitable adsorption geometry of substrate molecules on Cu surface, Cu catalysts are selective catalysts for many hydrogenation reactions. However, due to the low intrinsic activity for H_2 activation, which is often a limiting step, Cu catalysts are not widely used for selective hydrogenation reactions. In 2012, Kyriakou et al. reported the application of an alloy structure containing single-atom sites for selective hydrogenation reactions. As show in Figure 35, isolated Pd atoms deposited on Cu(111) surface can dissociate H_2, and those activated H species can spill over to the Cu(111) surface.[189] By this strategy, the bottleneck for Cu-based hydrogenation catalysts can be overcome, and due to the very low amount of Pd, the selectivity of Cu catalysts is not affected.[190] Therefore, Cu(111) surface modified with isolated Pd atoms showed excellent selectivity for selective hydrogenation of alkynes. Actually, this concept has already been demonstrated in 2009 on supported Au catalysts, in which ppm level of Pt was added to Au/TiO_2 catalyst to improve the activity without affecting the high selectivity of Au

DOI: 10.1021/acs.chemrev.7b00776
Chem. Rev. 2018, 118, 4981−5079

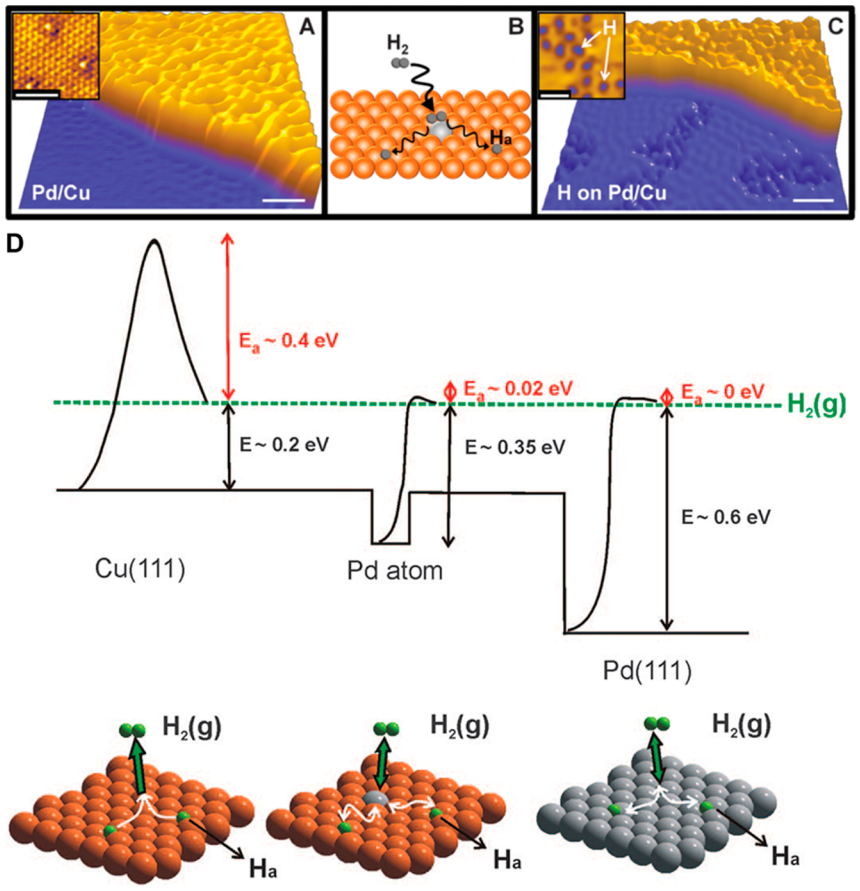

Figure 35. (A) STM image of single Pd atoms deposited on Cu(111) surface. (B) Schematic illustration of the activation of H_2 molecules on isolated Pd atoms and the subsequent H-spill-over on Cu(111) surface. (C) STM image of the dissociated H on Pd/Cu(111) surface. (D) Activation energy of H_2 on different types of surface. Adapted with permission from ref 189. Copyright 2012 The American Association for the Advancement of Science.

catalysts.[191] Besides, this concept has also been proved by practical catalysts containing PdCu alloy nanoparticles with a very low amount of Pd.[192] Lately, the concept of single-atom alloy structures has been extended to other combinations of metals and show promising performances for selective hydrogenation reactions. For instance, Pt−Cu alloys containing Pt single atoms show excellent activity and selectivity for hydrogenation of 1,3-butadiene to butenes.[193] Ag alloyed Pd single-atom catalysts are efficient catalysts for selective hydrogenation of acetylene to ethene in excess ethene.[194]

Single-atom alloy structures also show special properties in other heterogeneous reactions.[185] By galvanic replacement, Au single atoms can be generated on Pd nanoparticles by substituting the Pd atoms at the corners. Because of the electronic interaction between Au atoms and the surrounding Pd atoms, Au single atoms become electron-rich sites according to theoretical calculations. As shown in Figure 36, Au−Pd bimetallic structures with different Au loading and spatial distributions show distinct performances in oxidation of glucose. Considering that the activation of O_2 on metal surface is greatly related to the electronic properties of metal sites, the superior catalytic performances of Au−Pd single-atom alloyed nanoparticles can be ascribed to their unique electronic structures. Recently, it has been reported that Au−Pd bimetallic nanoparticles containing isolated Pd atoms show remarkable activity for selective hydrosilylation and Ullmann coupling of aryl chlorides in H_2O.[196,197] Nevertheless, doping with a single Pd atom aids the activity of Au_{25} clusters for selective oxidation of alcohol.[198]

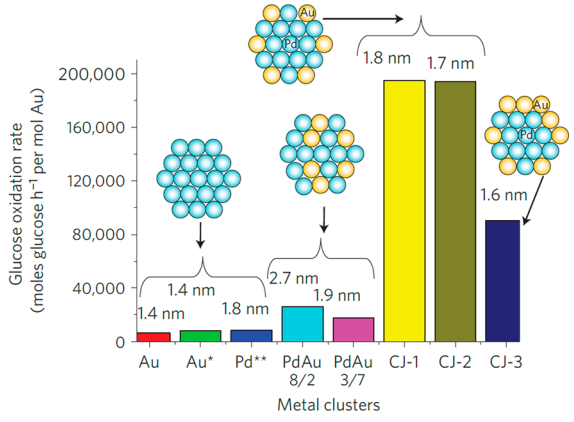

Figure 36. Comparison of the catalytic performances of various Au−Pd bimetallic nanostructures with different amounts and distributions of Au. The activity results have already been normalized to TOFs based on the amounts of Au atoms in the catalysts. Adapted with permission from ref 195. Copyright 2011 Macmillan Publishers Limited, part of Springer Nature.

In the above examples, isolated metal atoms are separated and stabilized on a surface or on a nanoparticle of the other metal. Recently, Tao et al. have proposed another type of single-atom alloy structure that contains one isolated atom and several other atoms surrounding it, as described in Figure 37.[199] By choosing the suitable support and carefully controlling the pretreatments on the heterogeneous catalyst, it may be possible to generate

DOI: 10.1021/acs.chemrev.7b00776
Chem. Rev. 2018, 118, 4981−5079

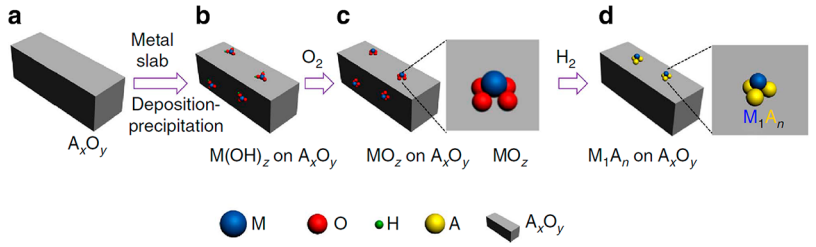

Figure 37. Generation of singly dispersed bimetallic clusters containing isolated atoms on metal oxides. Adapted with permission from ref 199. Copyright 2015 Macmillan Publishers Limited, part of Springer Nature.

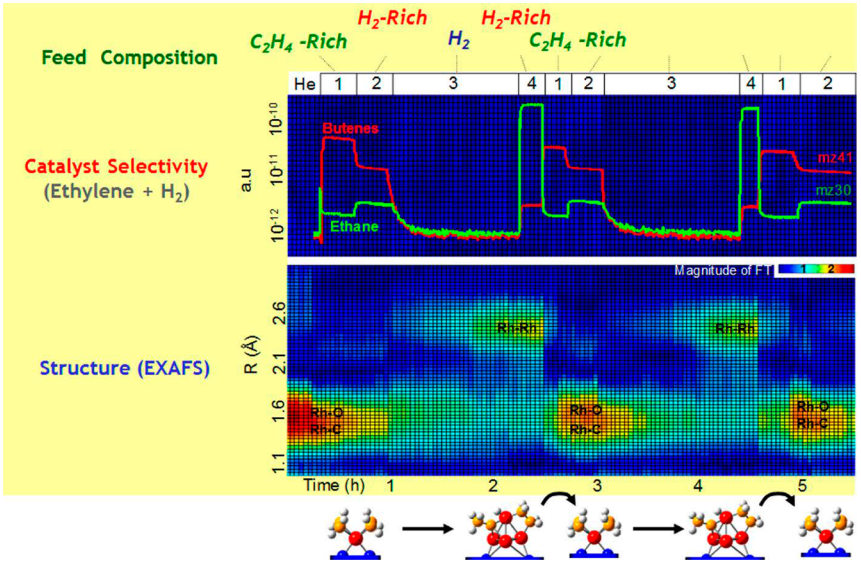

Figure 38. Evolution in selectivity of mononuclear $Rh(C_2H_4)_2$ complexes supported on HY zeolite with time on stream during the consecutively changed feed gases (ethylene and H_2). The coordination environment of Rh species is followed by EXAFS spectroscopy. In the bottom panel, the horizontal axis and vertical axis represent time on stream and the Rh-backscatter distance, and the intensity of various contributions is represented by colors (change from red to yellow to green to blue shows a decrease in intensity of the contribution). Adapted with permission from ref 203. Copyright 2011 American Chemical Society.

such bimetallic sites. With the help of various in situ techniques, it is proposed that bimetallic clusters containing a single Rh atom surrounded by several Co atoms from the CoO_x support are formed after reduction treatment, and these singly dispersed bimetallic clusters are very active for NO+CO reaction. A similar mechanism has also been proposed for Pt/CoO_x catalyst for NO $+H_2$ reaction.[200]

The unique role of isolated atoms in bimetallic particles has also been demonstrated in electrocatalytic reactions. For example, Pd atoms in AuPd alloy nanoparticles can serve as hot-spot sites for electrocatalytic reduction of O_2 to H_2O_2 with high selectivity.[201] AuPd alloy nanoparticles with low Pd contents ($\leq$10% in atomic ratio) showed much higher selectivity to H_2O_2 than those alloy nanoparticles with higher Pd contents. Combining electrocatalytic studies and theoretical calculations, it was proposed that the individual Pd atoms separated by Au atoms were the active and selective sites for O_2 reduction to H_2O_2. In contrast, O_2 would be directly reduced to H_2O on segregated Pd domains.

4.11. Evolution of Single-Atom Catalysts under Reaction Conditions

One critical issue related to single-atom catalysts is their stability under reaction conditions. Considering the intrinsic instability of single-atom species, they have a strong tendency to agglomerate into clusters or nanoparticles, especially in reductive atmosphere, in the situation without strong protection from sintering.[202] Gates et al. have investigated the evolution of mononuclear Ir complexes supported on zeolites in H_2 atmosphere at room temperature. In the case of supported $Ir(C_2H_4)_2/HY$, the bonding between Ir and zeolite would be broken after the formation of iridium hydride species, leading to the formation of Ir clusters. Furthermore, they have also studied how mononuclear metal species transform into metal clusters during the hydrogenation reaction.[203] In situ EXAFS allows one to correlate the catalyst selectivity with the structural information on supported Rh species, as shown in Figure 38. In C_2H_4-rich environment, butene was the major product, and Rh mainly exists in the mononuclear form. When these mononuclear Rh's were treated with H_2, Rh_4 clusters appear and ethane turned to be the major product in H_2-rich environment. Interestingly, the dynamic transformation between mononuclear Rh and Rh_4 clusters can be modulated by the reaction atmosphere.

When the reaction is performed in the liquid phase, the evolution of single-atom catalysts will be more complicated than under gas-phase reaction conditions. In a typical example, Finke et al. have studied the stability of zeolite-supported mononuclear Ir complex under the reaction conditions for liquid-phase hydrogenation of cyclohexene at 22 °C.[204] According to the experimental results from kinetic, spectroscopic, and electron microscopy characterizations, it was proven that those mononuclear Ir complexes are stable at 22 °C, and the

DOI: 10.1021/acs.chemrev.7b00776
Chem. Rev. 2018, 118, 4981−5079

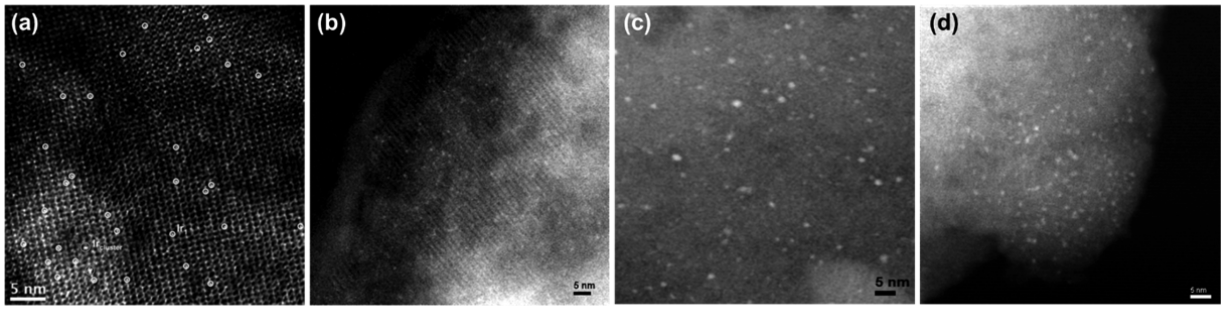

Figure 39. (a) High-resolution STEM images of the pristine Ir_1/Y catalyst, showing the presence of single Ir atoms with fine dispersion. (b) High-resolution STEM images of the Ir/Y catalyst after the first run of hydrogenation of cyclohexene, showing the presence of Ir clusters around 0.4 nm with 4−6 Ir atoms. (c) High-resolution STEM images of the Ir/Y catalyst after the second run of hydrogenation of cyclohexene, showing the presence of Ir clusters around 1 nm with ca. 40 Ir atoms. (d) High-resolution STEM images of the Ir/Y catalyst after the third run of hydrogenation of cyclohexene, showing the presence of Ir clusters around 1.3 nm with ca. 70 Ir atoms. Adapted with permission from ref 205. Copyright 2015 American Chemical Society.

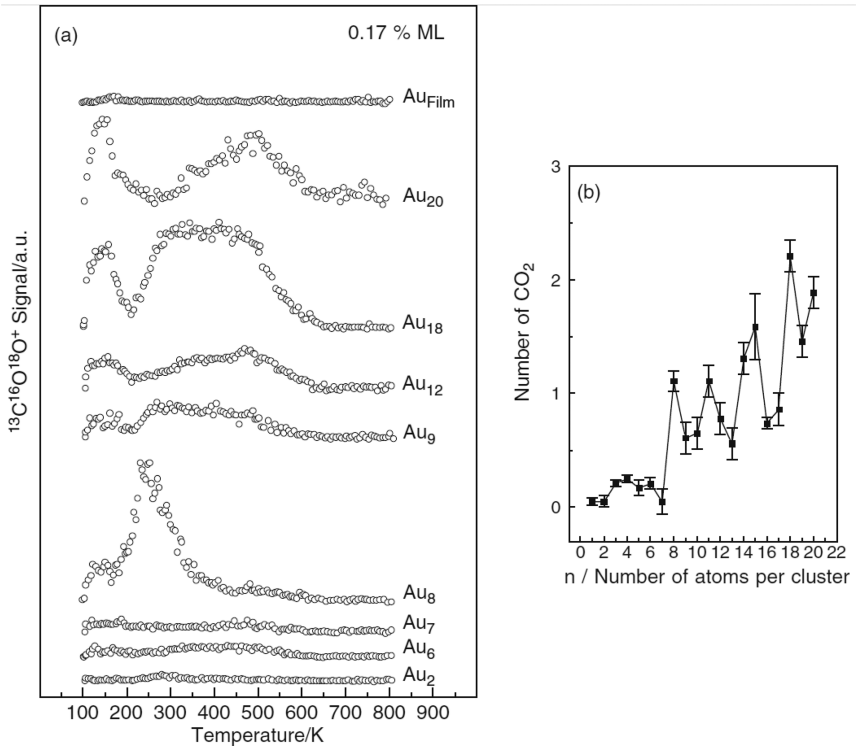

Figure 40. (a) Temperature-programmed reaction profiles for the CO oxidation on size-selected Au_n (n = 2−20) clusters on defect-rich MgO(100) surface. The model catalysts were saturated at 90 K with ^{13}CO and $^{18}O_2$, and the reaction product ($^{13}C^{18}O^{16}O$) was detected with a mass spectrometer, as a function of temperature. (b) The number of formed CO_2 molecules on each Au cluster with different atomicity. Adapted with permission from ref 214. Copyright 1999 American Chemical Society.

agglomeration of Ir single atoms into clusters or nanoparticles was not observed. However, when the reaction temperature increases for liquid-phase hydrogenation of cyclohexene, the situation changes.[205] The size of Ir species has been followed by both high-resolution STEM and EXAFS. As shown in Figure 39, three stages of evolution of mononuclear Ir species into Ir clusters (4−6 atom) and then to Ir nanoparticles (around 1 nm) were clearly observed during the three cycles of hydrogenation of cyclohexene. During the sequential sintering of Ir species, the activity for hydrogenation of cyclohexene was also decreasing.

In most of the above-mentioned works on catalytic applications of single-atom catalysts, the evolution of single-atom metal species has not been intensively studied. In many cases, only the fresh catalyst has been well characterized. It has been demonstrated in nanoparticulate metal catalysts that dynamic structural transformation is quite common in heterogeneous catalytic reactions. Taking that point into consideration, it is required to study the stability of single-atom catalysts under reaction conditions by different types of characterization techniques.

4.12. Perspectives on Single-Atom Catalysts

In the past few years, various single-atom catalysts have been prepared by different methods. For instance, singly dispersed Co in N-doped carbon can be generated using Co-complex or Co-containing metal−organic framework as precursor. Moreover, the morphologies of the resultant singly dispersed Co−N−C catalysts also show different morphologies. In those published works, Co−N−C catalysts from different methods have been

DOI: 10.1021/acs.chemrev.7b00776
Chem. Rev. 2018, 118, 4981−5079

tested for the same reaction (electrocatalytic oxygen reduction reaction). Spectroscopic and electron microscopic characterizations suggest that those Co−N−C catalysts show similar structures. However, although the reaction conditions may be different in different works, it is clear that the catalytic performances of different Co−N−C catalysts are different.[206−209] The differences between those Co−N−C catalysts are still unknown. A similar phenomenon has also been observed with Fe−N−C catalysts.[210−213]

It has been proposed that single-atom catalysts are thought to be analogous to homogeneous coordination compounds. It has been well established that the electronic structure of the metal center in coordination complex is strongly dependent on the ligand, which has significant influence on the catalytic properties. Therefore, it can be speculated that the coordination environment of single atoms in heterogeneous catalysts can also influence their catalytic behavior. Therefore, the differences observed in recent published works on different Co−N−C catalysts may originate from their different coordination structure of the singly dispersed Co sites, which cannot be fully reflected by the current characterization results.

There is no doubt that totally dispersed metals, and more specifically noble metals, is a way to minimize metal use, especially when they present high activity. These single metal atoms on organic and inorganic supports are very sensitive to electronic and geometric interactions with the atoms of the support. In some way, they can bridge homogeneous and heterogeneous catalysis, offering new perspectives for controlling activity and selectivity as well as for catalyzing less usual reactions.

Therefore, to have better understanding on the catalytic behavior of single-atom catalysts, it is necessary to correlate the catalytic behavior with the local coordination environment of the metal sites. Furthermore, it is also necessary to follow the evolution of the structures of single-site metal centers under reactions conditions. The geometric configuration of the metal site and its coordination environment may change during the catalytic cycles, in a way analogous to the catalytic cycle in homogeneous catalysis.

5. CATALYTIC APPLICATIONS OF METAL NANOCLUSTERS

5.1. CO Oxidation

CO oxidation is an excellent reaction test to discuss similarities and differences between single-atom and subnanometric clusters of different metals. Because much work on the reaction mechanism has been already carried out, it is of interest to use CO oxidation as a probe reaction to investigate how the size of metal species and the potential role of the support affect the activity. It should be considered that the electronic characteristics of metal species should be key to explain their catalytic behavior. We will now review the recent works on metal clusters for CO oxidation and will comment on the differences observed with single-atom metal catalysts.

5.1.1. CO Oxidation on Au Clusters. In 1999, Heiz et al. performed the first model study on size-selected metal nanoclusters for $^{13}CO+^{18}O_2$ reaction.[214] As shown in Figure 40a, ^{13}CO and $^{18}O_2$ were pumped into the reaction chamber at low temperature, and the reaction was monitored with a mass spectrometer. Notably, low activity for CO oxidation was observed for Au_n clusters with less than 10 atoms except Au_8. Moreover, two peaks in the temperature-programmed reaction (TPR) profiles of Au_8 and larger Au clusters were observed, suggesting that there may be two reaction pathways for CO oxidation at different temperature ranges. Later, Anderson et al. studied the activity of supported size-selected Au_n species (n = 1, 2, 3, and 4) for CO oxidation. They observed that Au_1 and Au_2 were inert for this reaction, and Au_3 is more active than Au_4. The authors claimed that the lack of activity of Au_1 and Au_2 may be related to the strong binding between Au and CO.[215] When the atomicity increased to 10−20, the CO oxidation activity of Au nanoclusters also increased, although in an odd−even oscillation way. As shown in Figure 40b, the reactivity of Au nanoclusters may change significantly by just changing one atomicity. Such a variation pattern is similar to the size-dependent electronic structures of Au nanoclusters as discussed before in this Review.[216] Notably, Au_8 clusters were found to be much more active than Au clusters with less than 8 atoms, implying that low-temperature CO oxidation may require multiple metal sites for the activation of CO and O_2.[217]

Furthermore, the role of the support on the catalytic behavior of Au clusters has been studied. It has been reported that Au_8 clusters deposited on a MgO(100) film, rich in oxygen defects, exhibited higher activity than those supported on defect-poor MgO(100) film. The reason for the enhanced activity of Au_8 clusters supported on defective MgO(100) could be related to the charge-transfer from MgO to Au clusters.[218] However, it should also be considered that the electronic interaction between MgO and Au clusters could also affect the geometric structure of the Au clusters.[219] Indeed, if Au_{20} clusters were deposited on a MgO(100) film, the optimized geometric structure of Au_{20} cluster corresponded to a three-dimensional tetrahedron. However, when the support was two-layer MgO film on Mo(100), Au preferred to be in the form of a two-dimensional Au island.

In the above-mentioned works, Au nanoclusters were generated by size-selected method and then deposited on support and used as model system. Actually, the catalytic behavior of Au nanoclusters prepared by conventional wet-chemistry methods, which is closer to practical heterogeneous catalysts, has also been investigated for CO oxidation. Gold catalysts supported on metal oxides (such as TiO_2, FeO_x, Al_2O_3, etc.) have been prepared by impregnation or coprecipitation methods. The resultant catalysts usually contain various types of Au species (including singly dispersed Au atoms, subnanometric Au clusters, and Au nanoparticles), and it becomes very difficult to measure those subnanometric Au species by conventional TEM due to the resolution limitation.[220] With the help of aberration-corrected STEM, it is possible to quantify the contribution of different types of Au species for CO oxidation. In 2008, Kiley and Hutchings reported the identification of active sites in Au/FeO_x catalysts for CO oxidation.[221] By comparing the size of Au species present in two Au/FeO_x samples (one active and the other catalytically inactive), the authors concluded that subnanometric Au clusters (around 0.5 nm) play a dominant role for the high activity in CO oxidation. Meanwhile, singly dispersed Au atoms and large Au nanoparticles (>5 nm) hardly contributed to the activity. In a recent work, these authors have performed a more systematic study on the contribution of different types of Au species in Au/FeO_x catalyst.[222] By quantitatively analyzing the population of different types of Au species, they have concluded that both subnanometric Au clusters (~0.5 nm) and small Au nanoparticles (1−3 nm) are the active species with similar turnover frequencies for CO oxidation, showing much higher TOF values than Au single atoms supported on FeO_x.

DOI: 10.1021/acs.chemrev.7b00776
Chem. Rev. 2018, 118, 4981−5079

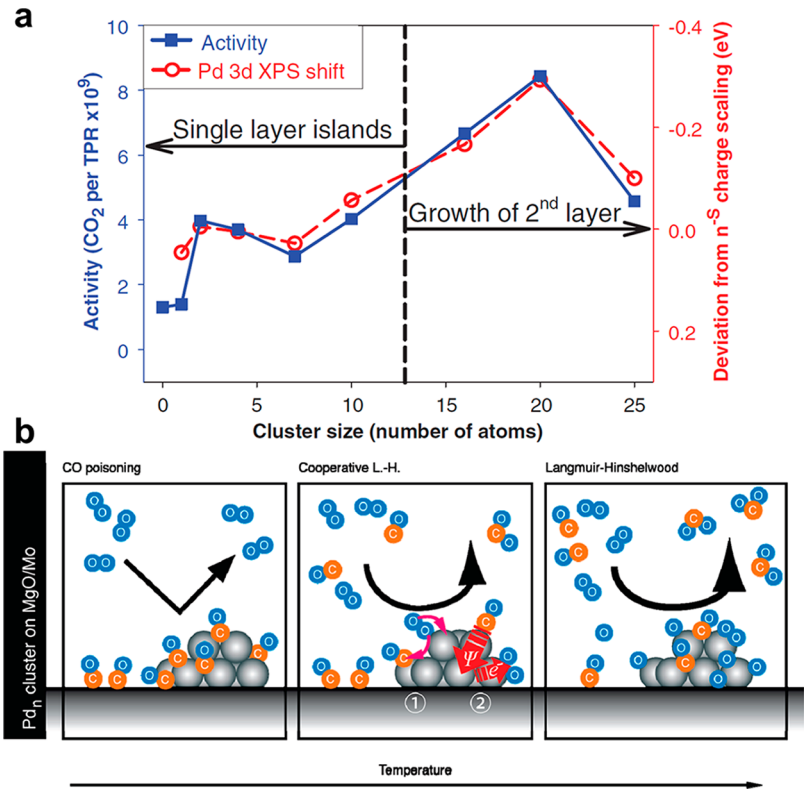

Figure 41. (a) Correlation between CO oxidation activity observed during temperature-programmed reaction (TPR) and the shifts of the Pd 3d binding energy observed by XPS. The XPS and TPR data for each type of Pd cluster were taken on the same sample. Adapted with permission from ref 213. Copyright 2009 The American Association for the Advancement of Science. (b) Mechanism of CO oxidation on Pd clusters from low to high temperature. At low temperature, Pd clusters will be poisoned by CO and cannot catalyze the CO oxidation. When the temperature increases to ca. 300 K, part of the Pd clusters are exposed to O_2 molecules and become able to activate O_2 and catalyze the CO+O_2 reaction. At ca. 400 K, a Langmuir−Hinshelwood-type reaction can be observed on Pd clusters for CO oxidation. Adapted with permission from ref 225. Copyright 2010 American Chemical Society.

5.1.2. CO Oxidation on Pt-Group Metal Clusters. The catalytic properties of Pt-group metal clusters have also been studied for CO oxidation. Anderson et al. have prepared size-selected Pd_n clusters deposited on TiO_2(110) as model catalysts, and attempted to correlated the catalytic activity with the electronic structures.[223] For doing that, the CO oxidation activity (determined by TPR) and the Pd 3d binding energy shifts relative to bulk Pd (measured by XPS) were plotted as a function of the atomicity of Pd_n clusters (Figure 41a). Obviously, these two plots showed a similar tendency when varying the cluster size. It could be seen there that CO oxidation activity increased substantially from Pd_2 to Pd_4, and then declined slowly when the cluster size increased to Pd_7. For larger clusters, activity increased gradually before dropping again for Pd_{25}. The good correlation between the Pd 3d binding energy shift and the catalytic activity suggests that electronic structures of metal clusters have a significant influence on the catalytic properties. Indeed, it has been found that the catalytic properties of Pd clusters supported on alumina could be affected by the thickness of the alumina film and geometric structures of Pd_{20} clusters.[224] In this way, when the thickness of Re-doped alumina film was around 2 nm, the CO oxidation activity of Pd clusters was the lowest.

To investigate how the size of the Pd cluster affects the catalytic properties, Kunz et al. studied the catalytic behavior of three Pd clusters (Pd_8, Pd_{13}, and Pd_{30}).[225] They found that these size-selected Pd clusters show temperature-dependent reaction mechanisms for CO+O_2 reaction. A schematic illustration of the proposed reaction mechanisms over Pd clusters is given in Figure 41b. When working in the low-temperature region, Pd clusters were poisoned by CO, and almost no CO_2 production was observed. When the temperature was increased to above 300 K, some of the Pd atoms in Pd clusters were exposed to O_2, leading to activation of O_2 and oxidation of CO. When the temperature was further increased, a Langmuir−Hinshelwood (L−H) mechanism occurred, in which adsorbed CO exhibited a promoting instead of a blocking effect for oxygen dissociation. Finally, the activity results for CO oxidation at $T > 400$ K showed that larger Pd clusters were active. Although no explanation for these results was given, it may occur that the CO poisoning effect was larger for small Pd clusters. If this is so, more Pd atoms could be exposed to O_2 in larger Pd clusters, which could facilitate the CO oxidation. The above reaction mechanism is also supported by theoretical calculations.[226]

Besides the size, the oxidation state and geometric structure of Pd clusters also play an important role in CO oxidation. Moseler et al. have studied the influence of oxidation state and geometric structures on magnesia-supported $Pd_{13}O_x$ clusters by TPR measurements, isotopic labeling experiments, and first-principles spin density functional theory.[227] When O_2 was adsorbed on Pd_{13} clusters, two types of $Pd_{13}O_x$ species were formed, $Pd_{13}O_4$ clusters with C_{4v} symmetry and nonsymmetric $Pd_{13}O_6$ clusters. The symmetric $Pd_{13}O_4$ showed higher activation energy for CO oxidation via reaction of an adsorbed CO molecule with one of the oxygen atoms of the $Pd_{13}O_4$ cluster. After the removal of CO_2, $Pd_{13}O_{4-x}$ clusters were formed that presented a lower activation energy for further CO oxidation. In contrast, the

DOI: 10.1021/acs.chemrev.7b00776
Chem. Rev. 2018, 118, 4981−5079

nonsymmetric $Pd_{13}O_6$ clusters were quite active at low temperature.

In the case of CeO_2-supported Pd catalysts, it has recently been reported that Pd nanoparticles can be transformed into Pd clusters after hydrothermal treatment. The amount of hydroxyl groups on CeO_2 increased significantly after hydrothermal treatment, which promoted the dispersion of Pd on CeO_2.[228] Those redispersed Pd clusters are highly active for CO oxidation, showing much higher activity than Pd single atoms supported on CeO_2.[86]

In 1999, Heiz et al. reported their work on size-selected Pt clusters for CO oxidation.[229] According to the TPR profiles, the CO_2 molecules produced per Pt_n clusters and per Pt atom were calculated, as shown in Figure 42a. For Pt_n clusters ($n \leq 8$), the

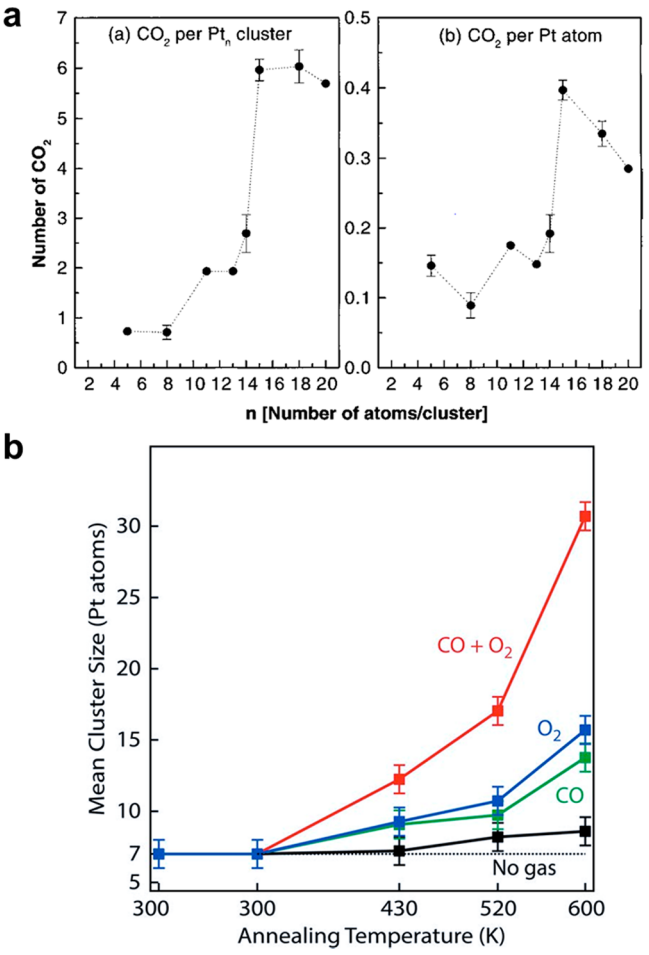

Figure 42. (a) Total number of catalytically produced CO_2 molecules as a function of cluster size of Pt. Total number of produced CO_2 molecules per Pt atom as a function of cluster size. Adapted with permission from ref 229. Copyright 1999 American Chemical Society. (b) Evolution of the average size of deposited Pt_7 clusters on $TiO_2(110)$ after annealing in a vacuum (black) and exposure to O_2 (blue), CO (green), and both reactants (red). Adapted with permission from ref 230. Copyright 2014 American Chemical Society.

production of CO_2 was quite low. The activity increased from Pt_{11} and reaches a maximum for Pt_{15} clusters. Pt_{15}, Pt_{18}, and Pt_{20} showed similar activity measured as CO_2 production per cluster. If CO_2 production per Pt atom was considered, then Pt_{15} gave the highest activity. It appeared that, to understand the size-dependent catalytic behavior of Pt clusters, both the electronic and the geometric factors should be considered. Small Pt_n clusters ($n \leq 6$) tend to be planar structures. In contrast, larger Pt_n clusters ($n \geq 10$) prefer to be in the form of three-dimensional structures. The change in the reactivity of individual Pt clusters appears between Pt_6 and Pt_{10}, which implies that three-dimensional structures are favorable for CO oxidation, as it has also been observed in the case of Au and Pd. However, it should be taken into account that the electronic structures of Pt clusters will also change with the size. Indeed, the energy level of the HOMO in Pt clusters will increase gradually when increasing their size. According to DFT calculations, the HOMO of Pt_{15} is close to the HOMO (π_{2g}*) of O_2, which should result in a larger back-donation between Pt_{15} and O_2 in the process of activation of O_2. This combination of geometry and HOMO energy can explain why Pt_{15} clusters show the highest activity per Pt atom.

When the support switched to $TiO_2(110)$, the situation changes. In a recent work, size-selected Pt_3, Pt_7, and Pt_{10} clusters were deposited on $TiO_2(110)$ to investigate the size evolution for CO oxidation.[230] After calculating the CO_2 production per Pt atom, it was found that Pt_3 shows the highest activity, with Pt_{10} exhibiting the lowest activity. However, these results are different from those obtained by other groups. For instance, Watanabe et al. have reported the structural transformation of Pt clusters from planar to three-dimensional structure when the atomicity is above 8, and highest CO oxidation activity was also observed on Pt_7 and Pt_8 clusters, while smaller Pt clusters (like Pt_4) show the lowest activity.[231] In another work, it was reported that Pt_{10} clusters supported on amorphous Al_2O_3 also showed high activity for CO oxidation.[232] These contradictory conclusions may be caused by the different properties of the TiO_2 supports, because the activation of O_2 occurs at the Pt−TiO_2 interface.[233]

One factor that should be considered when working with metal clusters is their evolution under different atmosphere during the annealing process. As shown in Figure 42b, Pt_7 clusters were quite stable below 300 K. When the temperature was increased to 430 K, the growth in size was not obvious in vacuum, CO, or O_2. Significant growth of Pt_7 clusters was observed, when the temperature was 520 K in vacuum. The ripening of Pt_7 clusters was quite apparent in CO+O_2 atmosphere. During the CO oxidation reaction, Pt_7 clusters were mobile on the surface of $TiO_2(110)$ due to the strong interaction between Pt clusters and CO, favoring the aggregation of Pt_7 clusters. A similar ripening phenomenon has also been observed by STM or grazing incidence small-angle X-ray scattering (GISAXS).[234,235]

For practical reasons, metal clusters are usually deposited on some support, and, in that case, the catalytic performance of the metal clusters can also be affected by the supports.[236] In a recent work, Brune et al. have deposited size-selected Pt_7 clusters on $TiO_2(110)$ surface with low-reduction (LR-TiO_2) and high-reduction (HR-TiO_2) states, respectively. These two types of $TiO_2(110)$ surfaces have different concentrations of oxygen vacancies. Catalytic measurements performed by pulses of CO and O_2 while simultaneously annealing the sample from 300 to 600 K showed that the maximum CO_2 production rate of the Pt clusters was 2 orders of magnitude higher when they were supported on LR- than on HR-TiO_2. The quenching of the CO_2 production on Pt/HR-TiO_2 was due to the depletion of the adsorbed O_2 on the Pt clusters via spillover to the support and consumption of O_2 by reaction with Ti^{3+} sites.

The unique role of Pt-group metal clusters for CO oxidation has also been reflected in catalysts prepared by coprecipitation. Pt/FeO_x (with ~2 wt % of Pt) containing Pt clusters and Pt

DOI: 10.1021/acs.chemrev.7b00776
Chem. Rev. 2018, 118, 4981−5079

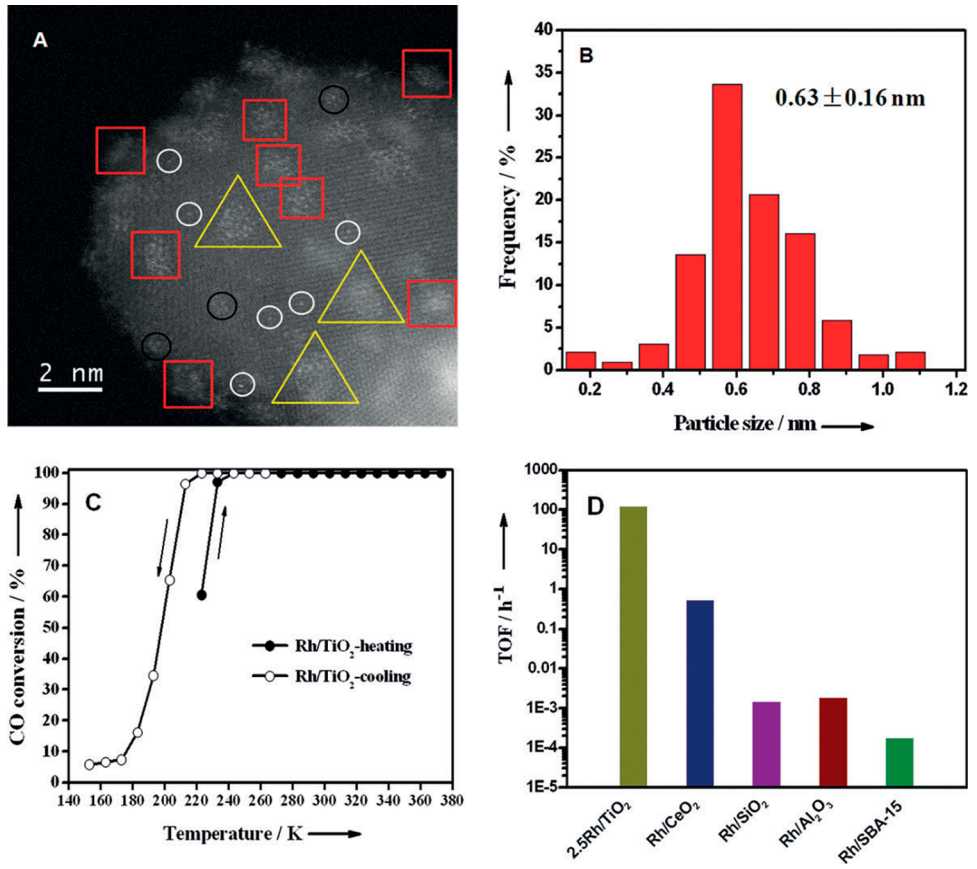

Figure 43. (A) High-resolution STEM image of Rh/TiO_2 sample, containing subnanometric Rh species and small Rh nanoparticles. (B) Size distribution of Rh species in this Rh/TiO_2 sample. (C) CO oxidation activity as a function of temperature on Rh/TiO_2 catalyst. (D) Comparison of TOFs at 293 K on various supported Rh catalysts for CO oxidation reaction. Adapted with permission from ref 238. Copyright 2016 Wiley-VCH Verlag GmbH & Co. KGaA, Weinheim.

single atoms show excellent activity for preferential oxidation of CO in the presence of rich H_2 at room temperature.[237] Although the TOF of Pt clusters (0.181 s^{-1}) is slightly lower than that of Pt singles (0.212 s^{-1}) under the same reaction conditions, the Pt loading of the Pt/FeO_x with clusters is much higher than Pt/FeO_x with single Pt atoms. Therefore, from a practical point of view, the Pt/FeO_x containing Pt clusters are better catalysts for CO-PROX reaction than the Pt/FeO_x catalyst with single atoms. In a recent work, Zhang and his co-workers reported the application of Rh/TiO_2 prepared by impregnation method for low-temperature CO oxidation (see Figure 43).[238] By tuning the size of Rh species, full conversion in CO oxidation was achieved at 223 K on subnanometric Rh clusters (0.4−0.8 nm), which is comparable to the performance of the state-of-art Au catalysts. Spectroscopic characterizations and theoretical calculations show that O_2 can be activated at the $Rh-TiO_2$ interface and react with CO molecules absorbed on TiO_2, giving high activity for CO oxidation. When the size of Rh increases to ∼2 nm, the activity drops sharply, implying a strong particle size effect on the catalytic performance. In the above two examples, subnanometric Pt and Rh clusters show distinct electronic structures as compared to nanoparticles according to CO-IR adsorption spectra, and their different electronic properties will be reflected on their chemical states when deposited on solid supports, which should have a significant influence on their activity. Moreover, in many cases, metal clusters will become partially oxidized, and their chemical states can evolve under reaction conditions. For instance, when Pt clusters (∼0.5 nm) are highly oxidized and coordinated by oxygen, they show poor activity for CO oxidation. By following the evolution of Pt species by in situ EXAFS and XANES, Ke et al. have proposed that reduced Pt clusters with low Pt−O coordination contribution are more favorable for low-temperature CO oxidation.[239]

What we have learned up to now is that the electronic properties of the Pt group metals depend on the size and structure of the clusters, the interactions with the support, and the atmosphere at which they are exposed. Obviously, all of those factors will determine the final catalytic activity and selectivity of the metal catalyst. On this basis, we will now discuss the catalytic behavior of metal clusters for important catalytic applications, such as selective oxidation, selective hydrogenation, dehydrogenation, photocatalysis, and electrocatalysis.

5.2. Oxidation of Hydrocarbons

The oxidation of C−H bond is a promising green strategy to obtain functionalized products from abundant raw materials. For instance, direct oxidation of CH_4 to CH_3OH is a dream reaction for the valorization of natural gas. In nature, enzymes containing two-copper centers can catalyze this transformation at room temperature.[240,241] Inspired by nature, chemists try to mimic the active sites in natural enzymes and design heterogeneous catalysts for direct oxidation of CH_4 to CH_3OH. In the past decade, it has been reported that Cu-zeolite catalysts prepared by the ion-exchange process can make the selective transformation of CH_4 to CH_3OH through a cyclic process, as shown in Figure 44a.[242] In the case of Cu-exchanged ZSM-5, with the help of

DOI: 10.1021/acs.chemrev.7b00776
Chem. Rev. 2018, 118, 4981−5079

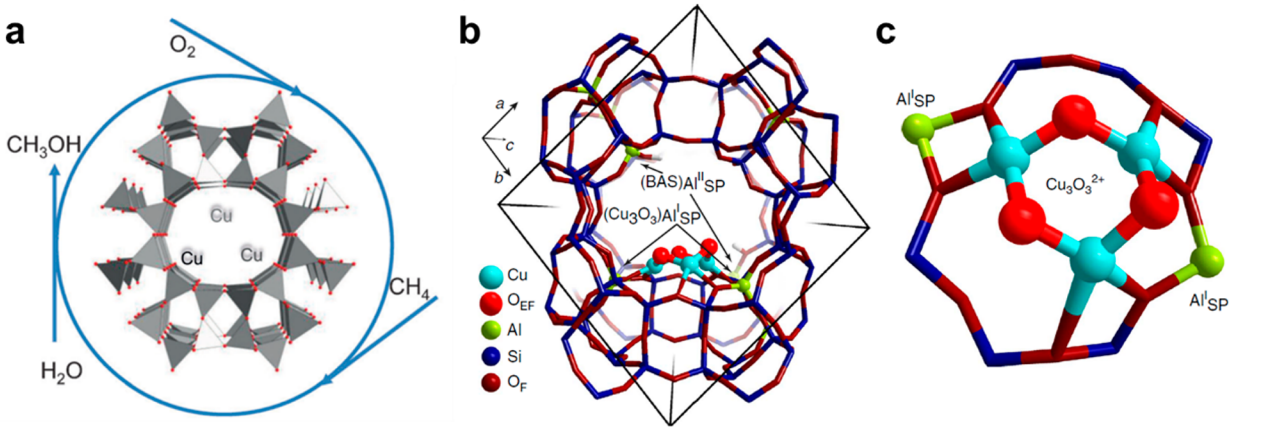

Figure 44. (a) Illustration of oxidation of CH_4 with Cu-exchanged zeolites through a cyclic process. Adapted with permission from ref 242. Copyright 2016 Wiley-VCH Verlag GmbH & Co. KGaA, Weinheim. (b,c) Schematic illustration of Cu_3 clusters located in the side pockets of MOR zeolites. The $Cu_3(\mu\text{-}O)_3$ clusters are proposed to be the active sites for oxidation of CH_4. Adapted with permission from ref 243. Copyright 2015 Macmillan Publishers Limited, part of Springer Nature.

Raman spectroscopy and isotopic studies, it has been proposed that binuclear Cu species located in ZSM-5 are the active species for CH_4 oxidation to CH_3OH.[243] In a recent work, the generation and stabilization of trinuclear copper oxygen clusters at the pore mouth of 8-ring side pockets in mordenite was reported, and these Cu_3 clusters showed activity and selectivity for oxidation of methane to CH_3OH.[244] Therefore, it can be seen that there is still some debate on the nature of the active sites in Cu-exchanged zeolites. Indeed, in another report, it is proposed that $Cu^{II}-O-Cu^{II}$ is the active site for methane oxidation to methanol.[245] Interestingly, when studying the Cu-zeolite catalysts by high-resolution TEM, it can be found that a large number of CuO_x nanoparticles (1−3 nm) are also present in the active Cu-exchanged zeolite catalysts, implying that Cu species other than Cu clusters may also be active for oxidation of CH_4.[246,247] Moreover, it should also be considered that the structures of the active Cu sites are also affected by the reaction conditions. Therefore, to clarify the role of Cu clusters for selective oxidation of methane, mechanistic studies based on catalysts with well-defined and stable metal species are required.[248] In a recent work, van Bokhoven et al. demonstrate an anaerobic approach for oxidation of methane to methanol using water as soft oxidant, giving very high selectivity (~97%) to methanol.[249] In that work, Cu-exchanged MOR zeolite was activated in He at 400 °C and then reacted with CH_4 at 200 °C, resulting in the reduction of Cu(II) to Cu(I). Afterward, the desorption of methanol and reoxidation of Cu(I) to Cu(II) can be realized by introducing H_2O into the Cu-MOR zeolite. The above catalytic cycles have also been verified by in situ XANES and FT-IR. Although progress on the identification of the nature of the active sites has been achieved in the past decade, the catalytic performance of Cu-exchanged zeolite materials is still far below the requirements for practical application, and exploring new materials for oxidation of methane to methanol is an emerging challenge.

The direct oxidation of C−H bond in benzene with O_2 for the production of phenol is another dream reaction for chemical industry. In 2006, Iwasawa et al. reported a Re/zeolite catalyst prepared by chemical vapor deposition (CVD) of organometallic Re compound on ZSM-5 crystallites for direct oxidation of benzene to phenol with O_2 in the presence of NH_3.[250] The catalyst could achieve 82.4−87.7% selectivity to phenol at 0.8−5.8% conversion of benzene under steady-state reaction. As described in Figure 45, EXAFS and XANES results reveal that Re_{10} clusters were the active sites under reaction conditions, and

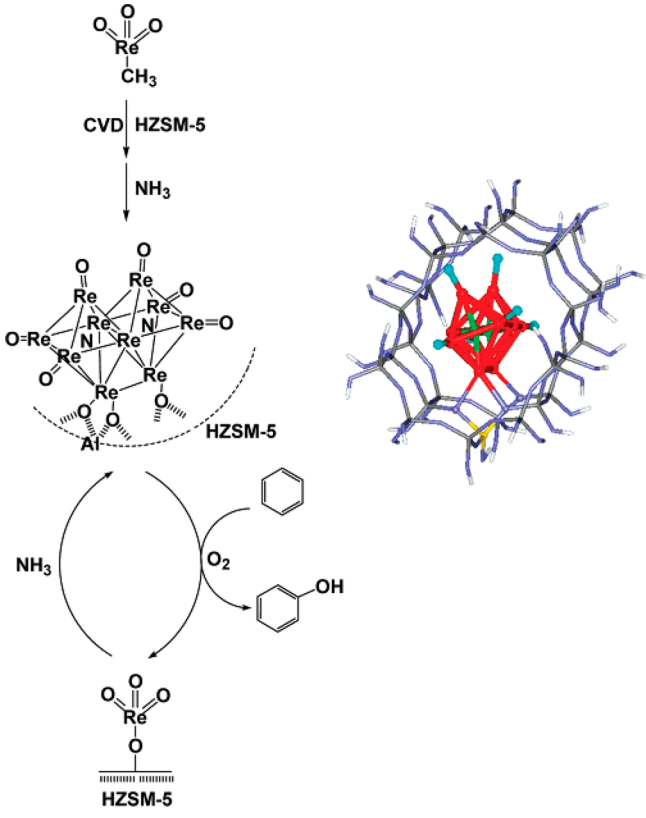

Figure 45. Generation of Re_{10} clusters in ZSM-5 by chemical vapor deposition and the dynamic transformation of Re_{10} clusters and mononuclear Re species under reaction conditions. Adapted with permission from ref 250. Copyright 2007 American Chemical Society.

they transformed into mononuclear Re under reaction conditions when there was no NH_3 in the feed gas. The presence of NH_3 is critical for the generation and stabilization of Re_{10} clusters in the pore channels of ZSM-5.[251]

In addition, Bao and his co-workers have also shown the application of Pt nanoclusters confined in carbon nanotubes for the catalytic oxidation of toluene.[252] In their work, Pt

DOI: 10.1021/acs.chemrev.7b00776
Chem. Rev. 2018, 118, 4981−5079

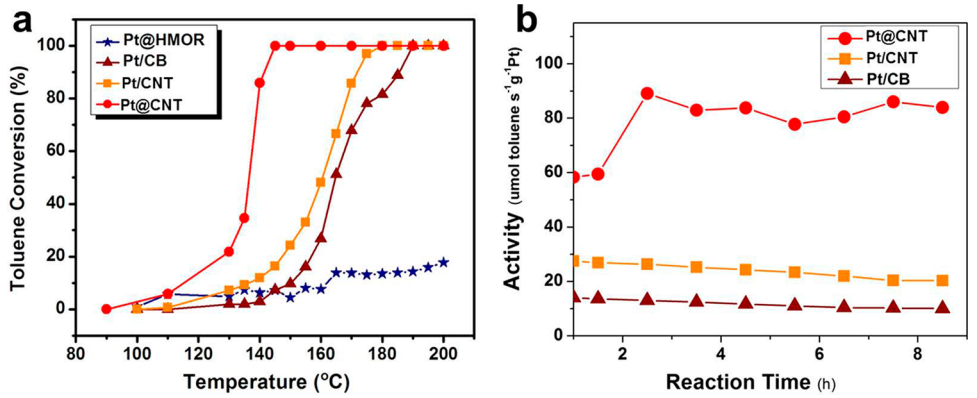

Figure 46. Activity and stability of Pt nanoclusters confined in carbon nanotubes (Pt@CNT) in comparison with Pt nanoclusters exposed on open surfaces of the carbon nanotubes exterior walls and carbon black (Pt/CNT and Pt/CB): (a) toluene conversion as a function of reaction temperatures; and (b) the stability test. Adapted with permission from ref 252. Copyright 2015 American Chemical Society.

nanoclusters and nanoparticles between 0.7 and 1.2 nm were loaded into the carbon nanotubes and on the surface of carbon nanotubes. Because of the electronic interaction between Pt clusters and carbon nanotubes, the Pt nanoclusters confined in carbon nanotubes were more difficult to be oxidized by O_2, which was favorable for the oxidation of toluene. In fact, Pt nanoclusters supported inside carbon nanotubes showed nearly 3-fold higher activity than those supported on the surface of carbon nanotubes (see Figure 46). Besides, the sintering of Pt clusters into Pt nanoparticles was also prevented by a confinement effect within carbon nanotubes.

Propene oxide is a large-scale raw material for the polymer industry. In 1998, Haruta et al. reported the application of Au/TiO_2 catalyst for the oxidation of propene to propene oxide using a mixture of H_2 and O_2. It was proposed that the metal nanoparticles were responsible for producing H_2O_2, which worked as oxidant to produce propene oxide when Au/TiO_2 was combined with a titanium silicate.[253] Spectroscopic investigations were carried out to identify the active sites for this reaction. The results indicated that small Au species (below 2 nm) are the active species for the production of propene oxide. Lee et al. generated size-selected Au_{6-10} clusters by a physical method and deposited them on amorphous alumina as catalyst for selective epoxidation of propene.[254] As shown in Figure 47, the conversion of C_3H_6 and product distributions depended on the composition of the feed gas. In the case of C_3H_6+O_2, higher propene conversion was achieved, but the stability of Au clusters was not good due to the loss of −OH groups at the perimeter of Au−Al_2O_3 interface. When H_2 or H_2O was introduced, the stability of Au clusters was improved. More importantly, the selectivity to propene oxide was greatly improved when H_2O was introduced into the feed gas. According to the results from theoretical calculations, it was suggested that the higher activity of Al_2O_3-supported Au clusters can be due to the easier formation of reaction intermediates (peroxo $^{\bullet}$OOH radicals). The above phenomenon has also been observed in other supported Au catalysts containing small Au nanoparticles (1−2 nm).[255] However, the nature of the active sites (subnanometric Au clusters or small Au nanoparticles between 1 and 2 nm) is still not well clarified for the epoxidation of propene.

Not only Au clusters, but subnanometric Ag clusters can also be active catalyst for epoxidation of propene. Vajda et al. showed that size-selected Ag_3 clusters deposited on Al_2O_3 were active and selective catalysts for epoxidation of propene at low temperature.[256] As shown in Figure 48A and B, Ag_3 clusters exhibited good conversion of propene at low temperature (<100 °C). Notably, propene could be readily converted into propene oxide and acrolein at 60 °C, which was remarkable as compared to conventional Ag-based catalysts. From room temperature to 60 °C, the major product was acrolein. When the temperature was increased to between 70 and 100 °C, higher propene oxide/acrolein ratios could be achieved. However, selectivity to CO_2 also increased from 30% to 60%. DFT calculations (Figure 48E) suggest that O_2 molecules are activated at the Ag/Al_2O_3 interface through formation of Ag_3O structure. Alumina-supported Ag_3O cluster has a substantial net spin density (~0.6) on the Ag and O in the cluster. In contrast, there is no spin density present when atomic oxygen is adsorbed on an Ag(111) surface, assuming low oxygen coverage. This work indicates that the flexibility of metal clusters may account for their higher catalytic performance by adapting their configuration during molecular activation. Notably, those Ag_3 clusters were not stable at above 120 °C, and they agglomerated into Ag nanoparticles of 2−3.5 nm, depending on the reaction temperature. The catalytic performance of those Ag nanoparticles has also been measured under the same conditions. As it can be seen in Figure 48C and D, Ag nanoparticles (~3.5 nm, generated from the sintering of Ag_3 clusters) show a turnover frequency (based on surface Ag atoms) similar to that of Ag_3 clusters for the production of propene oxide, implying that size effects are not so significant in this system. Further investigation on size effects with different types of Ag species may provide more insights on the nature of the active species for epoxidation of propene.

Metal clusters capped by organic groups have precise atomic structures, which can be ideal model catalysts to study the effects of components and structures on catalytic properties.[257] As it has been discussed in the part on size-selected Au clusters, activation of O_2 is an important advantage for the application of Au clusters. In this sense, Jin et al. showed the application of $Au_{25}(SR)_{18}$ clusters for selective oxidation of styrene.[258] The results summarized in Table 3 indicate that smaller Au clusters show higher conversion than larger ones, while the selectivity is similar for all of the catalysts. Nevertheless, the catalytic performance of $Au_{25}(SR)_{18}$ cluster can be further improved by doping with other metals. Single Pt-doping Au clusters[259] and single Pd-doping Au clusters[260] have been prepared to enhance the activity of Au clusters in selective oxidation reaction of styrene and alcohol, respectively. Indeed, doping with another atom can change the electronic structures of Au_{25} clusters so that the activation of O_2 could be further improved.

DOI: 10.1021/acs.chemrev.7b00776
Chem. Rev. 2018, 118, 4981−5079

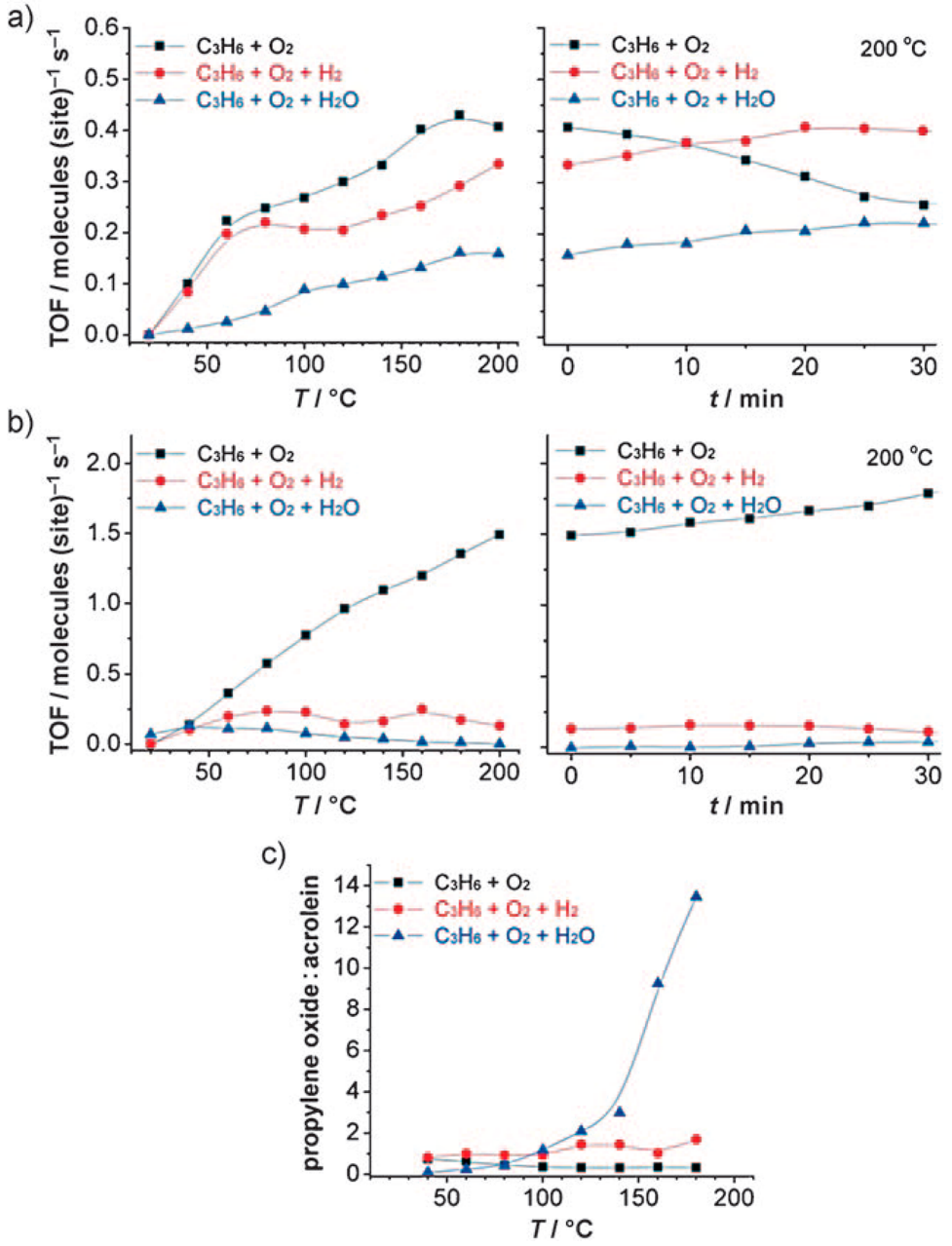

Figure 47. Catalytic performances of size-selected Au clusters deposited on Al_2O_3 for epoxidation of propene. (a) Turnover frequency based on the formation of propene oxide as a function of reaction temperature (left) and time on stream at 200 °C (right) for various compositions of feed gas. (b) Turnover frequency based on the formation of acrolein as a function of temperature (left) and time on stream at 200 °C (right) for various compositions of feed gas. (c) Temperature-dependent ratio of propene oxide to acrolein. ■, C_3H_6/O_2; ●, $C_3H_6/O_2/H_2$; ▲, $C_3H_6/O_2/H_2O$. Adapted with permission from ref 254. Copyright 2009 Wiley-VCH Verlag GmbH & Co. KGaA, Weinheim.

One important issue related to thiolate-protected metal clusters is their stability under reaction conditions. Au clusters capped by thiolate ligands may undergo oxidative decomposition under reaction conditions. Ackerson et al. have demonstrated that Au_{25} clusters decomposed to Au(I) species, which were the real active species for the oxidation of styrene with O_2.[261] It should be noticed, however, that the nature of the Au(I) species (size and structures) was not discussed in that paper. We have again to insist that for investigations on the catalytic behavior of metal clusters, it is critical to study their structures under reaction conditions.

5.3. Selective Hydrogenation

The hydrogenation of ethylene is generally accepted as a structure-insensitive reaction for Pt-based nanoparticulate catalysts. When the particle size of Pt species decreases to <1 nm, those Pt clusters can be treated as molecular sites, which show strong size-dependent electronic and geometric properties. In a recent work, Crampton et al. have investigated the catalytic behavior of size-selected Pt_n clusters (n = 8−15) in the subnanometric regime for hydrogenation of ethylene.[262] As shown in Figure 49a, Pt_{13} clusters showed the highest TOF value for production of ethane among a series of size-selected Pt clusters, indicating that the hydrogenation of ethylene on subnanometric Pt clusters is a structure-sensitive reaction. This

DOI: 10.1021/acs.chemrev.7b00776
Chem. Rev. 2018, 118, 4981−5079

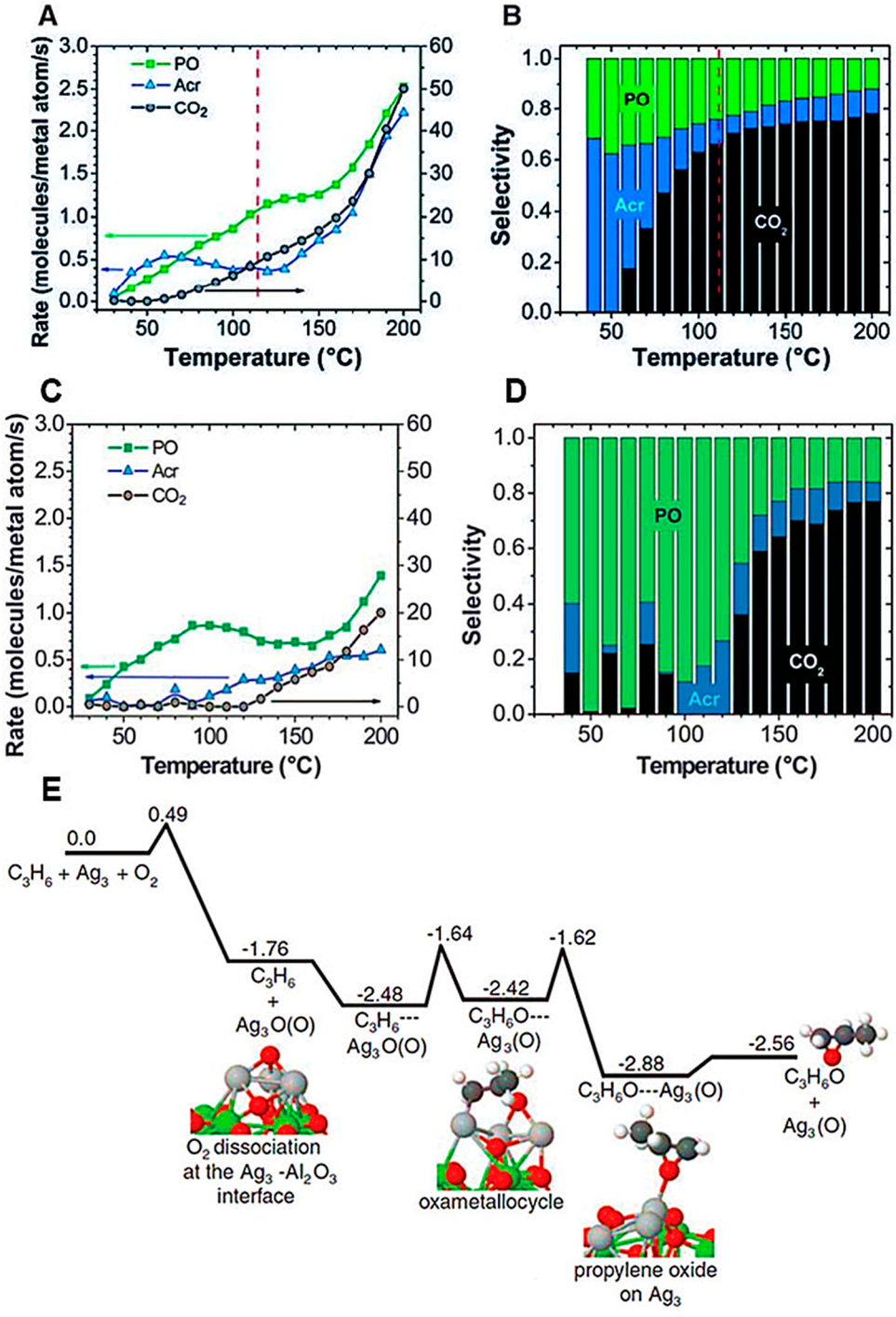

Figure 48. (A) Reaction rate of oxidation of propene to propene oxide (PO), acrolein (Acr), and CO_2 on Ag_3 clusters. (B) Selectivity toward different products at different temperature on Ag_3 clusters supported on Al_2O_3. (C) Reaction rate of oxidation of propene to propene oxide (PO), acrolein (Acr), and CO_2 on Ag nanoparticles (~3.5 nm). (D) Selectivity toward different products at different temperature on Ag_3 clusters supported on Al_2O_3. (E) Reaction mechanism of oxidation of propene to propene oxide catalyzed by Ag_3 clusters based on DFT calculations. Adapted with permission from ref 256. Copyright 2010 The American Association for the Advancement of Science.

is in contrast with established experiences on Pt nanoparticles or extended Pt surface.[263,264] Theoretical calculations show that the energy barrier for activation of H_2 and addition of dissociated H to adsorbed C_2H_4 molecules is the lowest on Pt_{13} clusters.

Theoretical calculations have also predicted one reaction pathway with low activation barrier for dehydrogenation of ethylene to ethylidyne on Pt clusters at higher temperature (>350 K). To test the calculation results, subnanometric Pt clusters were exposed to ethylene at 400 K, and the activity for hydrogenation of ethylene dropped for most of the Pt clusters, which was probably caused by the formation of ethylidyne on Pt clusters, according to the CO-IR spectroscopic results (see Figure 49b). Those ethylidyne absorbed on Pt clusters could block the active sites for hydrogenation of ethylene. This work implies that the interaction between subnanometric metal clusters and substrate molecules and the catalytic processes on

DOI: 10.1021/acs.chemrev.7b00776
Chem. Rev. 2018, 118, 4981−5079

Table 3. Catalytic Performance of Thiolate Capped $Au_n(SR)_m$ Clusters for the Selective Oxidation of Styrene with O_2[a]

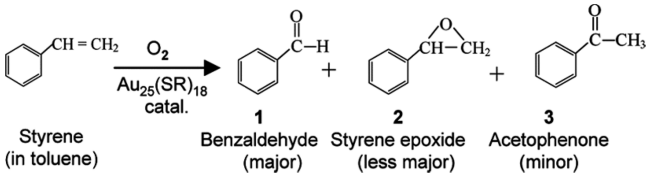

		selectivity/%		
catalyst	conversion/%	1	2	3
$Au_{25}(SCH_2CH_2Ph)_{18}$	27 ± 1.0	70	24	6
$Au_{25}(SC_6H_{13})_{18}$	25 ± 0.8	69	26	5
$Au_{38}(SCH_2CH_2Ph)_{24}$	14 ± 1.2	72	24	4
$Au_{38}(SC_{12}H_{25})_{18}$	15 ± 1.2	71	25	4
$Au_{144}(SCH_2CH_2Ph)_{60}$	12 ± 0.5	80	20	trace
$Au_{144}(SC_{12}H_{25})_{18}$	11 ± 0.8	84	16	trace
~3 nm Au nanoparticles	6 ± 1.2	82	18	trace

[a]Adapted with permission from ref 248. Copyright 2010 Wiley-VCH Verlag GmbH & Co. KGaA, Weinheim.

metal clusters can be different from the situation on conventional nanoparticles.[265] These authors also demonstrated that the activity of Pt_{13} clusters could be tuned by the support. When Pt_{13} clusters were supported on oxygen-deficient SiO_2 film, they showed activity similar to Pt(111) surface. However, when the support was changed to oxygen-rich SiO_2 film, a 3-fold increase of activity could be observed for hydrogenation of ethylene.[266]

In the above case, subnanometric Pt clusters were generated by a physical method and deposited on the surface as model catalysts. Actually, Pt clusters can also be generated by chemical method and used as catalysts for hydrogenation reactions under practical conditions. For instance, Pt_{12} clusters stabilized by dendrimer were prepared for hydrogenation of olefins, and its catalytic behavior was compared to that of Pt nanoparticles (ca. 2.2 nm).[267] As shown in Table 4, Pt_{12} clusters showed much higher TOF than did Pt NPs. In some cases, Pt_{12} clusters achieved 1 order of magnitude higher TOF than Pt NPs. More interestingly, Pt_{12} clusters also showed enhanced activity for the reductive amination of aldehydes with amines with a remarkable poison tolerance to amines without adding protic acid.[268]

In a recent work, Pt single atoms supported on phosphomolybdic acid were found to be active for the hydrogenation of C=C bonds. The TOF for hydrogenation of styrene at room temperature with 10 bar of H_2 was 1002 h^{-1}, which is lower than for Pt_{12} clusters, although the reaction conditions in these two works are different. In addition, Pd clusters encapsulated in G5-TEBA [fifth generation of triethoxybenzamide-terminated poly(propene imine) dendrimer] were also active for hydrogenation of olefins.[269] In the case of Pd_n clusters (n = 4, 8, and 16), the larger Pd clusters showed higher TOF. For Pd_{32} clusters, the TOF was almost the same as that for Pd_{16}.

As was previously shown for oxidation reactions, the hydrogenation activity can be further improved by preparing bimetallic clusters. For example, $Rh_{32}Fe_{28}$ nanoclusters show improved activity with respect to Rh_{60} nanoclusters in hydrogenation of C=C and nitroarenes.[270] The structure of dendrimers also has an influence on the hydrogenation activity. In the hydrogenation of C=C, Rh_{60} nanoclusters encapsulated in TPP-DPA G4 (fourth generation of phenylazomethine dendrimer) showed much higher activity than those in PAMAM G4-OH (fourth generation of polyamidoamine dendrimer).[271] However, when these two catalysts were used for the hydrogenation of nitroarenes, Rh clusters encapsulated in PAMAM G4-OH were much more active. It appears that the different molecular structures of two dendrimers should account for their distinct catalytic properties. Indeed, the solid shell of TPP-DPA G4 with a sufficient inner cavity allows a wide variety of hydrophobic substrates to access the surface of Rh nanoclusters. In contrast, the liquid shell of PAMAM G4-OH swelled with polar solvents, refused hydrophobic substrates to the interior space, whereas it can enhance the mass transportation of polar substrates, such as nitroarenes, to the Rh nanoclusters.

As shown before for selective oxidation reactions, thiolate-protected Au clusters can also be employed as catalyst for selective hydrogenation reactions. In their work, Jin et al. reported the application of $Au_{25}(SR)_{18}$ for the selective hydrogenation of α,β-unsaturated ketones and aldehydes.[272]

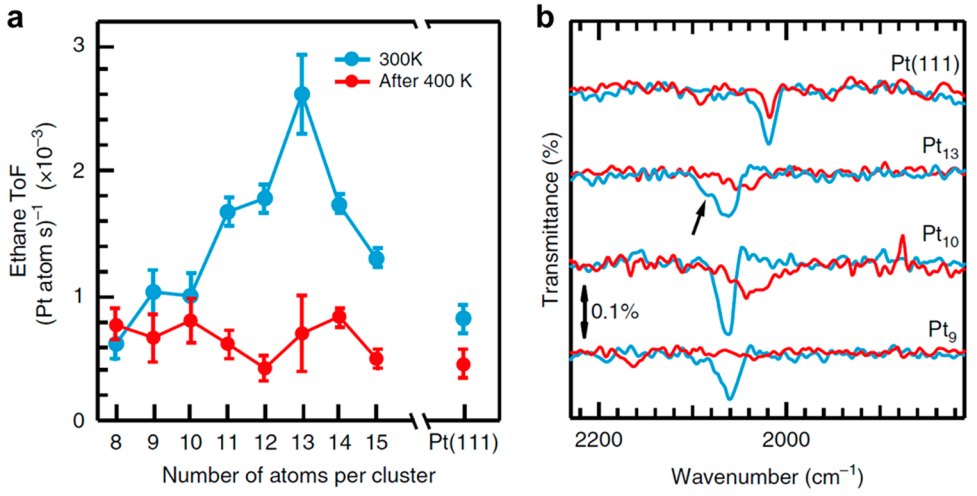

Figure 49. (a) TOF of hydrogenation of ethylene to ethane on Pt clusters with different atomicity at 300 K. The blue plots correspond to the TOF values measured for the fresh samples, and the red plots correspond to the TOF values measured after exposure to reaction gas at 400 K and then cooling to 300 K. (b) CO-IR spectra of Pt clusters and Pt(111) surface after hydrogenation of ethylene at 300 K (blue) and after exposure to reaction gas at 400 K and then cooling to 300 K (red). Adapted with permission from ref 262. Copyright 2016 Macmillan Publishers Limited, part of Springer Nature.

DOI: 10.1021/acs.chemrev.7b00776
Chem. Rev. 2018, 118, 4981−5079

Table 4. Turnover Frequencies of Olefin Hydrogenation in the Presence of Pt_{12} Cluster or Pt NPs (2.2 ± 0.8 nm) Supported on Graphitized Mesoporous Carbon (GMC)

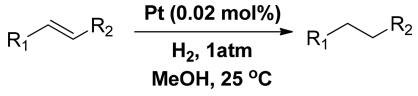

Entry	Substrate	Pt_{12}@TPM G4[a]/GMC (h^{-1})	Pt (2.2±0.8nm)[a]/GMC (h^{-1})
1		1.35×10^3	4.73×10^2
2	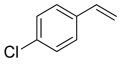	8×10^2	1.80×10 [b]
3	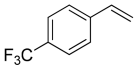	6.20×10 [b]	0
4		5.85×10^3	4.80×10^3
5		2.03×10^2	1.30×10
6	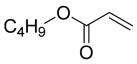	1.69×10^3	8.89×10^2

100% chemoselectivity to α,β-unsaturated alcohols was achieved with these cluster catalysts. It has been proposed that H_2 is dissociated by the surface Au atoms with lower coordination numbers, while C═O bonds are activated by the core Au atoms. Such a synergistic effect contributes to the high selectivity observed during the hydrogenation reaction. Subsequently, these authors have also investigated the size effects on the chemoselective hydrogenation of C═O bonds.[273] The catalytic activity (based on the conversion of 4-nitrobenzaldehyde) of the Au clusters increases with the size, $Au_{15}(SG)_{13}$ < $Au_{18}(SG)_{14}$ < $Au_{25}(SG)_{18}$ < $Au_{38}(SG)_{24}$. The results can be explained on the basis that catalysts with larger Au cluster cores have more metal surface that can be exposed to C═O bonds.

Thiolate- and phosphine-protected Au nanoclusters are also active for the partial hydrogenation of alkynes.[274] Terminal alkynes were converted to corresponding alkenes with >99% conversion of alkynes and ∼100% selectivity for *Z*-alkenes over both Au nanoclusters with different ligands. In contrast, hydrogenation of internal alkynes cannot be achieved because they cannot access the Au atoms due to the steric effect. As shown in Figure 50, Au atoms can be accessible to terminal alkynes through the interspace between the ligands. A special deprotonation activation pathway R′−C≡C $[Au_nL_m]$ (where L represents the protecting ligand on the cluster) is proposed on the basis of the catalytic results. Au_{38} clusters protected by alkynyl groups were found to be much more active than Au_{38} clusters protected by thiolate groups.[275]

Dendrimer-encapsulated Cu nanoclusters can also be active catalysts for selective hydrogenation reactions. In the work of Tsukuda et al., Cu^{2+} ions were reduced by $NaBH_4$ in the presence of PAMAM−OH(G6) dendrimers (sixth generation of poly(amidoamine) dendrimer with hydroxyl surface groups), leading to the formation of encapsulated Cu_{30} clusters.[276] These Cu_{30} clusters can catalyze the selective hydrogenation of C═O with up to 100% selectivity to alcohol in the presence of C═C. Moreover, Cu_{30} clusters can slowly be oxidized to Cu^{2+} by air, but they can be regenerated by $NaBH_4$ easily. However, in the case of Cu^0 NPs capped with PVP (polyvinylpyrrolidone), they cannot be regenerated by a second reduction, indicating the different redox properties between Cu clusters and Cu NPs.[277]

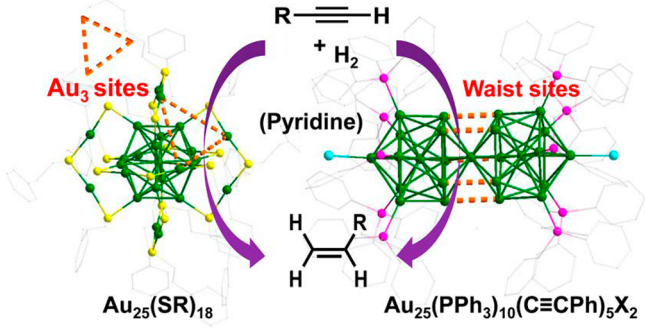

Figure 50. Proposed mechanism for selective hydrogenation of terminal alkynes to alkenes by the protected Au_{25} clusters. Left panel: $Au_{25}(SR)_{18}$ cluster. Right panel: $Au_{25}(PPh_3)_{10}(C{\equiv}CPh)_5X_2$ (X = Cl, Br) cluster. The models of these two protected Au clusters are presented according to their crystal structure. Color code: Au, green; S, yellow; C, gray; P, pink; X, cyan. Hydrogen atoms are not shown. The areas marked with organic lines are the Au_3 active sites (left panel) and the waist active sites (right panel) for the selective hydrogenation of alkyne, respectively. Adapted with permission from ref 274. Copyright 2014 American Chemical Society.

It was said before that the electronic and geometric structures are strongly related to the size of the metal clusters, and, consequently, it is not surprising that the catalytic properties of metal clusters also depend on the size. To this respect, Gates et al. have investigated the interactions between Ir species and H_2 to establish the size effects of metal clusters on hydrogenation of ethene.[278,279] A schematic illustration of different Ir species supported on MgO and zeolite is shown in Figure 51. When mononuclear Ir complexes were supported on electron-withdrawing zeolite support, single Ir atoms could activate C_2H_4 and H_2 simultaneously. On the other hand, when the support was basic MgO, mononuclear Ir complexes were electron-rich, and this situation was not favorable for the hydrogenation reaction. When Ir_4 clusters were loaded on MgO, activation of C_2H_4 and H_2 became easier, leading to higher TOF for ethene hydro-

DOI: 10.1021/acs.chemrev.7b00776
Chem. Rev. 2018, 118, 4981−5079

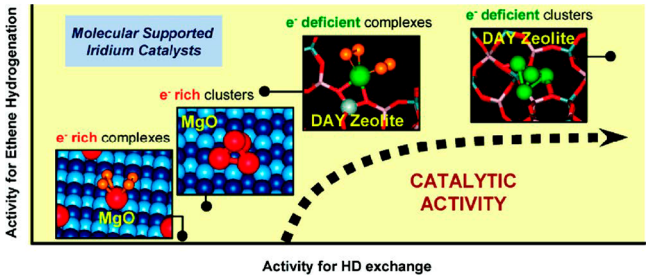

Figure 51. Schematic illustration of mononuclear Ir and Ir_4 clusters supported on MgO and DAY Zeolite. The relative activities for ethene hydrogenation are also presented. Adapted with permission from ref 279. Copyright 2011 American Chemical Society.

genation because the Ir_4 clusters could provide neighboring Ir sites for adsorption and activation of ethene and H_2. In contrast, for acid zeolite as support, Ir_4 clusters showed only minor improvement for the ethene hydrogenation reaction with respect to the mononuclear Ir complex, suggesting that the activation of ethene and H_2 on neighboring Ir sites is not the rate-determining step in zeolite-supported Ir catalysts.

The catalytic properties of supported Ir clusters can also be tuned through surface modification to introduce selective molecular recognition in the catalytic process. Thus, Ir_4 clusters were capped by calixarene-phosphine ligands, which blocked basal Ir sites in Ir_4 clusters and protect Ir_4 clusters from aggregation (see Figure 52). At the same time, the electronic and coordination environments of Ir_4 clusters were modulated. H−D exchange and ethene hydrogenation experiments provided evidence supporting that only the apical Ir were accessible for substrate molecules. Basal Ir sites were exposed after decarbonylation treatment. Yet they were not able to activate ethene molecules because of the blocking effect of calixarene-phosphine ligands as suggested by the simulation results.[280] This work demonstrates the possibility of controlling the catalytic properties of supported metal clusters in an accurate way, which now is an emerging task for cluster catalysis.[281]

When metal clusters are encapsulated in porous materials with well-defined pore structures, size-selective hydrogenation can be achieved. In a recent work from our research group, subnanometric Pt clusters have been introduced into MCM-22 zeolite (named as Pt@MCM-22) during transformation from a two-dimensional into a three-dimensional zeolite (see Figure 53a and b).[282] To test the accessibility of subnanometric Pt species in MCM-22, hydrogenation of light olefins with different molecular sizes was chosen as the model reaction. Considering the pore structures of MCM-22 and the synthesis principle, propene can diffuse into subnanometric Pt species located in the supercages or cavities while isobutene will have preferential access to Pt species located on the external surface of MCM-22 crystallites, but diffuse more slowly than propene to Pt species located in the internal space. For comparison, a Pt/MCM-22-imp catalyst containing Pt nanoparticles on the external surface of MCM-22 was also prepared by impregnation, and the catalytic results of two catalysts for hydrogenation of light olefins are shown in Figure 53c and d. Pt@MCM-22 showed much higher activity than Pt/MCM-22-imp for hydrogenation of propene, suggesting higher intrinsic activity of Pt clusters than Pt nanoparticles. Furthermore, Pt@MCM-22 and Pt/MCM-22-imp showed similar activity for hydrogenation of isobutene, indicating that a large proportion of subnanometric Pt species in Pt@MCM-22

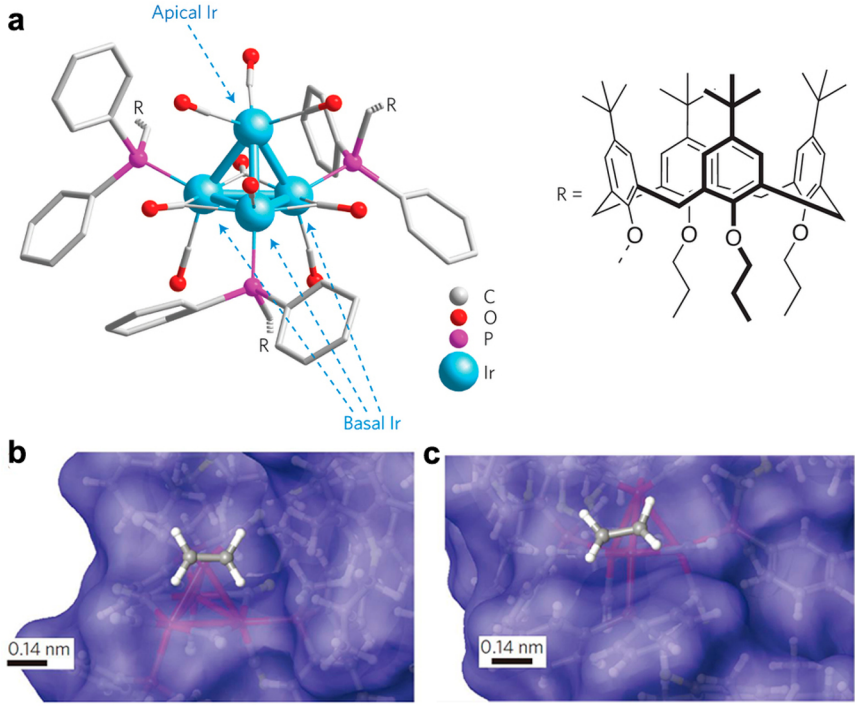

Figure 52. (a) Tetrahedral Ir_4 clusters stabilized by calixarene-phosphine ligands. Nine CO ligands are at first attached to the Ir_4 clusters. The CO ligands attached to the basal-plane Ir atoms can be removed with a thermal or gas-flowing treatment, creating "CO vacancy" sites that can take up new CO molecules, but prevent ethylene adsorption. Alternatively, the CO ligands attached to the apical Ir atom can be removed by reactive decarbonylation, creating a CO vacancy site that can bind both CO and ethylene. (b,c) Molecular graphics: Lowest free-energy structures of ethylene bonded to apical (b) and basal-plane (c) Ir atoms, in the calixarene-phosphine capped Ir_4 cluster. Adapted with permission from ref 280. Copyright 2014 Macmillan Publishers Limited, part of Springer Nature.

DOI: 10.1021/acs.chemrev.7b00776
Chem. Rev. 2018, 118, 4981−5079

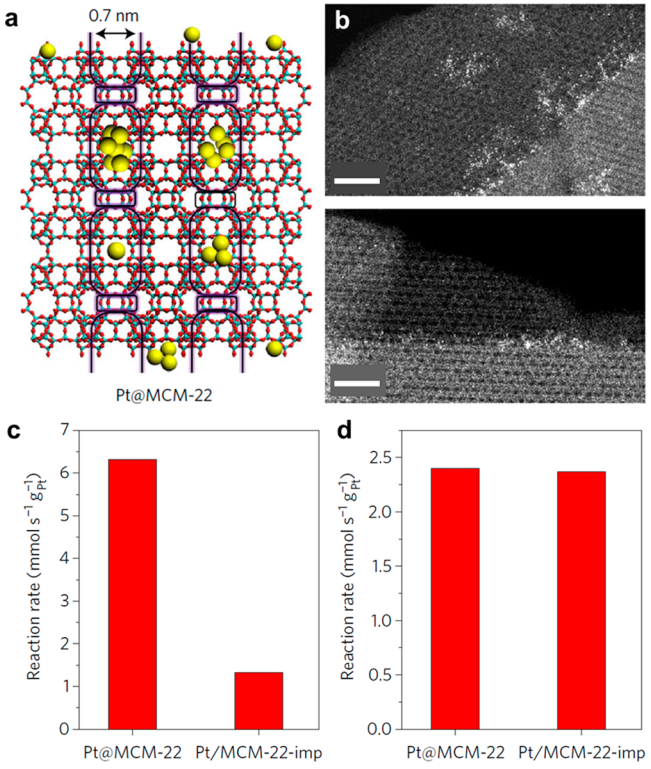

Figure 53. (a) Encapsulation of subnanometric Pt species in MCM-22 zeolite during the transformation of two-dimensional zeolite into three-dimensional. (b) High-resolution STEM images of Pt@MCM-22 catalyst, showing the presence of subnanometric Pt species (including Pt single atoms and Pt clusters). (c) Catalytic activity of Pt@MCM-22 and Pt/MCM-22-imp for hydrogenation of propene. (d) Catalytic activity of Pt@MCM-22 and Pt/MCM-22-imp for hydrogenation of isobutene. Adapted with permission from ref 282. Copyright 2017 Macmillan Publishers Limited, part of Springer Nature.

sample was located in the internal space of MCM-22 zeolite, resulting in size-selective catalytic properties.

As we have discussed in the part of the generation of supported metal clusters, bimetallic clusters can be prepared in a controllable way through the thermal decomposition of bimetallic or trimetallic organometallic clusters. Thomas et al. have carried out systematic work on the catalytic properties of bimetallic and multimetallic clusters for selective hydrogenation reactions.[283] The composition of the bimetallic clusters and the reaction scopes are described in Figure 54. In those reactions, it is clearly demonstrated that the reactivity and selectivity of metal clusters are tunable by the chemical composition. For example, for the hydrogenation of benzoic acid, nearly 100% selectivity to hydrogenation of the aromatic ring was achieved with $Ru_{10}Pt_2$ clusters, giving cyclohexanecarboxylic acid as product, while the other Ru-based bimetallic clusters gave products of partial hydrogenation. More interestingly, when Ru_6Sn clusters were used as catalysts for hydrogenation of 1,5-cyclooctadiene, only cyclooctene was obtained with 100% selectivity, while other Ru-based bimetallic clusters could give full hydrogenation product (cyclooctane) in some extent. These results demonstrate that the selectivity of metal clusters can be modulated by addition of a second metal component.

The catalytic performances of bimetallic clusters can be further tuned by adding a third metal.[284] Trimetallic Ru_5PtSn clusters were immobilized in mesoporous Davison silica (with a pore diameter of 3.8 nm) and used as catalyst for hydrogenation of dimethyl terephthalate (DMT). As compared to RuPt bimetallic clusters, the introduction of Sn can improve the activity and selectivity to desired products, simultaneously.[285]

Hydrogenation of syngas (CO, CO_2, and H_2) to methanol is an important industrial reaction, and the world's demand for methanol keeps increasing. So far, this reaction is performed on $Cu/ZnO/Al_2O_3$ catalyst under high pressure (50−100 bar), which consumes plenty of energy. Therefore, developing new catalysts for CO and CO_2 hydrogenation to methanol under mild conditions is of great importance for a sustainable future.[286,287] Moreover, when using CO_2 as a carbon source, designing more efficient catalysts to minimize the production of CO via the reverse water−gas shift reaction pathway is also important for a more efficient process.[288] Liu et al. have shown the promising catalytic performance of size-selected Cu_4 clusters for CO_2 hydrogenation under mild conditions.[289] As shown in Table 5, Cu_4 clusters deposited on Al_2O_3 showed higher turnover rates than the reported nanoparticulate catalysts. Especially, the production of methane was negligible, indicating the unique catalytic properties of Cu_4 clusters. Theoretical calculations show that, due to the different geometric structures of Cu_4 clusters as compared to conventional Cu nanoparticles, the methanation of CO_2 was not favorable. However, the selectivity to CO from the reverse water−gas shift reaction as well as the stability of subnanometric Cu clusters were not mentioned in this work.

In classic Fischer−Tropsch (F−T) synthesis, metal nanoparticles (such as Co, Fe, Ru, etc.) serve as the active species for $CO+H_2$ or CO_2+H_2.[290] Recently, it was reported that subnanometric Co clusters were also active for F−T synthesis and the activity and selectivity of Co clusters could be tuned by the cluster size and the supports.[291] As shown in Figure 55, small Co_4 clusters showed lower activity for F−T synthesis. In the case of larger Co_{27} clusters supported on ultrananocrystalline diamond (UNCD), better activity and higher selectivity to C_{4-8} products were obtained as compared to Co_4 clusters supported on Al_2O_3 and MgO. The cluster−support interaction could affect the binding energies of intermediates on Co clusters, which led to their different activity and selectivity. Notably, the selectivity to higher hydrocarbons (C_{4+}) was much lower than those obtained in the conventional F−T process, which may be caused by the much lower reaction pressure in this work.

Subnanometric Fe clusters can also serve as the active sites for F−T synthesis.[292] Partially reduced FeO_x clusters supported on CeO_2 nanorods showed performance comparable to that of other reported Fe-based catalysts (containing Fe nanoparticles). Spectroscopic characterizations indicate that the chemical states of FeO_x clusters and the interaction between Fe and CeO_2 support play a key role on the activity and selectivity of this catalyst for F−T synthesis.

Noble metal catalysts such as Pt- and Pd-based are widely used heterogeneous catalysts for the hydrogenation of unsaturated bonds (like C═C, C═O, etc.) in organic compounds, while it has been found recently that Fe- and Co-based non-noble metal catalysts can also work under similar mild conditions as noble metal catalysts.[293] However, the catalytic active species are not clearly identified due to the complexity of the catalytic process in solution and the dynamic structural transformation of the precatalyst under reaction conditions.

There is some experimental proof on the in situ transformation of organometallic compounds into metal nanoparticles, which can work as the active sites for hydrogenation reactions.[294] In a recent work, Gieshoff et al. have isolated series of subnanometric Fe clusters (Fe_4, Fe_6, and Fe_7) from the reaction mixture when

DOI: 10.1021/acs.chemrev.7b00776
Chem. Rev. 2018, 118, 4981−5079

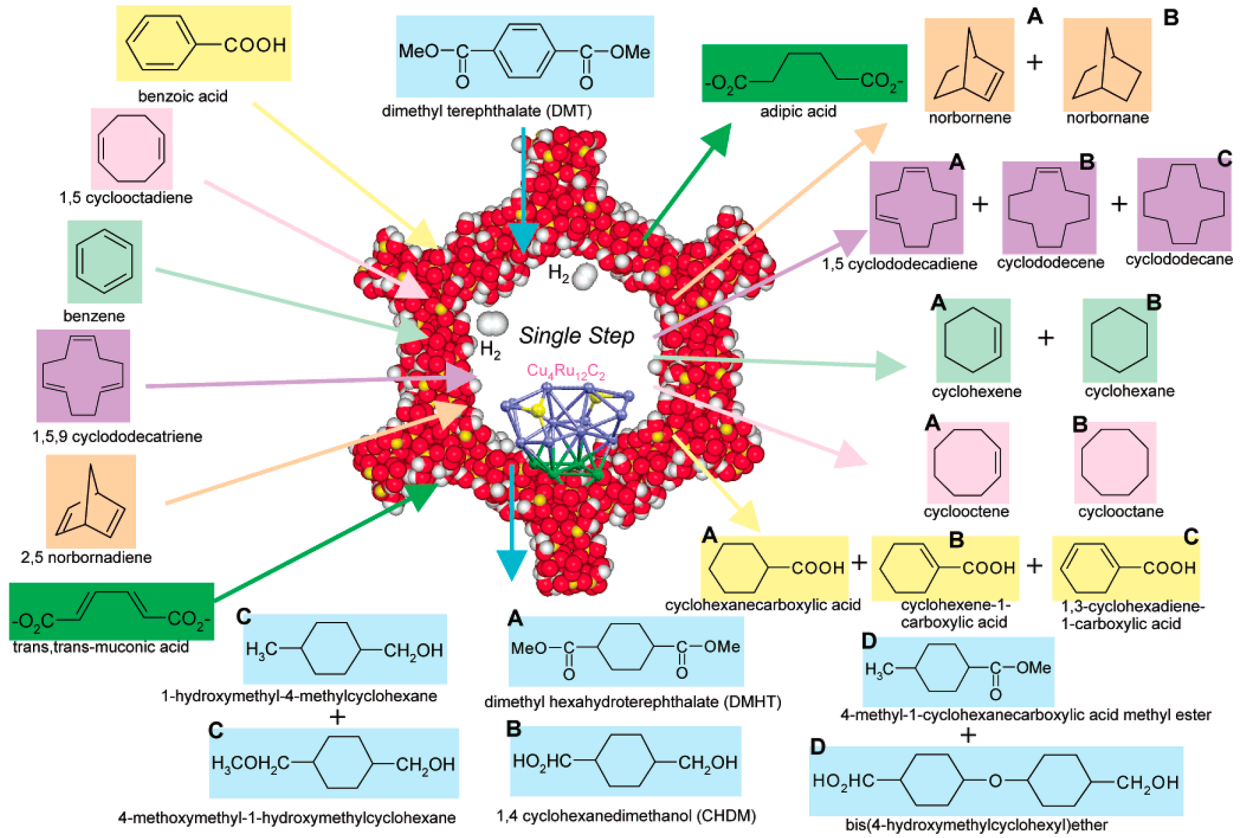

Figure 54. Single-step hydrogenation of some organic compounds using bimetallic cluster catalysts ($Cu_4Ru_{12}C_2$, in this case) supported on mesoporous solid carriers. Adapted with permission from ref 283. Copyright 2003 American Chemical Society.

Table 5. Comparison of TOR/TOF in the Present Work and in Previous Studies[a]

catalyst	temperature (°C)	total pressure (atm)	partial pressure of H_2 (atm)	partial pressure of CO_2 (atm)	max TOR/TOF of CH_3OH (s^{-1})
Cu_4/Al_2O_3	225	1.25	0.038	0.013	4.0×10^{-4}
Ni_5Ga_3/SiO_2	200−220	1	0.75	0.25	6.7×10^{-5}
$Cu/ZnO/Al_2O_3$	200−220	1	0.75	0.25	6.7×10^{-5}
Cu foil	237	5	4.6	0.4	1.2×10^{-3}

[a]Adapted with permission from ref 289. Copyright 2015 American Chemical Society.

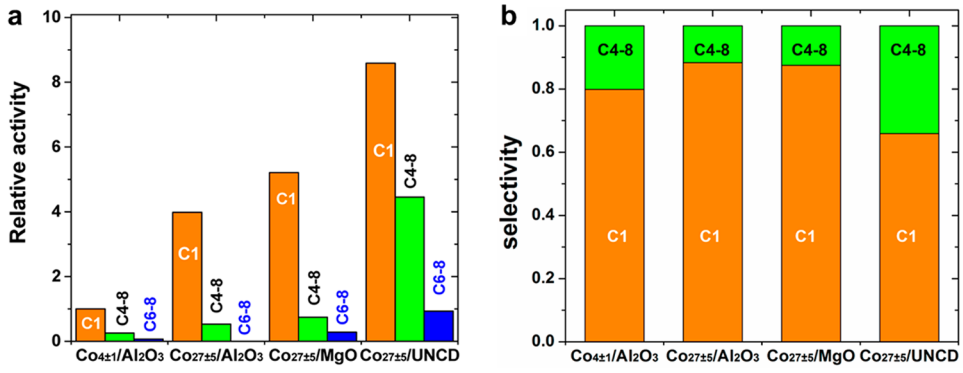

Figure 55. Catalytic performance for Fischer−Tropsch synthesis on Co_4 and Co_{27} clusters supported on various supports. $Co_{4±1}/Al_2O_3$, $Co_{27±5}/Al_2O_3$, $Co_{27±5}/MgO$, and $Co_{27±5}/UNCD$ at 225 °C (feed compostion, H_2:CO:He = 1:0.5:98.5, p_{H2} = 0.01 bar, p_{CO} = 0.005 bar). (a) Relative activity of different catalysts with respect to methane produced on the $Co_{4±1}/Al_2O_3$ sample. (b) Selectivity to methane and higher hydrocarbons. In this case, only methane and C4−8 are considered for calculating the selectivity. The reactivity of various cluster catalysts is normalized by the number of total deposited Co atoms. Adapted with permission from ref 291. Copyright 2015 American Chemical Society.

using mononuclear Fe compound as the precatalyst in the presence of ligands for hydrogenation of alkenes.[295] Kinetic studies and structural analysis showed that those subnanometric Fe clusters were more efficient than Fe nanoparticles and were able to perform hydrogenation of alkenes under very mild conditions (1−4 bar of H_2 at 20 °C), being promising substitutes

DOI: 10.1021/acs.chemrev.7b00776
Chem. Rev. 2018, 118, 4981−5079

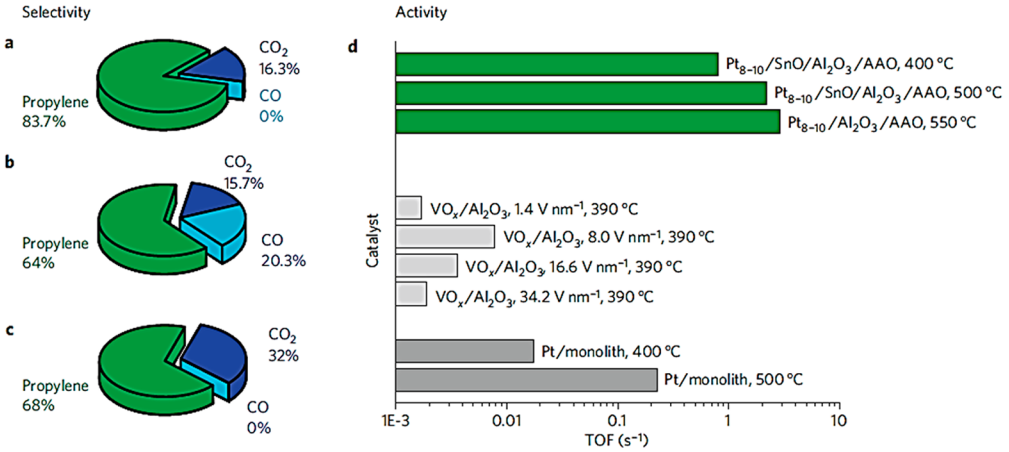

Figure 56. Catalytic performances of Pt-based and VO_x/Al_2O_3 catalysts for oxidative dehydrogenation of propane to propene. (a–c) Selectivity to different products by the Pt_{8-10} clusters deposited on various supports catalysts at different temperatures: (a) Pt clusters on SnO/Al_2O_3 at 400 °C, (b) SnO/Al_2O_3 at 500 °C, and (c) Al_2O_3 at 550 °C. (d) TOFs of propene produced on the Pt_{8-10} catalysts (green) and conventional VO_x/Al_2O_3 and Pt/monolith catalysts for oxidative dehydrogenation of propane to propene. The TOF values have already been normalized to single metal atoms in all catalysts. Adapted with permission from ref 300. Copyright 2009 Macmillan Publishers Limited, part of Springer Nature.

for noble metal catalysts. Considering that there are also reports on the application of Co-, Ni-, and Mn-based organometallic complexes as catalysts for hydrogenation of unsaturated bonds, it can be speculated that the active species under reaction conditions may also be different from the starting complexes.[296−298] It will be necessary to study the structural transformation of organometallic complexes under reaction conditions and identify their atomic structures.

5.4. Dehydrogenation Reactions

The production of light alkenes from dehydrogenation of alkanes is an important route for chemical industry.[299] Currently, metal nanoparticles such as Pt supported on metal oxides are used in industrial plants for dehydrogenation of propane to propene. The dehydrogenation of alkanes is an endothermic process, which requires a large consumption of energy. Therefore, developing new stable and active catalyst for dehydrogenation reaction, especially if they are based on non-noble metals or they are coupled with other reactions or separation systems that allow one to shift the dehydrogenation equilibrium, is a matter of much interest.

Vajda et al. deposited size-selected Pt clusters on anodized aluminum oxide (AAO, Anopore) membranes modified with Al_2O_3 and SnO and used this material for oxidative dehydrogenation of propane to propene.[300] The product distributions and a comparison of catalytic performance between Pt_{8-10} clusters and traditional catalysts (VO_x/Al_2O_3 and Pt/monolith) are presented in Figure 56. Pt clusters (Pt_{8-10}) on various supports showed very high activity as well as high selectivity to propene, being 40−100 times more active for the oxidative dehydrogenation of propane than conventional Pt-based and V-based catalysts. According to DFT calculations, Pt atoms with unsaturated coordination sites in Pt_{8-10} clusters favor the dissociation of C−H bonds rather than C−C or C═C bonds. Therefore, lower amounts of CO_2 and CO were produced on subnanometric Pt clusters rather than on Pt nanoparticles.

In a recent work, Anderson et al. have studied the dehydrogenation of ethylene to acetylene on size-selected Pt clusters (Pt_4, Pt_7, and Pt_8 clusters).[301] It was found that Pt_7 clusters showed the highest activity for ethylene dehydrogenation, while Pt_4 and Pt_8 clusters showed similar activity. Experimental results and theoretical calculations indicate that the bonding of ethylene with Pt_7 clusters is stronger than that with Pt_4 and Pt_8 clusters. On the other hand, the higher affinity of Pt_7 clusters to ethylene molecules will lead to faster deactivation and agglomeration of Pt_7 clusters due to coke formation.

Non-noble metal clusters can also work for dehydrogenation reactions, and it has been found that Co clusters were active for the oxidative dehydrogenation of cyclohexene.[302] $Co_{27\pm4}$ clusters were deposited on various metal oxide supports (Al_2O_3, ZnO, and TiO_2 and MgO) to study the influence of support on the catalytic performances. Co clusters supported on MgO showed the highest initial reactivity to formation of benzene for the dehydrogenation of cyclohexane. The strong interaction between Co clusters and MgO may facilitate the dehydrogenation of cyclohexene. However, Co clusters supported on MgO deactivated with time on stream, due to the formation of a Co−Mg−O solid solution at high temperatures. After comparing four supports (Al_2O_3, ZnO, MgO, and ultrananocrystalline diamond), the diamond support was found to be the best support for Co clusters during cyclohexane dehydrogenation.[303] It is proposed in that work that the different surface properties of various supports account for their different catalytic behavior.

So far, there are no reports on nonoxidative dehydrogenation of alkanes with subnanometric metal clusters, which is probably due to the low stability of subnanometric metal clusters at high temperature. In the absence of oxygen, subnanometric metal clusters may agglomerate into nanoparticles, which serve as the active sites for nonoxidative dehydrogenation of alkanes. It can be expected that, if subnanometric metal clusters can be stabilized on a suitable support under the dehydrogenation reaction conditions, higher activity may be achieved on those clusters.

5.5. deNO$_x$ Reactions

Pt-group metal catalysts (including Pt, Pd, and Rh) are the main active components of industrial three-way catalysts. Because the metal components mainly exist as nanoparticles, developing new catalysts with smaller metal crystalline size and higher activity as well as the introduction of non-noble metals to save the use of noble metals is an active research field. Heiz et al. have studied in an UHV system the catalytic properties of size-selected Pd_n clusters ($4 \leq n \leq 30$) deposited on MgO(100) for NO+CO, that is, $2NO + 2CO \rightarrow N_2 + 2CO_2$, as a model reaction for deNO$_x$

DOI: 10.1021/acs.chemrev.7b00776
Chem. Rev. 2018, 118, 4981−5079

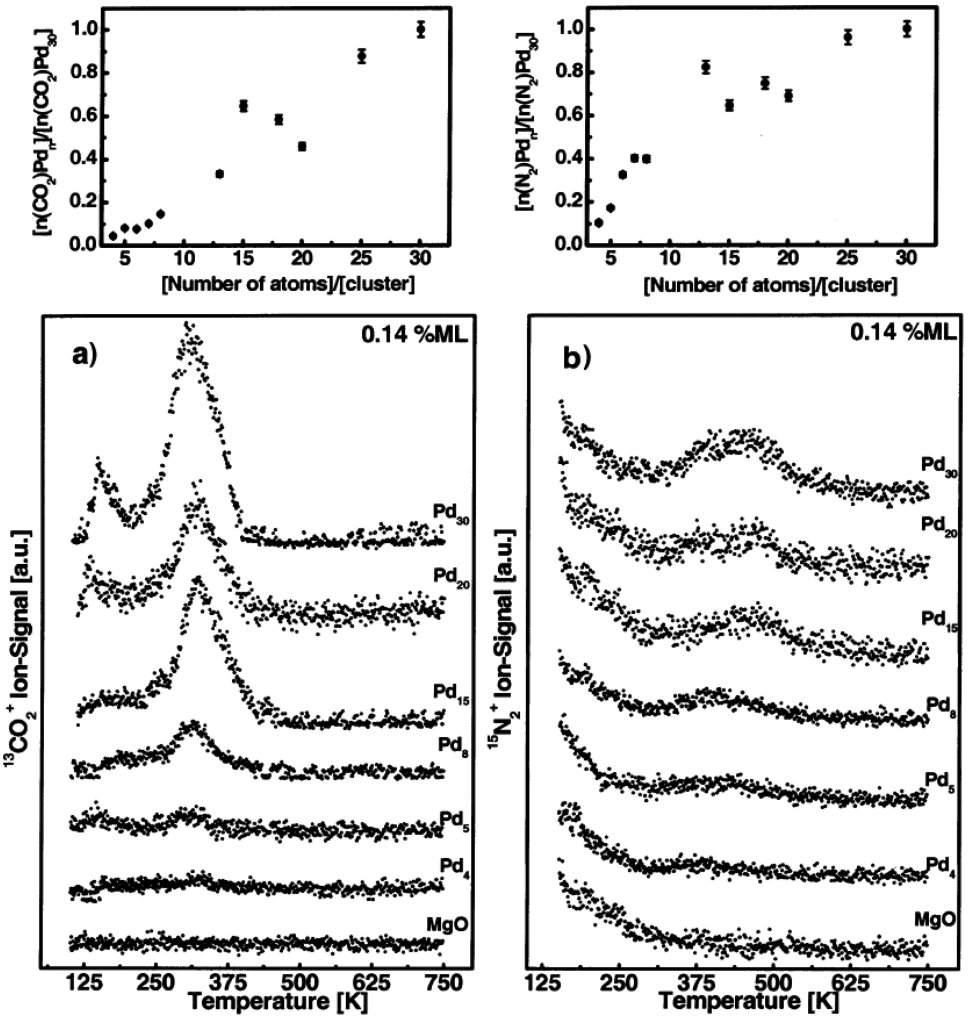

Figure 57. Temperature programed reaction (TPR) profiles of the reaction products $^{13}CO_2$ and $^{15}N_2$ as a function of cluster size. The Pd clusters were deposited on a clean MgO film and then were first exposed to ^{13}CO and then to ^{15}NO at 90 K. The activity of various Pd clusters for $^{13}CO_2$ and $^{15}N_2$ expressed as the number of product molecules formed per cluster and normalized to the reactivity of Pd_{30} are presented. Adapted with permission from ref 304. Copyright 2004 American Chemical Society.

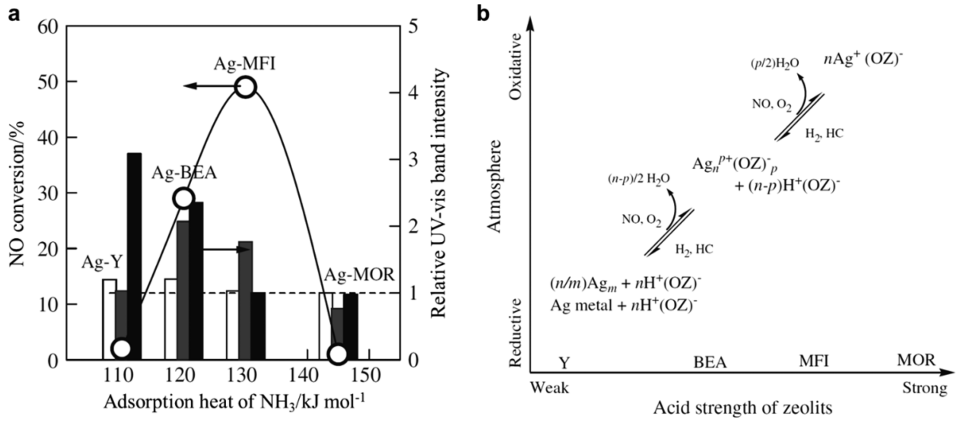

Figure 58. (a) Increment of NO conversion for C_3H_8-SCR with 0.5% H_2 at 573 K as compared to the activity obtained in the absence of H_2 as a function of adsorption heat of NH_3 on H-form zeolites (○). The bars represent the intensity of UV−vis bands corresponding to different types of Ag species: 212 nm (Ag^+, white bar), 260 nm ($Ag_n^{\delta+}$ cluster, gray bar), and 312 nm (metallic Ag_m cluster, black bar) under C_3H_8-SCR with 0.5% H_2. Those intensity values have already been normalized to those bands obtained on the same catalyst under similar reaction conditions but in the absence of H_2. (b) Schematic diagram of the evolution of Ag species, depending on the acidity of zeolite support and the reaction atmosphere. (OZ) represents the zeolite ion-exchange site in this figure. Adapted with permission from ref 310. Copyright 2005 Springer, Inc.

DOI: 10.1021/acs.chemrev.7b00776
Chem. Rev. 2018, 118, 4981−5079

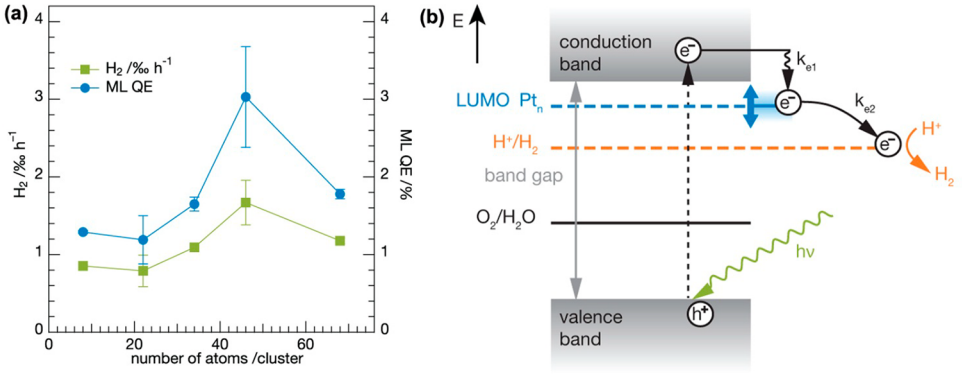

Figure 59. (a) Influences of Pt particle size on photocatalytic activity of the CdS nanorods with size-selected Pt clusters as cocatalysts. The average H_2 evolution rate as well as the quantum efficiency clearly change with the size of Pt clusters. (b) Schematic illustration of the generation of electrons and holes in CdS after excitation by light. The photogenerated electrons will transfer to Pt clusters and then catalyze the reduction of protons for the evolution of H_2. Adapted with permission from ref 313. Copyright 2012 American Chemical Society.

application.[304] The temperature programed reaction (TPR) profiles of the reaction products $^{13}CO_2$ and $^{15}N_2$ as a function of cluster size are shown in Figure 57. In the case of Pd_4 clusters, almost no product was observed. When the atomicity increased from 5 to 30, the activity based on the production of CO_2 at 300 K also increased gradually with the particle size, except for a relative drop between Pd_{15} and Pd_{20}. Interestingly, the formation of $^{13}CO_2$ was readily observed at very low temperature (140 K) when the atomicity was larger than 20. For Pd_n ($n \leq 20$) clusters, the NO+CO reaction could only occur at >300 K. It was proposed that adsorption and dissociation of NO can be the rate-determining step in this reaction. According to their results from FT-IR study, the authors have proposed two different reaction mechanisms for reaction temperatures of 140 and 300 K, respectively. At higher temperature, NO can be dissociated to atomic N and O bonded to Pd clusters. CO can be oxidized to CO_2 by atomic oxygen. However, at low temperature, the oxidation of CO can only occur through the adsorbed molecular NO. For Pd clusters with atomicity below 20, NO adsorption is not favorable, resulting in their low activity below 300 K.[305] The adsorption and dissociation of NO on Pd clusters with different sizes was also investigated by means of theoretical calculations.[306,307] Those works indicate that both the electronic and the geometric structures of Pd clusters will affect the interaction between Pd and substrate molecules, which further affects the reaction pathway, especially at different temperature range.

Ag-based catalysts also perform very well for selective catalytic reduction of NO by hydrocarbons (HC-SCR), and can serve as a substitute for expensive Pt-group catalysts.[308] Among different types of supported Ag catalysts, Ag/zeolite catalysts (usually prepared by ion-exchange process) show promising activity and stability for HC-SCR reaction.[309,310] As shown in Figure 58a, the addition of H_2 in the feed gas can significantly promote the NO conversion in C_3H_8-SCR reaction. The evolution of Ag species under reaction conditions was followed by EXAFS and UV−vis spectroscopy. In the case of Ag supported on zeolites with weaker acidity, Ag species tend to form metallic Ag nanoparticles under reaction conditions while they tend to form cationic Ag species on zeolites with stronger acidity. By correlating the activity with the contributions of different types of Ag species in various Ag/zeolite catalysts (see Figure 58b), it is proposed that positive charged Ag clusters (Ag_4^{2+} on average) are the active sites for HC-SCR reaction. Dynamic structural transformation of Ag species can occur when tuning the reaction conditions. By tuning the atmosphere (reductive or oxidative), the atomicity and chemical states of Ag species can be modulated, which will further affect the catalytic properties in the HC-SCR reaction.

5.6. Photocatalytic Reactions

In photocatalytic reactions such as water splitting and CO_2 reduction, metal nanoparticles are usually used as cocatalysts. Similarly, metal clusters can also work as cocatalysts. It has been well demonstrated that the size of metal cocatalysts has significant influence on the photocatalytic properties.[311,312] With suitable particle size, the promotion effect of metal species can be maximized for photocatalytic reactions.

Pt is widely used as a cocatalyst in heterogeneous photocatalysts, especially for the photocatalytic water splitting to produce H_2. In some works, Pt clusters were prepared through a simple coprecipitation method for the study of size effects on the photocatalytic H_2 evolution reaction. However, the Pt clusters obtained by this method presented wide size distributions, which are not ideal model catalysts for fundamental studies. To properly discuss the metal size effects, Berr et al. employed size-selected Pt nanoclusters with different sizes as cocatalysts on CdS nanorods for photocatalytic H_2 production.[313] As shown in Figure 59a, H_2 evolution efficiency below 1‰ h^{-1} was obtained for smaller clusters (Pt_8 and Pt_{22}), and this value increased to over 1‰ h^{-1} for Pt_{34}. After reaching a maximum H_2 production rate for Pt_{46} nanoclusters, the H_2 production rate dropped for Pt_{68}. Considering the reaction mechanism presented in Figure 59b, the catalytic efficiency was mainly associated with the higher charge separation efficiency between CdS and Pt nanoclusters, which is further related to the electronic structure of Pt nanoclusters. As it is known, the electronic structure (especially the position of lowest unoccupied molecular orbitals, LUMO) of metal clusters is strongly dependent on the atomicity of clusters. Therefore, by tuning the size, the charge-transfer process between CdS and Pt nanoclusters can be modulated, which would further affect the photocatalytic performance.[314] On the other hand, the reduction of protons to H_2 on Pt nanoclusters is also related to the electronic structure of Pt. The LUMO of Pt nanoclusters has to be higher than the H^+/H_2 redox potential. Therefore, Pt_{46} may have the suitable LUMO positions, which can facilitate the electron transfer from CdS to Pt_{46} nanoclusters and the subsequent reduction of H^+ to H_2.

Similarly, the size effects on the photocatalytic activity can also be reflected on Au nanoclusters.[315] Au_n clusters (n = 10−39) have been loaded on $BaLa_4Ti_4O_{15}$ as the cocatalyst for overall

DOI: 10.1021/acs.chemrev.7b00776
Chem. Rev. 2018, 118, 4981−5079

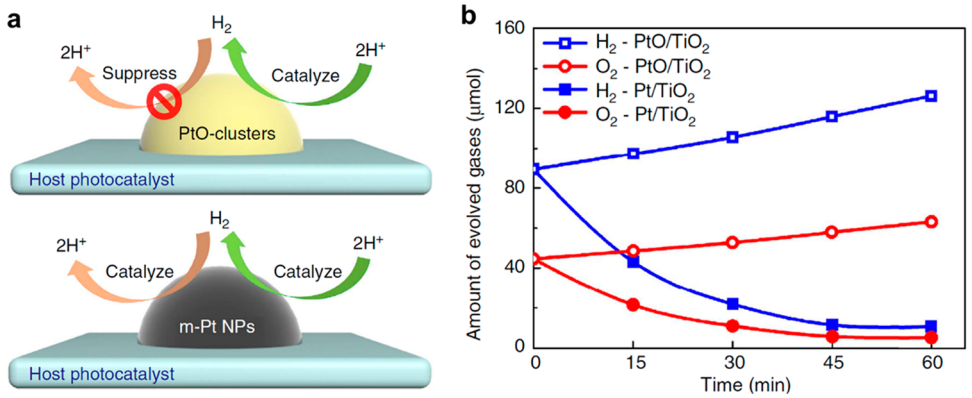

Figure 60. (a) Schematic illustration of the H_2 evolution and the H_2 oxidation by O_2 on PtO clusters and metallic Pt nanoparticles, respectively. (b) Evolution of the amount of H_2 and O_2 on PtO/TiO_2 and Pt/TiO_2 photocatalysts under ultraviolet−visible light irradiation (>300 nm). In a typical experiment, 2 mL of H_2 and 1 mL of O_2 were injected into the reaction cell for photocatalytic water splitting at time zero. Adapted with permission from ref 316. Copyright 2013 Macmillan Publishers Limited, part of Springer Nature.

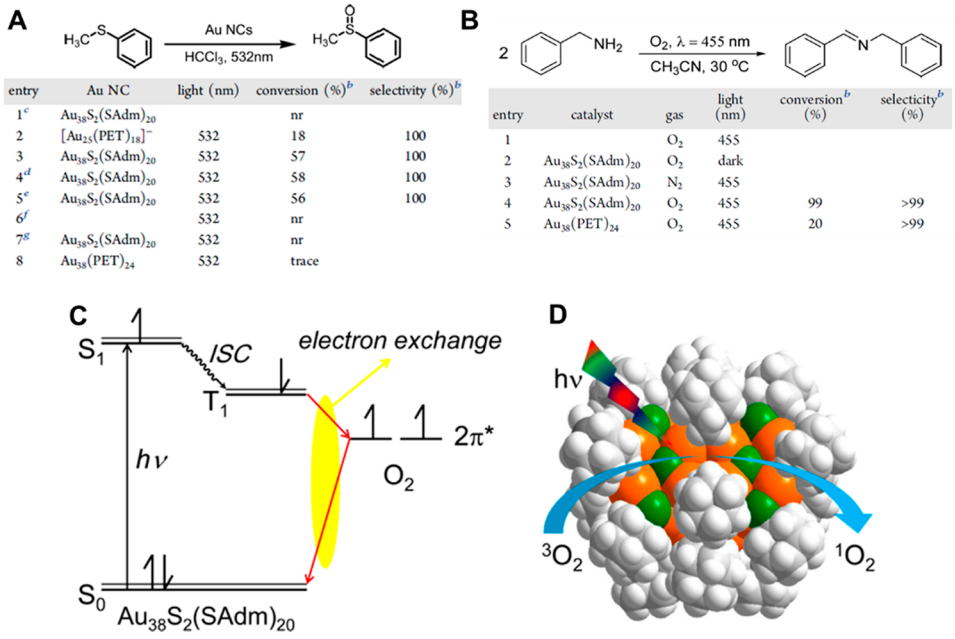

entry	Au NC	light (nm)	conversion (%)[b]	selectivity (%)[b]
1[c]	$Au_{38}S_2(SAdm)_{20}$		nr	
2	$[Au_{25}(PET)_{18}]^-$	532	18	100
3	$Au_{38}S_2(SAdm)_{20}$	532	57	100
4[d]	$Au_{38}S_2(SAdm)_{20}$	532	58	100
5[e]	$Au_{38}S_2(SAdm)_{20}$	532	56	100
6[f]		532	nr	
7[g]	$Au_{38}S_2(SAdm)_{20}$	532	nr	
8	$Au_{38}(PET)_{24}$	532	trace	

entry	catalyst	gas	light (nm)	conversion[b] (%)	selectivity[b] (%)
1		O_2	455		
2	$Au_{38}S_2(SAdm)_{20}$	O_2	dark		
3	$Au_{38}S_2(SAdm)_{20}$	N_2	455		
4	$Au_{38}S_2(SAdm)_{20}$	O_2	455	99	>99
5	$Au_{38}(PET)_{24}$	O_2	455	20	>99

Figure 61. (A) Comparison of catalytic activity of different types of Au clusters for selective oxidation of methyl phenyl sulfide to sulfoxide under visible light (532 nm). (B) Photocatalytic oxidation of benzylamine to imine in the presence of O_2 and $Au_{38}S_2(SAdm)_{20}$ clusters under LED irradiation (455 nm) at 30 °C. (C) Illustration of Dexter-type electron exchange coupling between Au_{38} cluster and O_2 for the generation of singlet O_2. (D) Schematic illustration of conversion of $^3O_2$ to $^1O_2$ on $Au_{38}S_2(SAdm)_{20}$ clusters under light irradiation. Adapted with permission from ref 318. Copyright 2017 American Chemical Society.

water splitting. It was found that the photoactivity decreased slowly with the size of Au nanoclusters. Notably, all of the catalysts with Au clusters as cocatalysts showed significantly higher activity than Au nanoparticles.

Nevertheless, the oxidation state of metal clusters can also affect the photocatalytic H_2 evolution activity. In a recent work, Yang et al. have prepared two kinds of Pt−TiO_2 catalysts for water splitting: PtO/TiO_2 and Pt/TiO_2. The size of the Pt species was below 1 nm and was mainly located on the {001} facets of TiO_2 nanosheets. As described in Figure 60a, PtO clusters can work as the reduction sites for H_2 evolution and simultaneously suppress the oxidation of H_2 by O_2. However, in the case of metallic Pt nanoparticles as cocatalyst, both H_2 evolution and H_2 oxidation could occur on Pt nanoparticles. As it can be seen in Figure 60b, when PtO/TiO_2 was used as catalyst, the amount of H_2 was continuously increasing under light irradiation, indicating that H_2 was produced from the photocatalytic water splitting and the amount of H_2 evolved from water splitting was more than that consumed by the side oxidation reaction. However, in the case of Pt/TiO_2, the amount of H_2 decreased with the reaction time, suggesting that the oxidation of H_2 by O_2 was the dominating reaction.[316,317] On the basis of DFT calculations, it is proposed that oxidized Pt clusters can make the overall water splitting possible because O_2 dissociation over PtO clusters is not favorable, and thus the back reaction (H_2+O_2) is suppressed.

Besides water splitting, it has also been reported that Au clusters can work as photocatalysts for selective oxidation reaction.[318] In a recent work, Li et al. have presented the catalytic properties of thiolate-protected Au clusters for aerobic oxidation of phenyl sulfide and benzylamine. As shown in Figure 61, in the presence of visible light generated by a LED lamp, the aerobic

DOI: 10.1021/acs.chemrev.7b00776
Chem. Rev. 2018, 118, 4981−5079

oxidations could be achieved with Au clusters. However, no reaction occurred without light irradiation. Mechanistic studies showed that singlet oxygen was the active species, and they were generated on Au clusters under visible light through a Dexter-type electron exchange coupling mechanism. Besides, the catalytic performance of Au clusters was related to their ligands, which maybe related to the electronic structure. Taking into consideration that the electronic structures of Au clusters are greatly dependent on the particle size and nature of the ligands, their photocatalytic properties can be modulated by tuning the preparation conditions. Nevertheless, as we have mentioned before, the stability of thiolate-protected Au clusters is a critical issue under reaction, and in this referred work, the stability of the Au clusters under photocatalytic aerobic oxidation conditions was not mentioned.

5.7. Electrocatalytic Reactions

By employing size-selected Pt clusters as model catalysts, Anderson et al. have performed systematic studies on the size-dependent electrocatalytic properties of Pt clusters.[319] In one of their publications, size-selected Pt_n clusters (n = 1−14) were deposited on indium tin oxide (ITO) for electrocatalytic ethanol oxidation reaction (EOR).[320] As shown in Figure 62b, the EOR

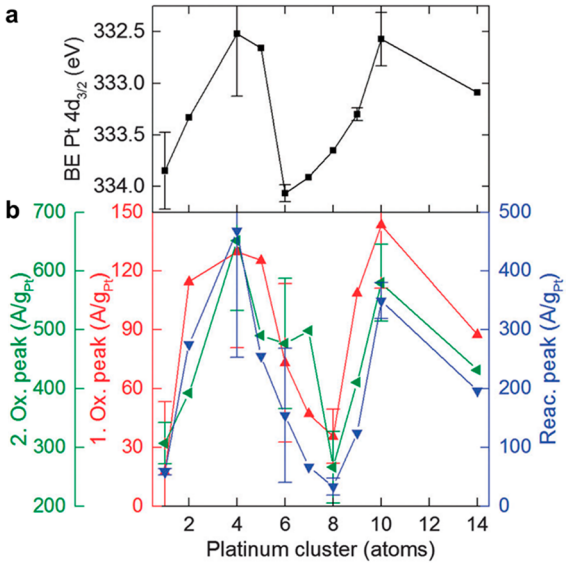

Figure 62. (a) Binding energy of Pt $4d_{3/2}$ in XPS spectra of Pt clusters with various sizes. (b) The electrocatalytic activity of Pt clusters with different atomicity for ethanol oxidation reaction (EOR). Red plot, first oxidation peak; green plot, second oxidation peak; blue plot, reactivation peak. Higher peak current corresponds to higher activity in EOR. Adapted with permission from ref 320. Copyright 2016 American Chemical Society.

activity of Pt clusters varied with their atomicity, and Pt_4 and Pt_{10} clusters showed the highest activity among them, which was also, based on normalized mass activity, much higher than conventional nanoparticulate Pt catalysts. Interestingly, the variation trend of Pt clusters for EOR can be well correlated with the binding energy of Pt $4d_{3/2}$ in XPS spectra (see Figure 62a), indicating that the electronic structures of Pt clusters may be the key factor that affects the electrocatalytic properties. Pt clusters with a lower binding energy correspond to electron-rich Pt species, which may further affect the activation of ethanol molecules at the electrode−substrate interface, and the electron-transfer process between Pt clusters and ethanol.

Size-selected Pt clusters have also been used as model catalysts for oxygen reduction reaction (ORR). It has been found that Pt_7, Pt_{10}, and Pt_{11} clusters supported on glassy carbon electrodes can catalyze the ORR with activity similar to that of conventional nanoparticulate Pt catalysts.[321] However, when other Pt clusters (such as Pt_4) were used as catalysts, low ORR activity was observed, while oxidation of carbon by water occurred on those catalysts. Considering the anomalous high Pt $4f_{7/2}$ core level binding energy of those three Pt clusters (Pt_7, Pt_{10}, and Pt_{11}), their unique electronic structures may be the reason for their distinct catalytic behaviors. However, when Pt clusters are deposited on indium tin oxide (ITO) electrodes for ORR, Pt clusters prefer to catalyze the two-electron reduction process to H_2O_2 instead of the four-electron reduction process to H_2O like in the case of conventional Pt nanoparticles.[322] When size-selected Pt clusters were deposited on glassy carbon substrate, the ORR activity was not only dependent on the particle size, but also dependent on the proximity of Pt clusters (the distance between the particles to each other).[323] As shown in Figure 63,

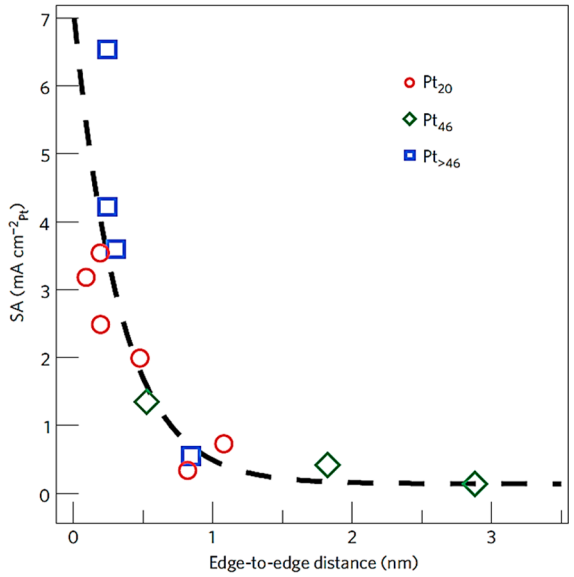

Figure 63. Relationship between specific activity (determined at 0.85 V) and edge-to-edge distance for Pt_{20}, Pt_{46}, and $Pt_{>46}$ clusters. The activity is plotted versus the average nearest edge-to-edge distance calculated from the nanocluster density assuming a random nanocluster distribution on the glassy carbon surface. Adapted with permission from ref 323. Copyright 2013 Macmillan Publishers Limited, part of Springer Nature.

when Pt clusters were in closely packed assembly on the electrode surface, their activity would approach to the surface activity of bulk Pt. On the basis of theoretical simulations, it was proposed that the increase in the activity should be related to a change of the electric double layer (EDL) structure and its potential distribution.

Size-selected Pd clusters can also be efficient electrocatalysts, and Vajda et al. have measured the electrocatalytic properties of Pd_n clusters (n = 4, 6, 17) for ORR.[324] It was found that Pd_4 shows no reaction, while Pd_6 and Pd_{17} clusters were very active (in terms of turnover rate per single Pd atom). Theoretical calculations suggested that this large difference may demonstrate that bridging Pd−Pd sites (which are only present in three-dimensional clusters) were active for the oxygen evolution reaction with the Pd_6 cluster.

DOI: 10.1021/acs.chemrev.7b00776
Chem. Rev. 2018, 118, 4981−5079

As we have discussed before, the preparation methodology can have a significant influence on the catalytic properties of metal clusters. Yamamoto et al. have prepared a series of subnanometric Pt clusters with different sizes stabilized by dendrimers. In this way, the authors performed a fundamental study on the size effects of Pt clusters for ORR.[325] From a comparison of the catalytic properties of Pt_{12}, Pt_{28}, and Pt_{60} clusters, it can be seen that Pt_{12} clusters showed much higher mass activity than did Pt_{28} and Pt_{60}. Notable, Pt_{12} clusters showed 1 order of magnitude higher mass activity as compared to state-of-the-art Pt/C catalyst. Furthermore, the doping of Pt clusters with Sn also improves the specific mass activity significantly, indicating the synergistic effects for bimetallic clusters. Recently, a series of Pt clusters stabilized in dendrimer have been generated and compared for ORR.[326] As shown in Figure 64, oscillation of mass activity with

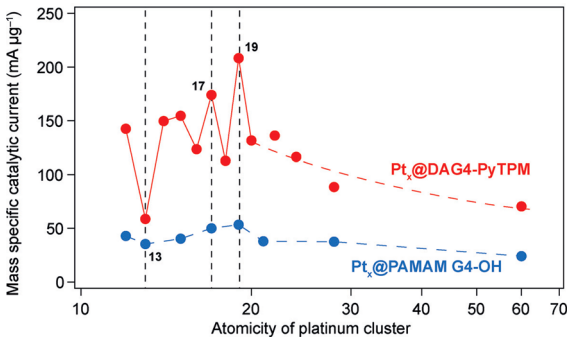

Figure 64. ORR activity of Pt clusters with different atomicity. These Pt clusters are prepared using dendrimer as template, and their atomicity can be tuned with high precision. Adapted with permission from ref 326. Copyright 2015 Wiley-VCH Verlag GmbH & Co. KGaA, Weinheim.

atomicity of Pt clusters has been observed. Notably, Pt_{17} and Pt_{19} clusters showed higher activity than the others. According to theoretical calculations, it was proposed that the rich edges sites in Pt_{17} and Pt_{19} contribute to their high activity. Nevertheless, it is highly interesting to observe that, although they have only one-atom difference, Pt_{12} clusters show almost 3-fold higher activity than Pt_{13} clusters.[327] To understand this effect, the geometric structures of Pt_{12} and Pt_{13} clusters were resolved by EXAFS. Pt_{13} clusters showed icosahedral shape, while Pt_{12} clusters appeared as double-layer structure with C_{2v} symmetry. According to the calculated oxygen adsorption energy, the binding energy of O_2 on Pt_{13} was much stronger than that on Pt_{12}, which would make the regeneration of the reduced surface difficult in the former during ORR.

Recently, Wang et al. have prepared Ag clusters protected by 2-mercaptobenzothiazole (MB) as electrocatalyst for ORR.[328] MALDI-TOF mass spectra showed that Ag clusters mainly consist of 2−5 Ag atoms. Electrocatalytic properties showed that these small Ag clusters exhibit superior activity over commercial Pt/C. Considering the low cost of Ag, they may be promising substitutes for Pt-based catalysts. Because the sizes of the O_2 molecule and protons are quite small, the blocking effect of thiolate-ligands seems not to be a problem for ORR. Therefore, electron transfer between the electrode and thiolate-protected metal clusters can be realized.[329]

Strong size effects on the oxygen reduction reaction activities are also observed on Au nanoclusters in ORR.[330] The overall limiting current density decreased with the increase of the size of Au nanoclusters, Au_{11} > Au_{25} > Au_{55} > Au_{140}. The catalytic performance of Au_{11} clusters was even comparable to that of commercial Pt/C catalyst, and the electrocatalytic properties of Au clusters were also related to their electronic property. The reaction pathway can be modulated through the electronic properties of metal clusters. When $Au_{25}(SR)_{18}$ clusters were negatively charged, about 90% production of H_2O_2 was achieved through two-electron reduction of O_2.[331] In another work, the electrocatalytic properties of Au_{25}^{q} clusters with different charge states (q = −1, 0, +1) have been tested with several model reactions.[332] These authors have found that negatively charged Au_{25}^{-} clusters showed enhanced activity in CO_2 reduction to CO, while positive charged Au_{25}^{+} clusters showed enhanced CO oxidation activity. Theoretical calculations demonstrate that the charge states of Au_{25} cluster can affect the adsorption and stabilization of intermediates, leading to the charge-dependent electrocatalytic performances.

Co_{27} clusters deposited on Fe_2O_3 film also showed activity for electrocatalytic water oxidation.[333] Stability tests showed that Co_{27} clusters were resistant to dissolution in harsh electrochemical water oxidation conditions and were also stable under solar light irradiation. The turnover rates for water oxidation on Co_{27} clusters were comparable to those reported for Pd- and Co-based nanoparticulate catalysts.

From a point view of electronic structure, metal clusters may show distinct catalytic behavior for electrocatalysis, especially for electrocatalytic reduction of CO_2 due to the complexity of products, which is dependent on the number of electrons transferred to CO_2 molecules. However, the stability of metal clusters at the electrode−electrolyte interface under electrocatalytic conditions, together with the production of metal clusters in large quantity with well-controlled atomicity, is still a challenge.

5.8. Catalysis with In Situ Formed Metal Clusters

5.8.1. In Situ Formed Pd Clusters. It is common to find that, in many catalytic reactions, a reaction induction period can be observed, and in situ evolution of the catalyst occurs during the catalytic processes. This means that the "real" catalyst is not the one initially added into the system. The in situ transformation of metal catalysts often occurs during liquid-phase organic reactions, as a consequence of the interactions between metal species, substrates, and solvent in the liquid phase. For some metal-catalyzed reactions, metal clusters can be in situ formed from the precursors (metal salts, transition metal complexes, or metal NPs), and those metal clusters will work as the "real" catalysts. In the following section, we will discuss a number of reports showing the reactivity and mechanistic studies of the metal clusters formed during the reactions.

One typical example about the dynamic transformation of metal species under reaction conditions is the evolution of Pd species for C−C coupling reactions. For the classic C−C coupling reaction using Pd-based catalysts, it has been reported that catalytic reactions can be initiated by virtually any source of Pd (Pd salts, Pd complexes, Pd NPs, Pd colloids, etc.).[334−336] Spectroscopic and high-resolution TEM have confirmed that leaching and recrystallization of Pd-based NPs occur under reaction conditions.[337−340] Subnanometric Pd species will leach from Pd NPs, resulting in the formation of Pd clusters, which can catalyze the C−C coupling reaction.[341] On the other hand, mononuclear Pd salts have also been found to aggregate to Pd clusters during the C−C coupling reactions.[342,343] These works infer that the real catalytic active species may be formed in situ during the reaction from different Pd sources. However, little is

DOI: 10.1021/acs.chemrev.7b00776
Chem. Rev. 2018, 118, 4981−5079

known about the nature of the in situ formed Pd species, including their size and their transformation pathway.

Recently, it has been presented that water-stabilized Pd_3 and Pd_4 clusters are excellent catalysts for C−C coupling reaction.[344] Nucleophilic molecules like water or amines can promote the formation of Pd clusters from Pd NPs and stabilize them. Those subnanometric Pd clusters show very high TOF and TON values for various C−C coupling reactions. When strongly bound ligands (like biaryl phosphines) are added to the reaction system, single Pd atoms can be coordinated by these ligands. These Pd complexes are highly active and can activate aryl chlorides that are considerably much less reactive than other aryl halides.[345] Thus, it seems that the existing state of Pd species under C−C coupling reaction conditions is dependent on the coordination environment, but the nature of the species formed is still unrevealed.

Because it was indicated that Pd clusters could play an important role in liquid-phase catalysis, Fu et al. prepared well-defined and highly stable $[Pd_3Cl(PPh_2)_2(PPh_3)_3]^+[SbF_6]^-$ clusters (named as Pd_3Cl clusters), and these Pd_3Cl clusters showed high activity for C−C coupling reaction while no induction period was observed, being consistent with previous works from Corma group.[346] In that work, a new mechanism was proposed for the classic Suzuki−Miyaura reaction (see Figure 65). In the classic mechanism, the oxidative addition of aryl

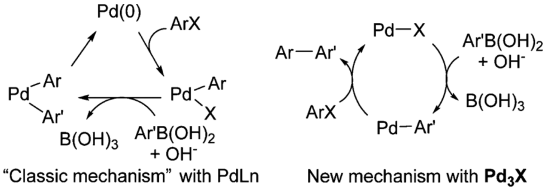

Figure 65. Comparison between the classic mechanism of Suzuki−Miyaura reaction and the newly proposed mechanism with Pd_3Cl clusters. Adapted with permission from ref 346. Copyright 2017 American Chemical Society.

halides on Pd(0) species is the initial step, followed by the transmetalation and reductive elimination. However, in situ EXAFS and mass spectroscopy led the authors to propose that the Pd_3Cl cluster first reacts with phenylboronic acid to generate the intermediate (Pd_3Ar). On the basis of the above works, plausible pathways of the Pd species transformation during the catalytic reaction have been proposed, and they are shown in Figure 66.[347,348]

When using Pd complexes as precursors, they may decompose in some cases, and Pd atoms can aggregate together to form Pd_nL_m clusters with simultaneous replacement of ligands and reduction of metal ions. These Pd clusters can also contribute, and, in some cases, be responsible for the final catalytic results. For reactions using Pd NPs as precursors, surface Pd atoms will detach to form Pd_nL_m clusters in the reaction solution through oxidative addition between Pd and the organic substrates. Probably, in the reaction environment, there is a dynamic transformation process between Pd complex, Pd clusters, and Pd NPs, depending on the concentration of the organic substrates and the products.

The in situ transformation of Pd species has also been found in various reactions.[349] For instance, Jiang et al. have reported the application of trinuclear Pd clusters for the conversion of CS_2 into CO_2 in the presence of HNO_3 at room temperature. As shown in Figure 67, the mononuclear Pd(II) complex first

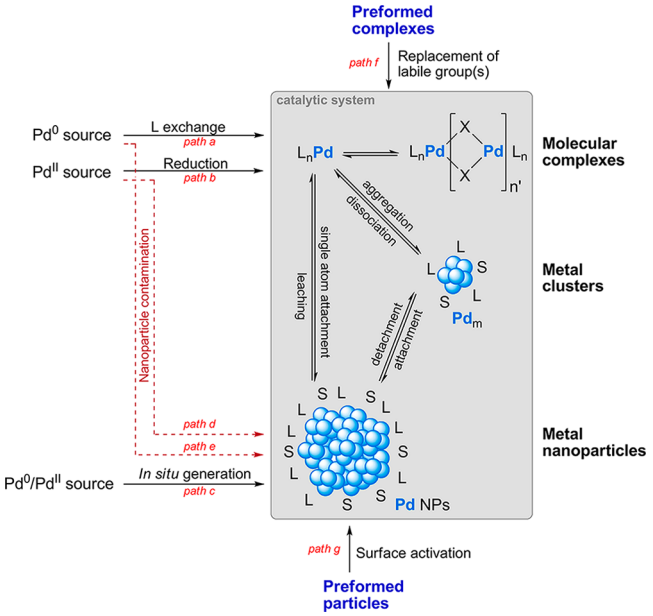

Figure 66. Plausible evolution of the palladium species transformation under reaction conditions (L, ligand; S, solvent; X, heteroatom). Adapted with permission from ref 347. Copyright 2013 American Chemical Society.

transformed into binuclear Pd complex, with further cleavage of the C−S bond in the CS_2 molecules, leading to the formation of CO_2. As a consequence, a trinuclear Pd complex was formed, which could be further transformed into mononuclear precatalyst in the presence of an excess of HNO_3.

5.8.2. In Situ Formed Au Clusters. As observed with Pd, we have found that the in situ formed Au clusters were the "real" active species for some Au-catalyzed reactions, such as ester-assisted hydration of alkyne and in the bromination reaction.[350] As shown in Figure 68, when mononuclear Au compounds ($HAuCl_4$ and AuCl) were used as the precatalyst, an induction period was observed. Fluorescence spectroscopy and MALDI-TOF prove that Au_3−Au_5 clusters were in situ formed under reaction conditions, and they were the catalytically active species for the ester-assisted hydration reaction. In the bromination reaction, a similar phenomenon was observed. However, in this case, Au_7−Au_9 clusters were the catalytically relevant Au species for the bromination reaction, suggesting that different reactions may need Au clusters of different sizes. To confirm the size-dependent catalytic properties of Au clusters, dendrimer (poly(amineamide-ethanol), PAMAM) encapsulated Au_5 and Au_8 clusters were prepared and tested for the hydration and bromination reactions. Au_5-PAMAM was able to catalyze the hydration reaction without induction period, while Au_8-PAMAM shows poor activity for this reaction. In the case of the bromination reaction, the situation was reversed. Au_8-PAMAM worked better than Au_5-PAMAM, and both of them showed no induction period. It should be noted that dendrimer-encapsulated Au clusters showed much lower activity than in situ formed Au clusters, implying that in situ formed Au clusters have optimized structures and coordination environment for catalysis.

By a top-down approach, subnanometric Au clusters can be generated on solid support (such as Al_2O_3, TiO_2, ZnO, CeO_2, and carbon) after the treatment of supported Au nanoparticles with I_2 solution, and those Au clusters are efficient catalyst for ester-assisted hydration of the alkyne.[351] Because it has also been observed that the in situ formation of Au clusters (Au_3−Au_6) play

DOI: 10.1021/acs.chemrev.7b00776
Chem. Rev. 2018, 118, 4981−5079

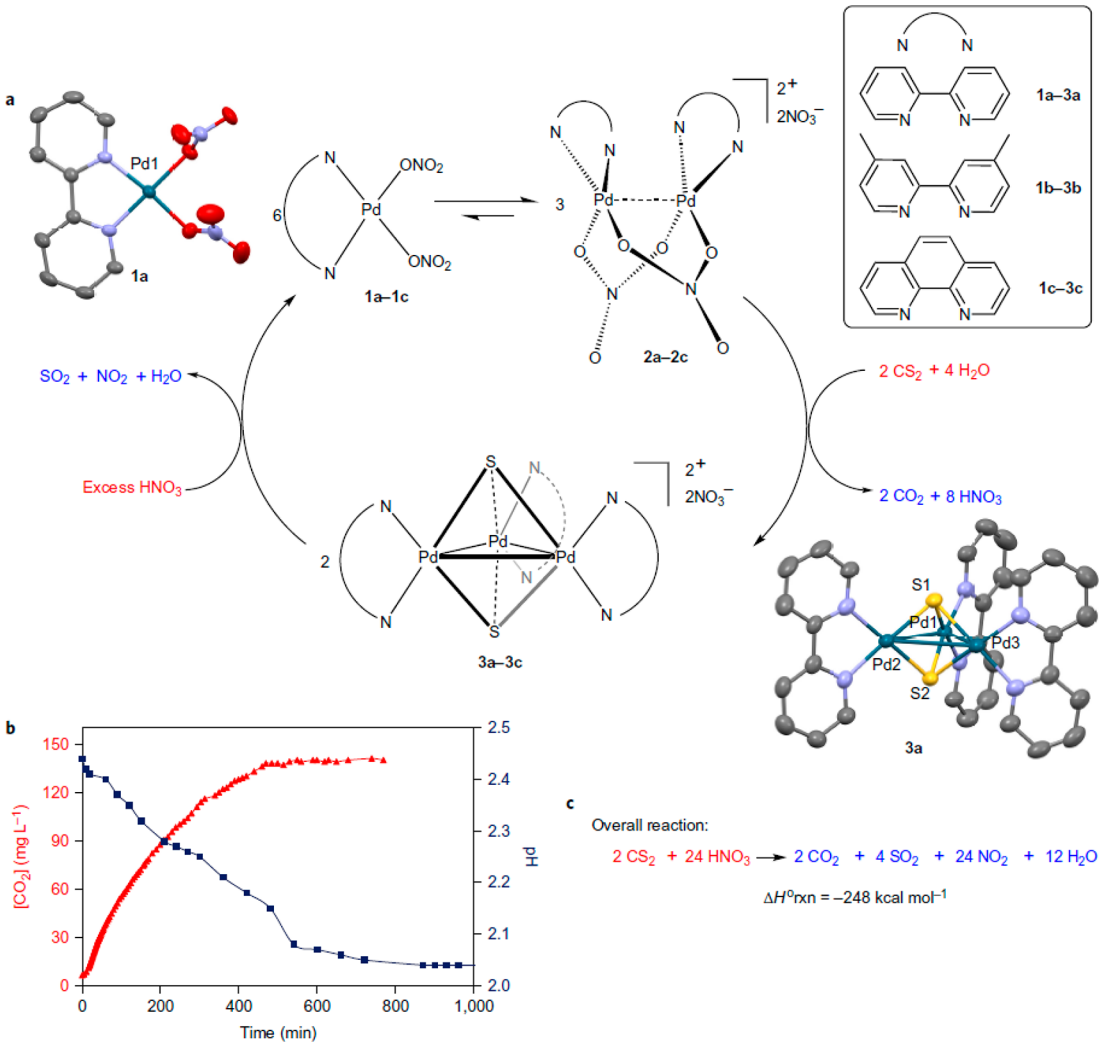

Figure 67. Conversion of CS_2 into CO_2 in HNO_3 by Pd complex at room temperature. (a) The transformation of mononuclear Pd precatalyst under reaction conditions is described. Trinuclear Pd clusters are the key active species for the conversion of CS_2 to CO_2. Notably, attempts to make the reaction working in HNO_3 aqueous were not successful. (b) Change of the CO_2 concentration and the pH values of the reaction solution with reaction time. (c) Overall reaction of the conversion of CS_2 to CO_2 in HNO_3. Adapted with permission from ref 349. Copyright 2017 Macmillan Publishers Limited, part of Springer Nature.

a key role in some other reactions, this may indicate that the transformation of mononuclear Au precursor into Au clusters can be a common phenomenon in Au-catalyzed organic reactions, including phenol synthesis from alkynylfurans rearrangement, *w*-bromination of phenylacetylene, bromination-hydration cascade reaction, and Conia−ene reaction of alkyne.[352] The in situ formation process of Au clusters can be affected by the reaction environment. When a strong acid like HOTf (with a Bronsted acidity near that of $HSbF_6$) was added to the reaction medium, the ester-assisted hydration of alkyne worked very fast without induction period. However, if basic ligands were added into the ester-assisted hydration of alkyne, the deactivation of Au clusters occurred because Au clusters were strongly capped by these ligands.[353]

Direct oxidation of olefins to epoxides with O_2 is a very attractive and challenging reaction. Hutchings et al. have reported that Au nanoparticles supported on carbon can catalyze the epoxidation of olefins (such as cyclohexene, *cis*-cyclooctene, styrene) with O_2 in the presence of *t*-butyl hydroperoxide (TBHP) as initiator.[354] In a following work, Lambert et al. have demonstrated the application of Au_{55} nanoparticles (~1.5 nm) as efficient catalyst for direct epoxidation of styrene to styrene oxide without initiator.[355] In that work, Au_{55} nanoparticles could achieve such transformation while other Au nanoparticles with larger size (>3 nm) did not work. These results imply that the particle size of Au species should affect the epoxidation reaction. However, the catalytic mechanism was not fully revealed.

Also, for the epoxidation reaction, it has been recently reported that subnanometric Au clusters with less than 10 Au atoms are the active species for epoxidation of *cis*-cyclooctene with O_2.[356] As shown in Figure 69, both heterogeneous and homogeneous Au catalysts (including Au/SiO_2, AuCl, and $AuCl_3$) could catalyze the epoxidation of *cis*-cyclooctene, with an induction period in all cases, indicating that some transformation of Au species may occur under reaction conditions as we have discussed in the above-mentioned examples. Furthermore, hot filtration experiments showed that leaching of Au from supported Au/SiO_2 catalyst into the reaction solution occurred. After the filtrate solution was checked by high-resolution STEM, it was found that subnanometric Au clusters were formed. In addition, spectroscopic characterizations (UV−vis and fluorescence spectroscopy) also confirmed the formation of Au

DOI: 10.1021/acs.chemrev.7b00776
Chem. Rev. 2018, 118, 4981−5079

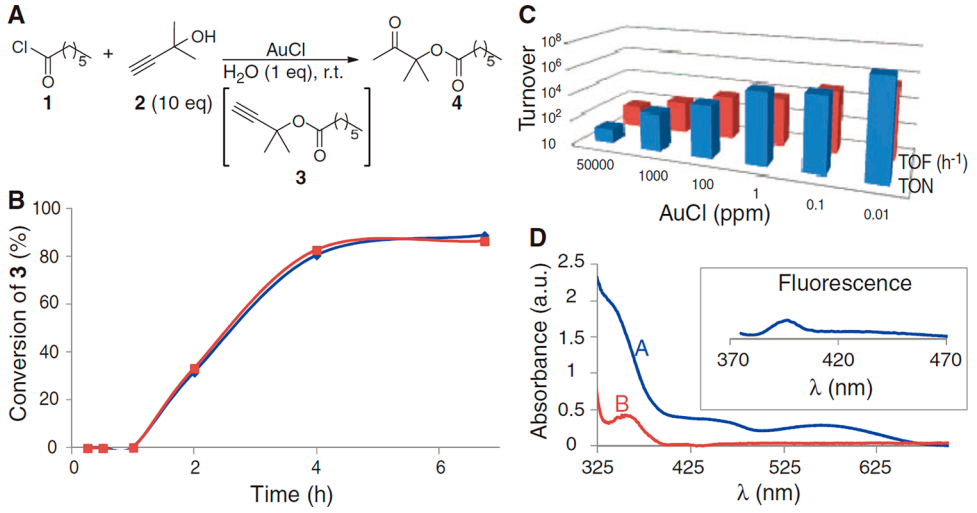

Figure 68. Ester-assisted hydration of alkyne by in situ formed Au clusters. (A) Scheme for the reaction. (B) Conversion for ester-assisted hydration of alkyne promoted by AuCl (squares) and $HAuCl_4$ (diamonds) at 100 ppm, after correction with the blank experiment. (C) Turnover number (TON) and turnover frequency (TOF) for different amounts of AuCl, calculated as moles of product formed per mole of AuCl at final conversion (TON) and as the initial reaction rate after the induction time per mole of AuCl (TOF). (D) UV−vis spectra of the reaction mixture for the hydration of alkyne containing the Au active species along the induction time (curve A) and when the reaction proceeds (curve B) with the corresponding fluorescence spectrum (inset, irradiated at 349 nm). Adapted with permission from ref 350. Copyright 2012 The American Association for the Advancement of Science.

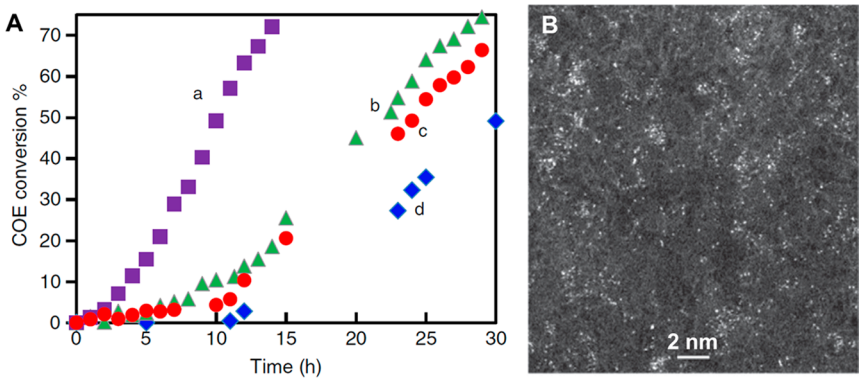

Figure 69. (A) Cyclooctene conversion with reaction time using different catalysts or without addition of Au catalyst. Au/SiO_2-A (a, ■), 6 mg AuCl (b, ▲), 7 mg $AuCl_3$ (c, ●), or no Au (d, ◆). (B) TEM images of filtrate solution from Au/SiO_2-A collected after conversion reached 18%. Au single atoms as well as subnanometric Au clusters are observed. Adapted with permission from ref 356. Copyright 2017 Macmillan Publishers Limited, part of Springer Nature.

clusters. Combining the above experimental results, it was concluded that in situ formed subnanometric Au clusters were the active species for epoxidation of *cis*-cyclooctene.

5.8.3. In Situ Formed Metal Clusters Other than Pd and Au. Besides Pd and Au clusters, Fe and Cu clusters have also been detected in the reaction mixture when Fe and Cu salts are used for C−C coupling reactions.[357,358] Although there is still some debate on the true active species in coupling reactions for Cu and Fe, the formation of metal clusters or even metal NPs was confirmed by EXAFS. For the Fe-catalyzed C−C coupling reaction, Fe−Fe dimers were detected after the addition of 1 equiv of PhMgCl. With 2 equiv of PhMgCl, the coordination number of Fe increased to 5.1, indicating that Fe clusters with 13 ± 2 atoms should be formed. This study indicates that there may be some common rules in metal-catalyzed C−C coupling reactions, the cluster-catalyzed mechanism. Recently, binuclear compounds are used for C−C coupling reactions, which is also compatible with the cluster-catalyzed mechanism.[359,360]

Besides C−C coupling reactions, Cu-catalyzed C−heteroatom coupling reactions can also follow a cluster-involved mechanism.[361] As shown in Figure 70, an induction period was observed for the Goldberg reaction when 0.5 mol % Cu salts were used as the starting catalyst. Electrospray ionization mass spectrometry (ESI−MS) confirmed the presence of Cu clusters of 2−7 atoms in solution only when the coupling starts, but not during the induction time. Furthermore, Cu NPs were also prepared as precatalyst for the Goldberg reaction. An induction period was also observed, and the in situ formation of Cu clusters was also confirmed by UV−vis and fluorescence spectroscopy. A series of experiments were performed to identify the chemical nature of the active Cu clusters. Neutral Cu(0) clusters were prepared by an electrochemical method and showed an induction period in the C−N coupling reaction (presented in the left panel in Figure 70c). In addition, Cu nanoparticles with surface Cu(II) species also showed induction period, indicating that the catalytically active clusters were neither Cu(0) nor Cu(II) but in some form of deoxygenated Cu(I) species. To

DOI: 10.1021/acs.chemrev.7b00776
Chem. Rev. 2018, 118, 4981−5079

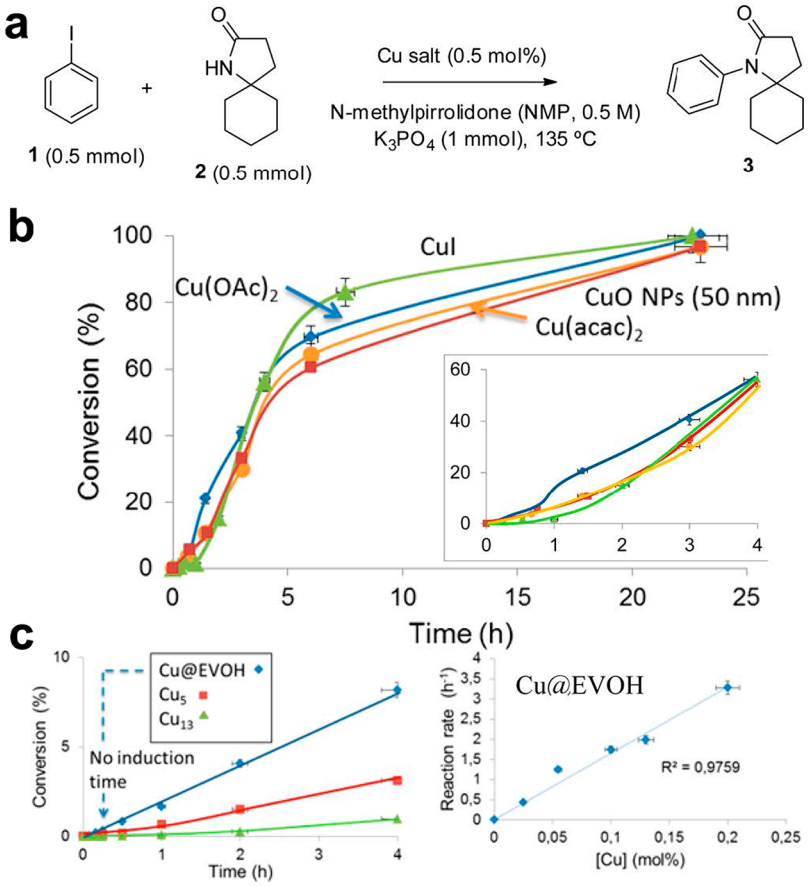

Figure 70. (a) Scheme of the C−N coupling reaction. (b) Kinetic results for the cross-coupling reaction between iodobenzene and amide catalyzed by commercially available 0.5 mol % of Cu compounds: $Cu(OAc)_2$ (blue ◆), CuO nanoparticles of ∼50 nm (red ■), $Cu(acac)_2$ (orange ●), and CuI (green ▲). The inset shows a magnification of the initial stage of the curves, where an induction period of ∼1 h can be observed for all of the Cu catalysts tested. (c) Left: Initial stage of the kinetic curves for the C−N cross coupling reaction in the presence of 0.05 mol % of Cu clusters. Right: Linear correlation between the initial reaction rate for the Goldberg reaction and the amount of Cu clusters containing ethylene-vinyl alcohol copolymer (EVOH) polymer (Cu@EVOH) used as a catalyst. No induction time was found in any case. Adapted with permission from ref 361. Copyright 2015 American Chemical Society.

prove that hypothesis, deoxygenated Cu(I) clusters were prepared by a one-pot reduction-stabilization method within an oxygen-protective polymer. As shown in Figure 70c, no induction period was observed when the Cu clusters stabilized in polymer were used as the catalyst. Thus, deoxygenated Cu(I) clusters were proved to be the active species for the Goldberg reaction. On the basis of that point, the in situ formed Cu clusters were also used for other types of coupling reactions, like C−O, C−S, and C−P coupling. As compared to the conventional Cu-diamine complexes, Cu clusters showed a better reactivity (lower amount of catalyst and higher TON) with different nucleophiles under optimized conditions, while Cu-diamine complexes can work at milder conditions and with a wider scope for more demanding reactions.

The Pt-catalyzed hydrosilylation of alkynes is widely used for organic synthesis of vinylsilanes and their derivatives. It is well-known that only β-vinylsilanes (through an anti-Markovnikov addition mechanism) are obtained with simple Pt catalysts such as Kardstedt catalyst and H_2PtCl_6, whereas α-vinylsilanes (through a Markovnikov addition mechanism) can only be obtained in very low yield. Recently, it has been reported that Pt_3 clusters can selectively catalyze the Markovnikov hydrosilylation of alkynes to α-vinylsilanes with very high turnover frequency (see Figure 71).[362] By following the evolution of Pt species by spectroscopic techniques, it was found that simple Pt compounds

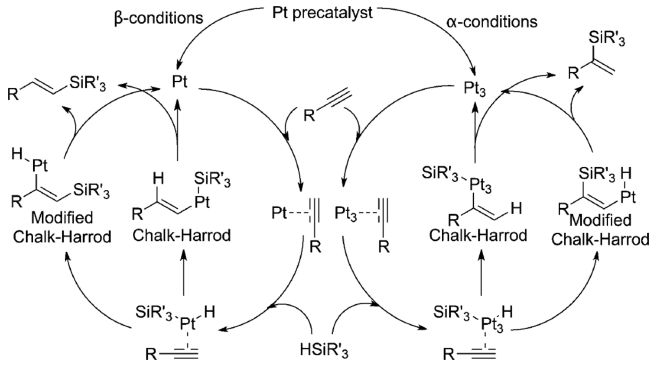

Figure 71. Possible pathways for the hydrosilylation of alkynes to obtain β-vinylsilanes (left) and α-vinylsilanes (right) through both Chalk−Harrod and modified Chalk−Harrod mechanism. Adapted with permission from ref 362. Copyright 2017 Wiley-VCH Verlag GmbH & Co. KGaA, Weinheim.

or the Kardstedt's catalyst would transform into Pt_3 clusters under reaction conditions, and those in situ formed Pt_3 clusters can afford a wide variety of new α-vinylsilanes with good yields. As compared to the classic catalytic mechanism on mononuclear Pt species for β-vinylsilanes, the selectivity of Pt_3 cluster is

DOI: 10.1021/acs.chemrev.7b00776
Chem. Rev. 2018, 118, 4981−5079

different, indicating the distinct behavior of metal clusters in organic reactions.

5.9. Perspectives on Catalysis Based on Metal Clusters

In the above-mentioned works, it has been clearly demonstrated that atomicity of metal clusters has a significant influence on their catalytic behavior. However, the influence of geometric structure on the catalytic properties of metal clusters is rarely studied. For metal clusters with a given atomicity, there should be several possible geometric configurations, which could have different catalytic reactivities under the same conditions. Furthermore, when metal clusters are supported on solid carriers, metal clusters with the same atomicity may have different geometric configurations in their local environment. Such variables make the situation of catalysis based on metal clusters more complicated than single-atom catalysis. Characterizations of the three-dimensional structure of supported metal clusters and tracking their dynamic structural evolution behavior should be key to establishing the structure−activity relationship.

So far, the preparation of metal clusters with a few atoms in a controllable manner is still a challenge. When introducing organic ligands, well-defined metal clusters can be generated by wet-chemistry approach. However, the removal of those ligands will destroy the homogeneity of the as-prepared metal clusters. Therefore, developing more robust synthetic methodologies will also be critical for understanding and improving the catalysis based on metal clusters.

6. CATALYTIC APPLICATIONS OF METALLIC AND BIMETALLIC NANOPARTICLES

The size, shape, chemical composition, and metal−support interaction effects of metal nanoparticles on the catalytic properties have been intensively studied in the last two decades, and a number of comprehensive reviews and perspectives on these topics have already been published.[363−366] In this part of the Review, we have considered metal nanoparticles with size above 1 nm. We will discuss how they can be prepared individually or supported on solid carriers, and the experimental and theoretical techniques required for in-depth characterizations to establish structure−reactivity correlations. We will highlight the recent insightful reports on size and shape effects of metal nanoparticles for heterogeneous catalysis, putting them in perspective with the results obtained with clusters and single atoms.

6.1. CO Oxidation

As shown in Figure 72, several types of Au nanostructures were deposited on metal oxide surface as model catalysts for CO oxidation.[367,368] Bilayer Au films showed the highest CO oxidation activity as compared to atomically dispersed Au or three-dimensional nanoparticles. With respect to the electronic factor, a nonmetallic to metallic transition of Au nanoparticles was observed on bilayer Au films, and bilayer Au films can provide adsorption sites for CO and active sites for O_2 activation, simultaneously.[369−371] Because of both electronic and geometric factors, bilayer Au structures showed the highest activity for CO oxidation. These studies based on surface science techniques match the results obtained on supported Au catalysts with Au nanoparticles. By systematic studies, Haruta et al. have demonstrated that the formation of Au/metal oxide interface is crucial for achieve high CO oxidation activity, and the perimeter of Au/oxide interface is key for catalysis.[372] Furthermore, it has also been found that Au nanoparticles with an average size of ~2 nm show the highest activity for low-temperature CO

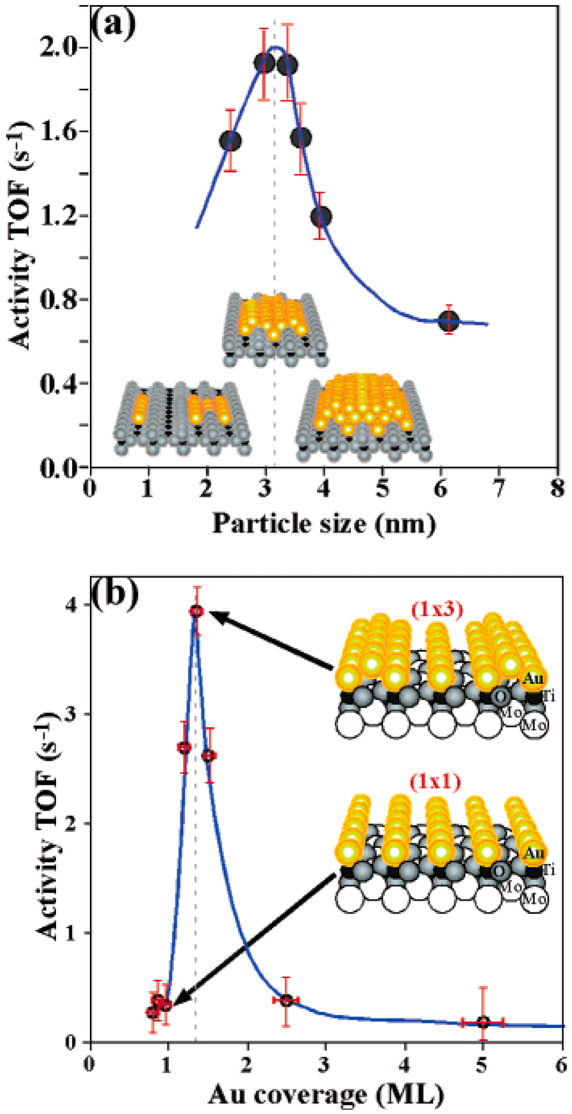

Figure 72. Catalytic activity for CO oxidation of different Au structures from single-layer to bilayer Au films and nanoparticles to three-dimensional hemispherical Au nanoparticles. (a) Influences of particle size on CO oxidation activity of Au supported on the TiO_2(110) at 353 K. (b) Influences of Au coverage on Au films supported on the Mo-(112)-(8×2)-TiO_x at room temperature. Adapted with permission from ref 367. Copyright 2006 American Chemical Society.

oxidation.[373] Therefore, for supported Au catalysts, the size of Au species also matters.

As discussed before, it has been reported that singly dispersed Au atoms and Au clusters supported on FeO_x are active for CO oxidation. However, it is also reported that an Au/FeO_x catalyst containing solely Au nanoparticles (1−5 nm) can be highly active for low-temperature CO oxidation.[374] Therefore, there is still discussion on the reactivity of different types of Au species.

From a mechanistic point of view, the CO oxidation reaction may follow different mechanisms at different reaction temperatures.[375] For instance, at $T > 80$ °C, O_2 can be activated directly on Au nanoparticles, giving the formation of atomic oxygen species for oxidation of CO. At lower temperature, O_2 can be activated at the metal−oxide interface. More interestingly, when the temperature decreases to <120 K, CO can be adsorbed on the support (TiO_2) and migrate to the Au−TiO_2 interface to react with O_2.[376] If this is so, then the active sites for CO oxidation at

DOI: 10.1021/acs.chemrev.7b00776
Chem. Rev. 2018, 118, 4981−5079

different temperatures may rely on different types of Au species, which should be further clarified.

The size effects of metal nanoparticles on CO oxidation reactivity have also been reflected on group VIII metals.[377] By a colloid chemical method, Pt nanoparticles with a narrow size distribution (from ca. 1 to 3 nm) have been deposited on FeO_x and tested for CO oxidation (under O_2-rich condition), showing that Pt nanoparticles around 2 nm give the highest activity. By correlating the catalytic results with spectroscopic characterizations, it was proposed that the chemical states of Pt species varied with the particle size, which may further affect the CO oxidation activity. However, the variation pattern may change with the metal element. In the case of Ru, the CO oxidation activity increased when increasing the particle size gradually. Ru nanoparticles around 6 nm showed almost 3 times higher activity than Ru nanoparticles of ~2 nm.[378] In situ spectroscopic characterizations indicated that the as-prepared metallic Ru nanoparticle transformed into core−shell structure ($Ru@RuO_2$) under reaction conditions, and the fraction of RuO_2 overlayer was related to the particle size.[379] A higher percentage of RuO_2 overlayer was observed in smaller Ru nanoparticles, while less RuO_2 overlayer was observed in larger Ru nanoparticles. Such size-dependent redox properties of Ru nanoparticles may account for their different reactivities in CO oxidation.

Similar to the case of supported nanoparticulate Au catalysts, the critical role of metal−support interface for CO oxidation has also been demonstrated on supported group VIII metal nanoparticles.[380] When Pt nanoparticles were supported on reducible metal oxides (like Co_3O_4, NiO), the activity for CO oxidation was significantly higher than when supported on relatively inert supports, like SiO_2. Furthermore, by tuning the size of metal nanoparticles and studying the kinetics, it has also been proposed that the active sites of supported group VIII metal nanoparticles are the corner metal atoms located at perimeter of the metal−CeO_2 interface.[381] As shown in Figure 73, the variation tendency of CO oxidation activity showed the same pattern with the number of corner atoms at the perimeter.

Considering the larger size of metal nanoparticles when compared to metal clusters or single atoms, it is possible to modify the surface properties of the former by loading a thin layer of metal oxide or metal hydroxide species.[382] For instance, when FeO monolayers were deposited on Pt nanoparticles, the unsaturated Fe(II) sites at the Pt−FeO interface could activate O_2 with a low energy barrier (see Figure 74), leading to high activity for the preferential oxidation of CO in rich H_2 (CO-PROX) at room temperature. In contrast, Pt nanoparticles without modification of transition metal oxides showed poor activity for CO oxidation.[383] However, such interface-confined ferrous centers were deactivated in O_2-rich atmosphere due to the over oxidation of Fe(II) sites to Fe(III) sites. This concept has also been extended to modification of Pt nanoparticles with hydroxide layers. In their work, Zheng et al. have prepared $Pt@NiFe(OH)_x$ composite nanoparticles, showing remarkable activity for CO oxidation in both oxidative (O_2-rich atmosphere) and reductive (H_2-rich atmosphere) conditions.[384] Theoretical calculations and mechanistic studies show that the unique interfacial structure between Pt and $NiFe(OH)_x$ can provide highly stable active sites for O_2 activation, and hydroxyl groups play a key role for maintaining the high activity. The above works provide new insights for understanding the metal−support interface at atomic scale.

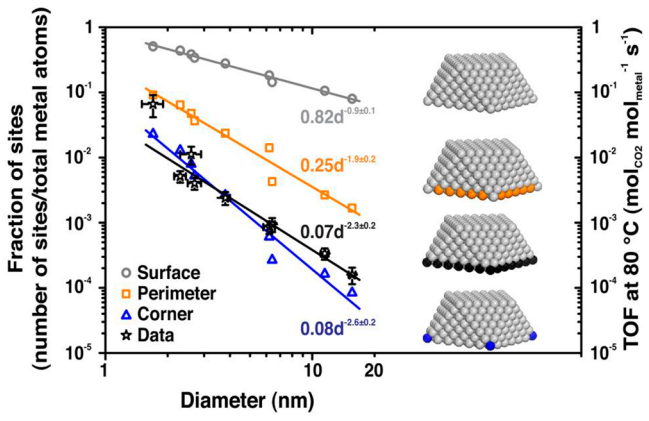

Figure 73. Calculated number of sites with a particular geometry (surface and perimeter or corner atoms in contact with the support) as a function of diameter and TOF at 80 °C of the nine ceria-based samples. Adapted with permission from ref 381. Copyright 2013 The American Association for the Advancement of Science.

6.2. Oxidation of Hydrocarbons

The production of ethylene oxide from epoxidation of ethylene is an important industrial process due to the large demand of ethylene oxide as bulk chemical intermediates. At present, the industrial catalysts for this reaction consist of large Ag nanoparticles (100−200 nm) supported on low-surface-area alumina, promoted with alkali (such as Cs) and other metals (such as Mo, W, Cr).[385] From a mechanistic point of view, the oxidation of ethylene on Ag surface goes through an oxometallacycle (OMC) intermediate, as confirmed by surface science experiments and kinetic isotopic studies.[386] The isomerization of the OMC on Ag leads to the formation of the desired product, ethylene oxide, or acetaldehyde as byproduct. According to theoretical calculations, the difference in the activation barrier for the formation of ethylene oxide and acetaldehyde is ~0.1 eV higher on Ag(100) than that on Ag(111), indicating that Ag(100) surface can be more selective for the production of ethylene oxide. Inspired by the theoretical calculations, Ag nanocrystals with different shapes have been prepared and tested for ethylene epoxidation reaction.[387] As compared to traditional supported Ag catalyst (spherical Ag nanoparticles exposed with (111) facets), Ag nanowires with (100) facets exposed showed higher selectivity toward ethylene oxide under the same reaction conditions. In a following work, Linic et al. have compared the catalytic performance of different Ag nanostructures for ethylene epoxidation reaction. As shown in Figure 75, Ag nanocubes with (100) facets exposed showed the highest selectivity, while Ag spherical nanoparticles showed the lowest selectivity to ethylene oxide.[388] According to the activity results, it is clear that Ag(100) facets have an advantage over Ag(111) facets for the selective production of ethylene oxide.

This concept has also been extended to the epoxidation of propene to propene oxide.[389] In this work, Pulido et al. have studied the aerobic epoxidation of propene on Ag(111) and Ag(100) surface by in situ spectroscopic techniques and theoretical calculations. Similar to epoxidation of ethylene, Ag(100) surface is more selective than Ag(111) for the production of propene oxide. However, it was found that under reaction conditions, the Ag(100) surface would reconstruct and transform into the less selectivity Ag(111) surface after longer reaction time. Therefore, preparing Ag-based catalysts with a large percentage of exposed (100) facets and stabilizing the (100) facets under reaction conditions can be a

DOI: 10.1021/acs.chemrev.7b00776
Chem. Rev. 2018, 118, 4981−5079

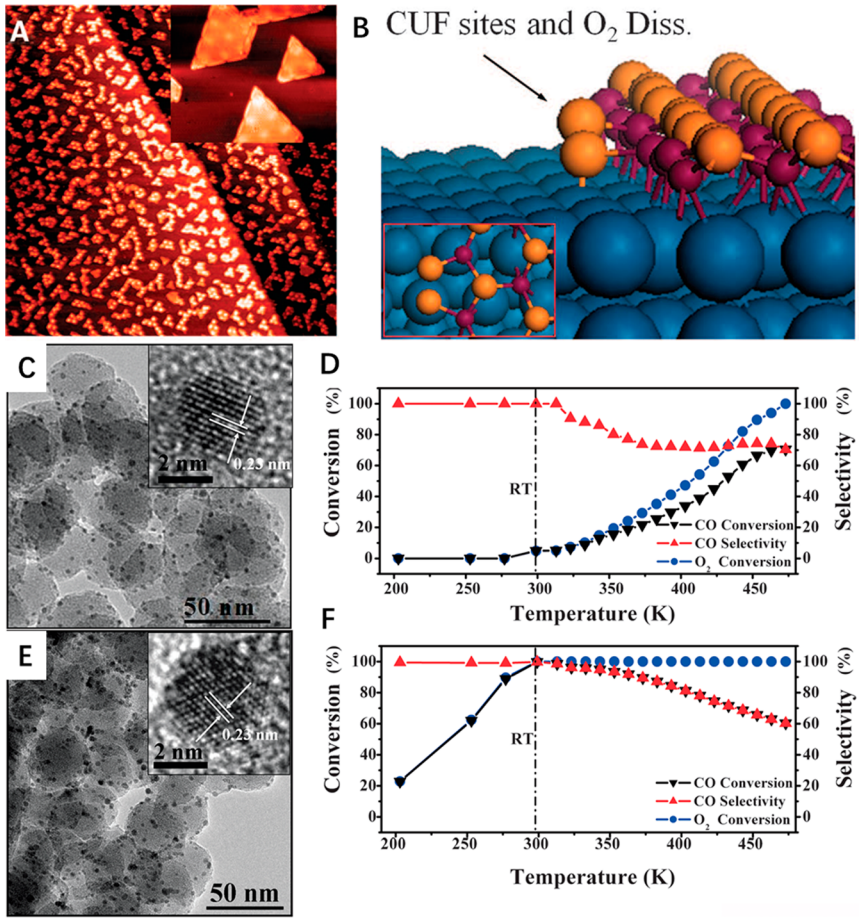

Figure 74. (A) STM image of 0.25 monolayer of FeO deposited on Pt(111). The inset image is a high-resolution STM image on the FeO monolayer nanoislands. (B) Schematic illustration of the coordinated-unsaturated ferrous (CUF) sites at the FeO−Pt interface and the transition states of O_2 dissociation at the CUF sites according to DFT calculations. (C) TEM images of Pt/SiO_2 catalyst and (D) its catalytic performance in CO-PROX reaction. (E) TEM images of bimetallic $Pt-Fe/SiO_2$ catalyst and (F) its catalytic performance in CO-PROX reaction. Adapted with permission from ref 382. Copyright 2010 The American Association for the Advancement of Science.

potential route to make promising catalyst for epoxidation of propene to propene oxide.

6.3. Oxidation of Alcohols

There are numerous works on the application of metal nanoparticles for selective oxidation of alcohols to aldehydes or ester. The particle size effect and the promotion effect from the support and synergistic effect of bimetallic nanoparticles have been intensively discussed.[99,390−392] Herein, we would like to emphasize the size effect of metal nanoparticles on their catalytic properties for oxidation of alcohols. As shown in Figure 76, Pd nanoparticles on three types of support showed the same variation on size-dependent activity for oxidation of benzyl alcohol. From a mechanistic point of view, during the oxidation of alcohol on metal surface, the alcohol molecule should be first adsorbed on the surface of metal nanoparticles, followed by activation of the O−H bond, resulting in the formation of an alkoxide intermediate. Subsequently, β-H elimination occurs to give aldehyde or ketone as product. Finally, the surface of metal nanoparticles can be recovered when adsorbed H species are removed by O_2 to form water.[393] Taking into consideration that several elemental steps can affect the overall reaction rate and the sites for adsorption of alcohol, and that β-H elimination and activation of O_2 are different on Pd nanoparticles, it is speculated that a certain balance can be achieved on Pd nanoparticles around 4 nm, to give the highest activity for oxidation of benzyl alcohol.

As we said before, not only the size of metal clusters and nanoparticles, but also the particle shape has an important impact on their catalytic properties, and such effects have been observed with Pt nanoparticles for alcohol oxidation reactions.[394] Cuenya et al. reported the influence of the shape on the reactivity of Pt particles (0.8−1 nm) supported on γ-Al_2O_3 for 2-propanol oxidation.[395] Four types of Pt nanoparticles with similar size and different shapes (illustrated in Figure 77a), according to EXAFS and STEM characterization respectively, were tested. These four supported Pt nanoparticles showed distinct activities for selective oxidation 2-propanol (as shown in Figure 77b), which implies that the shape of the cluster has a big impact on its catalytic properties. By correlating the coordination numbers of surface Pt atoms in four types of Pt clusters, they found that surface Pt atoms with lower coordination numbers showed a lower onset temperature, corresponding to the highest low-temperature activity. Among the four samples, the Pt nanoparticles with bilayer structure showed the highest activity for selective oxidation of 2-propanol. Furthermore, in the case of Pt nanoparticles with bilayer structure, the contact area between Pt and the Al_2O_3 support is larger, resulting in more perimetric Pt atoms. The interface effects between Pt and Al_2O_3 may also facilitate the oxidation reaction. A similar shape effect on catalytic

DOI: 10.1021/acs.chemrev.7b00776
Chem. Rev. 2018, 118, 4981−5079

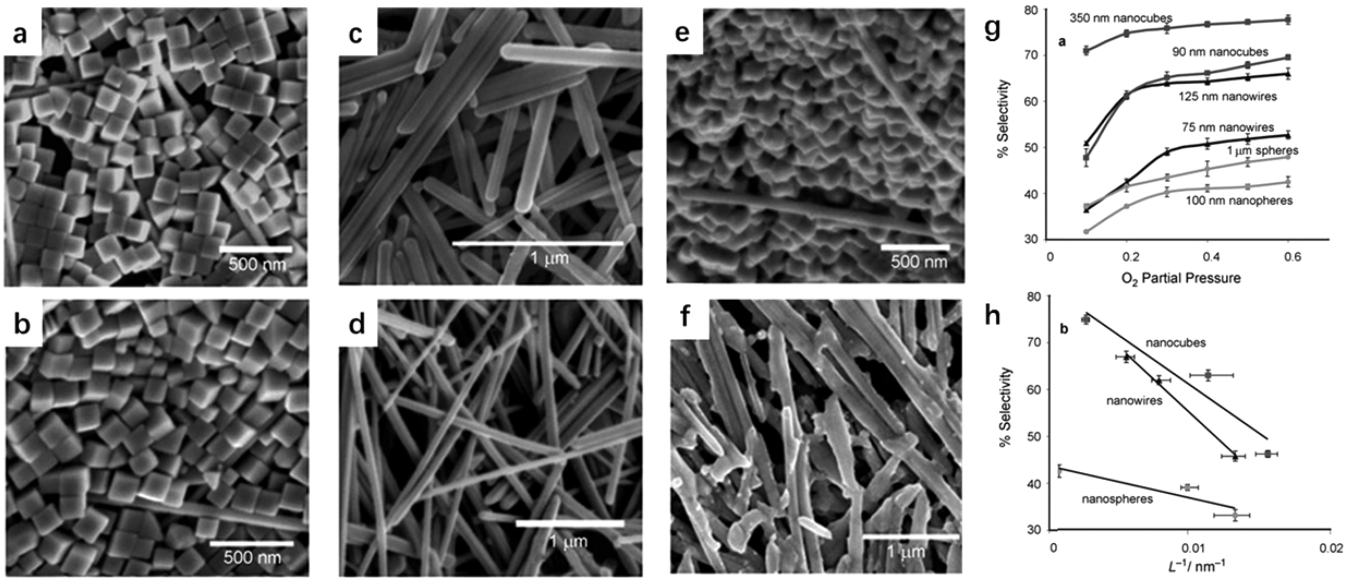

Figure 75. Scanning electron microscopy images of various Ag nanostructures. (a) Ag nanocubes (90 nm) deposited on Si water, (b) Ag nanocubes (90 nm) deposited on alumina support, (c) Ag nanowires (125 nm) deposited on Si water, (d) Ag nanowires (125 nm) deposited on alumina support, (e) Ag nanocubes (90 nm) after 48 h on stream under epoxidation reaction conditions, and (f) Ag nanowires (125 nm) after 48 h on stream under epoxidation reaction conditions. (g) Selectivity to ethylene oxide at different O_2 partial pressure for Ag nanocubes, nanowires, and spherical nanoparticles of different edge lengths and diameters. (h) Selectivity to ethylene oxide as a function of L^{-1} (inverse characteristic length) for Ag nanocubes, nanowires, and spherical Ag nanoparticles. Adapted with permission from ref 388. Copyright 2010 Wiley-VCH Verlag GmbH & Co. KGaA, Weinheim.

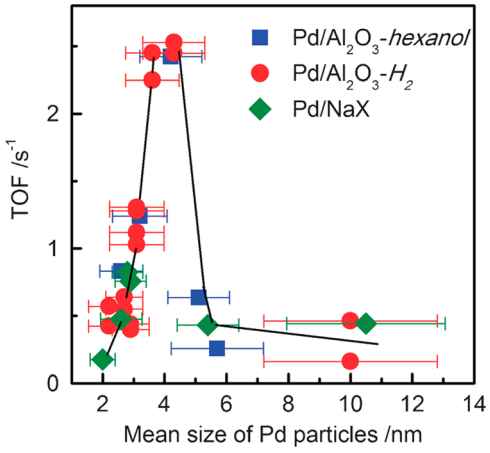

Figure 76. Dependence of turnover frequency on the mean size of Pd nanoparticles for the selective oxidation of benzyl alcohol. The TOF values for oxidation of benzyl alcohol to benzyl aldehyde from three different supported Pd catalysts are presented. Adapted with permission from ref 391. Copyright 2011 The Royal Society of Chemistry.

properties of Pt nanoparticles has also been reflected for the selective oxidation of 2-butanol.[396] Pt nanoparticles with more edge and corner sites show higher selectivity to 2-butanone, while Pt nanoparticles with less edge and corner sites show higher selectivity to combustion product (CO_2). Therefore, by tuning the geometric structure of metal nanoparticles, it is possible to modulate the selectivity during the selective oxidation of alcohols.

6.4. Selective Hydrogenation

Size effects of metal particles on catalytic properties for hydrogenation reactions have long been observed. In some reactions, the catalytic activity measured as turnover frequency (TOF) was found to be dependent on the particle size, and those reactions were named structure-sensitive reactions. However, in other cases, where catalytic activity did not depend on the particle size, those reactions were considered as structure-insensitive reactions.[397−399]

A typical example of a structure-sensitive reaction is the ammonia synthesis. Studies based on surface chemistry have already proved that the active sites for ammonia synthesis are the (111) facets of Fe.[400,401] Because the percentage of exposed (111) facets in Fe nanoparticles will increase when increasing the particle size, the reaction rate of ammonia synthesis will increase with the Fe particle size. The structure-sensitive phenomenon have also been observed in other hydrogenation reactions, such as the Fischer−Tropsch reaction on Co nanoparticles. Iglesia and other researchers have shown that the surface-specific activity (turnover frequency, TOF) is independent of the Co particle size in the range of 9−200 nm. It has been later observed that the TOF increases with the Co particle size in the range of 2−6 nm.[402,403] On the basis of systematic kinetic studies, de Jong et al. proposed an explanation for the size-dependent catalytic properties of Co nanoparticles.[404] The lower activity of Co particles with size <6 nm is caused by both blocking surface sites with unsaturated coordination and a lower intrinsic activity at the small terraces. Because the surface of small Co nanoparticles prefers to be covered by H_2, the selectivity to methane in the F−T synthesis is higher on small Co nanoparticles.

The hydrogenation of the C═C bond in light olefins is a typical structure-insensitive reaction. As shown in Figure 78, the TOF and activation energy of Pt nanoparticles are independent of the size for hydrogenation of cyclohexene. A similar phenomenon has also been observed during hydrogenation of ethylene on Pt nanoparticles, indicating that the above reactions are structure-insensitive.[405] When the substrate is switched from light olefins to aromatics, the situation changes. It was found that the full hydrogenation of benzene and toluene on Pt nanoparticles (from 1 to 7 nm) showed moderate size-sensitive

DOI: 10.1021/acs.chemrev.7b00776
Chem. Rev. 2018, 118, 4981−5079

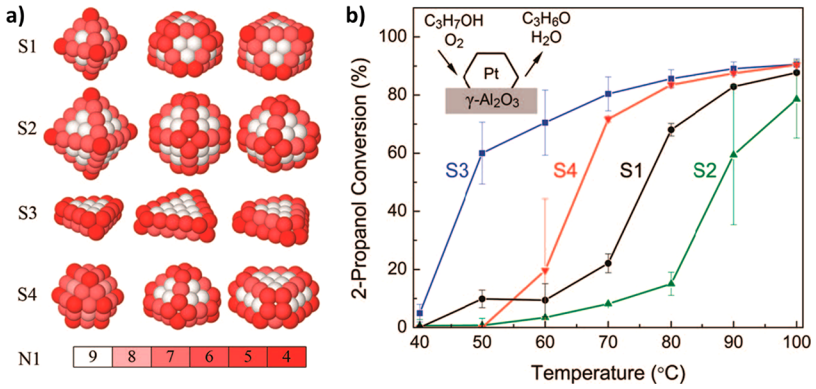

Figure 77. (a) Models of different Pt nanoparticles with similar particle size (~0.8 nm for S1 and ~1 nm for S2, S3, and S4) but different geometric shapes. The geometric shapes of different Pt/γ-Al_2O_3 samples (S1 to S4) were obtained on the basis of the fitting of EXAFS data as well as with the TEM measurements. The geometric shapes that give the best fitting results are shown in the left column. The color coding indicates the different number of first nearest neighbors (N1) of surface atoms in each Pt nanoparticle. (b) Catalytic activity for oxidation of 2-propanol to acetone by Pt/γ-Al_2O_3 samples measured in a packed-bed mass flow reactor by mass spectrometry. Adapted with permission from ref 395. Copyright 2010 American Chemical Society.

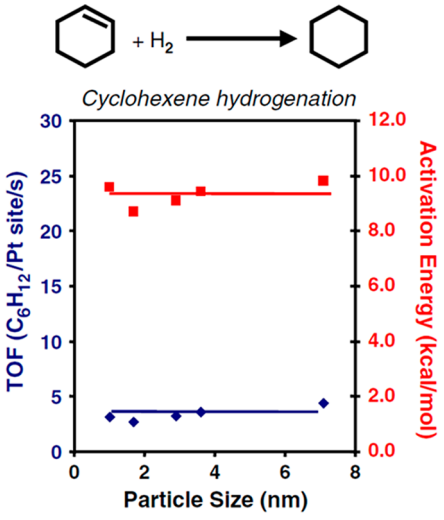

Figure 78. Turnover rate and activation energy over Pt nanoparticles as a function of particle size in cyclohexene hydrogenation to cyclohexane. Adapted with permission from ref 405. Copyright 2008 Springer.

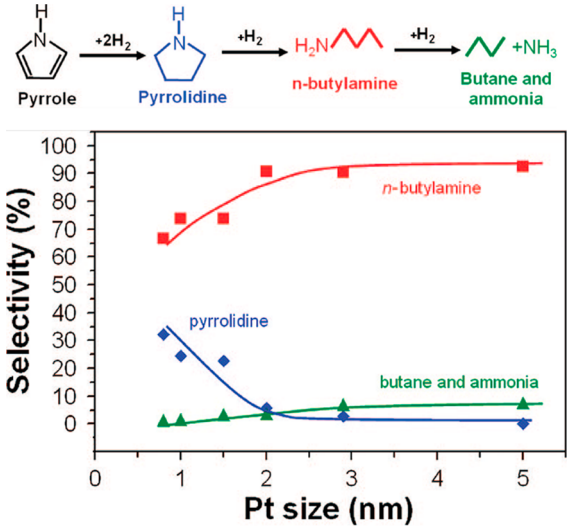

Figure 79. Hydrogenation of pyrrole by Pt nanoparticles with different particle size. The distributions of hydrogenation products are presented. Adapted with permission from ref 408. Copyright 2008 American Chemical Society.

behavior.[406,407] Pt nanoparticles with an average size of ~3 nm showed the highest turnover frequency for both reactions. However, the reaction order for H_2 and arenes (benzene and toluene) almost remained constant on Pt nanoparticles with different sizes.

From a geometric point of view, one Pt atom is already capable of absorbing one ethene molecule. However, when benzene or toluene molecules are absorbed on the surface of a Pt catalyst, multiple Pt atoms should be involved in the adsorption step. Therefore, when varying the size of Pt nanoparticles, the adsorption energy of benzene or toluene and the surface coverage will change, resulting in different activation energies and catalytic activities.

In some more complicated hydrogenation reactions, the size of metal nanoparticles will affect the product distributions. In a typical example, as shown in Figure 79, for hydrogenation of pyrrole, higher selectivity to pyrrolidine was observed on smaller Pt nanoparticles than on larger ones.[408] Similar effects can also be reflected on hydrogenation of 1,3-butadiene, furan, and furfural.[409−411] The different selectivity for those hydrogenation reactions on Pt nanoparticles can be associated with different reaction pathways on Pt nanoparticles with different sizes. More interestingly, significant differences between small Pt nanoparticles (≤2 nm) and larger nanoparticles (>2 nm) have been observed for different reactions. It appears that some electronic or geometric factors between small and large metal nanoparticles account for such differences. Further work is required to confirm if this is a general and reproducible fact.

When discussing the catalytic behavior of single atoms or metal clusters for hydrogenation reactions, the electronic structures of various metal species with different atomicity are usually claimed to be responsible for the differences observed. In the case of nanoparticles, due to their much larger size and many more possibilities in morphology, their geometric structures will also play a significant role.[412] For instance, as shown in Figure 80, only full hydrogenation product (cyclohexane) was observed on Pt cubes with (100) facets exposed for hydrogenation of benzene. However, in the case of cuboctahedras, with both (111) and (100) facets exposed, cyclohexene can be observed.[413]

Nevertheless, the catalytic behavior of metal surface can also be modulated by ligands, which is similar to the ligand effects

DOI: 10.1021/acs.chemrev.7b00776
Chem. Rev. 2018, 118, 4981−5079

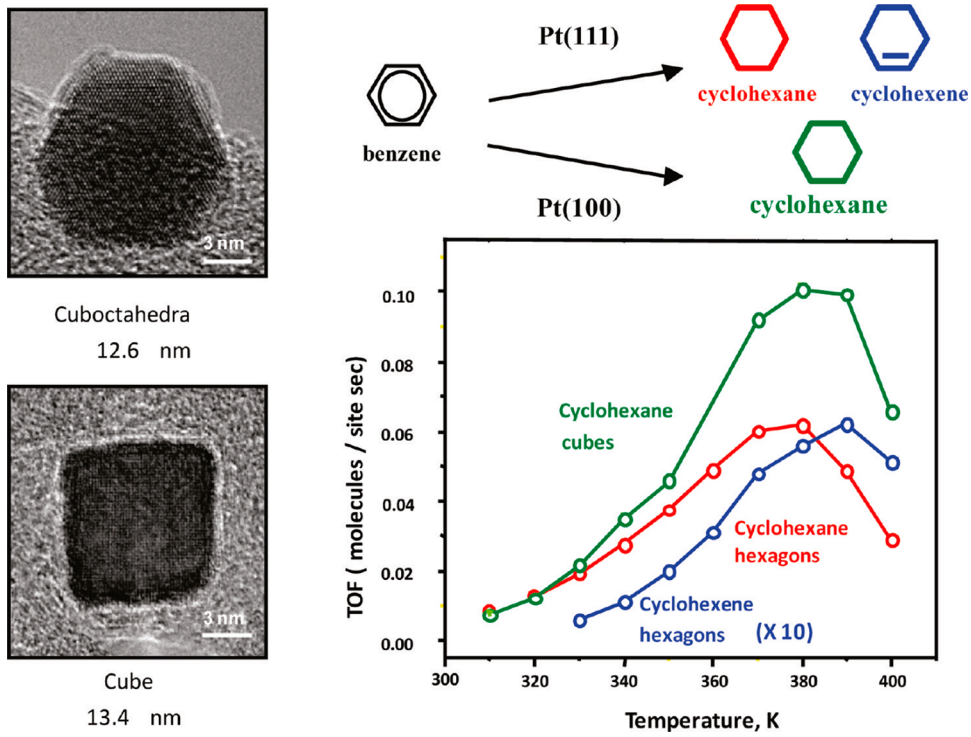

Figure 80. Morphology of Pt cuboctahedras and cubes and their catalytic performance for benzene hydrogenation. As it can be seen, only cyclohexane can be observed on Pt cubes, while both cyclohexane and cyclohexene can be observed on Pt cuboctahedras. Adapted with permission from ref 413. Copyright 2007 American Chemical Society.

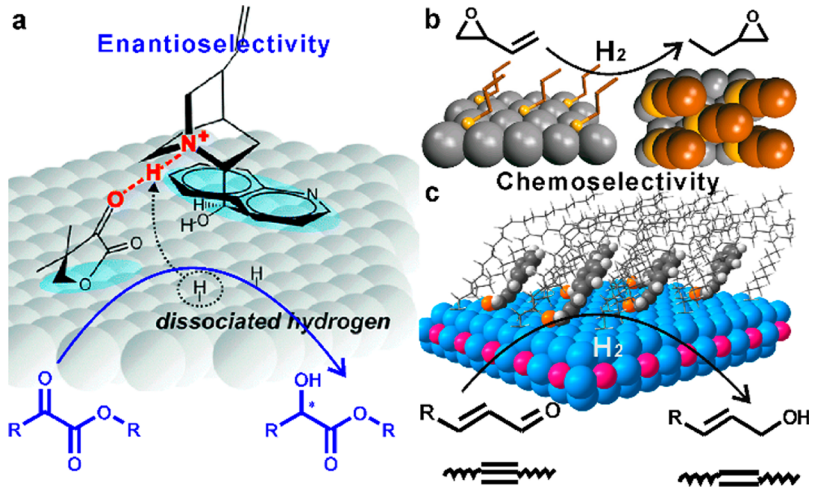

Figure 81. Introduction of metal−ligand interaction to modulate the chemoselectivity of metal nanoparticles for selective hydrogenation reactions. (a) Surface modification with cinchona alkaloids on Pt surface to enhance the enantioselectivity for hydrogenation of C = O bonds. (b) Surface modification of Pd surface with thiol ligands to modulate the selectivity for hydrogenation of epoxybutene to epoxybutane. (c) Surface modification of PtCo bimetallic nanoparticles with amine ligands for selectivity hydrogenation of conjugated unsaturated aldehyde to corresponding unsaturated alcohol. Adapted with permission from ref 415. Copyright 2017 American Chemical Society.

observed on catalysts containing single atoms and clusters. By introduction of suitable ligand to the surface of metal nanoparticles, the nanoscale environment of the surface of metal nanoparticles is changed, leading to the modulation of metal−substrate interaction, which can result in unique chemoselectivity as compared to naked metal nanoparticles.[414,415] As shown in Figure 81, enantioselective hydrogenation of C═C and C═O bonds can be realized by heterogeneous Pt catalysts after adsorption with chiral template molecules.[416] Notably, the shape of Pt nanoparticles can also affect the catalytic behavior in heterogeneous asymmetric hydrogenation reactions. It has been found that Pt nanoparticles with different ratios of (111)/(100) facets exposed could be prepared and modified with chiral template molecules for enantioselective hydrogenation of ketones.[417] It was found that the reaction rate and ee increased with the ratio of (111)/(100) facets in the Pt catalysts. According to spectroscopic characterizations and theoretical calculations, adsorption behavior of the cinchona alkaloid on different facets was thought to be the reason accounting for different enantioselective properties. Stronger adsorption of the chiral modifier was observed on (100) facets, which would block the active sites on Pt nanoparticles and also degrade the chiral

DOI: 10.1021/acs.chemrev.7b00776
Chem. Rev. 2018, 118, 4981−5079

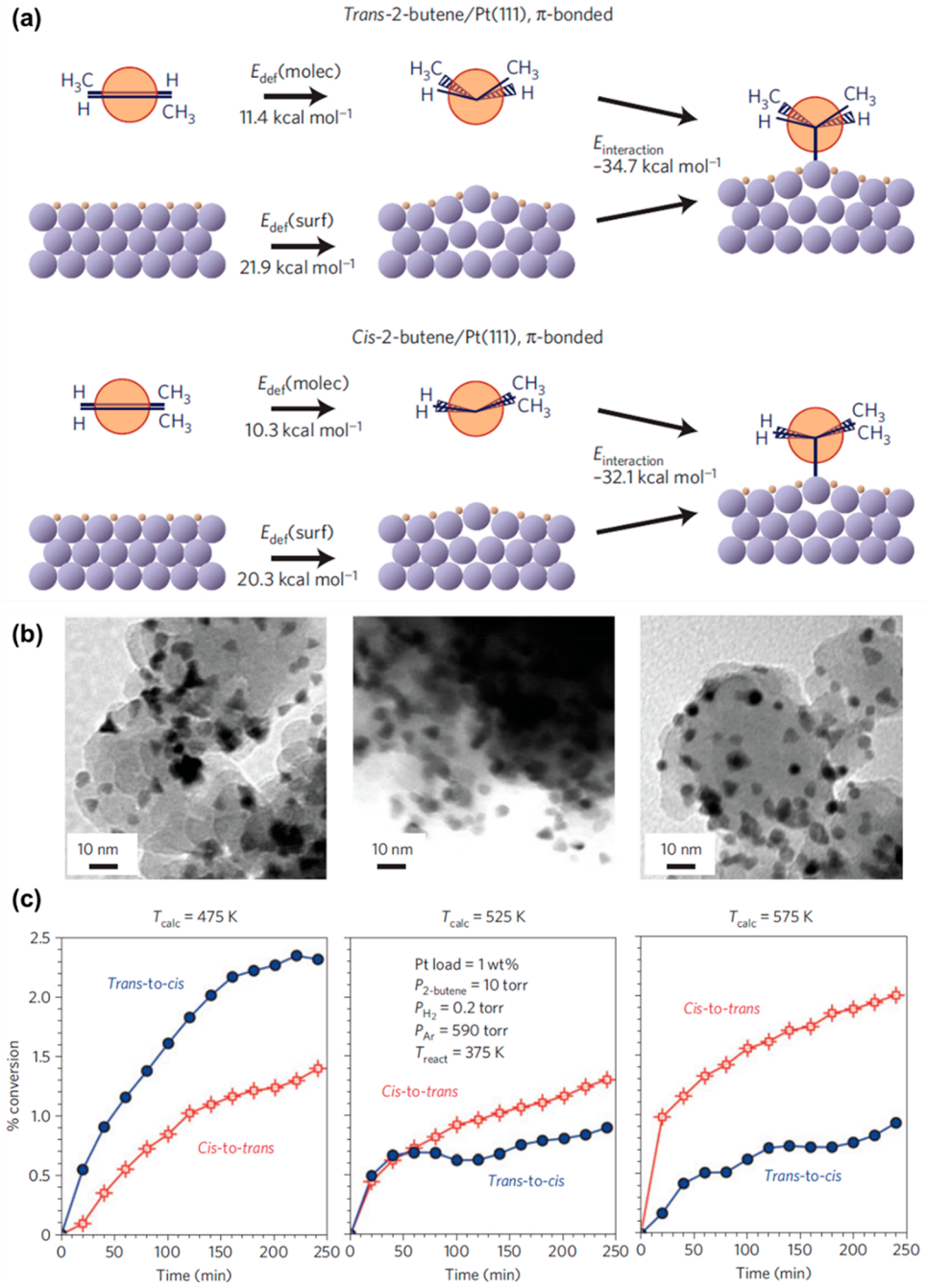

Figure 82. (a) Schematic illustration and corresponding DFT calculations of isomerization of *trans*-2-butene and *cis*-2-butene on Pt(111) surface. (b) Morphologies of three Pt/SiO_2 catalysts after calcination at different temperatures. The starting material consisted of Pt tetrahedras, with four (111) facets exposed. To remove the polymer capping agent, those Pt tetrahedras were calcined in air at 475, 525, and 575 K, followed by a reduction treatment with H_2. As a result of such oxidation−reduction treatment, the shape of Pt nanoparticles would change from tetrahedral to spherical shape stepwisely. (c) Corresponding kinetic data for the isomerization of *cis*- and *trans*-2-butene promoted by the Pt/SiO_2 catalyts with different shapes. The reaction conditions are also included. Adapted with permission from ref 422. Copyright 2009 Macmillan Publishers Limited, part of Springer Nature.

modifier. Besides, the presence of suitable ligands can also enhance the chemoselective hydrogenation of molecules with multiple functional groups. For instance, the presence of monolayer of thiol ligands on Pd nanoparticles can significantly improve the selectivity from <20% on naked Pd nanoparticles to >90% on modified Pd with octadecanethiol for hydrogenation of epoxybutene to epoxybutane.[418] Similar promotion effects can also be observed on amine-modified PtCo bimetallic nanoparticles for hydrogenation of α,β-unsaturated aldehydes to corresponding unsaturated alcohols.[419]

However, it should be pointed out that, due to the intrinsic heterogeneity of supported nanoparticulate metal catalysts, it will be very difficult to obtain uniform well-defined metal−ligand configuration on the surface of nanoparticles, which can cause the loss of chemoselectivity. Therefore, developing new methodologies for precise synthesis of heterogeneous metal catalysts with higher accuracy at molecular level is an emerging task.

DOI: 10.1021/acs.chemrev.7b00776
Chem. Rev. 2018, 118, 4981−5079

6.5. Isomerization Reactions

The isomerization of *trans* olefins to their less thermodynamically favorable *cis* configuration is an important reaction with implications in food chemistry and some other synthetic processes. Surface science experiments have demonstrated that the isomerization of light olefins follows the Horiuti−Polanyi mechanism, which involves the formation of a half-hydrogenated surface alkyl intermediate.[420] It has been observed that the isomerization of *trans*-2-butene to *cis*-2-butene is preferred over the transformation of *cis*-2-butene to *trans*-2-butene on Pt(111) surface.[421] The experimental results are consistent with theoretical calculations, as shown in Figure 82a. The *cis* configuration is more stable on H-saturated Pt(111) surface than its *trans* countpart. Furthermore, to extend the above insights to a more practical system, Pt nanoparticles with different shapes were prepared and tested for *cis*−*trans* isomerization in 2-butene. As shown in Figure 82b and c, Pt tetrahedras with dominating (111) facets exposed give a higher *trans*-to-*cis* reaction rate, while spherical Pt nanoparticles with more terrace surface sites exposed show a higher *cis*-to-*trans* reaction rate.[422,423] These results obtained on Pt nanoparticles are consistent with those obtained on model Pt(111) surface, indicating the possibility to tune reaction selectivity by controlling the surface structure of metal nanoparticles.

6.6. Electrocatalytic Reactions

For electrocatalytic reactions, the electronic and surface structures of metal nanoparticles also play a dominating role for controlling reactivity and selectivity.[424,425] To illustrate that, we have chosen here the oxygen reduction reaction (ORR) and electrocatalytic CO_2 reduction, as two important model reactions. They will be taken as typical examples to show how to modulate the electrocatalytic properties by tuning the morphology and chemical compositions of metal nanoparticles.

For ORR on the surface of Pt nanoparticles, the limiting reaction step is suggested by theoretical calculations to be the desorption of adsorbed oxygenated intermediates.[426] Therefore, by tuning the surface electronic structure of Pt nanoparticles, the ORR activity can also be modulated. According to experimental and calculation results, the specific activity of different crystal facets of Pt then is found to be Pt(100) ≪ Pt(111) ≈ Pt(110) (see Figure 83). For further tuning the electronic properties of Pt surface, the first strategy is to introduce a second metal to form Pt-based alloy nanoparticles.[427,428] Thus, by screening different combinations of Pt with another metal, it has been well established that PtNi bimetallic nanoparticles are highly active and robust catalyst for ORR. Specifically, the $Pt_3Ni(111)$ surface was proved to be extraordinarily active, showing 10 times higher specific activity than the Pt(111) surface, and 90 times higher than commercial Pt/C.[429] Following the results from surface science studies, many chemists started to develop methodologies for the preparation of PtNi bimetallic nanocrystals with well-defined morphologies, especially structures with (111) facets exposed. For instance, using DMF as solvent and weak reductant, octahedral PtNi nanocrystals with tunable chemical compositions can be obtained in a one-pot hydrothermal synthesis.[430] Moreover, it is possible to obtain Pt-based alloy nanocrystals with various morphologies by tuning the ligands for the synthesis of nanocrystals. For instance, icosahedral Pt_3Ni nanoscrystals with 20 (111) facets exposed have been prepared using CO as reductant and capping agent in a mixed solvent of oleylamine and oleic acid.[431] The morphological characterizations and catalytic performance of icosahedral Pt_3Ni nanocrystals are shown in Figure 84. As can be seen, icosahedral Pt_3Ni nanocrystals showed higher ORR activity than octahedral Pt_3Ni, which has been claimed to be caused by the higher surface strain in icosahedral Pt_3Ni nanocrystals according to theoretical modeling. In a recent work, biaxially strained PtPb@Pt core−shell nanoplates have been prepared, and they show exceptional high stability for ORR.[432] The Pt shell containing four-layer Pt atoms showed large tensile strains in the (110) crystal facets, which could optimize the Pt−O interaction during ORR. Furthermore, the intermetallic PtPd core also promoted the stability of Pt shells, resulting in negligible activity decay after even 50 000 ORR cycles.

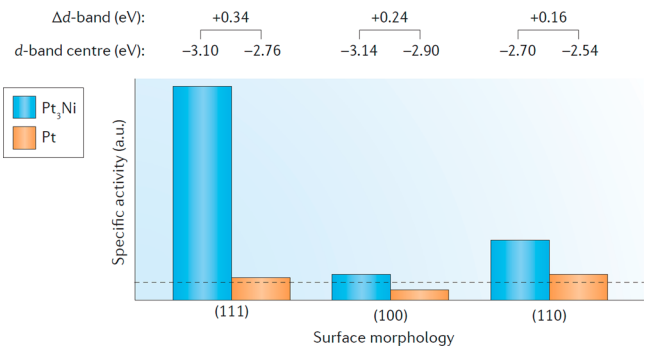

Figure 83. Influence of particle morphology and chemical compositions on the activity of Pt and Pt_3Ni for oxygen reduction reaction (ORR). Adapted with permission from ref 424. Copyright 2016 Macmillan Publishers Limited, part of Springer Nature.

Pt-based catalysts will also undergo surface reconstruction under electrocatalytic conditions, as it is commonly observed with heterogeneous catalysts. Transition metal, for instance, Ni, Co, Cu, in Pt-based alloy nanoparticles will be leaching into the electrolyte, and will form core−shell structures with a bimetallic Pt−M (M = Ni, Cu, Co, etc.) core and thin Pt skin on the surface. Such core−shell structures are proved to be stable and highly active for ORR, which is also consistent with the results obtained from surface science studies.[433−435] From the above understanding of structure−activity relationship on Pt-based catalysts, more complicated nanostructures have been prepared and show further enhanced ORR activity. For example, Chen et al. have reported the preparation of three-dimensional PtNi nanoframes with bimetallic PtNi as core and thin Pt skin as the shell. Such three-dimensional PtNi nanoframes showed high exposed surface sites and optimized surface structures, leading to high ORR activity and stability.[436] In addition, Li et al. have found the in situ formation of jagged Pt nanowires under oxygen reduction reaction conditions through electrochemical dealloying of PtNi bimetallic nanowires.[437] Those in situ formed Pt nanowires showed the highest mass activity for Pt-based catalyst up to now. It was proposed that the large percentage of Pt surface sites with unsaturated coordination environment and lattice strain account for its surprisingly high mass activity.

Electrocatalytic reduction of CO_2, as another important model reaction, is a hot topic in the electrocatalysis field. First, the particle size effect of metal nanoparticles for CO_2 reduction has been studied. For both Au and Cu nanoparticles, in the range from 2 to 10 nm, higher specific activity is achieved on smaller nanoparticles (Figure 85a), which can be ascribed to the higher percentage of metal atoms with unsaturated coordination environment.[438,439] Interestingly, by tuning the particle size of Au nanoparticles, it was possible to modulate the ratio of CO/H_2

DOI: 10.1021/acs.chemrev.7b00776
Chem. Rev. 2018, 118, 4981−5079

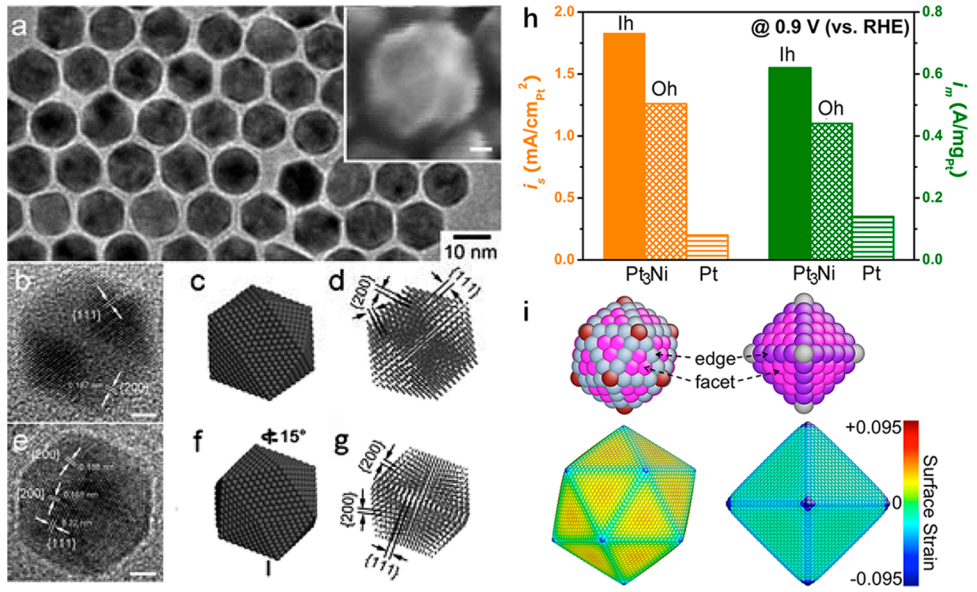

Figure 84. (a–g) Structural characterizations and determination of icosahedral Pt_3Ni nanocrystals. (h) Activity of icosahedral and octahedral Pt_3Ni nanocrystals as well as commercial Pt/C for oxygen reduction reaction. (i) Theoretical modeling of surface strain of icosahedral and octahedral Pt_3Ni nanocrystals. Adapted with permission from ref 431. Copyright 2012 American Chemical Society.

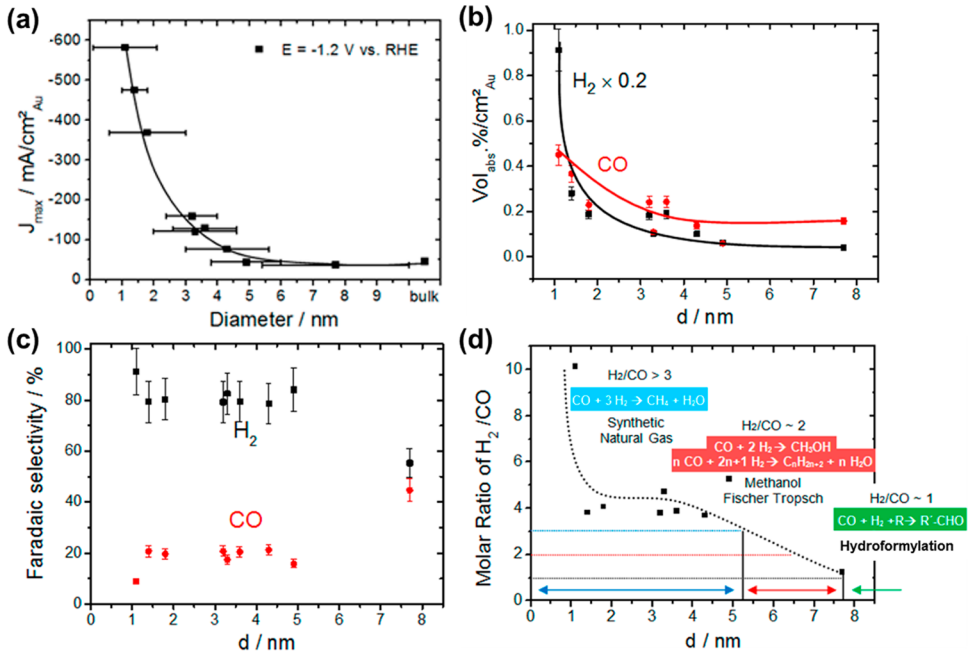

Figure 85. (a) Faradaic current densities at $E = -1.2$ V vs RHE on Au nanoparticles with different particle size. (b) Particle size dependence of the composition of gaseous products during electrocatalytic CO_2 reduction over Au nanoparticles. (c) Faradaic selectivity toward H_2 and CO as a function of size of Au nanoparticles in $KHCO_3$ solution (0.1 M) at $E = -1.2$ V vs RHE. (d) Ratio of gaseous CO/H_2 produced at $E = -1.2$ V vs RHE as a function of particle size of Au nanoparticles. Adapted with permission from ref 438. Copyright 2014 American Chemical Society.

in the evolved gas (see Figure 85). In the case of Pd nanoparticles, an optimized size of ~4 nm was observed for electrocatalytic CO_2 reduction to CO. Theoretical calculations show that the adsorption of CO_2 and the formation of COOH* (a key intermediate) are more favorable on edge and corner sites than on terrace sites of Pd nanoparticles. For Pd nanoparticles of ~4 nm, the amount of edge and corner sites is the highest, resulting in a better activity. Besides, the active sites for CO_2 reduction to CO on metal nanoparticles have also been proposed to be the grain boundary, and, in the case of Au nanoparticles, the electrocatalytic activity increases with the density of grain boundary.[440] Such structural-sensitive catalytic behaviors have also been observed on Ag-based and Cu-based catalysts for CO_2 reduction.[441,442]

CO_2 reduction can occur through different reaction pathways, leading to different products. However, so far, most of the reported work can only obtain CO as major product, as well as low yield of CH_4. Regarding other more valuable products (such as ethane, ethene, methanol, ethanol, etc.), they cannot be produced on most of the known systems. Recently, Gao et al. have reported the preparation of ultrathin Co nanosheets containing four layers of Co atoms for electrocatalytic reduction

DOI: 10.1021/acs.chemrev.7b00776
Chem. Rev. 2018, 118, 4981–5079

of CO_2 to formate.[443] It was found that the chemical state of Co has a significant influence on the electrocatalytic activity. When the Co nanosheets were partially oxidized, almost 1 order higher current density than the corresponding metallic Co nanosheets was observed. It was proposed that the partially oxidized Co species can facilitate the transfer of H species to CO_2 molecules adsorbed on Co nanosheets, which is a rate-limiting step in CO_2 reduction.

In recent years, progress has been achieved on Cu-based electrocatalyst for CO_2 reduction. By tuning the morphology and surface properties, the production of some more valuable products such as hydrocarbons and alcohols can be observed, although the yield is still too low for practical applications, if compared to conventional heterogeneous catalytic processes.[444−446] From a fundamental point of view, the reaction mechanism for electrocatalytic CO_2 reduction on the electrode and the electrode−electrolyte interface is still not clear. Because of the difficulty for performing kinetic studies and spectroscopic characterizations, the reaction pathways and limiting steps are far from being revealed. Besides, the morphology of nanoparticulate catalysts can also change during the electrocatalytic reactions, making it more complicated to address the active sites.[447] Nevertheless, the difficulty of electrocatalytic CO_2 reduction for large-scale operation will require further research and development efforts.

6.7. Organic Reactions

In traditional metal-catalyzed homogeneous organic reactions, the active species are usually thought to be isolated metal species, coordinated with ligands or solvents. In the section on catalytic properties of metal clusters, we have already discussed the in situ formed metal clusters under reaction conditions for some organic reactions. In those systems, although there is a difference between conventional mononuclear metal complexes and metal clusters, the in situ formed clusters still work as isolated active sites in homogeneous systems. In recent years, it has been reported that metal nanoparticles actually serve as the active sites for some organic reactions, including some important reactions with general interests, like C−H functionalization and C−C bond-forming reactions.[448−450] From a practical point of view, substituting conventional homogeneous catalysts with heterogeneous catalysts can help the organic transformations to meet the requirements for green and sustainable chemistry. Herein, we would like to highlight some typical examples on the application of metal nanoparticles for organic transformation and will make a brief discussion on the unique role that metal nanoparticles can play in some of those reactions.

In 2011, Stahl et al. reported the aerobic dehydrogenation of substituted cyclohexanones to phenols by Pd complexes.[451,452] In that paper, the starting catalyst was $Pd(OAc)_2$ or $Pd(TFA)_2$ (TFA = trifluoroacetate). 2-(*N*,*N*-Dimethylamino) pyridine as well as *p*-toluenesulfonic acid were also added to promote the yield. In their following papers, systematic kinetic investigations on the catalytic mechanism and active species were carried out. As shown in Figure 86a, cyclohexenone was formed as intermediate under those conditions and subsequently converted to phenol. In the first step from cyclohexanone to cyclohexenone, kinetic results indicated that the mononuclear Pd complexes could directly catalyze this transformation, while the formation of Pd nanoparticles under reaction conditions would slow the reaction rate (as shown in Figure 86b). To suppress the formation of Pd nanoparticles, DMSO was added and cyclohexenone was obtained in higher yield.[453] For the conversion of

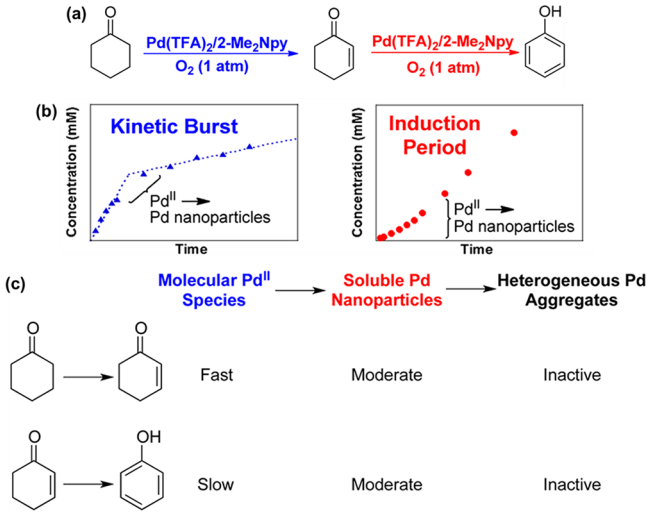

Figure 86. (a) Reaction scheme of aerobic dehydrogenation of cyclohexanone to cyclohexenone and then to phenol by Pd catalyst. (b) Kinetic results for the transformation from cyclohexanone to cyclohexanone (blue) and from cyclohexanone to phenol (red). (c) Summary of the evolution of Pd species under reaction conditions and their activity in the above two steps. Adapted with permission from ref 454. Copyright 2013 American Chemical Society.

cyclohexanone to phenol, an induction period corresponding to the formation of Pd nanoparticles from mononuclear Pd complex was observed, and the in situ formed Pd nanoparticles were more efficient than the Pd(II) complex for dehydrogenation of cyclohexanone to phenol.[454] However, those in situ formed Pd nanoparticles agglomerated into large nanoparticles (>100 nm) through a ripening process, leading to the deactivation of Pd catalysts (as summarized in Figure 86c). Therefore, to overcome the above problem, Xue et al. have prepared Pd nanoparticles capped with *β*-hydroxybutyric acid as heterogeneous catalyst for aerobic dehydrogenation of cyclohexanone to phenol.[455] These Pd nanoparticles capped by *β*-hydroxybutyric acid showed improved stability under reaction conditions, and a TON as high as 3000 was obtained. For comparison, $Pd(TFA)_2$ or commercial Pd/C catalyst can only achieve a TON less than 100 under the same conditions. It is then proposed that the presence of *β*-hydroxybutyric acid can protect Pd nanoparticles from leaching to the solution (proved by hot-filtration experiments) and sintering into large agglomerates. From a mechanistic point of view, by tuning the particle size and surface properties of Pd catalyst, it is possible to control the chemoselectivity and improve the stability for aerobic oxidative dehydrogenation of cyclohexanones.

Heterogeneous metal catalysts have also been reported as efficient catalysts for some C−H functionalization reactions. For instance, highly selective C3 C−H arylation of benzo[*b*]-thiophenes was achieved with commercial Pd/C and CuCl under mild conditions.[456] Control experiments using homogeneous catalysts like $PdCl_2(PPh_3)_2$ and $Pd(PPh_3)_4$ resulted exclusively in C2-arylation, which was different from the catalytic behavior of heterogeneous Pd/C catalyst. In addition, other experiments also confirm the heterogeneous nature of this process, which may account for the unique regioselectivity of Pd/C catalyst. In subsequent works, heterogeneous Pd catalysts have also been used for other arylation reactions, such as C−H thiolation of heteroarenes.[457,458] However, the origin of the

DOI: 10.1021/acs.chemrev.7b00776
Chem. Rev. 2018, 118, 4981−5079

unique catalytic properties of heterogeneous Pd catalysts is still not clear and requires further investigations.

There are also some other reports on the application of heterogeneous metal nanoparticles as catalyst for C−H functionalization. In a recent work, it has been demonstrated that Rh/C can catalyze the aerobic oxidative cross-coupling of aryl amines, resulting in the formation of asymmetric biaryl amines.[459] In another work, Warratz et al. show the *meta*-C−H bromination on purine bases by Ru/C catalyst.[460] It should be mentioned that the nature of active sites and catalytic mechanisms have not been clearly revealed in those works. Considering the critical role of the support on heterogeneous metal catalysts, the effects of metal−support interaction may have significant influences on the catalytic behavior. Furthermore, the structural evolution of heterogeneous metal catalysts under the experimental conditions for those organic reactions also needs to be considered. We believe that better understanding can be achieved in the future with more efforts from advanced and in situ characterizations, which proved new insights for developing more efficient and sustainable catalyst for organic reactions.

6.8. Catalysis with Alloyed Nanoparticles

Bimetallic and multimetallic nanoparticles have been shown to present quite distinct properties compared with monometallic nanoparticles.[461] Schematic illustrations of several typical types of bimetallic nanoparticles are shown in Figure 87. In bimetallic

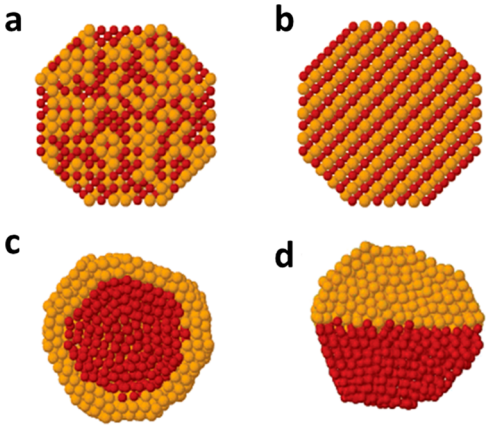

Figure 87. Schematic illustration of bimetallic nanoparticles with different types of spatial distributions of two elements. (a) Random alloyed, (b) intermetallic, (c) core−shell, and (d) heterojunction nanoparticles. Adapted with permission from ref 462. Copyright 2008 American Chemical Society.

or multimetallic nanoparticles, as a consequence of geometric stacking of two or more metal elements in a single nanoparticle, the size of the local segregation of each metal will be dependent on the chemical composition and atomic structures of the nanoparticles.[462]

By controllable synthesis of metal nanostructures, it is possible to modulate the physicochemical and catalytic properties. For instance, the spatial distributions of bimetallic alloy nanoparticles will have significant effects on the geometric and electronic structures. As it can be seen in Figure 87a and b, local enrichment of one metal element can exist in random alloyed nanoparticles. One metal can be separated by the other metal, leading to the formation of small patches. Those patches show different surface and electronic properties as compared to extended surface, and the size of the metal patches can be adjusted by the ratio of the two metal elements in bimetallic nanoparticles. Nevertheless, different spatial distributions of two metal elements should also affect the electronic interactions between them.[463] Besides, due to the heterogeneity in the distributions of the two metal elements, the geometric and electronic structures of randomly alloyed bimetallic nanoparticles are quite complicated. However, in the case of intermetallic nanoparticles, the whole nanoparticles have regular arrangement and homogeneous distribution of two metal elements.[464−466] The electronic and geometric structures of intermetallic nanoparticles can be well described on the basis of their well-defined atomic structures. More importantly, in suitable reactions, intermetallic nanoparticles show remarkable selectivity as compared to monometallic or randomly alloyed nanoparticles. For instance, as shown in Figure 88a, RuSb and RhSb intermetallic nanoparticles show remarkable selectivity for isomerization reaction of *cis*-alkene to *trans*-alkene.[467] Spectroscopic characterizations and theoretical calculations show that the selectivity to *trans*-alkene is strongly dependent on the geometric structure instead of the electronic structure of the catalyst. As shown in Figure 88b, the surface of RhSb intermetallic nanoparticles consists of a one-dimensional structure of Rh domains separated by Sb atoms. Therefore, when *cis*-alkene molecules were absorbed on RhSb nanoparticles, the inert Sb sites would block some reaction pathways for hydrogen addition reaction, which effectively suppress the hydrogenation of C═C bonds. In the other case of Ga@Rh core−shell structures shown in Figure 88c, the *cis*-alkene molecule could interact with a continuous Rh surface, on which the hydrogen addition reaction could undergo from several directions, leading to the hydrogenation of C═C bond (Figure 88d). Thus, intermetallic metal compounds provide a unique well-defined surface with spatial separated metal sites, which may enable one to make some highly selective transformations.

The stability of intermetallic compounds is a critical issue for catalytic applications. Pd_2Ga is an efficient catalyst for some selective hydrogenation reactions, like hydrogenation of CO_2 to methanol, hydrogenation of nitroarenes to anilines, and hydrogenation of alkynes to alkenes. By combing experimental results based on metal surface with well-defined structures and studies on nanoparticulate catalysts, it has been shown that the surface structure and chemical composition of the intermetallic Pd_2Ga compound are very sensitive to the environment. Furthermore, the chemoselectivity is strongly related to the intermetallic structure. Once the intermetallic structure is destroyed, the activity and selectivity irreversibly decline.[468,469]

One important reason for the application of bimetallic or multimetallic nanoparticles in catalytic reactions is the so-called synergistic effects between different elements as a result of their electronic interactions. Indeed, it has been observed in some reactions that bimetallic nanoparticles show better performance than catalysts made by each single metal component. For instance, AuPd alloy nanoparticles show significantly higher activity for oxidation of primary alcohols to aldehydes and oxidation of toluene to benzyl benzoate.[470,471] Moreover, AuPd bimetallic nanoparticles also show dramatically enhanced activity for hydrogenation of levulinic acid to γ-valerolactone.[472] However, in some cases like CO oxidation, water−gas shift, and decomposition of formic acid to CO_2 and H_2, AuPd bimetallic nanoparticles are less active than pure Au nanoparticles.[473] So far, there is no reasonable explanation on such synergistic effects. It is well-known that the electronic structures

DOI: 10.1021/acs.chemrev.7b00776
Chem. Rev. 2018, 118, 4981−5079

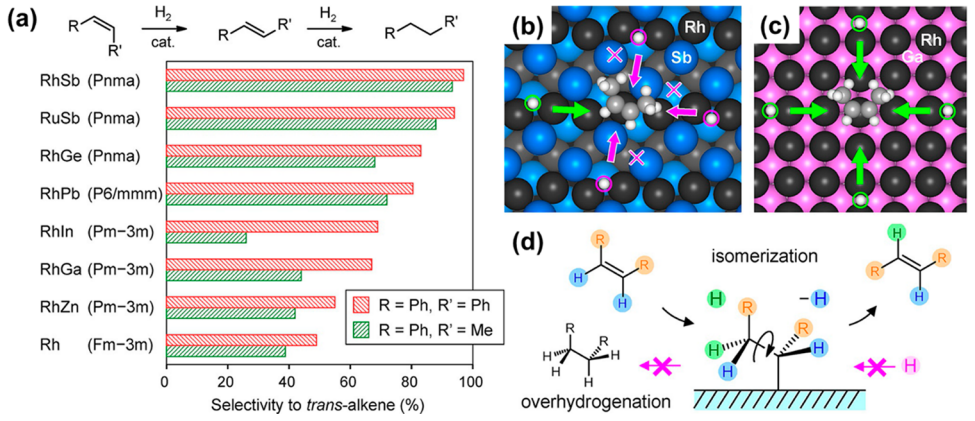

Figure 88. Selectivities to *trans*-alkenes during *cis*-stilbene and *cis*-methylstyrene isomerizations catalyzed by various Rh- and Ru-based intermetallic compounds and monometallic Rh supported on SiO_2. The reaction was performed under atmospheric pressure of H_2. Adapted with permission from ref 467. Copyright 2015 Wiley-VCH Verlag GmbH & Co. KGaA, Weinheim.

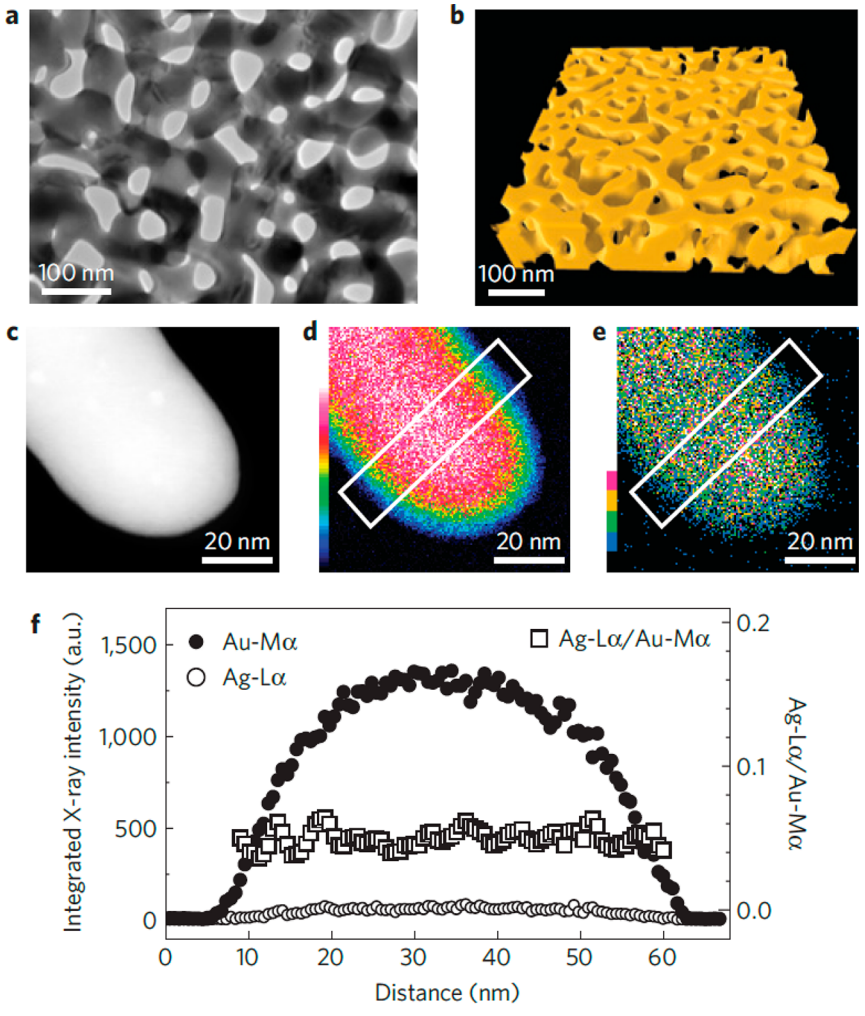

Figure 89. TEM micrographs and chemical analysis of nanoporous Au. (a,b) Low-magnification TEM image and the corresponding 3D tomographic reconstruction of nanoporous Au. (c) HAADF image of a gold ligament and the corresponding elemental mapping of Au (d) and Ag (e) in this area. (f) Line profile across the ligament, showing the relative amounts of Au and Ag in this area. Adapted with permission from ref 481. Copyright 2012 Macmillan Publishers Limited, part of Springer Nature.

as well as the geometric structures of bimetallic nanoparticles are different from the corresponding monometallic nanoparticles. However, the correlation between reactivity and structural factors is still unknown.

In the case of bimetallic catalysts with core−shell structures, the electronic properties of the metal shells in the nanoparticles can be modulated by tuning the thickness of the shell. Studies based on surface chemistry have already demonstrated the influences of the subsurface metal on the physicochemical

DOI: 10.1021/acs.chemrev.7b00776
Chem. Rev. 2018, 118, 4981−5079

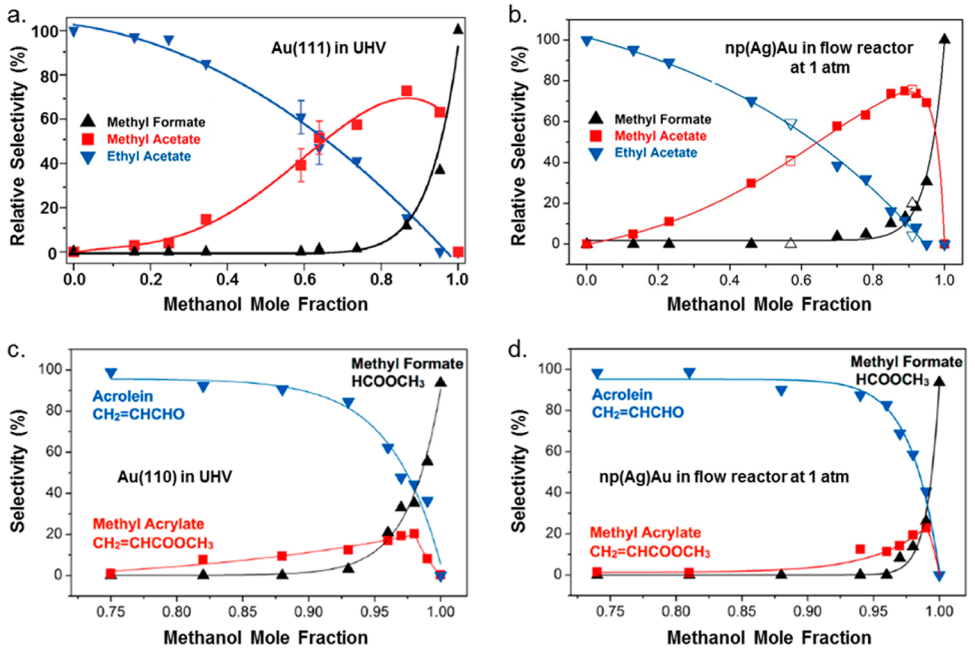

Figure 90. (a,b) Oxidative coupling of methanol and ethanol on Au(111) surface in UHV and on nanoporous Au in a fixed-bed flow reactor at atmosphere pressure. (c,d) Oxidative coupling of allylic alcohol and methanol on Au(111) surface in UHV and on nanoporous Au in a fixed-bed flow reactor at atmosphere pressure. Adapted with permission from ref 484. Copyright 2016 American Chemical Society.

properties of surface metal.[474] For example, the subsurface Pt−Ni−Pt(111) structure shows much higher hydrogenation activity as compared to Ni−Pt−Pt(111), Pt(111), and Ni(111).[475] The addition of subsurface 3d metal under Pt surface will shift the d-band center away from the Fermi energy level as compared to the Pt(111) surface, resulting in changes of adsorption properties of substrate molecules and activation energy for dissociation of H_2. We have already repeated throughout this Review that the lessons obtained from surface chemistry can be applied to the design of supported nanoparticulate metal catalysts. For example, in the preparation of Pd@Pt core−shell nanoparticles, electronic polarization will occur at the Pt−Pd interface, which results in the electron transfer from Pd to Pt.[476,477] The charge-transfer efficiency will be dependent on the thickness of Pt shells. Therefore, a series of electrocatalysts and photocatalysts with superior catalytic performances can be prepared on the basis of such principles.

6.9. Catalysis with Unsupported Metal Catalysts

In the above-mentioned works, metal nanoparticles are mainly supported on solid supports or exist as monodispersed nanoparticles in solution. In recent years, nanoporous Au has been prepared from acid leaching treatment of AuAg or AuAl alloy leaf (with thickness of hundreds of nanometers).[478] As shown in Figure 89a, the as-prepared nanoporous Au is composed of large Au particles (as compared to conventional supported Au catalysts) and macroporous structures. It is surprising to find that unsupported nanoporous Au shows remarkable activity in some catalytic oxidation reactions, including low-temperature CO oxidation.[479] For CO oxidation, it is well established that small Au nanoparticles or clusters supported on activated carriers (such as TiO_2, CeO_2, FeO_x) are the active species, while large or bulk Au particles are not active. Therefore, it is of interest to identify why nanoporous Au can be active for low-temperature CO oxidation. For that purpose, the chemical compositions of nanoporous Au have been carefully studied by electron microscopy, and it was found that the residual Ag in nanoporous Au plays a key role in selective oxidation reactions.[480] According to the EDS analysis shown in Figure 89 and surface analysis based on XPS, Ag was found to be enriched at the surface, and its concentration on the surface of nanoporous Au can be as high as 7 mol %. Furthermore, with the help of in situ TEM, the surface reconstruction of nanoporous Au under reaction conditions for CO oxidation has been investigated.[481,482] Aggregation of residual Ag to surface and the rapid diffusion of gold atoms at chemically active surface steps were observed simultaneously in the presence of $CO+O_2$ during the TEM measurements. These results indicate that nanoporous Au behaves differently from classic supported Au nanoparticles, and its active sites for oxidation reactions are related to the presence of Ag on the Au. Besides, the spatial distribution and chemical environment may also have significant influences. To show this potential effect, further detailed investigations are required, especially by in situ techniques.

Besides the CO oxidation discussed above, Friend et al. reported that methanol could be selectively converted into methyl formate ($HCOOCH_3$) at temperature as low as 80 °C on nanoporous Au.[483] It was also found that the amount of residual Ag in nanoporous Au could regulate the reactivity and selectivity for oxidation of methanol to methyl formate. With a higher amount of Ag, the selectivity to methyl formate decreased. For comparison, supported Ag nanoparticles only gave combustion product (CO_2) under the same conditions, indicating that tuning the size of Ag species in nanoporous Au is critical for selective oxidation of methanol. Moreover, other selective oxidation of alcohols (like ethanol) to the corresponding ester can also be carried out on nanoporous Au with remarkable selectivity under mild conditions (Figure 90).[484]

Kinetic studies show that the residual Ag species in nanoporous Au is an integral part of the active site for O_2 activation and the subsequent oxidative coupling of methanol to methyl formate.[485] In a recent work, the dynamic surface reconstruction of nanoporous Au has been investigated by means

DOI: 10.1021/acs.chemrev.7b00776
Chem. Rev. 2018, 118, 4981−5079

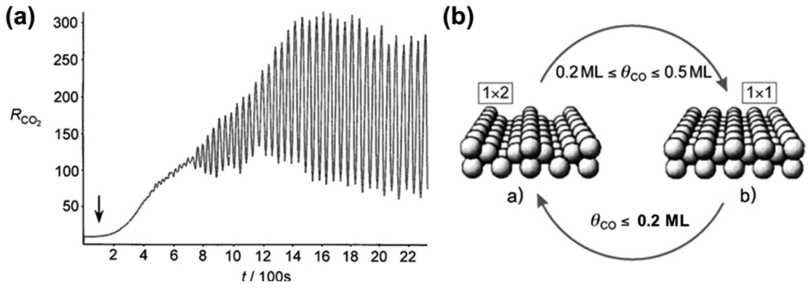

Figure 91. (a) Temporal oscillations of the production rate of CO_2 on Pt(110) surface at 470 K with a CO pressure of 3×10^{-5} mbar. (b) Surface reconstruction of Pt(110) surface between 1×1 and 1×2 structure under different CO coverage. Adapted with permission from ref 499. Copyright 2008 Wiley-VCH Verlag GmbH & Co. KGaA, Weinheim.

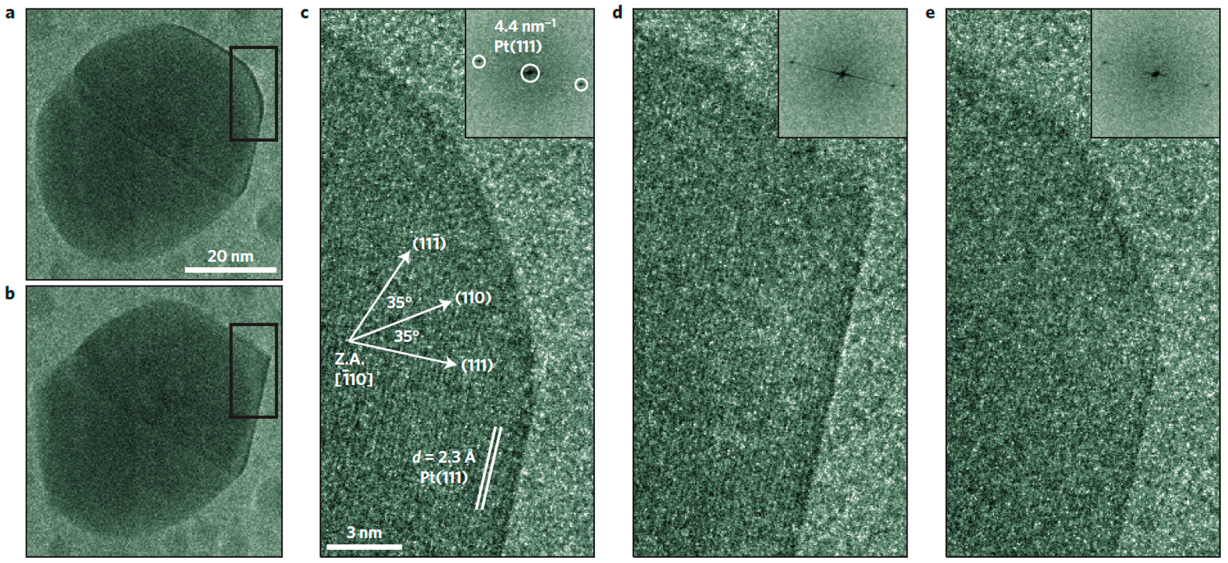

Figure 92. Visualization of the dynamic refacetting process of a Pt nanoparticle during the oscillatory CO oxidation at atomic scale by in situ high-resolution TEM. The TEM images show the more spherical shape (a,c,e, corresponding to lower CO conversion) and the more faceted shape (b,d, corresponding to higher CO conversion) during the oscillatory reaction. Adapted with permission from ref 498. Copyright 2014 Macmillan Publishers Limited, part of Springer Nature.

of in situ high-resolution TEM. It was clearly shown that after ozone treatment, the concentration of Ag species at the surface increased and those Ag species appeared as AgO_x patches, which was consistent with previous studies.[486,487] However, such AgO_x species were highly active and reacted with methanol to CO_2 directly. Further exposure of the nanoporous Au to CO would reduce those AgO_x species to Ag−Au alloy sites, which were quite selective for converting methanol into methyl formate. After reducion by methanol, Ag species would migrate to the subsurface, which could be regenerated by O_2 treatment. Therefore, a catalytic cycle for oxidative coupling of methanol to methyl formate can be envisaged.

6.10. Structural Evolution of Metal Nanoparticles under Reaction Conditions

Dynamic structural transformations of metal surface have already been well demonstrated in many systems.[488] The atomic arrangements on metal surface will reconstruct when interacting with different substrate molecules. Therefore, the surface structures of metal nanoparticles will be quite different under reaction conditions as compared to the situation in vacuum. The same will occur with catalysts based on single atoms and clusters.[489,490] As it has been mentioned and discussed before in this Review, the dynamic structural transformation of metal catalysts under various environments has already been realized by the catalysis community and reflected on in research works, including the changes of particle size, particle morphology, and spatial distributions of elements. In this part of the Review, we would like to emphasize the surface oscillation on metal surface and metal nanoparticles under reaction conditions.[491,492]

It was found in the 1970s that the production rate of CO_2 during CO oxidation reaction on supported Pt catalyst sometimes showed temporal oscillation behavior.[493] Such oscillation behavior of the CO_2 production rate was also observed on the Pt(110) surface, as shown in Figure 91a.[494] The oscillation patterns suggest that the CO oxidation reaction on Pt surface is far from equilibrium, which is similar to the population dynamics observed in nature.[495] Taking into consideration that the coverage of CO on Pt surface can affect the surface arrangements (see Figure 91b), the reaction kinetics of CO oxidation can be related to the dynamic oscillation of Pt surface structure. According to the results from surface science studies, it can be speculated that the oscillation behavior should occur in the following way. First, when Pt(110) surface is exposed to $CO+O_2$ mixture with a suitable CO/O_2 ratio, a transition from (1×2) pattern to (1×1) occurs. On (1×1) structure, the activation of O_2 will be favorable, leading to the consumption of CO. As a result, the CO coverage on (1×1) structure decreases, and the Pt(110) surface reconstructs into

DOI: 10.1021/acs.chemrev.7b00776
Chem. Rev. 2018, 118, 4981−5079

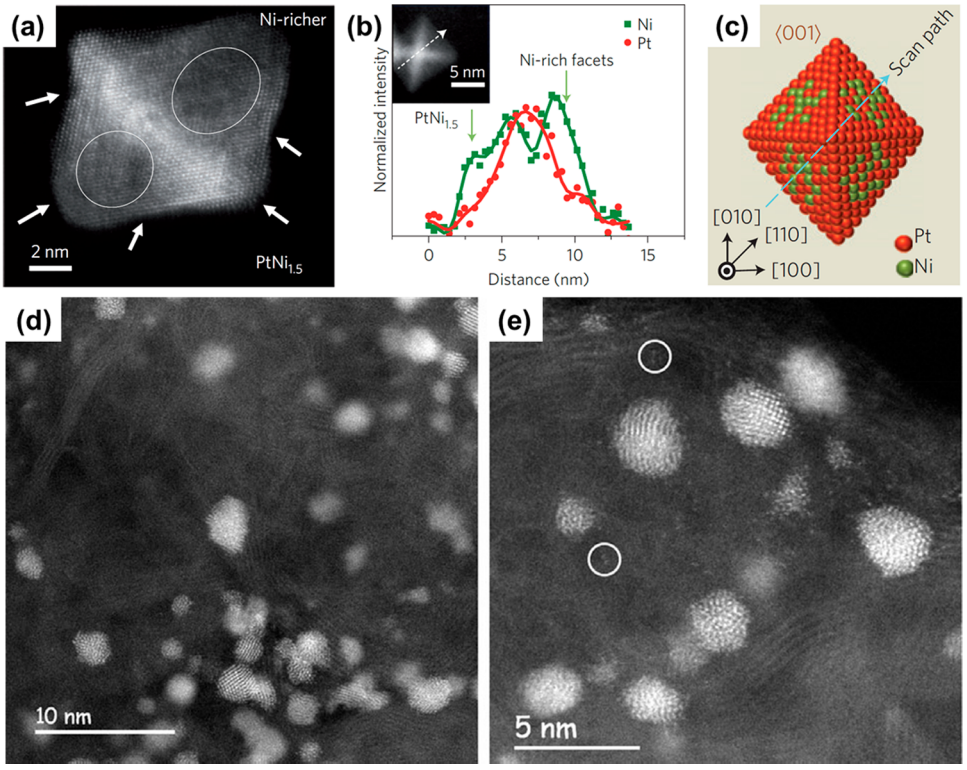

Figure 93. (a) High-resolution STEM image of PtNi bimetallic octahedral nanoparticle. The step sites on the surface of this particle are indicated by white arrows. Furthermore, local enrichment of Ni can also be found in this particle, suggesting the inhomogeneous distribution of Pt and Ni elements. (b,c) Elemental linescan of Pt and Ni and the corresponding schematic illustration of a PtNi bimetallic octahedral nanoparticle, showing the partially separation of Ni and Pt in a single nanocrystal. (d,e) High-resolution STEM image a typical Pd/C catalyst with a Pd loading of 5 wt % prepared by conventional wet impregnation. It can be clearly seen that Pd nanoparticles with irregular shapes are present in this sample. Those Pd nanoparticles show spherical shapes, with a large number of coordination unsaturated surface sites. Besides, some single Pd atoms also appear in this Pd/C catalyst. (a–c) Adapted with permission from ref 504. Copyright 2013 Macmillan Publishers Limited, part of Springer Nature. (d,e) Adapted with permission from ref 508. Copyright 2014 Wiley-VCH Verlag GmbH & Co. KGaA, Weinheim.

(1×2) structure. Notably, a key factor to achieve the above nonequilibrium oscillation process is the diffusion of reactants on Pt surface. By tuning the diffusion kinetics of CO and O_2, it should be possible to achieve different oscillation patterns on the Pt surface.[496] Moreover, when the reaction pressure increases from low pressure (for instance, 1×10^{-6} mbar) in UHV system to atmospheric pressure (1 bar), the oscillation behavior can also be observed, although the driving force becomes the dynamic transformation between metallic and metal oxide surface.[497]

The nonequilibrium oscillation behavior has also been observed on nanoparticulate catalysts. In a recent work, with the help of in situ TEM working at 1 bar, the surface oscillation of Pt nanoparticles under CO oxidation conditions was studied.[498] It is clearly shown in Figure 92 that the exposed facets of Pt nanoparticles showed oscillation behavior under CO oxidation conditions, changing between sharp facet (corresponding to higher conversion for CO+O_2) and rounded facet (corresponding to lower conversion for CO+O_2). By combining the data from mass and heat transport calculations as well as theoretical modeling, it was proposed that such refacetting behavior is related to the CO adsorption energy and reaction rate of CO+O_2.

Although there are still many open questions related to the oscillation behaviors of heterogeneous catalysts, it should be a common phenomenon and it has not been paid enough attention yet when studying supported metal catalysts.[499,500] For instance, oscillatory behavior has also been observed on partial oxidation of methane to syngas on supported Pd catalysts.[501] For studying the active sites in heterogeneous catalysis, the active sites are usually treated as "stable" species with identified structure and behavior. However, for acid–base and redox catalytic processes on metal catalysts, they are dynamic processes, which means the active sites should be "flexible" and can undergo structural transformation at each elementary step. Therefore, a cyclic oscillation phenomenon should occur, although the oscillation pattern may differ from reaction to reaction.

6.11. Perspectives on Catalysis Based on Metal Nanoparticles

As we discussed before, the effects of shape of metal nanocrystals on catalytic properties have been observed in numerous works, and it can be accepted that different catalytic performance (including activity, selectivity, and stability) can be obtained on metal nanocatalysts with various shapes. In most of the previous works, different atomic arrangements of different crystal facets of metal nanocatalysts were thought to be a key reason to explain the experimental results.[502,503] Indeed, from a theoretical point of view, the adsorption and interaction between metal surface and substrate molecules vary with the surface structures. Therefore, in many cases, the theoretical calculations can be well correlated with the results from surface science experiments. However, in practical heterogeneous catalysts, it will be extremely difficult to obtain a regular and stable metal surface with well-defined atomic arrangements. Nowadays, by sophisticated chemical synthesis, metal nanocrystals with well-controlled morphology can be obtained according to characterization by TEM. To show the morphology of metal nanocrystals, the

DOI: 10.1021/acs.chemrev.7b00776
Chem. Rev. 2018, 118, 4981–5079

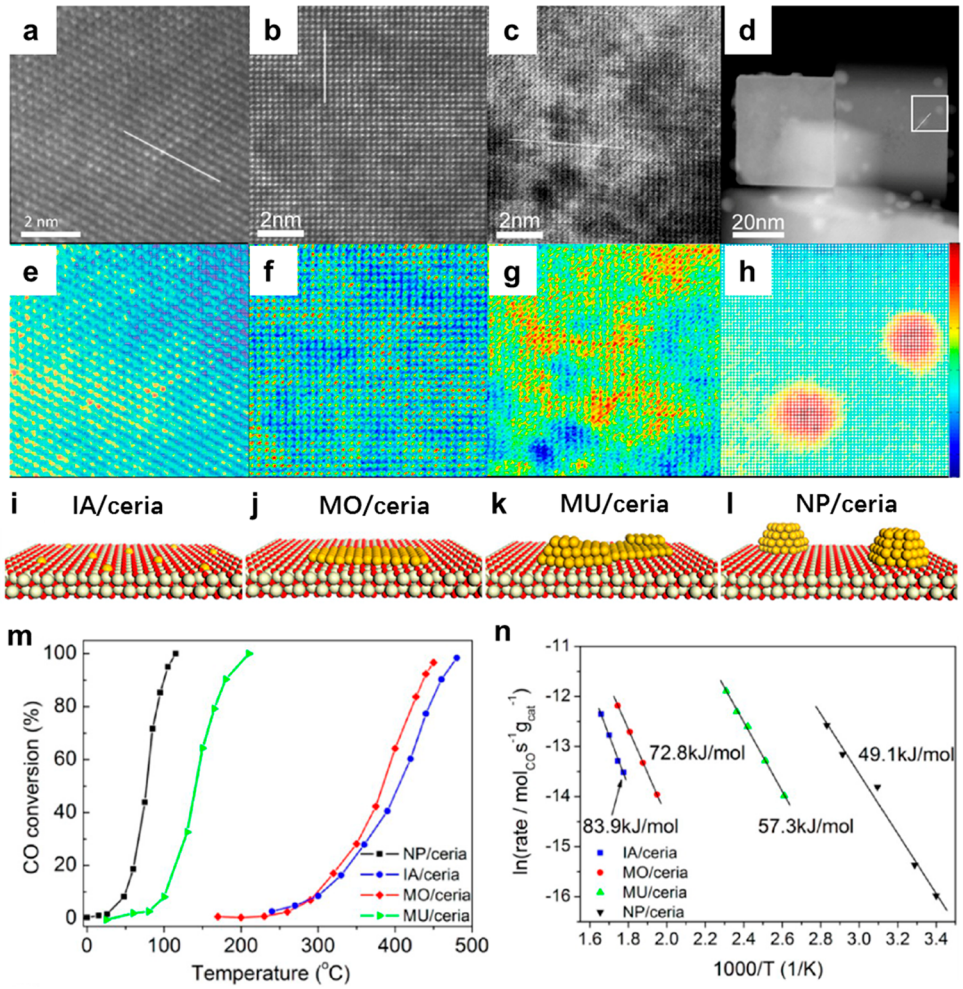

Figure 94. (a–h) High-resolution STEM images of various Au/CeO_2 and (i–l) corresponding schematic illustration of different types of Au species supported on CeO_2. (m) CO oxidation activity of various Au/CeO_2 catalysts. (n) Arrhenius plots of CO reaction rates of Au/CeO_2 catalysts with different types of Au species. IA/ceria, atomically dispersed Au; MO/ceria, single-layer Au; MU/ceria, multilayer Au; NP/ceria, Au nanoparticles. Adapted with permission from ref 512. Copyright 2015 American Chemical Society.

geometric scale of the TEM image is usually at nanometer range (usually larger than 10 nm). However, if those metal nanocrystals are studied with aberration-corrected electron microscopy with atomic resolution at subnanometric range, a large number of surface defects can be clearly observed. For instance, as shown in Figure 93a, some step and corner sites can be observed in a bimetallic PtNi nanocrystal with octahedral shape.[504] Actually, this is a quite common phenomenon for metal nanocrystals, in which the surface atomic arrangements do not perfectly match with their nanoscale geometric morphology. Local spatial separation of different elements should be a common situation for bimetallic or multimetallic nanoparticles, as displayed in Figure 93b. Moreover, in the case of bimetallic or multimetallic nanocrystals, the spatial distribution of different elements may not be precisely tuned at atomic scale. Taking into consideration that chemical reactions usually occur at the molecular level (subnanometric scale), there is a scale gap between the morphology of as-prepared metal nanocrystals and their surface atomic arrangements. If one considers the structural transformation of metal nanoparticles under reaction conditions, the situation will become even more complicated.

Nevertheless, according to research work based on surface science experiments, it is widely accepted in the catalysis community that the unsaturated surface sites (including terrace, step, kink, corner sites) may have higher reactivity than those surface sites with a saturated coordination environment. Therefore, it is supposed that nanocrystals with high-index crystal facets exposed may have higher catalytic activity than those with low-index crystal facets exposed. Indeed, in a large number of publications, it has been reported that metal nanocrystals with high-index crystal facets exposed show enhanced catalytic performance as compared to metal nanoparticles with low-index crystal facets, or metal nanoparticles prepared from conventional methods with irregular morphology.[505−507] However, if one looks into the atomic structures of conventional supported nanoparticulate catalysts (such as commercial Pt/C, Pd/C catalysts, or supported metal catalysts prepared by conventional impregnation or deposition-precipitation method), metal nanoparticles (1−5 nm) usually show spherical morphology.[508] In a typical example, the atomic STEM image of a Pd/C catalyst is shown in Figure 93d and e. From a structural point of view, a large number of coordination-unsaturated surface sites can be observed on those nanoparticles. Furthermore, taking into consideration their much smaller size as compared to those nanocrystals with well-controlled morphology (such as concaved nanocrystals or nanowires), the density of unsaturated surface sites should be much higher in conventional nanoparticulate catalysts.

DOI: 10.1021/acs.chemrev.7b00776
Chem. Rev. 2018, 118, 4981−5079

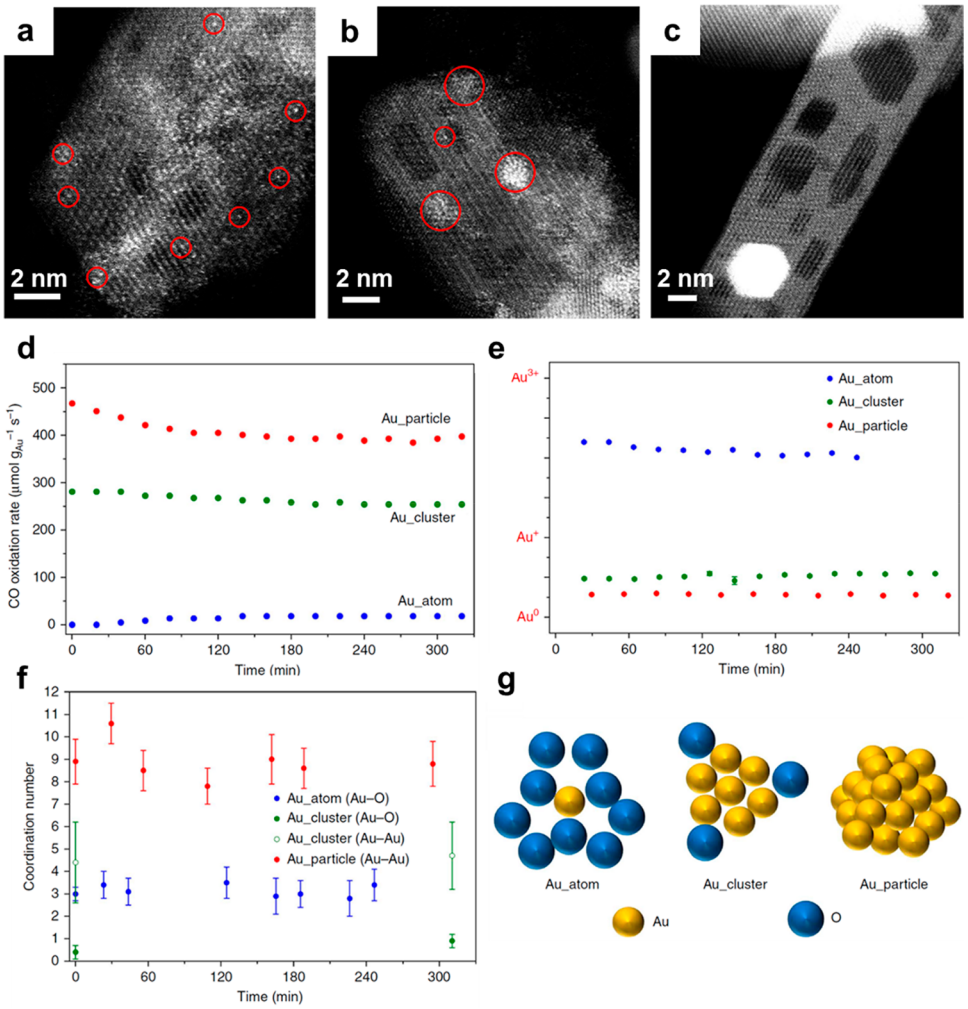

Figure 95. (a–c) High-resolution STEM images of single Au atoms, Au clusters, and nanoparticles supported on CeO_2 nanorods, respectively. (d) Reaction rates of three Au/CeO_2 samples for CO oxidation at room temperature. (e) Au oxidation state and (f) coordination number of Au–O/Au–Au as a function of reaction time, measured by XANES and EXAFS, respectively. (g) Schematic illustration of different types of Au species supported on CeO_2. In the case of Au single atoms, they exist as cationic Au ions. Au clusters exist as a mixture of metallic Au and cationic Au, and Au nanoparticles show metallic state. Adapted with permission from ref 513. Copyright 2016 Macmillan Publishers Limited, part of Springer Nature.

On the basis of the above analysis, it seems that some paradoxes can be found in the field of nanocatalysis. There is no doubt that the fast developments in the nanocatalysis field have brought lots of new insights for better understanding on heterogeneous catalysis, leading to the development of methodologies for preparation of new materials and new characterization techniques.[509−511] However, we want to emphasize that, to explain the catalytic phenomena at the molecular level, more emphasis should be done on establishing the correlations between reactivity and nanoscale morphology of metal nanoparticles for heterogeneous catalysis.

7. COMPARISON OF THE CATALYTIC BEHAVIOR OF SINGLE ATOMS, NANOCLUSTERS, AND NANOPARTICLES

7.1. CO Oxidation

As discussed before, different types of metal species (including single atoms, clusters, and nanoparticles) have been reported as active catalysts for CO oxidation reaction. When revisiting the work, we focused on different reports that were reaching contradictory conclusions on the relative activity of single atoms, clusters, and nanoparticles. We were emphasizing that catalytic activity should be compared under the same or similar experimental conditions. Otherwise, discussion on potential different reactivity of single atoms, clusters, and nanoparticles can be meaningless. We will carry out such a discussion here, trying to select situations in which their intrinsic reactivity can be comparable.

In the case of gold catalysts, Zhou et al. have prepared several types of Au species supported on CeO_2 nanoparticles to study the size and shape effects of Au for CO oxidation.[512] In their work, Au single atoms, Au monolayers, and Au nanoparticles were deposited on CeO_2 nanocubes as model catalysts. According to the temperature-programmed reduction (TPR) profiles, the reducibility of Au became difficult when decreasing the size from nanoparticles (ca. 3 nm) to single Au atoms, indicating the different redox properties of various Au species. As presented in Figure 94a, Au nanoparticles gave the best CO oxidation activity at low temperature range, and activity decreased when decreasing the particle size. In the case of isolated Au atoms supported on CeO_2, the sample required nearly 500 °C to reach total conversion of CO to CO_2. Furthermore, the TOF values of various Au/CeO_2 catalysts for

DOI: 10.1021/acs.chemrev.7b00776
Chem. Rev. 2018, 118, 4981−5079

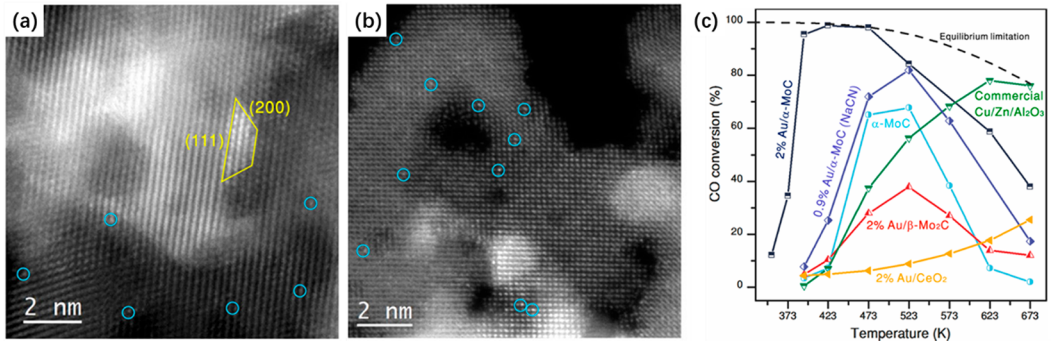

Figure 96. (a) High-resolution STEM image of 2%Au/α-MoC sample, showing the presence of both Au nanoparticles (~2 nm) and individual Au atoms. (b) High-resolution STEM image of 0.9%Au/α-MoC sample obtained by the NaCN leaching treatment on 2%Au/α-MoC sample. In this sample, only isolated Au atoms are observed. (c) Catalytic performance of different Au catalysts and the α-MoC support for water−gas shift reaction. Reaction condition: 10.5% CO, 21% H_2O, 20% N_2 in Ar; GHSV, 180 000 h^{-1}. Adapted with permission from ref 516. Copyright 2017 The American Association for the Advancement of Science.

CO oxidation at 240 °C have been calculated on the basis of all of the Au atoms in the catalyst. Au nanoparticles showed the highest TOF (9.88×10^{-1} s^{-1}), while isolated Au atoms showed the lowest TOF (1.07×10^{-2} s^{-1}). The nearly 2 order magnitude difference for CO oxidation activity shown above allows one to conclude that Au single atoms supported on CeO_2 are almost inert for CO oxidation, while Au nanoparticles (2−5 nm) are the most active species. The catalytic performance of subnanometric Au clusters was not studied in this work, but one could, in principle, extrapolate from the above results, that the catalytic activity of Au subnanometric metal clusters for CO oxidation may be smaller than for nanoparticles. However, because of the different electronic nature of the Au clusters with respect to Au nanoparticles, it could be risky to extrapolate the above results.

Interestingly, in a very recent work, a direct comparison between Au single atoms, clusters, and nanoparticles supported on CeO_2 nanorods has also been reported for CO oxidation (see Figure 95a−c).[513] As shown in Figure 95d, the catalytic activity normalized per Au atom for CO oxidation at room temperature showed that both Au nanoparticles and clusters are active at room temperature, while Au single atoms showed negligible activity for CO oxidation. Further in situ spectroscopic characterization showed that metallic Au species played a key role in CO oxidation reaction. Unfortunately, studies on the activation of O_2, which is a key step for CO oxidation, were not studied in this work. It should be mentioned that these above-mentioned results are consistent with the previous works from Goodman and Hutchings on Au/TiO_2 and Au/FeO_x, implying that the relative activity of Au single atoms, clusters, and nanoparticles for CO oxidation may follow a similar pattern on different supports.

As has been discussed before, Au/CeO_2 with low Au loading (0.05 wt %), containing singly dispersed Au atoms, was prepared and used for preferential oxidation of CO in the presence of H_2 (CO-PROX).[71] According to the data presented in that work, Au single atoms supported on CeO_2 also show poor activity as compared to Au nanoparticles for the CO-PROX reaction at room temperature. However, if the reaction is performed at 80 °C, Au single atoms show acceptable activity with good selectivity, while Au nanoparticles show lower selectivity to CO oxidation and considerable consumption of H_2. Thus, although the Au single atoms show lower intrinsic activity for CO oxidation, they may show higher selectivity for CO-PROX reaction. This is especially interesting because the CO-PROX process is best designed to operate around 80 °C.

In the case of CO oxidation on supported Pt catalyst, there are also contradictory results in the literature on the nature of the active sites and the relative activity of single atoms and nanoparticles. Stair et al. have simultaneously monitored different types of Pt species and their relative activity for CO oxidation by in situ IR spectroscopy.[514] After CO molecules were absorbed on Pt single atoms and nanoparticles, O_2 was introduced to the IR cell to oxidize the absorbed CO molecules to CO_2. It was claimed that only CO absorbed on Pt nanoparticles could react with O_2, while those absorbed on Pt single atoms remained stable up to 100 °C. On the basis of the IR results, it was claimed that under those reaction conditions, Pt single atoms do not participate in the CO oxidation reaction, while Pt nanoparticles were the catalytically active phase. It has to be mentioned here that in some other works, it has been claimed that single Pt atoms were active for CO oxidation. Thus, considering all previous reports on Pt single-atom catalysts, it seems that there are some contradictive conclusions on the active sites for Pt-catalyzed CO oxidation reaction.[72,73,75,78] However, it should be considered that the evolution of single atoms under reaction conditions is an important issue to be considered, and, so far, there is still not a clear global picture on the stability of single Pt atoms under reaction conditions, especially for those catalysts working at higher temperature (>90 °C).

Recently, the stability and evolution of atomically dispersed Pt species under reaction conditions has been studied in our research group by in situ TEM.[514] It has been seen that atomically dispersed Pt species will agglomerate into Pt clusters and small nanoparticles under CO+O_2 atmosphere at 100−300 °C. Furthermore, it has also been observed that those sintered Pt clusters and nanoparticles can redisperse into atomically dispersed Pt species when the reaction temperature is increased to 400 °C. These recent results imply that single atoms, clusters, and nanoparticles can show dynamic structural transformations between each other, and their state is strongly related to the reaction conditions. Therefore, it is highly recommended to establish reaction−structure correlations considering the catalytic species present during the catalytic reaction.

7.2. Water−Gas Shift

As already discussed in this Review, it has been reported that atomically dispersed Pt and Au species on various supports including zeolites, SiO_2, TiO_2, FeO_x, and CeO_2 are the active sites for water−gas shift reaction.[515] However, in a recent work, it has been shown that small Au nanoparticles (~2 nm) are the

DOI: 10.1021/acs.chemrev.7b00776
Chem. Rev. 2018, 118, 4981−5079

active sites for low-temperature WGS reaction, while Au single atoms are not active under the same conditions.[516] As it can be seen in Figure 96, the 2%Au/α-MoC sample containing Au nanoparticles showed exceptional high activity below 473 K, while the 0.9%Au/α-MoC sample containing Au single atoms showed much lower activity. These results are in contradiction to those observed with Au/oxide catalysts, which imply that the active species for low-temperature WGS reaction may depend on the support.

In a recent work from our research group, it has been observed by in situ TEM that atomically dispersed Pt species will agglomerate into Pt clusters and small nanoparticles under water−gas shift conditions, indicating the importance to investigate the stability of single atoms under WGS reaction conditions when trying to identify the nature of the active species.[514] A similar phenomenon has already been observed with Au/$CeZrO_4$ catalyst by TEM.[517] It was observed that subnanometric Au species agglomerated into Au nanoparticles (1−2 nm) during the water−gas shift reaction. According to previous studies from different groups, it seems that different types of metal species, from single atoms to clusters to nanoparticles, can be active for WGS reaction. However, the intrinsic activity of different types of metal species for WGS reaction is still not clear, which should be studied in future works.

7.3. Oxidation of Hydrocarbons

The oxidation of hydrocarbons to functional oxygenates is an important type of reaction for the preparation of valuable bulk chemicals. In most of the cases, a small amount of radical initiator is required to perform the reaction.[518] As we have discussed before, subnanometric Au clusters have been claimed to be active species for aerobic oxidation of cyclooctene in the absence of radical initiator. In that reaction, the role of Au clusters was to react with cyclooctene and generate radicals to initiate the oxidation reaction. However, leaching of Au nanoparticles into solution was also observed under reaction conditions.

When the substrate is switched from cyclooctene to cyclohexene, the catalytic behavior of Au catalyst changes. Donoeva et al. have prepared Au clusters and nanoparticles with different sizes and studied their catalytic behavior for oxidation of cyclohexene and the structural transformation of Au species under reaction conditions.[519,520] As can be seen in Figure 97, only Au nanoparticles larger than 2 nm were able to catalyze the oxidation of cyclohexene, while Au clusters and small Au nanoparticles (below 2 nm) showed negligible initial activity. Interestingly, an induction period was observed during the kinetic study when Au_9 clusters were used as catalyst. By tracking

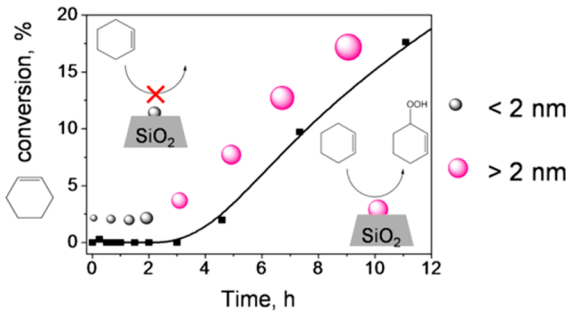

Figure 97. Relationships between the size of Au and the activity in the selective oxidation of cyclohexene into cyclohexenyl hydroperoxide. Adapted with permission from ref 519. Copyright 2013 American Chemical Society.

with UV−vis spectra, the in situ transformation of Au_9 clusters into Au nanoparticles was confirmed, and the catalyst containing Au nanoparticles did not show the induction period during the second run. These results suggest that the active species for aerobic oxidation of cyclohexene are Au nanoparticles larger than 2 nm instead of mononuclear Au compounds or Au clusters. Combining the results obtained from oxidation of cyclooctene and cyclohexene, it seems to us that either the type of active species is dependent on the substrate molecules or the role of leached gold species that aggregate to form nanoparticles requires further investigations.

The different catalytic behavior of mononuclear Au complex and Au nanoparticles can also be illustrated by the direct oxidative homocoupling of arenes. It has been reported that Au nanoparticles supported on TiO_2 can catalyze the direct oxidative coupling of nonactivated aromatics.[521] Although the yield is still low, this work opens a new strategy for the production of diphenyl compounds in an interesting way. In a recent work, Ishida et al. have reported the application of Au/Co_3O_4 catalysts for oxidative coupling of dimethyl phthalate, as shown in Figure 98a.[522] Mechanistic studies showed that metallic Au nano-

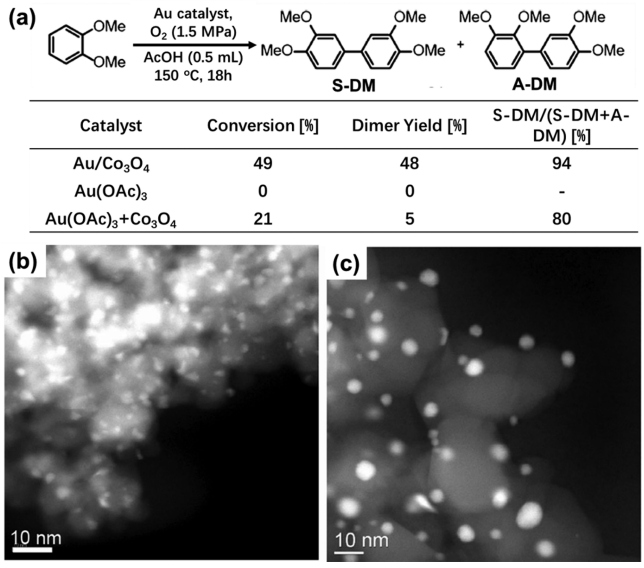

Catalyst	Conversion [%]	Dimer Yield [%]	S-DM/(S-DM+A-DM) [%]
Au/Co_3O_4	49	48	94
Au$(OAc)_3$	0	0	-
Au$(OAc)_3$+Co_3O_4	21	5	80

Figure 98. (a) Oxidative coupling of dimethyl phthalate with different Au catalysts. (b) STEM images of Au/Co_3O_4 catalyst (b) and Au$(OAc)_3$+Co_3O_4 (c) after the coupling of dimethyl phthalate. Adapted with permission from ref 522. Copyright 2015 Wiley-VCH Verlag GmbH & Co. KGaA, Weinheim.

particles were the active sites for the oxidative coupling of arenes, while mononuclear Au compounds would transform into metallic Au nanoparticles in the presence of the metal oxide support under reaction conditions (see Figure 98c). Previous kinetic results have already revealed that activation of O_2 does not appear to be the rate-limiting step, while activation of C−H bond in arenes is probably the rate-limiting step.[523] However, how the size of Au particles affects the activation of C−H bonds in arenes is still not clear, and it is probably related to the different electronic structures between Au nanoparticles and smaller Au species (Au single atoms or clusters).

The transformation of metal compounds under reaction conditions has also been studied for Cu-catalyzed oxidative coupling of alkynes. CuCl and other Cu compounds like $Cu(Ac)_2$ are classic catalysts for oxidative coupling of terminal

DOI: 10.1021/acs.chemrev.7b00776
Chem. Rev. 2018, 118, 4981−5079

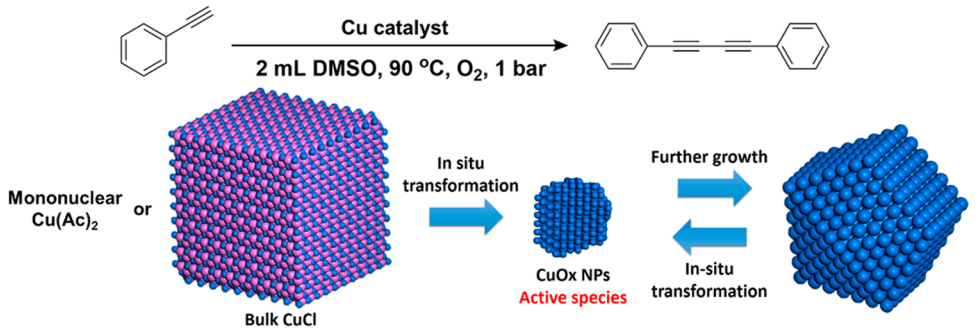

Figure 99. Oxidative coupling of phenylacetylene using mononuclear $Cu(Ac)_2$ or bulk CuCl as the starting catalyst. These Cu compounds would transform into monodispersed CuO_x nanoparticles (~2 nm) under reaction conditions, which serve as the active species. Besides, small CuO_x nanoparticles (~2 nm) would further grow into large CuO_x nanoparticles when a large amount of Cu catalyst is introduced into the reaction mixture. Larger CuO_x nanoparticles can transform back to small CuO_x nanoparticles under suitable reaction conditions. Adapted with permission from ref 524. Copyright 2016 American Chemical Society.

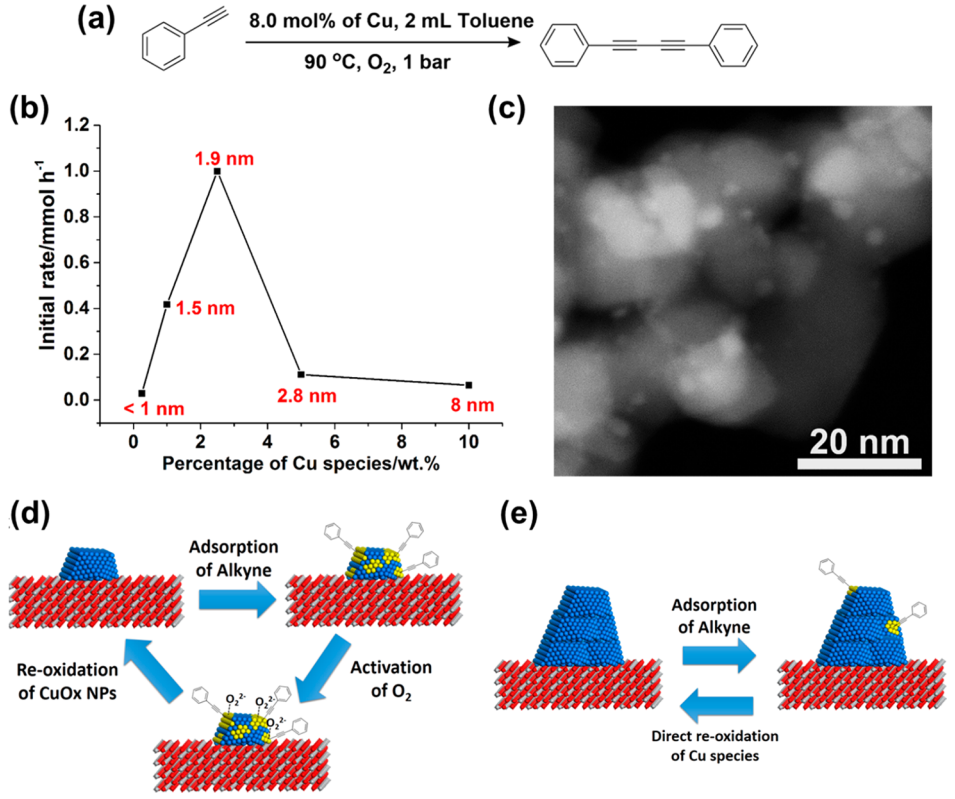

Figure 100. (a) Reaction scheme for the oxidative coupling of phenylacetylene with supported CuO_x/TiO_2 catalysts. (b) Initial reaction rates of CuO_x/TiO_2 catalysts with different Cu loading for oxidative coupling of phenylacetylene. (c) STEM image of CuO_x/TiO_2 sample with CuO_x nanoparticles of ~2 nm. (d) Schematic illustration of the proposed mechanism on CuO_x/TiO_2 sample with CuO_x nanoparticles of ~2 nm for oxidative coupling of phenylacetylene. O_2 molecules are activated through the formation of peroxides. (e) Schematic illustration of the proposed mechanism on CuO_x/TiO_2 sample with CuO_x nanoparticles of 5−10 nm for oxidative coupling of phenylacetylene. Adapted with permission from ref 524. Copyright 2016 American Chemical Society.

alkynes.[524] However, when a small amount of CuCl or $Cu(Ac)_2$ (<5 mol %) was used as the starting catalyst, a reaction induction period was observed. It was found that the starting catalyst (Cu salts) formed CuO_x nanoparticles (~2 nm) under reaction conditions. Furthermore, when large CuO_x nanoparticles (5−10 nm) were used as the starting catalyst, an induction period was also observed. By following the reaction and the evolution of the catalyst with reaction time, it was observed that the large particles were transformed into small CuO_x nanoparticles (~2 nm) under reaction conditions. On the other hand, subnanometric Cu clusters were found to be inactive for this reaction. Therefore, as described in Figure 99, a dynamic transformation between Cu species was observed during the reaction for oxidative coupling of terminal alkynes, when working in homogeneous phase. A series of supported CuO_x/TiO_2 catalysts were prepared and also tested for oxidative coupling of terminal alkynes. By tuning the loading of Cu, the particle size of CuO_x could be modulated, from the subnanometric regime to nearly 10 nm. As shown in Figure 100b, the catalytic results of these supported CuO_x/TiO_2 catalysts show that only the CuO_x/TiO_2 sample with CuO_x nanoparticles of ~2 nm was the active catalyst (see Figure 100c for the STEM image of the active catalyst). Samples with smaller

DOI: 10.1021/acs.chemrev.7b00776
Chem. Rev. 2018, 118, 4981−5079

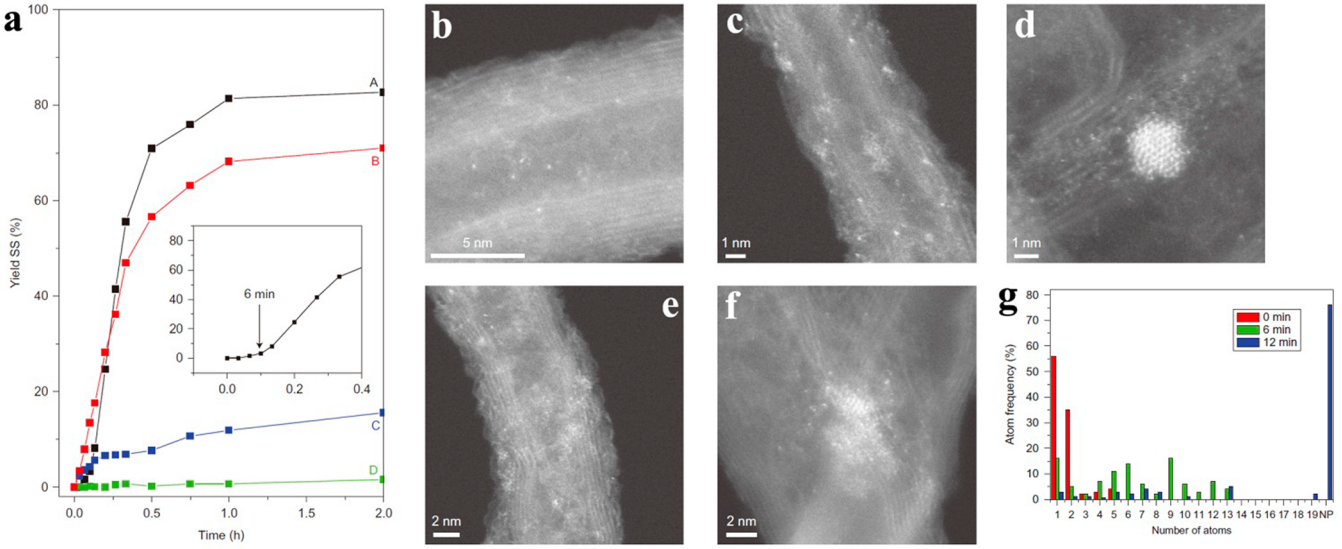

Figure 101. (a) Oxidation of thiophenol to disulfide in the presence of O_2 by Au catalysts. Single isolated gold atoms (sample A) are not active in the oxidation of thiophenol during the induction period of 6 min, which indicates that other types of Au species are being formed under reaction conditions. The evolution of the gold species was followed by stopping the reaction at different times. The catalyst (named as samples B, C, and D taken at 6, 12, and 120 min, respectively, during the reaction of sample A) were isolated from the reaction mixture and used to carry out a new reaction under the same conditions. The yields of disulfide with reaction time using samples A, B, C, and D as catalyst are shown. Inset shows the kinetic curve of sample A at the beginning of the reaction. (b−g) Evolution of the gold species present on the catalyst studied by high-resolution STEM. (b) Isolated gold atoms present on the as-prepared catalyst. (c) Catalyst taken after reaction for 6 min shows the presence of small clusters with 4−13 atoms. (d,e) Two different images of sample C taken at 12 min in which both small clusters and some Au nanoparticles can be observed. (f) In sample D, taken after 120 min of reaction, most of the gold aggregated into nanoparticles larger than 2 nm. (g) Size distribution of the Au species in samples A, B, and C. Adapted with permission from ref 525. Copyright 2013 Macmillan Publishers Limited, part of Springer Nature.

or larger CuO_x nanoparticles were much less active for this reaction, indicating a strong crystalline size effect. To understand these phenomenon, kinetic, spectroscopic, and isotopic studies were carried out. On the basis of the information acquired, the activation of O_2 was proved to be the rate-limiting step for oxidative coupling of alkynes, indicating the strong impact of the particle size of the Cu species on the activation of O_2. In fact, O_2 is activated in the form of peroxides, which are a key intermediate for oxidative coupling of alkynes on CuO_x nanoparticles of ∼2 nm. It appears quite clear that the size of CuO_x nanoparticles will determine how O_2 is activated, being the origin of the different catalytic performance of CuO_x nanoparticles with different sizes.

7.4. Oxidation of Alcohols and Thiophenol

It has also been found that Au clusters with low atomicity show enzyme-like activities for selective oxidation of thiophenol to disulfide.[525] Au single atoms were first supported on carbon nanotubes. As it can be seen in Figure 101a, a short induction period was observed when singly dispersed Au atoms were used as the starting catalyst, implying that single Au atoms were not the active species for oxidation of thiophenol. Interestingly, during the induction period, separated Au atoms aggregated to form Au clusters with 5−10 Au atoms, and the oxidation of thiophenol to disulfide started to occur. However, the reaction rate decreased when the conversion was higher than 70%, implying the deactivation of Au catalysts. High-resolution STEM at different reaction time (see Figure 101) indicated that subnanometric Au clusters agglomerated gradually to Au nanoparticles under reaction conditions, and then the reaction declined. Small Au nanoparticles (∼1 nm) were also prepared independently, and it was proved that Au nanoparticles were inactive for this reaction. Therefore, it can be concluded that only subnanometric Au clusters are active for oxidation of thiophenol to disulfide.

To understand the distinct catalytic behaviors of single Au atoms, clusters, and nanoparticles for the oxidation of thiophenol, theoretical calculations on the activation of thiophenol and O_2 on different Au species were performed. As shown in Figure 102, calculation results suggest that the interaction between thiophenol and Au clusters is strongly related to the atomicity of Au species. Thiophenol and O_2 can be activated on Au clusters, simultaneously. However, O_2 cannot be activated on single atoms, and Au nanoparticles are poisoned by thiophenol due to the formation of a stronger Au−S interaction.

The situation changes when Au is used as catalyst for the oxidation of alcohols. It is well established that supported Au nanoparticles are superior catalysts for selective oxidation of alcohols.[99] Aerobic oxidation of ethanol on Au_{38} nanoparticle and Au_3 cluster then was studied by theoretical calculations.[16] Following the calculation results, it appears that Au clusters are not active for oxidation of ethanol, while Au nanoparticles are quite active. The DFT results indicate that Au nanoparticles can activate O_2 through dissociation of O−O bond and facilitate the formation of a new bond by reductive elimination. In contrast, small Au clusters should be more active for reactions following radical pathways involving peroxo or hydroperoxo intermediates, such as the radical-initiated oxidation of cyclooctene. In the case of CuO_x, those hydroperoxo intermediates are formed on CuO_x nanoparticles of ∼2 nm, as shown before.

7.5. Selective Hydrogenation

Gates et al. have studied the evolution of Rh species under reaction conditions for hydrogenation of ethylene.[526] In the pristine catalyst, mononuclear Rh complexes were loaded in HY zeolite. After treatment in H_2 flow at 100 °C for 4 min, Rh dimers appeared, and longer H_2 treatment at 100 °C led to the formation of Rh clusters of around 0.5 nm, as described in Figure 103. The reactivity and selectivity for ethylene hydrogenation also changed

DOI: 10.1021/acs.chemrev.7b00776
Chem. Rev. 2018, 118, 4981−5079

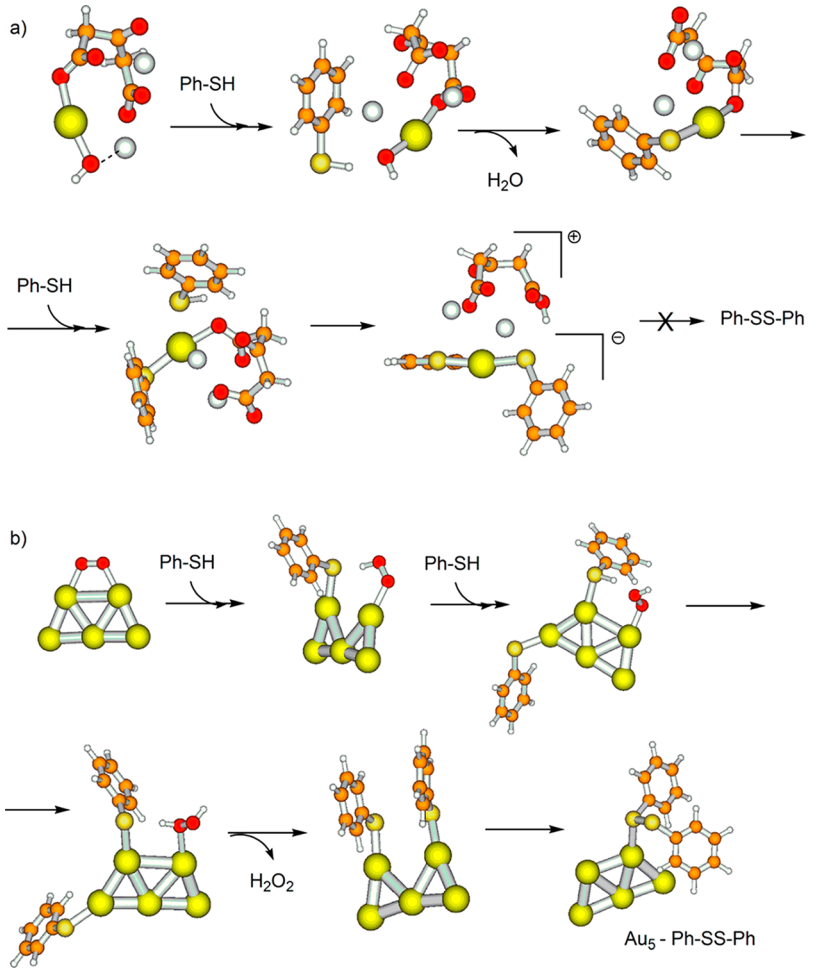

Figure 102. Structures involved in the mechanism of thiol oxidation catalyzed by (a) AuI species and (b) Au_5 cluster. Au, S, C, O, and H atoms are depicted in gold, yellow, orange, red, and white, respectively. Adapted with permission from ref 525. Copyright 2014 American Chemical Society.

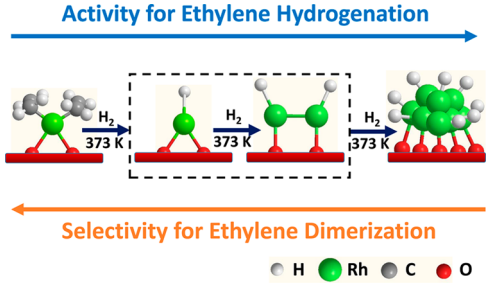

Figure 103. Evolution of mononuclear Rh complex supported on HY zeolite during the catalytic hydrogenation of ethylene and ethylene dimerization. In the presence of H_2, Rh atoms will agglomerate gradually into Rh clusters. The activity toward hydrogenation of ethylene and selectivity toward ethylene dimerization will also change with the atomicity of Rh species. Adapted with permission from ref 526. Copyright 2016 American Chemical Society.

with time on stream. As shown in Table 6, dimerization products (butenes) were the major products at time zero, because mononuclear Rh complex served as the Lewis acid sites for the dimerization of ethylene to butenes. After the H_2 reduction treatment, the conversion of ethylene as well as the selectivity to the hydrogenation product (ethane) increased significantly, indicating that the hydrogenation of ethylene was preferred on Rh clusters rather than on mononuclear Rh complex. In a recent work, Gates et al. demonstrate the unique role of pair-site Rh species supported on MgO for hydrogenation of ethene. It was found that pair-site Rh species (1.1 s^{-1}) are more than 2 orders more active than the single-site Rh species (<0.01 s^{-1}).[527] From a mechanistic point of view, one key step for the hydrogenation reaction is the dissociation of H_2, which normally requires a synergistic interaction between H_2 molecule and multiple metal sites.

The catalytic behavior of different Pt species has also been studied for hydrogenation of nitroarenes to aniline.[528] As shown in Figure 104a and b, single Pt atoms, clusters (with ∼10 Pt atoms), as well as nanoparticles (∼1 nm) were generated by size-selected method and deposited on silicon TEM grids. The three types of Pt species then were tested for hydrogenation of *p*-chloronitrobenzene in a batch reactor at 100 °C with 5 bar of H_2. As it can be seen in Figure 104c and d, Pt clusters showed the highest turnover number per Pt specie. However, if the turnover number was calculated on the basis of the Pt atoms, Pt single atoms showed the highest activity. After the hydrogenation reaction, the size and morphology of Pt species were preserved (see Figure 104e–h). These results indicate that single Pt atoms may be able to catalyze hydrogenation reaction, even when they are supported on an inert support like silicon wafer used in this work. However, the stability of Pt single atoms under reaction conditions should be carefully verified for a longer reaction time.

Regarding the influence of metal–support interaction on metal species with different atomicity, it has been presented that

DOI: 10.1021/acs.chemrev.7b00776
Chem. Rev. 2018, 118, 4981–5079

Table 6. Catalytic Activities Characterizing the Sample Initially Formed by Adsorption of $Rh(C_2H_4)_2(acac)$ on Y Zeolite after Various Treatments for Hydrogenation and Dimerization of Ethylene in a Flow Reactor at 298 K and 1 bar[a]

				selectivity in ethylene conversion (wt %)				
treatment conditions	Rh−Rh coordination number	ethylene conversion (%)	TOF for ethylene conversion (s^{-1})	ethane	*n*-butane	*trans*-2-butene	1-butene	*cis*-2-butene
none	0	2.2	0.11	18.5	0.7	50.1	11.8	18.9
H_2 at 373 K for 4 min	0.18	2.2	0.11	35.1	0.8	34.5	13.6	16.0
H_2 at 373 K for 60 min	4.4	4.9	0.25	64.1	3.1	19.9	4.5	8.4

[a]Adapted with permission from ref 527. Copyright 2016 American Chemical Society.

single-atom metal catalyst and metal clusters supported on acid support (zeolite) show higher activity for ethylene hydrogenation than those on basic support (MgO).[529] However, in a recent work, it is shown that the situation is more complicated when considering the reactivity of metal clusters with different atomicity.[530] No general trend has been observed after comparing the reactivity for ethylene hydrogenation of size-selected Pt clusters (from Pt_8 to Pt_{20}) deposited on MgO and SiO_2, suggesting the difficulty and complexity of the catalytic behavior of subnanometric metal clusters.

7.6. Dehydrogenation Reactions

As the reverse reaction of hydrogenation, dehydrogenation reactions follow a different behavior on Pt nanoparticles. As discussed before, the hydrogenation of cyclohexene to cyclohexane is a structure-insensitive reaction with constant activation energy on Pt nanoparticles with different size. However, the activation energy will increase when increasing the particle size for dehydrogenation of cyclohexene to benzene, resulting in a decreased TOF when increasing the particle size (as shown in Figure 105).[531] According to kinetic studies, it is suggested that the rate-limiting step for the dehydrogenation of propane is the first C−H bond activation, and that elemental step is favorable on Pt sites with unsaturated coordination environment.[532] Therefore, Pt particles with smaller size show higher activity. Taking a further look at the results shown in Figure 105, subnanometric Pt species were not studied for dehydrogenation reaction. To the best of our knowledge, there is a report on the catalytic properties of Pt clusters for dehydrogenation of hydrocarbons, while there is no report on the application of single Pt atoms for such reactions.[282] From a mechanistic point of view, it can be speculated that multiple metal sites should be required for the adsorption of the substrate molecule and activation of the C−H bond. Considering the poor stability of Pt single atoms and the harsh conditions for dehydrogenation reactions (usually >500 °C), it could be difficult to stabilize single Pt atoms under reaction conditions. Nevertheless, it has recently been proposed on the basis of in situ XAS characterization that single-site Ga species supported on SiO_2 are active species for propane dehydrogenation.[533] It is also found that single-site Ga species (probably as surface Ga−O species) can remain stable at very high temperature (>550 °C) under propane dehydrogenation conditions, without obvious agglomeration, according to EXAFS results, which is significantly different from the situation with Pt-based catalysts.[534] It can be speculated that the physicochemical properties and sintering behavior of Ga are different from those of Pt, probably due to a stronger interaction between the Ga and the surface oxygen species of the silica support.

7.7. Organic Reactions

As discussed before, it has been proved that Pd clusters with three or four atoms are the active species for C−C cross-coupling reactions. Besides, Au catalysts have also been reported to be efficient for Sonagashira reaction without the presence of Pd.[535,536] As shown in those works, heterogeneous Au/CeO_2 was found to be active and selective for the cross-coupling reaction between phenylacetylene and iodobenzene. The nature of the active sites for Au-catalyzed Sonagashira reaction has been investigated by experimental and theoretical works.[537,538] The mechanistic studies show that the Sonagashira cross-coupling reaction on supported Au catalyst follows a Langmuir−Hinshelwood mechanism, in which the surface bimolecular coupling is the rate-limiting step, as displayed in Figure 106. Furthermore, the calculation results indicate that C−I bond dissociation (activation of iodobenzene) occurs on high-coordinated Au^0 atoms present in the crystal facets of Au nanoparticles, while C−H dissociation (activation of phenylacetylene) occurs on Au atoms with low coordination located at the corners or even in Au clusters in solution. On the basis of the above discussion, the results reported in the literature could be explained.[539,540]

As we have discussed before, the catalytic behavior of metal clusters is distinct from that of metal nanoparticles. Taking into consideration that different molecules may be activated on different types of Au species, the combination of metal clusters and nanoparticles has been shown to enhance the activity of either cluster or nanoparticles for the Sonagashira reaction.[541] Following that idea, in a recent work, it has been demonstrated that the combination of Au nanoparticles and clusters shows significantly higher activity than a single type of catalyst for Sonogashira reaction. As described in Figure 107, supported Au clusters can leach into solution and activate the C−H bond terminal alkynes with the help of base. Moreover, the C−X bond in aryl halide can be activated on the Au^0 sites with high coordination in supported Au nanoparticles. Therefore, such bifunctional catalyst can give a higher yield of C−C coupling products than conventional Au/CeO_2 catalyst. This work demonstrates that, taking advantage of their distinct electronic structures of different metal species, it is possible to obtain synergistic effects to improve the catalytic performance.

In the part of catalytic applications of single atoms, it has been mentioned that single Au atoms are proposed to be the active sites for hydrochlorination of acetylene. In a recent work from our group, a different reaction mechanism is proposed for hydrochlorination of alkynes on Au nanoparticles when working in the liquid phase.[542] Metallic Au nanoparticles supported on TiO_2 are proved to be the most active catalyst for hydrochlorination of phenylacetylene, while mononuclear Au complexes or subnanometric Au clusters are not active under the same conditions. According to the results presented, the activation of HCl is found to be the rate-limiting step, and its activation is more favorable on metallic Au surface. Theoretical calculations also show that electron transfer from Au nanoparticles promotes the dissociation of H−Cl bond, and then the dissociated H and Cl can perform regioselective addition on the

DOI: 10.1021/acs.chemrev.7b00776
Chem. Rev. 2018, 118, 4981−5079

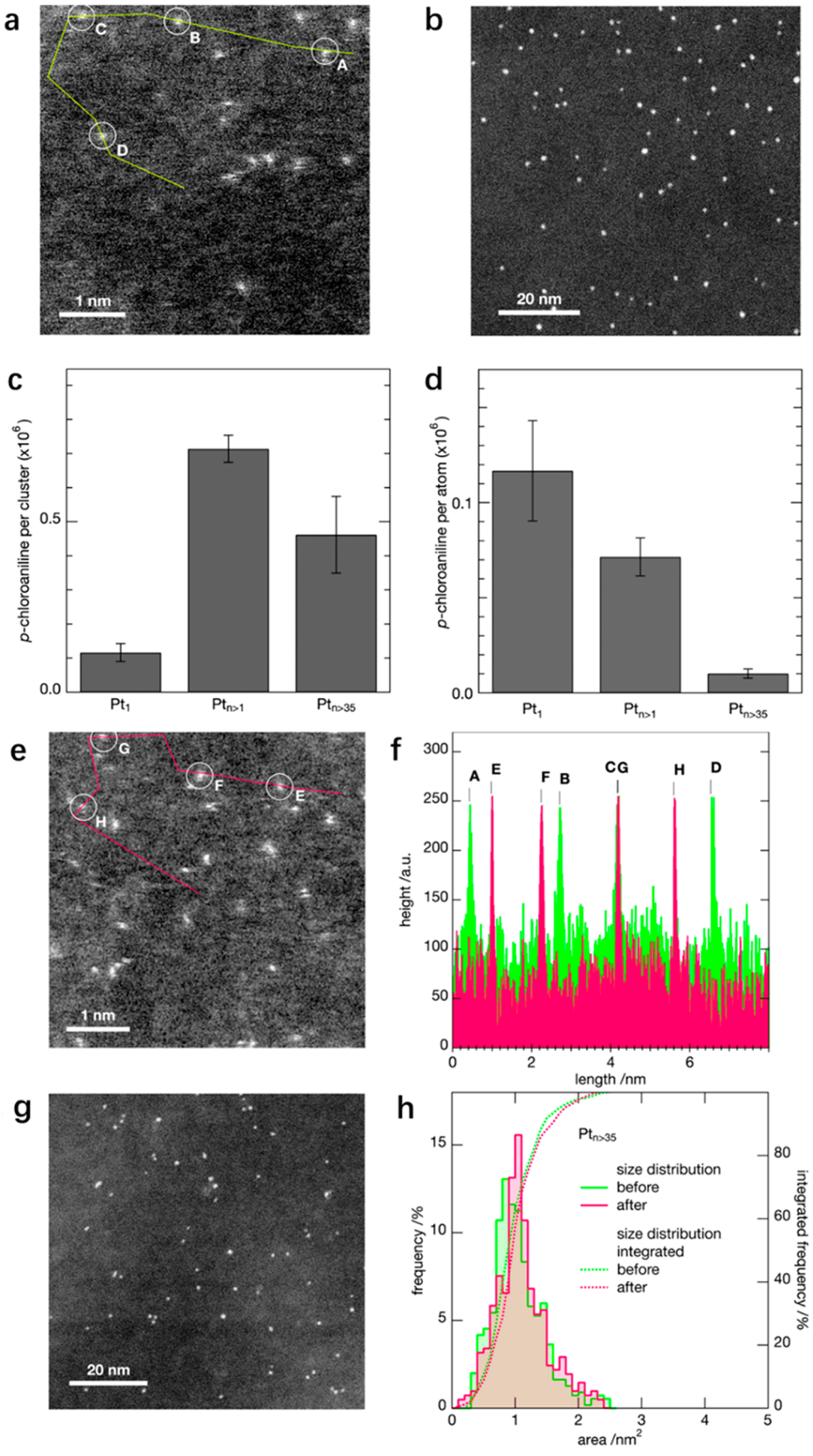

Figure 104. High-resolution STEM images of Pt single atoms (a) and Pt nanoparticles (b) before the hydrogenation reaction. Catalytic activity expressed as yield of *p*-chloroaniline after hydrogenation of *p*-chloronitrobenzene per Pt specie (c) and per Pt atom (d). (e–h) High-resolution STEM images of Pt single atoms and Pt nanoparticles after the hydrogenatrion of *p*-chloronitrobenzene. Adapted with permission from ref 528. Copyright 2017 American Chemical Society.

DOI: 10.1021/acs.chemrev.7b00776
Chem. Rev. 2018, 118, 4981–5079

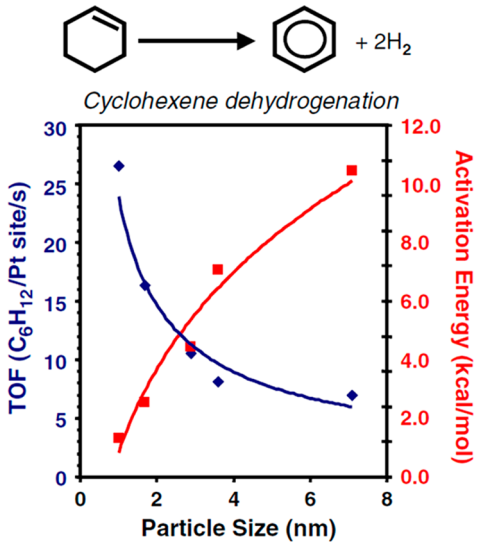

Figure 105. Particle size effect on catalytic properties of Pt nanoparticles for cyclohexene dehydrogenation to benzene. Adapted with permission from ref 531. Copyright 2008 Springer.

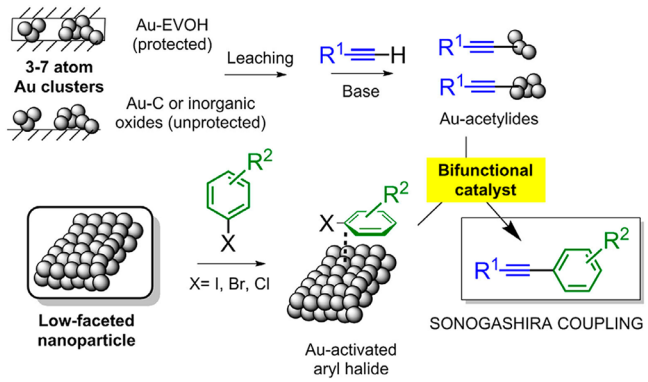

Figure 107. Mechanistic proposal for the Sonogashira coupling with Au clusters and Au Nanoparticles as bifunctional catalyst. Adapted with permission from ref 541. Copyright 2017 Wiley-VCH Verlag GmbH & Co. KGaA, Weinheim.

coadsorbed alkyne, leading to the formation of the syn-product. Notably, this process works with Au/TiO_2 in the liquid phase at 80 °C, and it is clearly different from that on Au/C in the gas phase at >150 °C. For the gas-phase hydrochlorination reaction, it has been reported that HCl is activated by an oxidation step on atomically dispersed cationic Au species. We show that, for the same type of reaction on the same metal catalyst, different types of active sites may be required when changing the reaction conditions, and the reaction occurs through a different mechanistic route.

In homogeneous systems, metal species often work as Lewis acid sites and catalyze C−C or C−X bond formation reactions.[543−545] For example, metal-catalyzed hydroamination reactions are powerful tools to construct C−N bonds for organic synthesis.[546] It has been widely reported that $PtCl_2$, AuCl, $RhCl_3$, and some other metal salts can catalyze hydroamination reactions. However, most of those salts are not soluble in the reaction solvents, as shown in Figure 108a. On the other hand, the active species for hydroamination reactions are thought to be isolated metal sites with positive charge, which should be soluble in the solvents.[547] To overcome such limitation of conventional metal salts, isolated cationic metal species confined in zeolites have been prepared by ion-exchange method, and they show excellent activity and recyclability for hydroamination reactions (see Figure 108b).

In the work of Somorjai et al., $PhICl_2$ was used as oxidation reagent to make positively charged Pt_{40} nanoclusters, which further served as heterogeneous acid sites for carbon−carbon and carbon−heteroatom bond-forming reactions that previously were only observed with homogeneous catalysis.[548] As shown in their work (see Figure 109), these electrophilic Pt_{40} nanoclusters show excellent activities in nitrogen- and oxygen-containing heterocycles through π-bond activation. Larger Pt nanoparticles with different sizes were also synthesized for comparison, and they showed a marked initial spike in activity, followed by rapid deactivation. Consequently, a longer reaction time was required to achieve full conversion. The authors confirmed that the catalysis was heterogeneous, not through a leaching mechanism during the reaction. Therefore, the authors claimed to have converted a homogeneous to a heterogeneous catalytic process.

This strategy has also been extended to other metal catalysts for electrophilic reactions.[549] For instance, Pd_{40} particles supported by SBA-15 were much more efficient than corresponding homogeneous catalysts. By a similar method, Au nanoparticles (~2 nm) encapsulated in dendrimer were

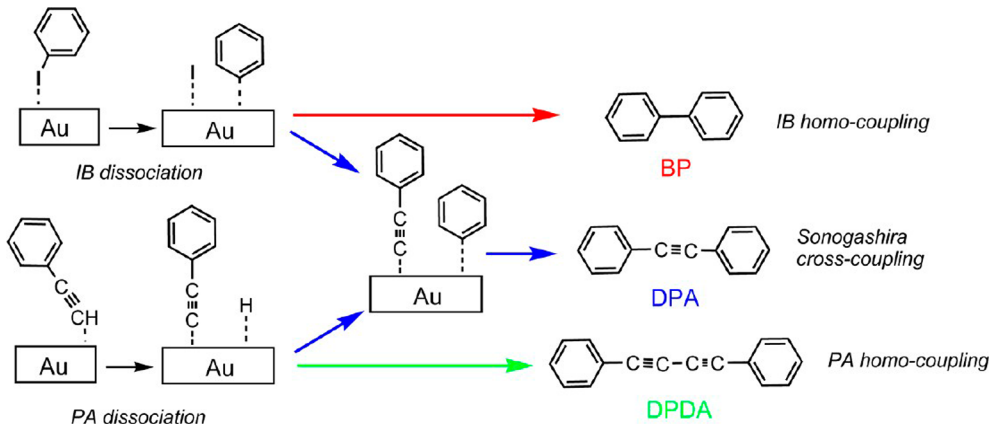

Figure 106. Reaction scheme for Au-catalyzed Sonagashira reaction (product DPA) including the illustration for activation of iodobenzene and phenylacetylene. The competitive homocoupling reactions of phenylacetylene (product DPDA) and iodobenzene (product BP) are also described. Adapted with permission from ref 537. Copyright 2012 American Chemical Society.

DOI: 10.1021/acs.chemrev.7b00776
Chem. Rev. 2018, 118, 4981−5079

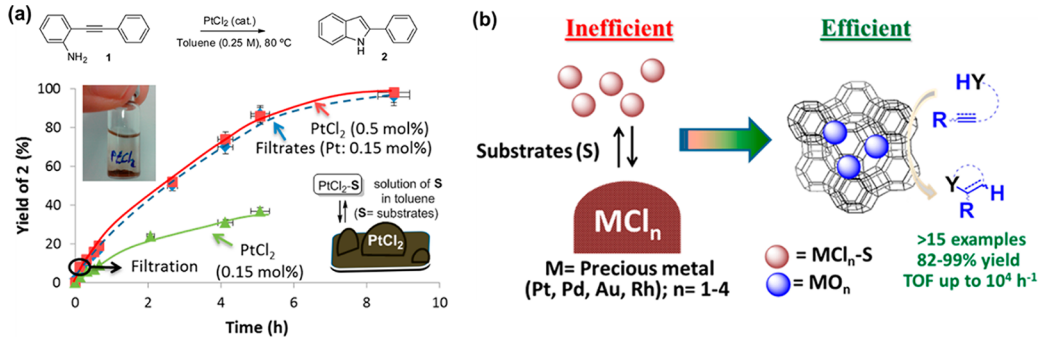

Figure 108. (a) Yield–time profile for the hydroamination of *o*-(phenylacetylen)aniline catalyzed by $PtCl_2$. The photograph on the left shows the precipitate of $PtCl_2$ in toluene under reaction conditions, and the illustration on the right describes the equilibrium-controlled dissolution of $PtCl_2$ with the substrates under reaction conditions. (b) Schematic illustration using metal-exchanged zeolite as substitute catalysts for hydroamination reactions with high activity. Adapted with permission from ref 547. Copyright 2015 American Chemical Society.

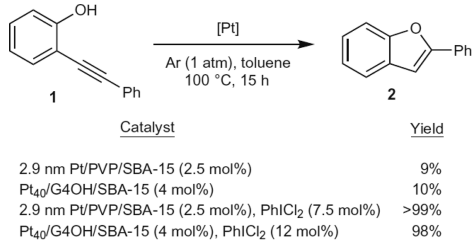

Catalyst	Yield
2.9 nm Pt/PVP/SBA-15 (2.5 mol%)	9%
Pt_{40}/G4OH/SBA-15 (4 mol%)	10%
2.9 nm Pt/PVP/SBA-15 (2.5 mol%), $PhICl_2$ (7.5 mol%)	>99%
Pt_{40}/G4OH/SBA-15 (4 mol%), $PhICl_2$ (12 mol%)	98%

Figure 109. Hydroalkoxylation using surface-oxidized Pt nanoparticles. To obtain electrophilic activity from the Pt nanoparticles, treatment with mild oxidant ($PhICl_2$) was performed. Afterward, the Pt_{40}/G4OH/SBA-15 sample was further reduced under H_2 atmosphere at 100 °C for 24 h before being used for catalytic tests. Adapted with permission from ref 548. Copyright 2010 Macmillan Publishers Limited, part of Springer Nature.

employed to catalyze cyclopropanation reactions using propargyl pivalate and styrene as reactants for production of *cis*- and *trans*-diastereomers of cyclopropane.[550] More interestingly, the selectivity could be modulated by the properties of Au nanoparticles and the reactor residence time. These results demonstrate the possibility of combining the potential advantages of heterogeneous catalysts for conventional homogeneous reactions.[551] Furthermore, with modification of chiral peptide (self-assembled monolayer, SAM), asymmetric catalytic reactions can also be performed with Au nanoclusters (~1.5 nm). In that work, Au clusters were encapsulated in chiral SAM/MCF-17 for synthesis of intermolecular cyclopropane, and the enantioselectivity is enhanced due to the chiral environment of the SAM matrix.[552] However, the reactivity of subnanometric Au clusters is not mentioned in those works, and should be an interesting topic to be discussed in future works. From an electronic point of view, the chemical states of metal clusters and nanoparticles are different, which should affect their reactivity for the above organic transformations. Nevertheless, considering the flexibility of the geometric structures of metal clusters, the transition state may also vary with the size of metal entities, which may result in different reaction pathways and selectivity.

In a recent work, it is reported that Pd_4 clusters confined in a metal–organic framework can serve as catalyst for carbene-mediated reactions.[553] Mononuclear Pd complex or Pd species supported on conventional solid carriers (metal oxides, zeolites, carbon, etc.) showed low activity under the same conditions, indicating the unique catalytic behavior of Pd_4 clusters confined in the MOF structure. Because homogeneous Pd_4 complex was not active under the same conditions, it also implies that the MOF structure may have influence on the catalytic properties of Pd_4 clusters.

It can be concluded that, by tuning the surface properties of metal nanoparticles and clusters, it is possible to prepare heterogeneous metal catalysts for some organic reactions that are usually catalyzed by homogeneous metal complex. It appears that the bridges between homogeneous and heterogeneous are being better established. The next challenge will be to perform enantioselective reactions by means of those heterogeneous catalysts. One way of doing that could be by using chiral auxiliaries that could adsorb weakly enough to avoid the blockage or deactivation of the active sites in the heterogeneous systems. Notice that some success was already achieved with metal nanoparticles by anchoring chiral molecules.[554]

7.8. Photocatalytic Reactions

For metal species, a very important character associated with the particle size is the size-dependent optical properties. For metal nanoparticles, it is well-known that particle size and morphology has significant influence on their plasmonic properties. In the case of metal clusters as well as small nanoparticles (<2 nm), their optical adsorption behavior is also strongly related to the size. As shown in Figure 110, the UV–vis adsorption band will generally shift to lower wavelength when decreasing the particle size. In the case of subnanometric Cu clusters with less than 13 atoms, they can only absorb UV light (<400 nm) and show characteristic fluorescence emission depending on the atomicity.[555] Therefore, as a consequence of their different light absorption properties and electronic structures, metal clusters and nanoparticles show

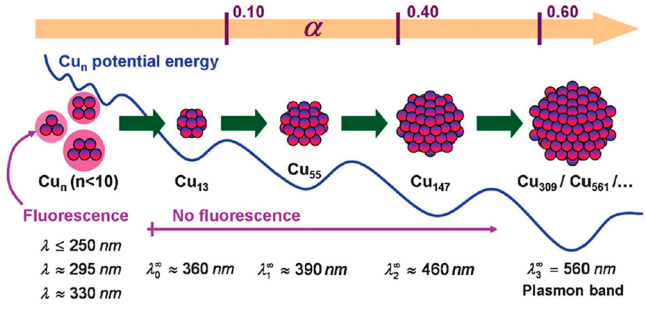

Figure 110. Schematic illustration of size-dependent optical properties of Cu clusters and nanoparticles. Estimated wavelengths of the plasmon band for Cu clusters or nanoparticles are shown at the bottom. Adapted with permission from ref 555. Copyright 2009 American Chemical Society.

DOI: 10.1021/acs.chemrev.7b00776
Chem. Rev. 2018, 118, 4981–5079

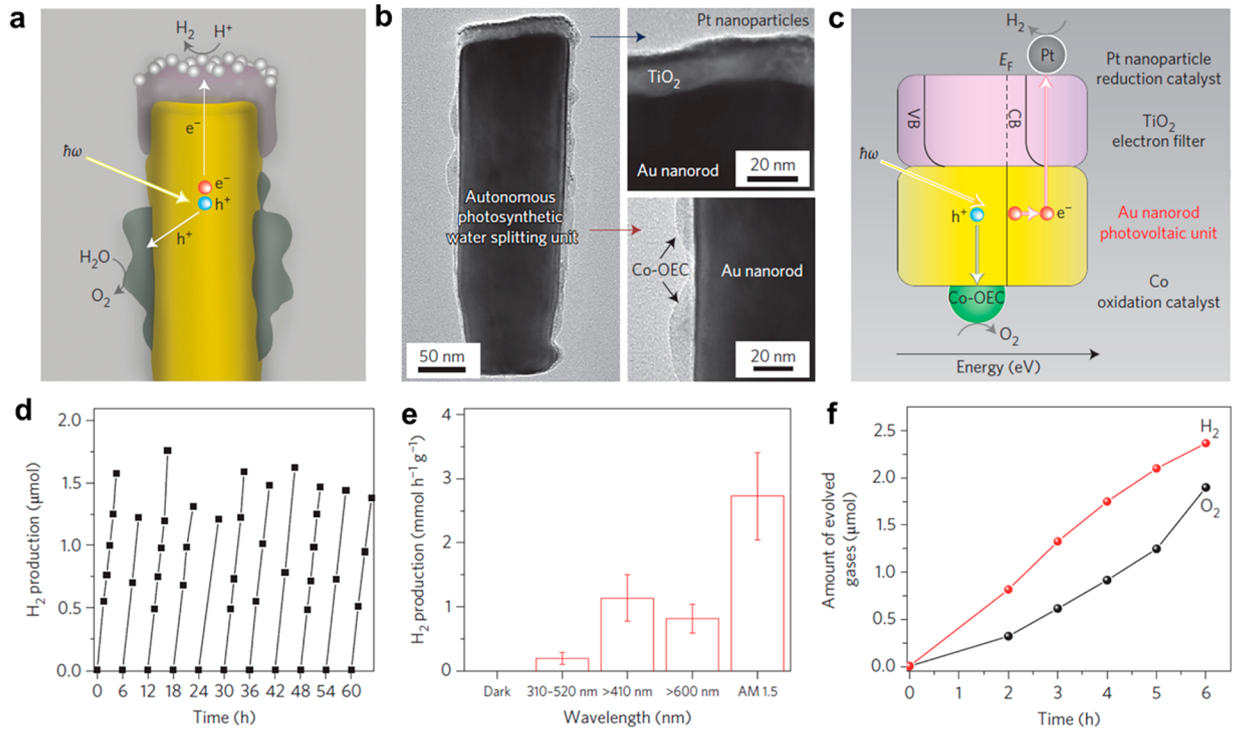

Figure 111. (a–c) Schematic illustrations and structural characterizations of plasmon-mediated overall water splitting on Au nanorods modified with cocatalysts. (d) Amount of H_2 produced on Au nanorods under visible light (>410 nm) irradiation. (e) H_2 production rate on Au nanorods under irradiation of light of different wavelength. (f) Measured O_2 and H_2 photoproducts as a function of time for a second device illuminated by 300 mW/cm^2 of white light (AM 1.5). Adapted with permission from ref 560. Copyright 2013 Macmillan Publishers Limited, part of Springer Nature.

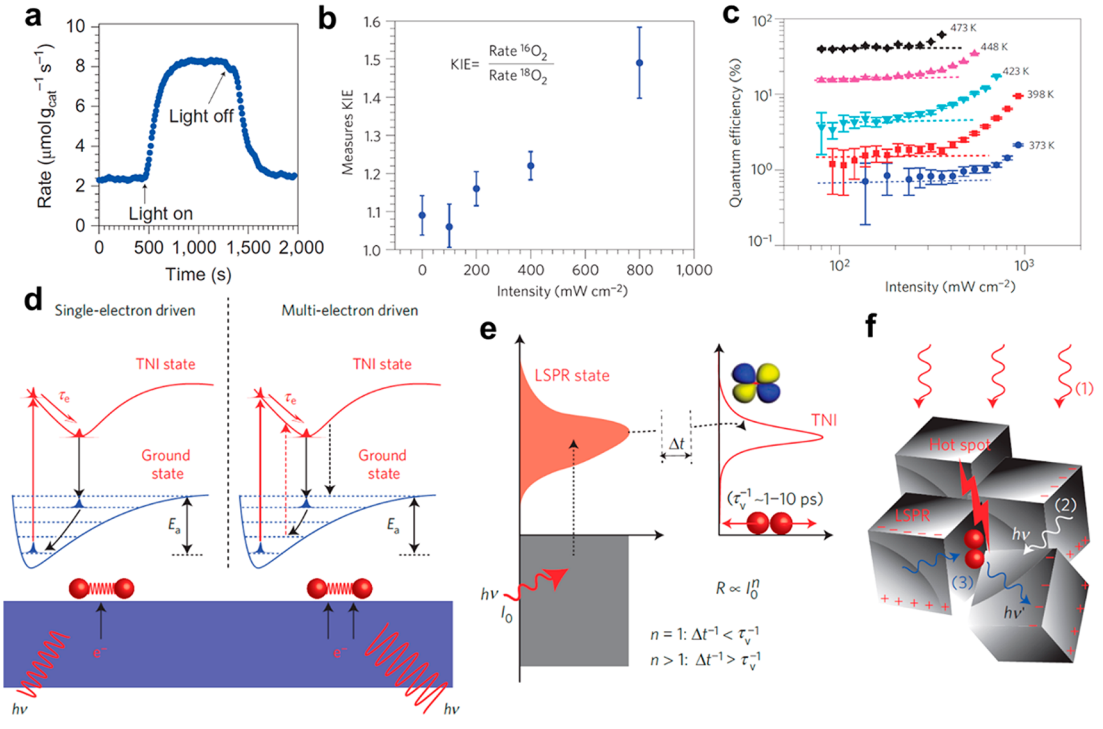

Figure 112. (a) Reaction rate for epoxidation of ethylene to ethylene oxide on Ag nanocubes with and without visible light irradiation at 450 K. (b) Isotopic studies on the influences of light intensity for epoxidation of ethylene on Ag nanocubes. (c) Influences of reaction temperature and light intensity on quantum efficiency for epoxidation of ethylene on plasmonic Ag nanocubes. (d) Schematic illustration of single-electron driven and multielectron driven reactions on metal surface under light irradiation. (e) Schematic illustration on the plasmon-mediated electron transfer from Ag to O_2. When the rate of plasmon excitation, Δt^{-1}, is lower than the vibrational decay rate of O_2, τ_v^{-1}, the photocatalytic rate is linear with respect to the light intensity. On the other hand, when $\Delta t^{-1} > \tau_v^{-1}$, the photocatalytic rate shifts to a superlinear dependence on light intensity. (f) Formation of a hot spot in a complex structure of Ag nanocubes for activation of O_2 under low-intensity visible light irradiation. Adapted with permission from refs 562 and 563. Copyright 2011 and 2012 Macmillan Publishers Limited, part of Springer Nature, respectively.

DOI: 10.1021/acs.chemrev.7b00776
Chem. Rev. 2018, 118, 4981−5079

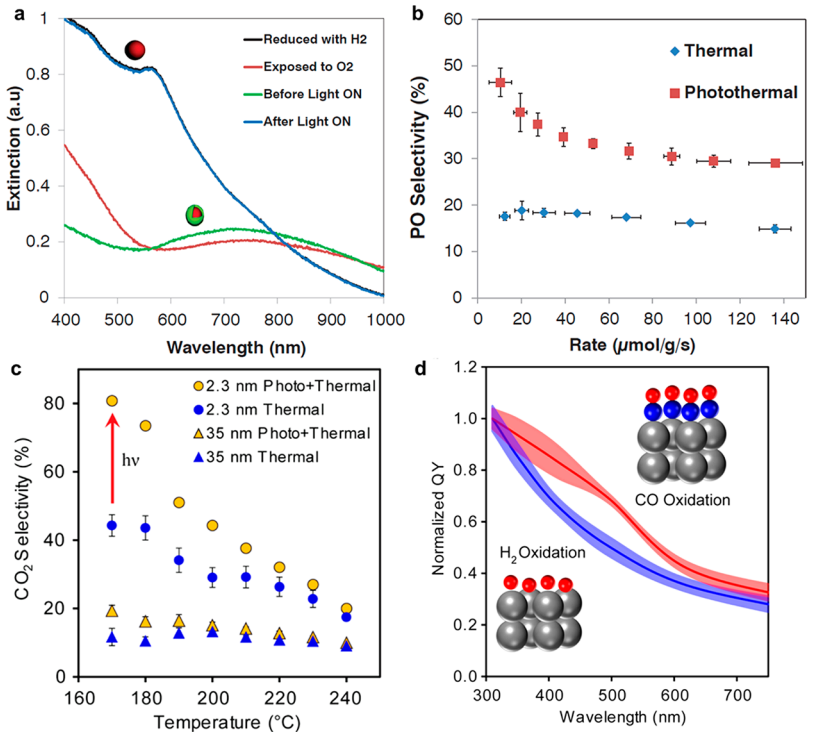

Figure 113. (a) UV−vis spectra of Cu nanoparticles under different conditions. (b) Selectivity to propene epoxide under photothermal and thermal conditions on Cu nanoparticles. (c) Influences of light irradiation on preferential oxidation of CO in rich H_2 on small and big Pt nanoparticles. (d) Normalized quantum yields for CO and H_2 oxidation driven by hot electrons after excitation of Pt states with a low intensity laser pulse obtained by theoretical calculations. The physical models of H_2 and CO adsorbed on Pt surface are also presented. The shaded regions represent variations in calculated quantum yield due to uncertainty in physical parameters used in the model. (a,b) Adapted with permission from ref 564. Copyright 2013 The American Association for the Advancement of Science. (c,d) Adapted with permission from ref 565. Copyright 2014 American Chemical Society.

distinct photocatalytic properties. Basically, metal species may act as light sensitizer or cocatalyst in photocatalytic systems. In the case of cocatalysts, as discussed before, the charge-transfer process between a semiconductor and a metal cocatalyst will vary with the particle size of the metal. Furthermore, the surface reaction kinetics will also be related to the particle size of the metal cocatalyst. This has already been demonstrated in some Pt/semiconductor photocatalysts.[556,557]

In recent years, mononuclear metal complexes have been employed as photocatalyst for photoredox transformations by reacting with substrate molecules to generate radicals after being excited by visible light.[558,559] However, for supported single atoms, the above process seems not to be applicable anymore due to their different electronic structures. In the following section, we would like to emphasize the different catalytic behaviors of metal nanoparticles and clusters when they are working as light absorbent without the involvement of semiconductor materials, and discuss how the particle size affects the metal−molecule interactions.

When metal clusters or nanoparticles are excited by light, electrons in the ground state will be transferred to higher energy levels, which can be further transferred to molecules or participate in surface reaction directly. For instance, it has been reported that Au nanorods can serve as light sensitizer for adsorption of visible light (>410 nm) and produce photogenerated electrons and holes (see Figure 111). Subsequently, those photoelectrons and holes can transfer to cocatalysts for overall water splitting to H_2 and O_2, simultaneously.[560] Besides, it has also been reported that photocatalytic conversion of CO_2 to HCOOH can be achieved on Au nanoparticles covered by reduced graphene oxide under visible-light irradiation through a plasmon-mediated mechanism.[561] So far, the efficiency of plasmon-based photocatalytic process is still much lower than that on traditional semiconductor-based photocatalysts, which is probably related to the short lifetime and low reactivity of photogenerated hot electrons.

On the other hand, photogenerated hot electrons can transfer to substrate molecules and favor the activation process. For instance, it has been demonstrated that under visible light irradiation, the activation of oxygen on Ag nanoparticles was promoted and thereof led to higher catalytic reactivity for epoxidation of ethylene to ethylene oxide by O_2 (as shown in Figure 112a).[562] Kinetic and isotopic studies show that the reaction rate on Ag nanoparticles under light irradiation exhibited a superlinear power law dependence on light intensity (rate ~ intensity^n, with $n > 1$), even at much lower intensity than that required for superlinear behavior on extended metal surfaces (see Figure 112b and c).[563] Nevertheless, the apparent quantum efficiency on plasmonic Ag nanoparticles for ethylene epoxidation increased when the light intensity and reaction temperature increased, which was also significantly different from the situation on traditional semiconductor photocatalysts. Considering that oxygen molecules are activated through the electron transferred from Ag nanoparticles, both single-electron and multielectron transfer between Ag and O_2 may occur, which was dependent on the light intensity. According to the experimental results and theoretical calculations, it was proposed that when the light intensity was higher than the threshold (~300 mW/cm^2), multielectron transfer between Ag and O_2 occurred, leading to the superlinear power law dependence on light intensity (as shown in Figure 112d and e). Nevertheless, according to simulation modeling, considering the intensity

DOI: 10.1021/acs.chemrev.7b00776
Chem. Rev. 2018, 118, 4981−5079

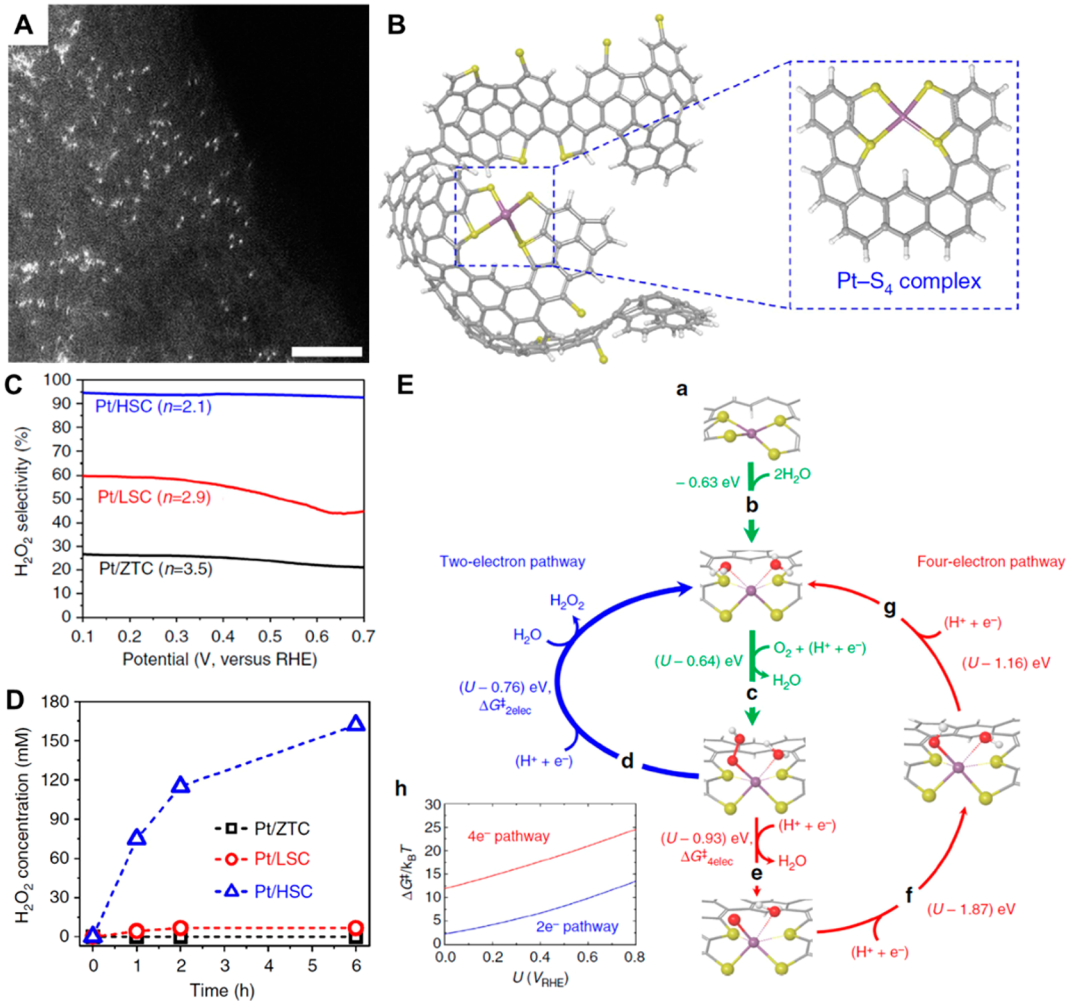

Figure 114. (A) High-resolution STEM image of atomically Pt species on S-functionalized carbon. A large number of Pt single atoms as well as a small fraction of Pt clusters can be seen. (B) A schematic illustration of the coordination environment of atomically dispersed Pt species in S-functionalized carbon. (C) Selectivity to H_2O_2 on three Pt catalysts estimated by rotating ring disk electrode experiments (Pt ring potential: 1.2 V_{RHE}). Pt/ZTC corresponds to Pt nanoparticles (ca. 4 nm) supported on zeolite-templated carbon without the functionalization with S. Pt/LSC corresponds to Pt nanoparticles (ca. 1−2 nm) supported on zeolite-templated carbon with 4 wt % of S. Pt/HSC corresponds to atomically dispersed Pt supported on zeolite-templated carbon with 17 wt % of S. (D) Accumulated H_2O_2 concentrations with reaction time on three Pt catalysts under short-circuit condition (at $V = 0$) at room temperature. (E) Proposed catalytic mechanism on atomically dispersed Pt catalysts for oxygen reduction to H_2O_2. Adapted with permission from ref 572. Copyright 2016 Macmillan Publishers Limited, part of Springer Nature.

distribution of electric field intensity on Ag nanocubes, it seemed impossible to realize the superlinear law between reactivity and light intensity on monodispersed Ag nanocubes at relatively low light intensity used in this work (300−400 mW/cm^2). Therefore, it was speculated that the enhanced electric field between composed Ag nanocubes could cause the experimental phenomenon, as described in Figure 112f. Therefore, it also implies that, by tuning the spatial assembly of plasmonic nanoparticles, their photocatalytic properties can be modulated.

The introduction of light−catalyst interaction can also change the chemoselectivity for heterogeneous catalytic processes. As shown in Figure 113a and b, Linic et al. have also reported the influence of visible light irradiation on epoxidation of propene with Cu nanoparticles. Under visible-light irradiation, the partially oxidized Cu−CuO_x nanoparticles will be reduced to metallic Cu and maintain stability under reaction conditions for epoxidation of propene. As a consequence, the selectivity to propene oxide is promoted as compared to thermal catalytic process under equal conditions because the selectivity to combustion product (CO_2) is much lower on metallic Cu nanoparticles.[564] When substrate molecules are absorbed on the metal surface, electronic interaction between metal and the absorbent will occur. In a recent work, Christopher et al. have demonstrated the tuning of selectivity by controlling the metal−absorbent interaction with light. In their work, CO oxidation by O_2 in rich H_2 is chosen as the model reaction. As shown in Figure 113c, under photothermal conditions, the selectivity to CO oxidation is improved in a wide temperature range. Specifically, selectivity to CO oxidation by O_2 is increased from 44% to 81% on Pt nanoparticles (ca. 2.3 nm) supported on Al_2O_3 at 170 °C. However, such enhancement is not observed on large Pt nanoparticles (ca. 35 nm).[565] When molecules are absorbed on the metal surface, electronic interaction between metal and molecules will occur. The bonding between the metal surface and substrate molecules can also be excited by incident light. Therefore, with the help of physical modeling and calculations, it is possible to obtain calculated quantum yields of photocatalytic reactions on metal surface. As shown in Figure 113d, the calculation results suggest that the absorbed CO and H_2 show different response behavior to visible light. Therefore, when the

DOI: 10.1021/acs.chemrev.7b00776
Chem. Rev. 2018, 118, 4981−5079

catalyst is irradiated by light between 400 and 600 nm, the CO−Pt bonding will be preferentially activated, resulting in improved CO selectivity in the CO-PROX reaction.

The modulation effects of light irradiation have also been reflected for the hydrogenation reaction. Halas et al. have prepared Pd nanoparticles supported on plasmonic Al nanoparticles (e.g., antenna-reactor nanocomposites catalyst) for selective hydrogenation reactions. Under laser irradiation, hot electrons are generated on plasmonic Al nanoparticles and are transferred to Pd nanoparticles, which has been confirmed by ultrafast spectroscopy. Subsequently, those light-induced hot electrons can promote the H_2 activation process on Pd nanoparticles according to the results from H_2-D_2 exchange experiments. More interestingly, activity and chemoselectivity for hydrogenation of acetylene on Pd nanoparticles can also be modulated by the incident light irradiation. Under laser irradiation, the catalytic activity for acetylene hydrogenation is decreased, and a C_2H_4/C_2H_6 ratio of ∼37 can be achieved with an incident laser powder of ∼14.3 W/cm^2. For comparison, the C_2H_4/C_2H_6 ratio in the products is only ∼7 under thermal conditions without laser irradiation.[566]

As compared to the numerous reports on applications of plasmonic nanoparticles for photocatalytic reactions, the number of reports on photocatalytic applications of metal nanoparticles is much less. As shown before, most of the reports are on the role of metal clusters as cocatalysts of semiconductor materials, and their different catalytic behavior is probably related to different electronic structures between clusters and nanoparticles. Notably, there are only a few reports on the application of metal clusters without the presence of other semiconductor materials. It has been reported that subnanometric Cu and Au clusters can serve as photocatalysts for the degradation of organic dyes under visible light, and their catalytic performance is dependent on their atomicity.[567,568] However, as compared to those classic semiconductor photocatalysts, the efficiency of metal clusters is much lower, and their stability is also a limitation.

Taking into consideration that metal clusters have been proved to be active species for various organic reactions, such as C−C and C−X (X = N, O, S, etc.) coupling reactions, there should be some influences of light irradiation on those catalytic processes. Indeed, there are some reports on light-promoted C−C coupling reactions with supported Pd catalysts.[569−571] With visible light irradiation, the reaction rates can be significantly enhanced. However, in those works, Pd mainly exist as nanoparticles, which seems not to be the real active species because Pd-leaching from nanoparticles into solution occurs under reaction conditions. Therefore, it is necessary to identify the mechanism that explains how visible light irradiation can promote Pd-catalyzed C−C coupling reactions. Electronic transfer between semiconductor support and Pd clusters may contribute the enhanced activity. On the other hand, as shown above, the introduction of light irradiation may also change the chemoselectivity of metal clusters.

7.9. Electrocatalytic Reactions

For electrocatalytic reactions, the catalytic behavior of metal catalysts can also be modulated by tuning their particle size. In the case of Pt-based catalysts, both Pt nanoparticles and Pt atoms are active for the electrocatalytic reduction of oxygen. Interestingly, the atomicity of Pt species will affect the selectivity for the electrocatalytic reduction of O_2.[572] Indeed, Choi et al. have prepared three Pt/C catalysts with different Pt particle sizes (from nanoparticles to clusters to single Pt atoms) and tested for oxygen reduction reaction in an acidic medium. As shown in Figure 114, atomically dispersed Pt species are stabilized by S-functionalized carbon and Pt nanoparticles, as well as Pt clusters are also prepared for comparison by tuning the amount of doped S in the carbon support. According to theoretical calculations, only atomically dispersed Pt species can selectively reduce O_2 into H_2O_2 (with a selectivity of ∼95%) through the two-electron pathway, while O_2 will be directly reduced to H_2O on both Pt clusters and nanoparticles through the conventional four-electron pathway. Similar unique selectivity toward H_2O_2 of Pt single atoms has also been demonstrated with Pt/TiN catalysts.[573]

Single-atom non-noble metal catalysts are shown to be promising substitutes for Pt-based catalysts for oxygen reduction reaction.[574] In most of the systems, it is claimed that isolated metal−N−C are the active sites, although the configuration of such metal−N−C species may be different in materials from different preparations. Interestingly, in a recent work, Wang et al. have demonstrated the generation of isolated Fe−Co−N−C bimetallic sites and tested their catalytic performance for H_2/O_2 fuel cell in comparison with commercial Pt/C catalyst.[575] The presence of Fe−Co bonding was confirmed by EXAFS, and it was proposed that O_2 activation on Fe−Co bimetallic sites was more favorable than on each single-component metal−N−C catalyst, leading to its much higher ORR activity. This work implies that modulating the interaction between atomically dispersed metal species may lead to better electrocatalysts.

From a mechanistic point of view, the different catalytic behavior between single atoms, clusters, and nanoparticles can have two explanations. One is related to the metal−substrate interface, which is similar to that in traditional heterogeneous catalytic processes and has been intensively discussed, and it is believed to be the origin of different reactivity. On the other hand, the charge-transfer process between the electrode and metal catalyst may also account for their different catalytic behavior between atomically dispersed metal species, clusters, and nanoparticles. However, the charge-transfer process has not been fully discussed. Considering the complexity for electrocatalytic process and the lack of efficient in situ characterization techniques, the fundamentals on size-dependent catalytic behaviors need to be clarified further.

8. PERSPECTIVES

It has been presented in this Review that, in the case of metal catalysts, and even more so with supported metal catalysts, the number of variables that can have an effect on the catalytic behavior is quite high. Among them, we can highlight the size and shape of the metal particles, the nature of the support and metal−support interaction, the presence of the other metals, from impurities to defined bimetallic or multimetallic particles, and the chemical states of the surface. However, among all, we would like to point out two: (a) the intrinsic electronic difference and binding capacities when going from single atoms to clusters and to nanoparticles; and (b) the dynamic characteristics of the catalytic process, which is directed by the metal−reactant and/or metal−solvent interaction. In this latter case, the size, shape, and electronic properties can be even dramatically modified by such interactions. These changes can be for the good or for the bad from a catalytic point of view, and it shows how difficult is to get sensible structure−reactivity correlations by combining catalytic results, catalyst characterizations, and molecular modeling,

DOI: 10.1021/acs.chemrev.7b00776
Chem. Rev. 2018, 118, 4981−5079

unless the dynamic characteristics of the catalyst during the reaction are considered.

When nanoparticles become smaller, especially metal clusters with less than 20 atoms or even single atoms supported on solid carriers, the size, shape, and electronic properties of the metal will also depend on the electronic structure and surface arrangement of the support. The extreme situation occurs with single metal atoms where the "ligands" of those will be atoms from the support. The presence and the number of vacancies, the oxidation state of the atoms of the solid carrier, and the characteristics of their frontier orbital and potential overlapping with those of the metal species not only will mark the final electronic properties of the "single" atom and their reactivity for catalysis, but also the metal sintering and/or metal leaching. Therefore, in the case of supported "single atoms", the real active site, where reactants are activated and transition states are stabilized, will be the "single metal atom", but the "ligand" atoms of the support will play an important role.

It has been proposed recently that heterogeneous single-atom catalysts can work analogously to homogeneous catalysts. Despite their difference in electronic structures, in our opinion, the geometric factor can be a significant difference between them. In the case of homogeneous catalysis, the metal centers are coordinated by ligands, and/or the reactants and the geometric structure of such complexes are quite flexible. The metal center can be accessible to large molecules and can adjust the coordination configuration between the metal and reactant during the catalytic cycles. However, in the case of supported single atoms, their geometric structures are partially restricted by the support, especially for those supported on inorganic solid carriers. Consequently, the catalytic applications of single-atom catalysts in the literature are mainly related to activation of small molecules, at least to date. It has been reported that, when Rh single atoms are stabilized by polymers, they can serve as stable and active sites for hydroformylation reactions. Considering the flexible geometric structure of polymers, it maybe a possible approach to overcome the geometric restriction of conventional inorganic solid carriers, making single-atom catalysts closer to its homogeneous counterpart. However, the stability and the potential leaching of single atoms should also be considered under those circumstances.

All of the above-mentioned factors may be key issues for preparing a successful single-atom catalyst. In the case of metal clusters, the nature of the support and the metal−support interaction will dictate the shape of the supported clusters, their stability, the atomic structure of the metal−cluster interface, and electronic interactions between the support and the metal clusters. The fact that the number of variables and their interdependence is so large in the case of subnanometric metal catalysts has made that many of the studies presented appear phenomenological and "specific" for a given catalyst−reaction system. Nevertheless, there are already some general lessons that could be extracted from the studies reported to date.

First is the important role that single atoms and small clusters can play in catalysis. While this could be intuitively deduced from older work, it is now possible to "see" those metal entities on supports and solution with the development of new catalyst preparation techniques and the development of aberration-corrected TEM and MALDI-TOF techniques. Furthermore, the direct observation of those subnanometric metal species leads to better discussions on their stability and catalytic role. All of the above together with the advances in molecular modeling have boosted our understanding of the catalytic behavior at the molecular level on those highly dispersed species.

It should be emphasized that the theoretical calculations and molecular modeling should match the experimental conditions as much as possible to obtain a reasonable interpretation on experimental results. Currently, in many works, the modeling of active sites in heterogeneous catalysts and the computational methods are still far from the realistic working catalyst.[576] With unrealistic parameters for theoretical calculations, the output results may be useless for understanding the behavior and reaction mechanism of heterogeneous catalysts. On the other hand, with suitable modeling on the experimental basis, the theoretical calculations and modeling can be very helpful to understand experimental phenomena and can even be used for predictions. It can be expected in the near future that, with the development of better hardware resources and especially with the help of new concepts from machine learning and artificial intelligence, the accuracy of theoretical calculations for heterogeneous catalytic reactions will be improved greatly.

It should be noticed that we normally build "static" models of the catalytic phenomena, while those catalysts are dynamic under reaction conditions. So, today we are still missing more deepness on this aspect. Therefore, in situ surface techniques such as XAS, XPS, XRD, and TEM that allow following catalyst evolution during reaction will be most helpful. It is true that in situ TEM studies on metal nanoparticles have been already performed and provided new insights on the atomic structures of metal particles when they interact with reactants. However, nanoparticles of 2−10 nm are already quite stable, and the critical issue is to apply such technique for catalysts based on single atoms and subnanometric clusters. As was said in this Review, the first steps along this direction are now being given.

If we want to go beyond the study of particular cases, we should work to establish a unified theory that will envelop and explain all of the cases in metal catalysis, regardless if that is based on homogeneous or heterogeneous chemical, photochemical, electrochemical, or photoelectrochemical catalysts. At the end, all of them are based on electronic interactions, and, to achieve global explanations, we can make use of the knowledge generated by the physicists and chemists on solid-state chemistry, physical chemistry of surface, and chemical reactivity. It is also true that if we attempt to achieve this global and unifying knowledge on catalysis, we will require more than just quick catalytic experiments. We should combine more "realistic" operando characterizations with high-quality adsorption, reaction kinetics, isotopic studies, as well as theoretical work. In other words, we should generate a deeper molecular mechanistic knowledge involving dynamic transformations of metal catalysts and molecular interactions at the gas/liquid−solid interface to deal with the complications introduced when going from molecular catalysis to heterogeneous catalysis with metal catalysts.

AUTHOR INFORMATION

Corresponding Author

*E-mail: acorma@itq.upv.es.

ORCID

Avelino Corma: 0000-0002-2232-3527

Notes

The authors declare no competing financial interest.

DOI: 10.1021/acs.chemrev.7b00776
Chem. Rev. 2018, 118, 4981−5079

Biographies

Lichen Liu is currently a Ph.D. student working with Prof. Avelino Corma in the Instituto de Tecnología Química (CSIC-UPV) in Valencia (Spain). He obtained his B.S. from Nanjing University in 2012 and M.S. from Universitat Politècnica de València (UPV) in 2014. His Ph.D. work is focused on the preparation and catalytic applications of heterogeneous metal catalysts.

Avelino Corma, professor and founder of the Instituto de Tecnología Química (CSIC-UPV) in Valencia (Spain), has been carrying out research in heterogeneous catalysis in academia and in collaboration with companies for nearly 35 years. He has worked on fundamental aspects of acid−base, redox, and multisite catalysis with the aim of understanding the nature of the active sites and reaction mechanisms. With these bases, he has developed catalysts from the concepts in laboratory to their applications in industrial processes.

ACKNOWLEDGMENTS

Financial support from the European Union through the European Research Council (grant ERC-AdG-2014-671093, SynCatMatch) and the Spanish government through the "Severo Ochoa Program" (SEV-2016-0683) is acknowledged.

REFERENCES

(1) Boudart, M. Catalysis by Supported Metals. *Adv. Catal.* **1969**, *20*, 153−166.
(2) Boudart, M. Heterogeneous Catalysis by Metals. *J. Mol. Catal.* **1985**, *30*, 27−38.
(3) Ertl, G., Knözinger, H., Weitkamp, J., Eds. *Handbook of Heterogeneous Catalysis*; Wiley-VCH: New York, 1997.
(4) Čejka, J., Corma, A., Zones, S., Eds. *Zeolites and Catalysis: Synthesis, Reactions and Applications*; Wiley-VCH: New York, 2010.
(5) Čejka, J., Morris, R. E., Nachtigall, P., Eds. *Zeolites in Catalysis: Properties and Applications*; Royal Society of Chemistry: UK, 2017.
(6) Somorjai, G. A.; Carrazza, J. Structure Sensitivity of Catalytic Reactions. *Ind. Eng. Chem. Fundam.* **1986**, *25*, 63−69.
(7) Che, M.; Bennett, C. O. The Influence of Particle Size on the Catalytic Properties of Supported Metals. *Adv. Catal.* **1989**, *36*, 55−172.
(8) Gates, B. C.; Guczi, L.; Knozinger, H. Metal clusters in Catalysis. *Studies in Surface Science Catalysis*; Elsevier: New York, 1986; Vol. *29*.
(9) Thomas, J. M.; Midgley, P. A. The Merits of Static and Dynamic High-Resolution Electron Microscopy (HREM) for the Study of Solid Catalysts. *ChemCatChem* **2010**, *2*, 783−798.
(10) Yang, J. C.; Small, M. W.; Grieshaber, R. V.; Nuzzo, R. G. Recent Developments and Applications of Electron Microscopy to Heterogeneous Catalysis. *Chem. Soc. Rev.* **2012**, *41*, 8179−8194.
(11) Roldan Cuenya, B.; Behafarid, F. Nanocatalysis: Size- and Shape-Dependent Chemisorption and Catalytic Reactivity. *Surf. Sci. Rep.* **2015**, *70*, 135−187.
(12) Corma, A. Attempts to Fill the Gap between Enzymatic, Homogeneous, and Heterogeneous Catalysis. *Catal. Rev.: Sci. Eng.* **2004**, *46*, 369−417.
(13) Chaudhuri, P.; Verani, C. N.; Bill, E.; Bothe, E.; Weyhermüller, T.; Wieghardt, K. Electronic Structure of Bis(o-iminobenzosemiquinonato)metal Complexes (Cu, Ni, Pd). The Art of Establishing Physical Oxidation States in Transition-Metal Complexes Containing Radical Ligands. *J. Am. Chem. Soc.* **2001**, *123*, 2213−2223.
(14) Zaanen, J.; Sawatzky, G. A.; Allen, J. W. Band Gaps and Electronic Structure of Transition-Metal Compounds. *Phys. Rev. Lett.* **1985**, *55*, 418−421.
(15) Taylor, K. J.; Pettiette-Hall, C. L.; Cheshnovsky, O.; Smalley, R. E. Ultraviolet Photoelectron Spectra of Coinage Metal Clusters. *J. Chem. Phys.* **1992**, *96*, 3319−3329.
(16) Boronat, M.; Leyva-Perez, A.; Corma, A. Theoretical and Experimental Insights into the Origin of the Catalytic Activity of Subnanometric Gold Clusters: Attempts to Predict Reactivity with Clusters and Nanoparticles of Gold. *Acc. Chem. Res.* **2014**, *47*, 834−844.
(17) Wang, J.; Wang, G.; Zhao, J. Density-Functional Study of Au_n (n = 2−20) Clusters: Lowest-Energy Structures and Electronic Properties. *Phys. Rev. B: Condens. Matter Mater. Phys.* **2002**, *66*, 035418.
(18) Buceta, D.; Piñeiro, Y.; Vázquez-Vázquez, C.; Rivas, J.; López-Quintela, M. Metallic Clusters: Theoretical Background, Properties and Synthesis in Microemulsions. *Catalysts* **2014**, *4*, 356−374.
(19) Kelly, K. L.; Coronado, E.; Zhao, L. L.; Schatz, G. C. The Optical Properties of Metal Nanoparticles: the Influence of Size, Shape, and Dielectric Environment. *J. Phys. Chem. B* **2003**, *107*, 668−677.
(20) Fernández, E. M.; Soler, J. M.; Garzón, I. L.; Balbás, L. C. Trends in the Structure and Bonding of Noble Metal Clusters. *Phys. Rev. B: Condens. Matter Mater. Phys.* **2004**, *70*, 165403.
(21) Schauermann, S.; Hoffmann, J.; Johánek, V.; Hartmann, J.; Libuda, J.; Freund, H.-J. Catalytic Activity and Poisoning of Specific Sites on Supported Metal Nanoparticles. *Angew. Chem., Int. Ed.* **2002**, *41*, 2532−2535.
(22) Janssens, T. V. W.; Clausen, B. S.; Hvolbæk, B.; Falsig, H.; Christensen, C. H.; Bligaard, T.; Nørskov, J. K. Insights into the Reactivity of Supported Au Nanoparticles: Combining Theory and Experiments. *Top. Catal.* **2007**, *44*, 15−26.
(23) Wu, J.; Li, P.; Pan, Y. T.; Warren, S.; Yin, X.; Yang, H. Surface Lattice-Engineered Bimetallic Nanoparticles and Their Catalytic Properties. *Chem. Soc. Rev.* **2012**, *41*, 8066−8074.
(24) Tauster, S. J. Strong Metal-Support Interactions. *Acc. Chem. Res.* **1987**, *20*, 389−394.
(25) Sasahara, A.; Pang, C. L.; Onishi, H. Probe Microscope Observation of Platinum Atoms Deposited on the TiO_2(110)-(1 × 1) Surface. *J. Phys. Chem. B* **2006**, *110*, 13453−13457.
(26) Novotny, Z.; Argentero, G.; Wang, Z.; Schmid, M.; Diebold, U.; Parkinson, G. S. Ordered Array of Single Adatoms with Remarkable Thermal Stability: Au/Fe_3O_4(001). *Phys. Rev. Lett.* **2012**, *108*, 216103.
(27) Gong, X. Q.; Selloni, A.; Dulub, O.; Jacobson, P.; Diebold, U. Small Au and Pt Clusters at the Anatase TiO_2(101) Surface: Behavior at Terraces, Steps, and Surface Oxygen Vacancies. *J. Am. Chem. Soc.* **2008**, *130*, 370−381.
(28) Campbell, C. T.; Parker, S. C.; Starr, D. E. The Effect of Size-Dependent Nanoparticle Energetics on Catalyst Sintering. *Science* **2002**, *298*, 811−814.
(29) Campbell, C. T. The Energetics of Supported Metal Nanoparticles: Relationships to Sintering Rates and Catalytic Activity. *Acc. Chem. Res.* **2013**, *46*, 1712−1719.
(30) Farmer, J. A.; Campbell, C. T. Ceria Maintains Smaller Metal Catalyst Particles by Strong Metal-Support Bonding. *Science* **2010**, *329*, 933−936.
(31) Hansen, T. W.; Delariva, A. T.; Challa, S. R.; Datye, A. K. Sintering of Catalytic Nanoparticles: Particle Migration or Ostwald Ripening? *Acc. Chem. Res.* **2013**, *46*, 1720−1730.
(32) Simonsen, S. B.; Chorkendorff, I.; Dahl, S.; Skoglundh, M.; Sehested, J.; Helveg, S. Direct Observations of Oxygen-Induced Platinum Nanoparticle Ripening Studied by in situ TEM. *J. Am. Chem. Soc.* **2010**, *132*, 7968−7975.
(33) Simonsen, S. B.; Chorkendorff, I.; Dahl, S.; Skoglundh, M.; Sehested, J.; Helveg, S. Ostwald Ripening in a Pt/SiO_2 Model Catalyst Studied by in situ TEM. *J. Catal.* **2011**, *281*, 147−155.
(34) Wettergren, K.; Schweinberger, F. F.; Deiana, D.; Ridge, C. J.; Crampton, A. S.; Rotzer, M. D.; Hansen, T. W.; Zhdanov, V. P.; Heiz, U.; Langhammer, C. High Sintering Resistance of Size-Selected Platinum Cluster Catalysts by Suppressed Ostwald Ripening. *Nano Lett.* **2014**, *14*, 5803−5809.
(35) Kang, J. H.; Menard, L. D.; Nuzzo, R. G.; Frenkel, A. I. Unusual Non-Bulk Properties in Nanoscale Materials: Thermal Metal-Metal Bond Contraction of Gamma-Alumina-Supported Pt Catalysts. *J. Am. Chem. Soc.* **2006**, *128*, 12068−12069.
(36) Sanchez, S. I.; Menard, L. D.; Bram, A.; Kang, J. H.; Small, M. W.; Nuzzo, R. G.; Frenkel, A. I. The Emergence of Nonbulk Properties in Supported Metal Clusters: Negative Thermal Expansion and Atomic

DOI: 10.1021/acs.chemrev.7b00776
Chem. Rev. 2018, 118, 4981−5079

Disorder in Pt Clusters Supported on γ-Al_2O_3. *J. Am. Chem. Soc.* **2009**, *131*, 7040−7054.
(37) Vayssilov, G. N.; Lykhach, Y.; Migani, A.; Staudt, T.; Petrova, G. P.; Tsud, N.; Skala, T.; Bruix, A.; Illas, F.; Prince, K. C.; et al. Support Nanostructure Boosts Oxygen Transfer to Catalytically Active Platinum Nanoparticles. *Nat. Mater.* **2011**, *10*, 310−315.
(38) Nilius, N.; Ganduglia-Pirovano, M. V.; Brazdova, V.; Kulawik, M.; Sauer, J.; Freund, H. J. Counting Electrons Transferred Through a Thin Alumina Film into Au Chains. *Phys. Rev. Lett.* **2008**, *100*, 096802.
(39) Lin, X.; Nilius, N.; Freund, H. J.; Walter, M.; Frondelius, P.; Honkala, K.; Hakkinen, H. Quantum Well States in Two-Dimensional Gold Clusters on MgO Thin Films. *Phys. Rev. Lett.* **2009**, *102*, 206801.
(40) Lykhach, Y.; Kozlov, S. M.; Skala, T.; Tovt, A.; Stetsovych, V.; Tsud, N.; Dvorak, F.; Johanek, V.; Neitzel, A.; Myslivecek, J.; et al. Counting Electrons on Supported Nanoparticles. *Nat. Mater.* **2016**, *15*, 284−288.
(41) Bamwenda, G. R.; Tsubota, S.; Nakamura, T.; Haruta, M. The Influence of the Preparation Methods on the Catalytic Activity of Platinum and Gold Supported on TiO_2 for CO Oxidation. *Catal. Lett.* **1997**, *44*, 83−87.
(42) Serna, P.; Corma, A. Transforming Nano Metal Nonselective Particulates into Chemoselective Catalysts for Hydrogenation of Substituted Nitrobenzenes. *ACS Catal.* **2015**, *5*, 7114−7121.
(43) Sun, B.; Vorontsov, A. V.; Smirniotis, P. G. Role of Platinum Deposited on TiO_2 in Phenol Photocatalytic Oxidation. *Langmuir* **2003**, *19*, 3151−3156.
(44) Sterrer, M.; Risse, T.; Martinez Pozzoni, U.; Giordano, L.; Heyde, M.; Rust, H. P.; Pacchioni, G.; Freund, H. J. Control of The Charge State of Metal Atoms on Thin MgO Films. *Phys. Rev. Lett.* **2007**, *98*, 096107.
(45) Pacchioni, G.; Giordano, L.; Baistrocchi, M. Charging of Metal Atoms on Ultrathin MgO/Mo(100) Films. *Phys. Rev. Lett.* **2005**, *94*, 226104.
(46) Giordano, L.; Pacchioni, G.; Goniakowski, J.; Nilius, N.; Rienks, E. D.; Freund, H. J. Charging of Metal Adatoms on Ultrathin Oxide Films: Au and Pd on FeO/Pt(111). *Phys. Rev. Lett.* **2008**, *101*, 026102.
(47) Schneider, W. D.; Heyde, M.; Freund, H. J. Charge Control in Model Catalysis: The Decisive Role of the Oxide-Nanoparticle Interface. *Chem. - Eur. J.* **2018**, *24*, 2317.
(48) Yin, C.; Zheng, F.; Lee, S.; Guo, J.; Wang, W. C.; Kwon, G.; Vajda, V.; Wang, H. H.; Lee, B.; DeBartolo, J.; et al. Size- and Support-Dependent Evolution of the Oxidation State and Structure by Oxidation of Subnanometer Cobalt Clusters. *J. Phys. Chem. A* **2014**, *118*, 8477−8484.
(49) Ferguson, G. A.; Yin, C.; Kwon, G.; Tyo, E. C.; Lee, S.; Greeley, J. P.; Zapol, P.; Lee, B.; Seifert, S.; Winans, R. E.; et al. Stable Subnanometer Cobalt Oxide Clusters on Ultrananocrystalline Diamond and Alumina Supports: Oxidation State and the Origin of Sintering Resistance. *J. Phys. Chem. C* **2012**, *116*, 24027−24034.
(50) Haller, G. L.; Resasco, D. E. Metal−Support Interaction: Group VIII Metals and Reducible Oxides. *Adv. Catal.* **1989**, *36*, 173−235.
(51) Fu, Q.; Wagner, T. Interaction of Nanostructured Metal Overlayers with Oxide Surfaces. *Surf. Sci. Rep.* **2007**, *62*, 431−498.
(52) Kitano, M.; Inoue, Y.; Yamazaki, Y.; Hayashi, F.; Kanbara, S.; Matsuishi, S.; Yokoyama, T.; Kim, S. W.; Hara, M.; Hosono, H. Ammonia Synthesis Using a Stable Electride as an Electron Donor and Reversible Hydrogen Store. *Nat. Chem.* **2012**, *4*, 934−940.
(53) Kanbara, S.; Kitano, M.; Inoue, Y.; Yokoyama, T.; Hara, M.; Hosono, H. Mechanism Switching of Ammonia Synthesis Over Ru-Loaded Electride Catalyst at Metal-Insulator Transition. *J. Am. Chem. Soc.* **2015**, *137*, 14517−14524.
(54) Zhang, Z.; Yates, J. T., Jr Band Bending in Semiconductors: Chemical and Physical Consequences at Surfaces and Interfaces. *Chem. Rev.* **2012**, *112*, 5520−5551.
(55) Subramanian, V.; Wolf, E. E.; Kamat, P. V. Catalysis with TiO_2/gold nanocomposites. Effect of Metal Particle Size on the Fermi Level Equilibration. *J. Am. Chem. Soc.* **2004**, *126*, 4943−4950.
(56) Lee, J.; Shim, H. S.; Lee, M.; Song, J. K.; Lee, D. Size-Controlled Electron Transfer and Photocatalytic Activity of ZnO−Au Nanoparticle Composites. *J. Phys. Chem. Lett.* **2011**, *2*, 2840−2845.
(57) Sitja, G.; Le Moal, S.; Marsault, M.; Hamm, G.; Leroy, F.; Henry, C. R. Transition from Molecule to Solid State: Reactivity of Supported Metal Clusters. *Nano Lett.* **2013**, *13*, 1977−1982.
(58) Yudanov, I. V.; Genest, A.; Schauermann, S.; Freund, H. J.; Rosch, N. Size Dependence of the Adsorption Energy of CO on Metal Nanoparticles: a DFT Search for the Minimum Value. *Nano Lett.* **2012**, *12*, 2134−2139.
(59) Meier, D. C.; Goodman, D. W. The Influence of Metal Cluster Size on Adsorption Energies: CO Adsorbed on Au Clusters Supported on TiO_2. *J. Am. Chem. Soc.* **2004**, *126*, 1892−1899.
(60) Lei, Y.; Zhao, H.; Rivas, R. D.; Lee, S.; Liu, B.; Lu, J.; Stach, E.; Winans, R. E.; Chapman, K. W.; Greeley, J. P.; et al. Adsorbate-Induced Structural Changes in 1−3 nm Platinum Nanoparticles. *J. Am. Chem. Soc.* **2014**, *136*, 9320−9326.
(61) Newton, M. A.; Belver-Coldeira, C.; Martinez-Arias, A.; Fernandez-Garcia, M. Dynamic In Situ Observation of Rapid Size and Shape Change of Supported Pd Nanoparticles During CO/NO Cycling. *Nat. Mater.* **2007**, *6*, 528−532.
(62) Nagai, Y.; Dohmae, K.; Ikeda, Y.; Takagi, N.; Tanabe, T.; Hara, N.; Guilera, G.; Pascarelli, S.; Newton, M. A.; Kuno, O.; et al. In Situ Redispersion of Platinum Autoexhaust Catalysts: an On-Line Approach to Increasing Catalyst Lifetimes? *Angew. Chem., Int. Ed.* **2008**, *47*, 9303−9306.
(63) Moliner, M.; Gabay, J. E.; Kliewer, C. E.; Carr, R. T.; Guzman, J.; Casty, G. L.; Serna, P.; Corma, A. Reversible Transformation of Pt Nanoparticles into Single Atoms inside High-Silica Chabazite Zeolite. *J. Am. Chem. Soc.* **2016**, *138*, 15743−15750.
(64) Sá, J.; Taylor, S. F. R.; Daly, H.; Goguet, A.; Tiruvalam, R.; He, Q.; Kiely, C. J.; Hutchings, G. J.; Hardacre, C. Redispersion of Gold Supported on Oxides. *ACS Catal.* **2012**, *2*, 552−560.
(65) Kim, D.; Becknell, N.; Yu, Y.; Yang, P. Room-Temperature Dynamics of Vanishing Copper Nanoparticles Supported on Silica. *Nano Lett.* **2017**, *17*, 2732−2737.
(66) Duan, X.; Tian, X.; Ke, J.; Yin, Y.; Zheng, J.; Chen, J.; Cao, Z.; Xie, Z.; Yuan, Y. Size Controllable Redispersion of Sintered Au Nanoparticles by Using Iodohydrocarbon and Its Implications. *Chem. Sci.* **2016**, *7*, 3181−3187.
(67) Morgan, K.; Goguet, A.; Hardacre, C. Metal Redispersion Strategies for Recycling of Supported Metal Catalysts: A Perspective. *ACS Catal.* **2015**, *5*, 3430−3445.
(68) Haruta, M. Size- and Support-Dependency in the Catalysis of Gold. *Catal. Today* **1997**, *36*, 153−166.
(69) Qiao, B.; Liang, J.-X.; Wang, A.; Xu, C.-Q.; Li, J.; Zhang, T.; Liu, J. J. Ultrastable Single-Atom Gold Catalysts with Strong Covalent Metal-Support Interaction (CMSI). *Nano Res.* **2015**, *8*, 2913−2924.
(70) Qiao, B.; Liang, J.-X.; Wang, A.; Liu, J.; Zhang, T. Single Atom Gold Catalysts for Low-Temperature CO Oxidation. *Chin. J. Catal.* **2016**, *37*, 1580−1586.
(71) Qiao, B.; Liu, J.; Wang, Y.-G.; Lin, Q.; Liu, X.; Wang, A.; Li, J.; Zhang, T.; Liu, J. Highly Efficient Catalysis of Preferential Oxidation of CO in H_2-Rich Stream by Gold Single-Atom Catalysts. *ACS Catal.* **2015**, *5*, 6249−6254.
(72) Qiao, B.; Wang, A.; Yang, X.; Allard, L. F.; Jiang, Z.; Cui, Y.; Liu, J.; Li, J.; Zhang, T. Single-Atom Catalysis of CO Oxidation Using Pt_1/FeOx. *Nat. Chem.* **2011**, *3*, 634−641.
(73) Moses-DeBusk, M.; Yoon, M.; Allard, L. F.; Mullins, D. R.; Wu, Z.; Yang, X.; Veith, G.; Stocks, G. M.; Narula, C. K. CO oxidation on Supported Single Pt Atoms: Experimental and ab initio Density Functional Studies of CO Interaction with Pt Atom on θ-Al_2O_3(010) Surface. *J. Am. Chem. Soc.* **2013**, *135*, 12634−12645.
(74) DeRita, L.; Dai, S.; Lopez-Zepeda, K.; Pham, N.; Graham, G. W.; Pan, X.; Christopher, P. Catalyst Architecture for Stable Single Atom Dispersion Enables Site-Specific Spectroscopic and Reactivity Measurements of CO Adsorbed to Pt Atoms, Oxidized Pt Clusters, and Metallic Pt Clusters on TiO_2. *J. Am. Chem. Soc.* **2017**, *139*, 14150−14165.
(75) Kistler, J. D.; Chotigkrai, N.; Xu, P.; Enderle, B.; Praserthdam, P.; Chen, C. Y.; Browning, N. D.; Gates, B. C. A Single-Site Platinum CO Oxidation Catalyst in Zeolite KLTL: Microscopic and Spectroscopic

DOI: 10.1021/acs.chemrev.7b00776
Chem. Rev. 2018, 118, 4981−5079

Determination of the Locations of the Platinum atoms. *Angew. Chem., Int. Ed.* **2014**, *53*, 8904−8907.
(76) Costello, C. K.; Yang, J. H.; Law, H. Y.; Wang, Y.; Lin, J. N.; Marks, L. D.; Kung, M. C.; Kung, H. H. On the Potential Role of Hydroxyl Hroups in CO Oxidation over Au/Al_2O_3. *Appl. Catal., A* **2003**, *243*, 15−24.
(77) Saavedra, J.; Whittaker, T.; Chen, Z.; Pursell, C. J.; Rioux, R. M.; Chandler, B. D. Controlling Activity and Selectivity Using Water in the Au-Catalysed Preferential Oxidation of CO in H_2. *Nat. Chem.* **2016**, *8*, 584−589.
(78) Wang, C.; Gu, X.-K.; Yan, H.; Lin, Y.; Li, J.; Liu, D.; Li, W.-X.; Lu, J. Water-Mediated Mars-Van Krevelen Mechanism for CO Oxidation on Ceria-Supported Single-Atom Pt_1 Catalyst. *ACS Catal.* **2017**, *7*, 887−891.
(79) Jones, J.; Xiong, H.; DeLaRiva, A. T.; Peterson, E. J.; Pham, H.; Challa, S. R.; Qi, G.; Oh, S.; Wiebenga, M. H.; Pereira Hernandez, X. I.; Wang, Y.; Datye, A. K. Thermally stable single-atom platinum-on-ceria catalysts via atom trapping. *Science* **2016**, *353*, 150−154.
(80) Zhang, Z.; Zhu, Y.; Asakura, H.; Zhang, B.; Zhang, J.; Zhou, M.; Han, Y.; Tanaka, T.; Wang, A.; Zhang, T.; et al. Thermally Stable Single Atom $Pt/m\text{-}Al_2O_3$ for Selective Hydrogenation and CO Oxidation. *Nat. Commun.* **2017**, *8*, 16100.
(81) Peterson, E. J.; DeLaRiva, A. T.; Lin, S.; Johnson, R. S.; Guo, H.; Miller, J. T.; Hun Kwak, J.; Peden, C. H.; Kiefer, B.; Allard, L. F.; Ribeiro, F. H.; Datye, A. K. Low-temperature Carbon Monoxide Oxidation Catalysed by Regenerable Atomically Dispersed Palladium on Alumina. *Nat. Commun.* **2014**, *5*, 4885.
(82) Huang, Z.; Gu, X.; Cao, Q.; Hu, P.; Hao, J.; Li, J.; Tang, X. Catalytically Active Single-Atom Sites Fabricated from Silver Particles. *Angew. Chem., Int. Ed.* **2012**, *51*, 4198−4203.
(83) Chen, Y.; Kasama, T.; Huang, Z.; Hu, P.; Chen, J.; Liu, X.; Tang, X. Highly Dense Isolated Metal Atom Catalytic Sites: Dynamic Formation and In Situ Observations. *Chem. - Eur. J.* **2015**, *21*, 17397−17402.
(84) Abbet, S.; Heiz, U.; Hakkinen, H.; Landman, U. CO Oxidation on a Single Pd Atom Supported on Magnesia. *Phys. Rev. Lett.* **2001**, *86*, 5950−5953.
(85) Liang, J.-X.; Lin, J.; Yang, X.-F.; Wang, A.-Q.; Qiao, B.-T.; Liu, J.; Zhang, T.; Li, J. Theoretical and Experimental Investigations on Single-Atom Catalysis: $Ir_1/FeOx$ for CO Oxidation. *J. Phys. Chem. C* **2014**, *118*, 21945−21951.
(86) Spezzati, G.; Su, Y.; Hofmann, J. P.; Benavidez, A. D.; DeLaRiva, A. T.; McCabe, J.; Datye, A. K.; Hensen, E. J. M. Atomically Dispersed Pd-O Species on $CeO_2(111)$ as Highly Active Sites for Low-Temperature CO Oxidation. *ACS Catal.* **2017**, *7*, 6887−6891.
(87) Su, Y.-Q.; Filot, I. A. W.; Liu, J.-X.; Hensen, E. J. M. Stable Pd-Doped Ceria Structures for CH_4 Activation and CO Oxidation. *ACS Catal.* **2018**, *8*, 75−80.
(88) Fu, Q.; Saltsburg, H.; Flytzani-Stephanopoulos, M. Active Nonmetallic Au and Pt Species on Ceria-Based Water-Gas Shift Catalysts. *Science* **2003**, *301*, 935−938.
(89) Zhai, Y.; Pierre, D.; Si, R.; Deng, W.; Ferrin, P.; Nilekar, A. U.; Peng, G.; Herron, J. A.; Bell, D. C.; Saltsburg, H.; Mavrikakis, M.; Flytzani-Stephanopoulos, M. Alkali-Stabilized Pt-OHx Species Catalyze Low-Temperature Water-Gas Shift Reactions. *Science* **2010**, *329*, 1633−1636.
(90) Yang, M.; Li, S.; Wang, Y.; Herron, J. A.; Xu, Y.; Allard, L. F.; Lee, S.; Huang, J.; Mavrikakis, M.; Flytzani-Stephanopoulos, M. Catalytically Active Au-O(OH)x Species Stabilized by Alkali Ions on Zeolites and Mesoporous Oxides. *Science* **2014**, *346*, 1498−1501.
(91) Yang, M.; Liu, J.; Lee, S.; Zugic, B.; Huang, J.; Allard, L. F.; Flytzani-Stephanopoulos, M. A Common Single-Site Pt(II)-O(OH)x Species Stabilized by Sodium on "Active" and "Inert" Supports Catalyzes the Water-Gas Shift Reaction. *J. Am. Chem. Soc.* **2015**, *137*, 3470−3473.
(92) Flytzani-Stephanopoulos, M. Gold Atoms Stabilized on Various Supports Catalyze the Water-Gas Shift Reaction. *Acc. Chem. Res.* **2014**, *47*, 783−792.
(93) Lin, J.; Wang, A.; Qiao, B.; Liu, X.; Yang, X.; Wang, X.; Liang, J.; Li, J.; Liu, J.; Zhang, T. Remarkable Performance of $Ir_1/FeOx$ Single-Atom Catalyst in Water Gas Shift Reaction. *J. Am. Chem. Soc.* **2013**, *135*, 15314−15317.
(94) Guan, H.; Lin, J.; Qiao, B.; Miao, S.; Wang, A.-Q.; Wang, X.; Zhang, T. Enhanced Performance of Rh_1/TiO_2 Catalyst Without Methanation in Water-Gas Shift Reaction. *AIChE J.* **2017**, *63*, 2081−2088.
(95) Zhang, S.; Shan, J. J.; Zhu, Y.; Frenkel, A. I.; Patlolla, A.; Huang, W.; Yoon, S. J.; Wang, L.; Yoshida, H.; Takeda, S.; Tao, F. F. WGS Catalysis and in situ Studies of CoO_{1-x}, $PtCo_n/Co_3O_4$, and $Pt_mCo_{m'}/CoO_{1-x}$ Nanorod Catalysts. *J. Am. Chem. Soc.* **2013**, *135*, 8283−8293.
(96) Gai, P. L.; Yoshida, K.; Ward, M. R.; Walsh, M.; Baker, R. T.; van de Water, L.; Watson, M. J.; Boyes, E. D. Visualisation of Single Atom Dynamics in Water Gas Shift Reaction for Hydrogen Generation. *Catal. Sci. Technol.* **2016**, *6*, 2214−2227.
(97) Carter, J. H.; Liu, X.; He, Q.; Althahban, S.; Nowicka, E.; Freakley, S. J.; Niu, L.; Morgan, D. J.; Li, Y.; Niemantsverdriet, J. W. H.; et al. Activation and Deactivation of Gold/Ceria-Zirconia in the Low-Temperature Water-Gas Shift Reaction. *Angew. Chem., Int. Ed.* **2018**, *56*, 16037.
(98) Davis, S. E.; Ide, M. S.; Davis, R. J. Selective Oxidation of Alcohols and Aldehydes over Supported Metal Nanoparticles. *Green Chem.* **2013**, *15*, 17−45.
(99) Abad, A.; Concepcion, P.; Corma, A.; Garcia, H. A Collaborative Effect between Gold and a Support Induces the Selective Oxidation of Alcohols. *Angew. Chem., Int. Ed.* **2005**, *44*, 4066−4069.
(100) Hackett, S. F.; Brydson, R. M.; Gass, M. H.; Harvey, I.; Newman, A. D.; Wilson, K.; Lee, A. F. High-Activity, Single-Site Mesoporous Pd/Al_2O_3 Catalysts for Selective Aerobic Oxidation of Allylic Alcohols. *Angew. Chem., Int. Ed.* **2007**, *46*, 8593−8596.
(101) Abad, A.; Almela, C.; Corma, A.; Garcia, H. Unique Gold Chemoselectivity for the Aerobic Oxidation of Allylic Alcohols. *Chem. Commun.* **2006**, 3178−3180.
(102) Jagadeesh, R. V.; Junge, H.; Pohl, M. M.; Radnik, J.; Bruckner, A.; Beller, M. Selective Oxidation of Alcohols to Esters Using Heterogeneous Co_3O_4-N@C Catalysts Under Mild Conditions. *J. Am. Chem. Soc.* **2013**, *135*, 10776−10782.
(103) Jagadeesh, R. V.; Junge, H.; Beller, M. Green Synthesis of Nitriles Using Non-Noble Metal Oxides-Based Nanocatalysts. *Nat. Commun.* **2014**, *5*, 4123.
(104) Zhang, L.; Wang, A.; Wang, W.; Huang, Y.; Liu, X.; Miao, S.; Liu, J.; Zhang, T. Co−N−C Catalyst for C−C Coupling Reactions: On the Catalytic Performance and Active Sites. *ACS Catal.* **2015**, *5*, 6563−6572.
(105) Xie, J.; Yin, K.; Serov, A.; Artyushkova, K.; Pham, H. N.; Sang, X.; Unocic, R. R.; Atanassov, P.; Datye, A. K.; Davis, R. J. Selective Aerobic Oxidation of Alcohols over Atomically-Dispersed Non-Precious Metal Catalysts. *ChemSusChem* **2017**, *10*, 359−362.
(106) Wei, H.; Liu, X.; Wang, A.; Zhang, L.; Qiao, B.; Yang, X.; Huang, Y.; Miao, S.; Liu, J.; Zhang, T. FeOx-Supported Platinum Single-Atom and Pseudo-Single-Atom Catalysts for Chemoselective Hydrogenation of Functionalized Nitroarenes. *Nat. Commun.* **2014**, *5*, 5634.
(107) Zhang, B.; Asakura, H.; Zhang, J.; Zhang, J.; De, S.; Yan, N. Stabilizing a Platinum Single-Atom Catalyst on Supported Phosphomolybdic Acid without Compromising Hydrogenation Activity. *Angew. Chem., Int. Ed.* **2016**, *55*, 8319−8323.
(108) Yan, H.; Cheng, H.; Yi, H.; Lin, Y.; Yao, T.; Wang, C.; Li, J.; Wei, S.; Lu, J. Single-Atom Pd_1/Graphene Catalyst Achieved by Atomic Layer Deposition: Remarkable Performance in Selective Hydrogenation of 1,3-Butadiene. *J. Am. Chem. Soc.* **2015**, *137*, 10484−10487.
(109) Vile, G.; Albani, D.; Nachtegaal, M.; Chen, Z.; Dontsova, D.; Antonietti, M.; Lopez, N.; Perez-Ramirez, J. A Stable Single-Site Palladium Catalyst for Hydrogenations. *Angew. Chem., Int. Ed.* **2015**, *54*, 11265−11269.
(110) Rossell, M. D.; Caparrós, F. J.; Angurell, I.; Muller, G.; Llorca, J.; Seco, M.; Rossell, O. Magnetite-Supported Palladium Single-Atoms Do Not Catalyse the Hydrogenation of Alkenes But Small Clusters Do. *Catal. Sci. Technol.* **2016**, *6*, 4081−4085.

DOI: 10.1021/acs.chemrev.7b00776
Chem. Rev. 2018, 118, 4981−5079

(111) Kwak, J. H.; Kovarik, L.; Szanyi, J. CO_2 Reduction on Supported Ru/Al_2O_3 Catalysts: Cluster Size Dependence of Product Selectivity. *ACS Catal.* **2013**, *3*, 2449−2455.
(112) Matsubu, J. C.; Yang, V. N.; Christopher, P. Isolated Metal Active Site Concentration and Stability Control Catalytic CO_2 Reduction Selectivity. *J. Am. Chem. Soc.* **2015**, *137*, 3076−3084.
(113) Mori, K.; Taga, T.; Yamashita, H. Isolated Single-Atomic Ru Catalyst Bound on a Layered Double Hydroxide for Hydrogenation of CO_2 to Formic Acid. *ACS Catal.* **2017**, *7*, 3147−3151.
(114) Lu, J.; Serna, P.; Gates, B. C. Zeolite- and MgO-Supported Molecular Iridium Complexes: Support and Ligand Effects in Catalysis of Ethene Hydrogenation and H−D Exchange in the Conversion of H_2+D_2. *ACS Catal.* **2011**, *1*, 1549−1561.
(115) Lu, J.; Serna, P.; Aydin, C.; Browning, N. D.; Gates, B. C. Supported Molecular Iridium Catalysts: Resolving Effects of Metal Nuclearity and Supports as Ligands. *J. Am. Chem. Soc.* **2011**, *133*, 16186−16195.
(116) Yang, D.; Odoh, S. O.; Borycz, J.; Wang, T. C.; Farha, O. K.; Hupp, J. T.; Cramer, C. J.; Gagliardi, L.; Gates, B. C. Tuning Zr_6 Metal−Organic Framework (MOF) Nodes as Catalyst Supports: Site Densities and Electron-Donor Properties Influence Molecular Iridium Complexes as Ethylene Conversion Catalysts. *ACS Catal.* **2016**, *6*, 235−247.
(117) Yang, D.; Odoh, S. O.; Wang, T. C.; Farha, O. K.; Hupp, J. T.; Cramer, C. J.; Gagliardi, L.; Gates, B. C. Metal-Organic Framework Nodes as Nearly Ideal Supports for Molecular Catalysts: NU-1000- and UiO-66-Supported Iridium Complexes. *J. Am. Chem. Soc.* **2015**, *137*, 7391−7396.
(118) Liu, P.; Zhao, Y.; Qin, R.; Mo, S.; Chen, G.; Gu, L.; Chevrier, D. M.; Zhang, P.; Guo, Q.; Zang, D.; et al. Photochemical Route for Synthesizing Atomically Dispersed Palladium Catalysts. *Science* **2016**, *352*, 797−801.
(119) Bond, G. C.; Sermon, P. A. Gold Catalysts for Olefin Hydrogenation. *Gold Bull.* **1973**, *6*, 102−105.
(120) Guzman, J.; Gates, B. C. Structure and Reactivity of a Mononuclear Gold-Complex Catalyst Supported on Magnesium Oxide. *Angew. Chem., Int. Ed.* **2003**, *42*, 690−693.
(121) Zhang, X.; Shi, H.; Xu, B. Q. Catalysis by Gold: Isolated Surface Au^{3+} Ions Are Active Sites for Selective Hydrogenation of 1,3-Butadiene over Au/ZrO_2 Catalysts. *Angew. Chem., Int. Ed.* **2005**, *44*, 7132−7135.
(122) Zhang, X.; Shi, H.; Xu, B.-Q. Comparative Study of Au/ZrO_2 Catalysts in CO Oxidation and 1,3-Butadiene Hydrogenation. *Catal. Today* **2007**, *122*, 330−337.
(123) Zhang, X.; Llabrés i Xamena, F. X.; Corma, A. Gold(III)−Metal Organic Framework Bridges the Gap between Homogeneous and Heterogeneous Gold Catalysts. *J. Catal.* **2009**, *265*, 155−160.
(124) Kovtunov, K. V.; Zhivonitko, V. V.; Corma, A.; Koptyug, I. V. Parahydrogen-Induced Polarization in Heterogeneous Hydrogenations Catalyzed by an Immobilized Au(III) Complex. *J. Phys. Chem. Lett.* **2010**, *1*, 1705−1708.
(125) Corma, A.; Salnikov, O. G.; Barskiy, D. A.; Kovtunov, K. V.; Koptyug, I. V. Single-Atom Gold Catalysis in the Context of Developments in Parahydrogen-Induced Polarization. *Chem. - Eur. J.* **2015**, *21*, 7012−7015.
(126) Westerhaus, F. A.; Jagadeesh, R. V.; Wienhofer, G.; Pohl, M. M.; Radnik, J.; Surkus, A. E.; Rabeah, J.; Junge, K.; Junge, H.; Nielsen, M.; et al. Heterogenized Cobalt Oxide Catalysts for Nitroarene Reduction by Pyrolysis of Molecularly Defined Complexes. *Nat. Chem.* **2013**, *5*, 537−543.
(127) Liu, L.; Concepción, P.; Corma, A. Non-Noble Metal Catalysts for Hydrogenation: A Facile Method for Preparing Co Nanoparticles Covered with Thin Layered Carbon. *J. Catal.* **2016**, *340*, 1−9.
(128) Liu, L.; Gao, F.; Concepción, P.; Corma, A. A New Strategy to Transform Mono and Bimetallic Non-Noble Metal Nanoparticles into Highly Active and Chemoselective Hydrogenation Catalysts. *J. Catal.* **2017**, *350*, 218−225.
(129) Liu, W.; Zhang, L.; Yan, W.; Liu, X.; Yang, X.; Miao, S.; Wang, W.; Wang, A.; Zhang, T. Single-Atom Dispersed Co−N−C Catalyst: Structure Identification and Performance for Hydrogenative Coupling of Nitroarenes. *Chem. Sci.* **2016**, *7*, 5758−5764.
(130) Combita, D.; Concepción, P.; Corma, A. Gold Catalysts for the Synthesis of Aromatic Azocompounds from Nitroaromatics in One Step. *J. Catal.* **2014**, *311*, 339−349.
(131) Liu, X.; Li, H. Q.; Ye, S.; Liu, Y. M.; He, H. Y.; Cao, Y. Gold-Catalyzed Direct Hydrogenative Coupling of Nitroarenes to Synthesize Aromatic Azo Compounds. *Angew. Chem., Int. Ed.* **2014**, *53*, 7624−7628.
(132) Sun, X.; Olivos-Suarez, A. I.; Osadchii, D.; Romero, M. J. V.; Kapteijn, F.; Gascon, J. Single Cobalt Sites in Mesoporous N-Doped Carbon Matrix for Selective Catalytic Hydrogenation of Nitroarenes. *J. Catal.* **2018**, *357*, 20−28.
(133) Ji, P.; Manna, K.; Lin, Z.; Urban, A.; Greene, F. X.; Lan, G.; Lin, W. Single-Site Cobalt Catalysts at New $Zr_8(\mu_2\text{-}O)_8(\mu_2\text{-}OH)_4$ Metal-Organic Framework Nodes for Highly Active Hydrogenation of Alkenes, Imines, Carbonyls, and Heterocycles. *J. Am. Chem. Soc.* **2016**, *138*, 12234−12242.
(134) Li, Z.; Schweitzer, N. M.; League, A. B.; Bernales, V.; Peters, A. W.; Getsoian, A. B.; Wang, T. C.; Miller, J. T.; Vjunov, A.; Fulton, J. L.; et al. Sintering-Resistant Single-Site Nickel Catalyst Supported by Metal-Organic Framework. *J. Am. Chem. Soc.* **2016**, *138*, 1977−1982.
(135) Cohen, S. M.; Zhang, Z.; Boissonnault, J. A. Toward "metalloMOFzymes": Metal−Organic Frameworks with Single-Site Metal Catalysts for Small-Molecule Transformations. *Inorg. Chem.* **2016**, *55*, 7281−7290.
(136) Hu, B.; Schweitzer, N. M.; Zhang, G.; Kraft, S. J.; Childers, D. J.; Lanci, M. P.; Miller, J. T.; Hock, A. S. Isolated Fe^{II} on Silica As a Selective Propane Dehydrogenation Catalyst. *ACS Catal.* **2015**, *5*, 3494−3503.
(137) Getsoian, A. B.; Das, U.; Camacho-Bunquin, J.; Zhang, G.; Gallagher, J. R.; Hu, B.; Cheah, S.; Schaidle, J. A.; Ruddy, D. A.; Hensley, J. E.; et al. Organometallic Model Complexes Elucidate the Active Gallium Species in Alkane Dehydrogenation Catalysts Based on Ligand Effects in Ga K-edge XANES. *Catal. Sci. Technol.* **2016**, *6*, 6339−6353.
(138) Wang, C.; Garbarino, G.; Allard, L. F.; Wilson, F.; Busca, G.; Flytzani-Stephanopoulos, M. Low-Temperature Dehydrogenation of Ethanol on Atomically Dispersed Gold Supported on ZnZrOx. *ACS Catal.* **2016**, *6*, 210−218.
(139) De, S.; Saha, B.; Luque, R. Hydrodeoxygenation Processes: Advances on Catalytic Transformations of Biomass-Derived Platform Chemicals into Hydrocarbon Fuels. *Bioresour. Technol.* **2015**, *178*, 108−118.
(140) Liu, G.; Robertson, A. W.; Li, M. M.-J.; Kuo, W. C. H.; Darby, M. T.; Muhieddine, M. H.; Lin, Y.-C.; Suenaga, K.; Stamatakis, M.; Warner, J. H.; et al. MoS_2 Monolayer Catalyst Doped with Isolated Co Atoms for the Hydrodeoxygenation Reaction. *Nat. Chem.* **2017**, *9*, 810.
(141) Chianelli, R. R. Fundamental Studies of Transition Metal Sulfide Hydrodesulfurization Catalysts. *Catal. Rev.: Sci. Eng.* **1984**, *26*, 361−393.
(142) Zhu, Y.; Ramasse, Q. M.; Brorson, M.; Moses, P. G.; Hansen, L. P.; Kisielowski, C. F.; Helveg, S. Visualizing the Stoichiometry of Industrial-Style Co-Mo-S Catalysts with Single-Atom Sensitivity. *Angew. Chem., Int. Ed.* **2014**, *53*, 10723−10727.
(143) Spivey, J. J.; Hutchings, G. Catalytic Aromatization of Methane. *Chem. Soc. Rev.* **2014**, *43*, 792−803.
(144) Guo, X.; Fang, G.; Li, G.; Ma, H.; Fan, H.; Yu, L.; Ma, C.; Wu, X.; Deng, D.; Wei, M.; et al. Direct, Nonoxidative Conversion of Methane to Ethylene, Aromatics, and Hydrogen. *Science* **2014**, *344*, 616−619.
(145) Sakbodin, M.; Wu, Y.; Oh, S. C.; Wachsman, E. D.; Liu, D. Hydrogen-Permeable Tubular Membrane Reactor: Promoting Conversion and Product Selectivity for Non-Oxidative Activation of Methane over an Fe©SiO_2 Catalyst. *Angew. Chem., Int. Ed.* **2016**, *55*, 16149−16152.
(146) Gu, X.-K.; Qiao, B.; Huang, C.-Q.; Ding, W.-C.; Sun, K.; Zhan, E.; Zhang, T.; Liu, J.; Li, W.-X. Supported Single Pt_1/Au_1 Atoms for Methanol Steam Reforming. *ACS Catal.* **2014**, *4*, 3886−3890.
(147) Zhu, Y.; An, Z.; He, J. Single-Atom and Small-Cluster Pt Induced by Sn (IV) sites Confined in an LDH Lattice for Catalytic Reforming. *J. Catal.* **2016**, *341*, 44−54.
(148) Meriaudeau, P.; Naccache, C. Dehydrocyclization of Alkanes Over Zeolite-Supported Metal Catalysts: Monofunctional or Bifunctional Route. *Catal. Rev.: Sci. Eng.* **1997**, *39*, 5−48.

DOI: 10.1021/acs.chemrev.7b00776
Chem. Rev. 2018, 118, 4981−5079

(149) Nielsen, M.; Alberico, E.; Baumann, W.; Drexler, H. J.; Junge, H.; Gladiali, S.; Beller, M. Low-Temperature Aqueous-Phase Methanol Dehydrogenation to Hydrogen and Carbon Dioxide. *Nature* **2013**, *495*, 85−89.
(150) Shabaker, J. Aqueous-Phase Reforming of Methanol and Ethylene Glycol over Alumina-Supported Platinum Catalysts. *J. Catal.* **2003**, *215*, 344−352.
(151) Lin, L.; Zhou, W.; Gao, R.; Yao, S.; Zhang, X.; Xu, W.; Zheng, S.; Jiang, Z.; Yu, Q.; Li, Y. W.; et al. Low-Temperature Hydrogen Production from Water and Methanol Using Pt/α-MoC Catalysts. *Nature* **2017**, *544*, 80−83.
(152) Franke, R.; Selent, D.; Borner, A. Applied Hydroformylation. *Chem. Rev.* **2012**, *112*, 5675−5732.
(153) Horvath, I. T.; Rabai, J. Facile Catalyst Separation Without Water: Fluorous Biphase Hydroformylation of Olefins. *Science* **1994**, *266*, 72−75.
(154) Nowotny, M.; Maschmeyer, T.; Johnson, B. F.; Lahuerta, P.; Thomas, J. M.; Davies, J. E. Heterogeneous Dinuclear Rhodium(II) Hydroformylation Catalysts-Performance Evaluation and Silsesquioxane-Based Chemical Modeling. *Angew. Chem., Int. Ed.* **2001**, *40*, 955−958.
(155) Sun, Q.; Dai, Z.; Liu, X.; Sheng, N.; Deng, F.; Meng, X.; Xiao, F. S. Highly Efficient Heterogeneous Hydroformylation over Rh-Metalated Porous Organic Polymers: Synergistic Effect of High Ligand Concentration and Flexible Framework. *J. Am. Chem. Soc.* **2015**, *137*, 5204−5209.
(156) Li, C.; Yan, L.; Lu, L.; Xiong, K.; Wang, W.; Jiang, M.; Liu, J.; Song, X.; Zhan, Z.; Jiang, Z.; Ding, Y. Single Atom Dispersed Rh-Biphephos&PPh_3@Porous Organic Copolymers: Highly Efficient Catalysts for Continuous Fixed-Bed Hydroformylation of Propene. *Green Chem.* **2016**, *18*, 2995−3005.
(157) Lang, R.; Li, T.; Matsumura, D.; Miao, S.; Ren, Y.; Cui, Y. T.; Tan, Y.; Qiao, B.; Li, L.; Wang, A.; et al. Hydroformylation of Olefins by a Rhodium Single-Atom Catalyst with Activity Comparable to $RhCl(PPh_3)_3$. *Angew. Chem., Int. Ed.* **2016**, *55*, 16054−16058.
(158) Wang, L.; Zhang, W.; Wang, S.; Gao, Z.; Luo, Z.; Wang, X.; Zeng, R.; Li, A.; Li, H.; Wang, M.; et al. Atomic-level Insights in Optimizing Reaction Paths for Hydroformylation Reaction over Rh/CoO Single-Atom Catalyst. *Nat. Commun.* **2016**, *7*, 14036.
(159) Li, Y. H.; Xing, J.; Yang, X. H.; Yang, H. G. Cluster Size Effects of Platinum Oxide as Active Sites in Hydrogen Evolution Reactions. *Chem. - Eur. J.* **2014**, *20*, 12377−12380.
(160) Xing, J.; Chen, J. F.; Li, Y. H.; Yuan, W. T.; Zhou, Y.; Zheng, L. R.; Wang, H. F.; Hu, P.; Wang, Y.; Zhao, H. J.; et al. Stable Isolated Metal Atoms as Active Sites for Photocatalytic Hydrogen Evolution. *Chem. - Eur. J.* **2014**, *20*, 2138−2144.
(161) Li, X.; Bi, W.; Zhang, L.; Tao, S.; Chu, W.; Zhang, Q.; Luo, Y.; Wu, C.; Xie, Y. Single-Atom Pt as Co-Catalyst for Enhanced Photocatalytic H_2 Evolution. *Adv. Mater.* **2016**, *28*, 2427−2431.
(162) Zhang, H.; Wei, J.; Dong, J.; Liu, G.; Shi, L.; An, P.; Zhao, G.; Kong, J.; Wang, X.; Meng, X.; et al. Efficient Visible-Light-Driven Carbon Dioxide Reduction by a Single-Atom Implanted Metal-Organic Framework. *Angew. Chem., Int. Ed.* **2016**, *55*, 14310−14314.
(163) Seh, Z. W.; Kibsgaard, J.; Dickens, C. F.; Chorkendorff, I.; Norskov, J. K.; Jaramillo, T. F. Combining Theory and Experiment in Electrocatalysis: Insights into Materials Design. *Science* **2017**, *355*, 1.
(164) Cheng, N.; Stambula, S.; Wang, D.; Banis, M. N.; Liu, J.; Riese, A.; Xiao, B.; Li, R.; Sham, T. K.; Liu, L. M.; Botton, G. A.; Sun, X. Platinum Single-Atom and Cluster Catalysis of the Hydrogen Evolution Reaction. *Nat. Commun.* **2016**, *7*, 13638.
(165) Kamai, R.; Kamiya, K.; Hashimoto, K.; Nakanishi, S. Oxygen-Tolerant Electrodes with Platinum-Loaded Covalent Triazine Frameworks for the Hydrogen Oxidation Reaction. *Angew. Chem., Int. Ed.* **2016**, *55*, 13184−13188.
(166) Fei, H.; Dong, J.; Arellano-Jimenez, M. J.; Ye, G.; Dong Kim, N.; Samuel, E. L.; Peng, Z.; Zhu, Z.; Qin, F.; Bao, J.; et al. Atomic Cobalt on nitrogen-doped Graphene for Hydrogen Generation. *Nat. Commun.* **2015**, *6*, 8668.
(167) Liang, H. W.; Bruller, S.; Dong, R.; Zhang, J.; Feng, X.; Mullen, K. Molecular Metal-Nx Centres in Porous Carbon for Electrocatalytic Hydrogen Evolution. *Nat. Commun.* **2015**, *6*, 7992.
(168) Qiu, H. J.; Ito, Y.; Cong, W.; Tan, Y.; Liu, P.; Hirata, A.; Fujita, T.; Tang, Z.; Chen, M. Nanoporous Graphene with Single-Atom Nickel Dopants: An Efficient and Stable Catalyst for Electrochemical Hydrogen Production. *Angew. Chem., Int. Ed.* **2015**, *54*, 14031−14035.
(169) Chen, Z.; Higgins, D.; Yu, A.; Zhang, L.; Zhang, J. A Review on Non-Precious Metal Electrocatalysts for PEM Fuel Cells. *Energy Environ. Sci.* **2011**, *4*, 3167−3192.
(170) Dombrovskis, J. K.; Palmqvist, A. E. C. Recent Progress in Synthesis, Characterization and Evaluation of Non-Precious Metal Catalysts for the Oxygen Reduction Reaction. *Fuel Cells* **2016**, *16*, 4−22.
(171) Lefevre, M.; Proietti, E.; Jaouen, F.; Dodelet, J. P. Iron-Based Catalysts with Improved Oxygen Reduction Activity in Polymer Electrolyte Fuel Cells. *Science* **2009**, *324*, 71−74.
(172) Koslowski, U. I.; Abs-Wurmbach, I.; Fiechter, S.; Bogdanoff, P. Nature of the Catalytic Centers of Porphyrin-Based Electrocatalysts for the ORR: A Correlation of Kinetic Current Density with the Site Density of Fe−N_4 Centers. *J. Phys. Chem. C* **2008**, *112*, 15356−15366.
(173) Zitolo, A.; Goellner, V.; Armel, V.; Sougrati, M. T.; Mineva, T.; Stievano, L.; Fonda, E.; Jaouen, F. Identification of Catalytic Sites for Oxygen Reduction in Iron- and Nitrogen-Doped Graphene Materials. *Nat. Mater.* **2015**, *14*, 937−942.
(174) Jiang, W. J.; Gu, L.; Li, L.; Zhang, Y.; Zhang, X.; Zhang, L. J.; Wang, J. Q.; Hu, J. S.; Wei, Z.; Wan, L. J. Understanding the High Activity of Fe-N-C Electrocatalysts in Oxygen Reduction: Fe/Fe_3C Nanoparticles Boost the Activity of Fe-Nx. *J. Am. Chem. Soc.* **2016**, *138*, 3570−3578.
(175) Yin, P.; Yao, T.; Wu, Y.; Zheng, L.; Lin, Y.; Liu, W.; Ju, H.; Zhu, J.; Hong, X.; Deng, Z.; et al. Single Cobalt Atoms with Precise N-Coordination as Superior Oxygen Reduction Reaction Catalysts. *Angew. Chem., Int. Ed.* **2016**, *55*, 10800−10805.
(176) Huan, T. N.; Ranjbar, N.; Rousse, G.; Sougrati, M.; Zitolo, A.; Mougel, V.; Jaouen, F.; Fontecave, M. Electrochemical Reduction of CO_2 Catalyzed by Fe-N-C Materials: A Structure−Selectivity Study. *ACS Catal.* **2017**, *7*, 1520−1525.
(177) Chen, X.; Zhu, H.; Wang, W.; Du, H.; Wang, T.; Yan, L.; Hu, X.; Ding, Y. Multifunctional Single-Site Catalysts for Alkoxycarbonylation of Terminal Alkynes. *ChemSusChem* **2016**, *9*, 2451−2459.
(178) Duan, H.; Li, M.; Zhang, G.; Gallagher, J. R.; Huang, Z.; Sun, Y.; Luo, Z.; Chen, H.; Miller, J. T.; Zou, R.; et al. Single-Site Palladium(II) Catalyst for Oxidative Heck Reaction: Catalytic Performance and Kinetic Investigations. *ACS Catal.* **2015**, *5*, 3752−3759.
(179) Metzger, E. D.; Brozek, C. K.; Comito, R. J.; Dincă, M. Selective Dimerization of Ethylene to 1-Butene with a Porous Catalyst. *ACS Cent. Sci.* **2016**, *2*, 148−153.
(180) Metzger, E. D.; Comito, R. J.; Hendon, C. H.; Dincă, M. Mechanism of Single-Site Molecule-Like Catalytic Ethylene Dimerization in Ni-MFU-4*l*. *J. Am. Chem. Soc.* **2017**, *139*, 757−762.
(181) Rozhko, E.; Bavykina, A.; Osadchii, D.; Makkee, M.; Gascon, J. Covalent Organic Frameworks as Supports for a Molecular Ni Based Ethylene Oligomerization Catalyst for the Synthesis of Long Chain Olefins. *J. Catal.* **2017**, *345*, 270−280.
(182) Díaz, U.; Corma, A. Ordered Covalent Organic Frameworks, COFs and PAFs. From Preparation to Application. *Coord. Chem. Rev.* **2016**, *311*, 85−124.
(183) Periana, R. A.; Taube, D. J.; Gamble, S.; Taube, H.; Satoh, T.; Fujii, H. Platinum Catalysts for the High-Yield Oxidation of Methane to a Methanol Derivative. *Science* **1998**, *280*, 560−564.
(184) Palkovits, R.; Antonietti, M.; Kuhn, P.; Thomas, A.; Schuth, F. Solid Catalysts for the Selective Low-Temperature Oxidation of Methane to Methanol. *Angew. Chem., Int. Ed.* **2009**, *48*, 6909−6912.
(185) Soorholtz, M.; Jones, L. C.; Samuelis, D.; Weidenthaler, C.; White, R. J.; Titirici, M.-M.; Cullen, D. A.; Zimmermann, T.; Antonietti, M.; Maier, J.; et al. Local Platinum Environments in a Solid Analogue of the Molecular Periana Catalyst. *ACS Catal.* **2016**, *6*, 2332−2340.

DOI: 10.1021/acs.chemrev.7b00776
Chem. Rev. 2018, 118, 4981−5079

(186) Nkosi, B.; Coville, N. J.; Hutchings, G. J. Vapour Phase Hydrochlorination of Acetylene with Group VIII and IB Metal Chloride Catalysts. *Appl. Catal.* **1988**, *43*, 33−39.
(187) Johnston, P.; Carthey, N.; Hutchings, G. J. Discovery, Development, and Commercialization of Gold Catalysts for Acetylene Hydrochlorination. *J. Am. Chem. Soc.* **2015**, *137*, 14548−14557.
(188) Malta, G.; Kondrat, S. A.; Freakley, S. J.; Davies, C. J.; Lu, L.; Dawson, S.; Thetford, A.; Gibson, E. K.; Morgan, D. J.; Jones, W.; et al. Identification of Single-Site Gold Catalysis in Acetylene Hydrochlorination. *Science* **2017**, *355*, 1399−1403.
(189) Kyriakou, G.; Boucher, M. B.; Jewell, A. D.; Lewis, E. A.; Lawton, T. J.; Baber, A. E.; Tierney, H. L.; Flytzani-Stephanopoulos, M.; Sykes, E. C. Isolated Metal Atom Geometries as a Strategy for Selective Heterogeneous Hydrogenations. *Science* **2012**, *335*, 1209−1212.
(190) Lucci, F. R.; Marcinkowski, M. D.; Lawton, T. J.; Sykes, E. C. H. H_2 Activation and Spillover on Catalytically Relevant Pt−Cu Single Atom Alloys. *J. Phys. Chem. C* **2015**, *119*, 24351−24357.
(191) Serna, P.; Concepción, P.; Corma, A. Design of Highly Active and Chemoselective Bimetallic Gold−Platinum Hydrogenation Catalysts Through Kinetic and Isotopic Studies. *J. Catal.* **2009**, *265*, 19−25.
(192) Boucher, M. B.; Zugic, B.; Cladaras, G.; Kammert, J.; Marcinkowski, M. D.; Lawton, T. J.; Sykes, E. C.; Flytzani-Stephanopoulos, M. Single Atom Alloy Surface Analogs in $Pd_{0.18}Cu_{15}$ Nanoparticles for Selective Hydrogenation Reactions. *Phys. Chem. Chem. Phys.* **2013**, *15*, 12187−12196.
(193) Lucci, F. R.; Liu, J.; Marcinkowski, M. D.; Yang, M.; Allard, L. F.; Flytzani-Stephanopoulos, M.; Sykes, E. C. Selective Hydrogenation of 1,3-Butadiene on Platinum-Copper Alloys at the Single-Atom Limit. *Nat. Commun.* **2015**, *6*, 8550.
(194) Pei, G. X.; Liu, X. Y.; Wang, A.; Lee, A. F.; Isaacs, M. A.; Li, L.; Pan, X.; Yang, X.; Wang, X.; Tai, Z.; et al. Ag Alloyed Pd Single-Atom Catalysts for Efficient Selective Hydrogenation of Acetylene to Ethylene in Excess Ethylene. *ACS Catal.* **2015**, *5*, 3717−3725.
(195) Zhang, H.; Watanabe, T.; Okumura, M.; Haruta, M.; Toshima, N. Catalytically Highly Active Top Gold Atom on Palladium Nanocluster. *Nat. Mater.* **2012**, *11*, 49−52.
(196) Miura, H.; Endo, K.; Ogawa, R.; Shishido, T. Supported Palladium−Gold Alloy Catalysts for Efficient and Selective Hydrosilylation under Mild Conditions with Isolated Single Palladium Atoms in Alloy Nanoparticles as the Main Active Site. *ACS Catal.* **2017**, *7*, 1543−1553.
(197) Zhang, L.; Wang, A.; Miller, J. T.; Liu, X.; Yang, X.; Wang, W.; Li, L.; Huang, Y.; Mou, C.-Y.; Zhang, T. Efficient and Durable Au Alloyed Pd Single-Atom Catalyst for the Ullmann Reaction of Aryl Chlorides in Water. *ACS Catal.* **2014**, *4*, 1546−1553.
(198) Xie, S.; Tsunoyama, H.; Kurashige, W.; Negishi, Y.; Tsukuda, T. Enhancement in Aerobic Alcohol Oxidation Catalysis of Au_{25} Clusters by Single Pd Atom Doping. *ACS Catal.* **2012**, *2*, 1519−1523.
(199) Zhang, S.; Nguyen, L.; Liang, J.-X.; Shan, J.; Liu, J.; Frenkel, A. I.; Patlolla, A.; Huang, W.; Li, J.; Tao, F. Catalysis on Singly Dispersed Bimetallic Sites. *Nat. Commun.* **2015**, *6*, 7938.
(200) Nguyen, L.; Zhang, S.; Wang, L.; Li, Y.; Yoshida, H.; Patlolla, A.; Takeda, S.; Frenkel, A. I.; Tao, F. Reduction of Nitric Oxide with Hydrogen on Catalysts of Singly Dispersed Bimetallic Sites Pt_1Co_m and Pd_1Co_n. *ACS Catal.* **2016**, *6*, 840−850.
(201) Jirkovsky, J. S.; Panas, I.; Ahlberg, E.; Halasa, M.; Romani, S.; Schiffrin, D. J. Single Atom Hot-Spots at Au-Pd Nanoalloys for Electrocatalytic H_2O_2 Production. *J. Am. Chem. Soc.* **2011**, *133*, 19432−19441.
(202) Lu, J.; Aydin, C.; Browning, N. D.; Gates, B. C. Hydrogen Activation and Metal Hydride Formation Trigger Cluster Formation from Supported Iridium Complexes. *J. Am. Chem. Soc.* **2012**, *134*, 5022−5025.
(203) Serna, P.; Gates, B. C. Zeolite-Supported Rhodium Complexes and Clusters: Switching Catalytic Selectivity by Controlling Structures of Essentially Molecular Species. *J. Am. Chem. Soc.* **2011**, *133*, 4714−4717.
(204) Bayram, E.; Lu, J.; Aydin, C.; Uzun, A.; Browning, N. D.; Gates, B. C.; Finke, R. G. Mononuclear Zeolite-Supported Iridium: Kinetic, Spectroscopic, Electron Microscopic, and Size-Selective Poisoning Evidence for an Atomically Dispersed True Catalyst at 22 °C. *ACS Catal.* **2012**, *2*, 1947−1957.
(205) Bayram, E.; Lu, J.; Aydin, C.; Browning, N. D.; Özkar, S.; Finney, E.; Gates, B. C.; Finke, R. G. Agglomerative Sintering of an Atomically Dispersed Ir_1/Zeolite Y Catalyst: Compelling Evidence Against Ostwald Ripening but for Bimolecular and Autocatalytic Agglomeration Catalyst Sintering Steps. *ACS Catal.* **2015**, *5*, 3514−3527.
(206) Han, Y.; Wang, Y.-G.; Chen, W.; Xu, R.; Zheng, L. R.; Zhang, J.; Luo, J.; Shen, R.-A.; Zhu, Y.; Cheong, W.-C.; et al. Hollow N-doped Carbon Spheres with Isolated Cobalt Single Atomic Sites: Superior Electrocatalysts for Oxygen Reduction. *J. Am. Chem. Soc.* **2017**, *139*, 17269−17272.
(207) Yin, P.; Yao, T.; Wu, Y.; Zheng, L.; Lin, Y.; Liu, W.; Ju, H.; Zhu, J.; Hong, X.; Deng, Z.; et al. Single Cobalt Atoms with Precise N-Coordination as Superior Oxygen Reduction Reaction Catalysts. *Angew. Chem., Int. Ed.* **2016**, *55*, 10800−10805.
(208) Cheng, Q.; Yang, L.; Zou, L.; Zou, Z.; Chen, C.; Hu, Z.; Yang, H. Single Cobalt Atom and N Codoped Carbon Nanofibers as Highly Durable Electrocatalyst for Oxygen Reduction Reaction. *ACS Catal.* **2017**, *7*, 6864−6871.
(209) Zheng, Y.; Jiao, Y.; Zhu, Y.; Cai, Q.; Vasileff, A.; Li, L. H.; Han, Y.; Chen, Y.; Qiao, S. Z. Molecule-Level g-C_3N_4 Coordinated Transition Metals as a New Class of Electrocatalysts for Oxygen Electrode Reactions. *J. Am. Chem. Soc.* **2017**, *139*, 3336−3339.
(210) Chen, Y.; Ji, S.; Wang, Y.; Dong, J.; Chen, W.; Li, Z.; Shen, R.; Zheng, L.; Zhuang, Z.; Wang, D.; et al. Isolated Single Iron Atoms Anchored on N-Doped Porous Carbon as an Efficient Electrocatalyst for the Oxygen Reduction Reaction. *Angew. Chem., Int. Ed.* **2017**, *56*, 6937−6941.
(211) Chung, H. T.; Cullen, D. A.; Higgins, D.; Sneed, B. T.; Holby, E. F.; More, K. L.; Zelenay, P. Direct Atomic-Level Insight Into the Active Sites of a High-Performance PGM-free ORR Catalyst. *Science* **2017**, *357*, 479−484.
(212) Zhu, C.; Fu, S.; Song, J.; Shi, Q.; Su, D.; Engelhard, M. H.; Li, X.; Xiao, D.; Li, D.; Estevez, L. Self-Assembled Fe-N-Doped Carbon Nanotube Aerogels with Single-Atom Catalyst Feature as High-Efficiency Oxygen Reduction Electrocatalysts. *Small* **2017**, *13* (15), 1603407.
(213) Zhang, Z.; Gao, X.; Dou, M.; Ji, J.; Wang, F. Biomass Derived N-Doped Porous Carbon Supported Single Fe Atoms as Superior Electrocatalysts for Oxygen Reduction. *Small* **2017**, *13* (22), 1604290.
(214) Sanchez, A.; Abbet, S.; Heiz, U.; Schneider, W. D.; Häkkinen, H.; Barnett, R. N.; Landman, U. When Gold Is Not Noble: Nanoscale Gold Catalysts. *J. Phys. Chem. A* **1999**, *103*, 9573−9578.
(215) Lee, S.; Fan, C.; Wu, T.; Anderson, S. L. CO Oxidation on Au_n/TiO_2 Catalysts Produced by Size-Selected Cluster Deposition. *J. Am. Chem. Soc.* **2004**, *126*, 5682−5683.
(216) Arenz, M.; Landman, U.; Heiz, U. CO Combustion on Supported Gold Clusters. *ChemPhysChem* **2006**, *7*, 1871−1879.
(217) Landman, U.; Yoon, B.; Zhang, C.; Heiz, U.; Arenz, M. Factors in Gold Nanocatalysis: Oxidation of CO in the Non-Scalable Size Regime. *Top. Catal.* **2007**, *44*, 145−158.
(218) Yoon, B.; Hakkinen, H.; Landman, U.; Worz, A. S.; Antonietti, J. M.; Abbet, S.; Judai, K.; Heiz, U. Charging Effects on Bonding and Catalyzed Oxidation of CO on Au_8 Clusters on MgO. *Science* **2005**, *307*, 403−407.
(219) Harding, C.; Habibpour, V.; Kunz, S.; Farnbacher, A. N.; Heiz, U.; Yoon, B.; Landman, U. Control and Manipulation of Gold Nanocatalysis: Effects of Metal Oxide Support Thickness and Composition. *J. Am. Chem. Soc.* **2009**, *131*, 538−548.
(220) Ohyama, J.; Esaki, A.; Koketsu, T.; Yamamoto, Y.; Arai, S.; Satsuma, A. Atomic-Scale Insight into the Structural Effect of a Supported Au Catalyst based on a Size-Distribution Analysis Using Cs-STEM and Morphological Image-Processing. *J. Catal.* **2016**, *335*, 24−35.
(221) Herzing, A. A.; Kiely, C. J.; Carley, A. F.; Landon, P.; Hutchings, G. J. Identification of Active Gold clusters on Iron Oxide Supports for CO Oxidation. *Science* **2008**, *321*, 1331−1335.

DOI: 10.1021/acs.chemrev.7b00776
Chem. Rev. 2018, 118, 4981−5079

(222) He, Q.; Freakley, S. J.; Edwards, J. K.; Carley, A. F.; Borisevich, A. Y.; Mineo, Y.; Haruta, M.; Hutchings, G. J.; Kiely, C. J. Population and Hierarchy of Active Species in Gold Iron Oxide Catalysts for Carbon Monoxide Oxidation. *Nat. Commun.* **2016**, *7*, 12905.
(223) Kaden, W. E.; Wu, T.; Kunkel, W. A.; Anderson, S. L. Electronic Structure Controls Reactivity of Size-Selected Pd Clusters Adsorbed on TiO_2 Surfaces. *Science* **2009**, *326*, 826−829.
(224) Kane, M. D.; Roberts, F. S.; Anderson, S. L. Effects of Alumina Thickness on CO Oxidation Activity over Pd_{20}/Alumina/Re(0001): Correlated Effects of Alumina Electronic Properties and Pd_{20} Geometry on Activity. *J. Phys. Chem. C* **2015**, *119*, 1359−1375.
(225) Kunz, S.; Schweinberger, F. F.; Habibpour, V.; Röttgen, M.; Harding, C.; Arenz, M.; Heiz, U. Temperature Dependent CO Oxidation Mechanisms on Size-Selected Clusters. *J. Phys. Chem. C* **2010**, *114*, 1651−1654.
(226) Yoon, B.; Landman, U.; Habibpour, V.; Harding, C.; Kunz, S.; Heiz, U.; Moseler, M.; Walter, M. Oxidation of Magnesia-Supported Pd_{30} Clusters and Catalyzed CO Combustion: Size-Selected Experiments and First-Principles Theory. *J. Phys. Chem. C* **2012**, *116*, 9594−9607.
(227) Moseler, M.; Walter, M.; Yoon, B.; Landman, U.; Habibpour, V.; Harding, C.; Kunz, S.; Heiz, U. Oxidation State and Symmetry of Magnesia-Supported $Pd_{13}O_x$ Nanocatalysts Influence Activation Barriers of CO Oxidation. *J. Am. Chem. Soc.* **2012**, *134*, 7690−7699.
(228) Jeong, H.; Bae, J.; Han, J. W.; Lee, H. Promoting Effects of Hydrothermal Treatment on the Activity and Durability of Pd/CeO_2 Catalysts for CO Oxidation. *ACS Catal.* **2017**, *7*, 7097−7105.
(229) Heiz, U.; Sanchez, A.; Abbet, S.; Schneider, W. D. Catalytic Oxidation of Carbon Monoxide on Monodispersed Platinum Clusters: Each Atom Counts. *J. Am. Chem. Soc.* **1999**, *121*, 3214−3217.
(230) Bonanni, S.; Ait-Mansour, K.; Harbich, W.; Brune, H. Reaction-Induced Cluster Ripening and Initial Size-Dependent Reaction Rates for CO Oxidation on $Pt_n/TiO_2(110)$-(1 × 1). *J. Am. Chem. Soc.* **2014**, *136*, 8702−8707.
(231) Watanabe, Y.; Wu, X.; Hirata, H.; Isomura, N. Size-Dependent Catalytic Activity and Geometries of Size-Selected Pt Clusters on TiO_2(110) Surfaces. *Catal. Sci. Technol.* **2011**, *1*, 1490.
(232) Yin, C.; Negreiros, F. R.; Barcaro, G.; Beniya, A.; Sementa, L.; Tyo, E. C.; Bartling, S.; Meiwes-Broer, K.-H.; Seifert, S.; Hirata, H.; et al. Alumina-Supported Sub-Nanometer Pt_{10} Clusters: Amorphization and Role of the Support Material in a Highly Active CO Oxidation Catalyst. *J. Mater. Chem. A* **2017**, *5*, 4923−4931.
(233) Jiang, D.-e.; Overbury, S. H.; Dai, S. Structures and Energetics of Pt Clusters on TiO_2: Interplay Between Metal−Metal Bonds and Metal−Oxygen Bonds. *J. Phys. Chem. C* **2012**, *116*, 21880−21885.
(234) Gerber, T.; Knudsen, J.; Feibelman, P. J.; Granas, E.; Stratmann, P.; Schulte, K.; Andersen, J. N.; Michely, T. CO-Induced Smoluchowski Ripening of Pt Cluster Arrays on the Graphene/Ir(111) moire. *ACS Nano* **2013**, *7*, 2020−2031.
(235) Chaâbane, N.; Lazzari, R.; Jupille, J.; Renaud, G.; Avellar Soares, E. CO-Induced Scavenging of Supported Pt Clusters: A GISAXS Study. *J. Phys. Chem. C* **2012**, *116*, 23362−23370.
(236) Bonanni, S.; Ait-Mansour, K.; Harbich, W.; Brune, H. Effect of the TiO_2 Reduction State on the Catalytic CO Oxidation on Deposited Size-Selected Pt Clusters. *J. Am. Chem. Soc.* **2012**, *134*, 3445−3450.
(237) Qiao, B.; Wang, A.; Li, L.; Lin, Q.; Wei, H.; Liu, J.; Zhang, T. Ferric Oxide-Supported Pt Subnano Clusters for Preferential Oxidation of CO in H_2-Rich Gas at Room Temperature. *ACS Catal.* **2014**, *4*, 2113−2117.
(238) Guan, H.; Lin, J.; Qiao, B.; Yang, X.; Li, L.; Miao, S.; Liu, J.; Wang, A.; Wang, X.; Zhang, T. Catalytically Active Rh Sub-Clusters on TiO_2 for CO Oxidation at Cryogenic Temperatures. *Angew. Chem., Int. Ed.* **2016**, *55*, 2820−2824.
(239) Ke, J.; Zhu, W.; Jiang, Y.; Si, R.; Wang, Y.-J.; Li, S.-C.; Jin, C.; Liu, H.; Song, W.-G.; Yan, C.-H.; et al. Strong Local Coordination Structure Effects on Subnanometer PtOx Clusters over CeO_2 Nanowires Probed by Low-Temperature CO Oxidation. *ACS Catal.* **2015**, *5*, 5164−5173.
(240) Sirajuddin, S.; Rosenzweig, A. C. Enzymatic Oxidation of Methane. *Biochemistry* **2015**, *54*, 2283−2294.
(241) Himes, R. A.; Barnese, K.; Karlin, K. D. One is Lonely and Three is a Crowd: Two Coppers Are for Methane Oxidation. *Angew. Chem., Int. Ed.* **2010**, *49*, 6714−6716.
(242) Tomkins, P.; Ranocchiari, M.; van Bokhoven, J. A. Direct Conversion of Methane to Methanol under Mild Conditions over Cu-Zeolites and beyond. *Acc. Chem. Res.* **2017**, *50*, 418−425.
(243) Woertink, J. S.; Smeets, P. J.; Groothaert, M. H.; Vance, M. A.; Sels, B. F.; Schoonheydt, R. A.; Solomon, E. I. A $[Cu_2O]^{2+}$ Core in Cu-ZSM-5, the Active Site in the Oxidation of Methane to Methanol. *Proc. Natl. Acad. Sci. U. S. A.* **2009**, *106*, 18908−18913.
(244) Grundner, S.; Markovits, M. A.; Li, G.; Tromp, M.; Pidko, E. A.; Hensen, E. J.; Jentys, A.; Sanchez-Sanchez, M.; Lercher, J. A. Single-Site Trinuclear Copper Oxygen Clusters in Mordenite for Selective Conversion of Methane to Methanol. *Nat. Commun.* **2015**, *6*, 7546.
(245) Haack, P.; Limberg, C. Molecular Cu^{II}-O-Cu^{II} Complexes: Still Waters Run Deep. *Angew. Chem., Int. Ed.* **2014**, *53*, 4282−4293.
(246) Tomkins, P.; Mansouri, A.; Bozbag, S. E.; Krumeich, F.; Park, M. B.; Alayon, E. M.; Ranocchiari, M.; van Bokhoven, J. A. Isothermal Cyclic Conversion of Methane into Methanol over Copper-Exchanged Zeolite at Low Temperature. *Angew. Chem., Int. Ed.* **2016**, *55*, 5467−5471.
(247) Narsimhan, K.; Iyoki, K.; Dinh, K.; Roman-Leshkov, Y. Catalytic Oxidation of Methane into Methanol over Copper-Exchanged Zeolites with Oxygen at Low Temperature. *ACS Cent. Sci.* **2016**, *2*, 424−429.
(248) Alayon, E. M. C.; Nachtegaal, M.; Bodi, A.; van Bokhoven, J. A. Reaction Conditions of Methane-to-Methanol Conversion Affect the Structure of Active Copper Sites. *ACS Catal.* **2014**, *4*, 16−22.
(249) Sushkevich, V. L.; Palagin, D.; Ranocchiari, M.; van Bokhoven, J. A. Selective Anaerobic Oxidation of Methane Enables Direct Synthesis of Methanol. *Science* **2017**, *356*, 523−527.
(250) Bal, R.; Tada, M.; Sasaki, T.; Iwasawa, Y. Direct Phenol Synthesis by Selective Oxidation of Benzene with Molecular Oxygen on an Interstitial-N/Re Cluster/Zeolite Catalyst. *Angew. Chem., Int. Ed.* **2006**, *45*, 448−452.
(251) Tada, M.; Bal, R.; Sasaki, T.; Uemura, Y.; Inada, Y.; Tanaka, S.; Nomura, M.; Iwasawa, Y. Novel Re-Cluster/HZSM-5 Catalyst for Highly Selective Phenol Synthesis from Benzene and O_2: Performance and Reaction Mechanism. *J. Phys. Chem. C* **2007**, *111*, 10095−10104.
(252) Zhang, F.; Jiao, F.; Pan, X.; Gao, K.; Xiao, J.; Zhang, S.; Bao, X. Tailoring the Oxidation Activity of Pt Clusters via Encapsulation. *ACS Catal.* **2015**, *5*, 1381−1385.
(253) Hayashi, T.; Tanaka, K.; Haruta, M. Selective Vapor-Phase Epoxidation of Propene over Au/TiO_2 Catalysts in the Presence of Oxygen and Hydrogen. *J. Catal.* **1998**, *178*, 566−575.
(254) Lee, S.; Molina, L. M.; Lopez, M. J.; Alonso, J. A.; Hammer, B.; Lee, B.; Seifert, S.; Winans, R. E.; Elam, J. W.; Pellin, M. J.; et al. Selective Propene Epoxidation on Immobilized Au_{6-10} Clusters: the Effect of Hydrogen and Water on Activity and Selectivity. *Angew. Chem., Int. Ed.* **2009**, *48*, 1467−1471.
(255) Huang, J.; Akita, T.; Faye, J.; Fujitani, T.; Takei, T.; Haruta, M. Propene Epoxidation with Dioxygen Catalyzed by Gold Clusters. *Angew. Chem., Int. Ed.* **2009**, *48*, 7862−7866.
(256) Lei, Y.; Mehmood, F.; Lee, S.; Greeley, J.; Lee, B.; Seifert, S.; Winans, R. E.; Elam, J. W.; Meyer, R. J.; Redfern, P. C.; et al. Increased Silver Activity for Direct Propene Epoxidation via Subnanometer Size Effects. *Science* **2010**, *328*, 224−228.
(257) Li, G.; Jin, R. Atomically Precise Gold Clusters as New Model Catalysts. *Acc. Chem. Res.* **2013**, *46*, 1749−1758.
(258) Zhu, Y.; Qian, H.; Zhu, M.; Jin, R. Thiolate-Protected Au_n Clusters as Catalysts for Selective Oxidation and Hydrogenation Processes. *Adv. Mater.* **2010**, *22*, 1915−1920.
(259) Qian, H.; Jiang, D. E.; Li, G.; Gayathri, C.; Das, A.; Gil, R. R.; Jin, R. Monoplatinum Doping of Gold Clusters and Catalytic Application. *J. Am. Chem. Soc.* **2012**, *134*, 16159−16162.
(260) Xie, S.; Tsunoyama, H.; Kurashige, W.; Negishi, Y.; Tsukuda, T. Enhancement in Aerobic Alcohol Oxidation Catalysis of Au_{25} Clusters by Single Pd Atom Doping. *ACS Catal.* **2012**, *2*, 1519−1523.

DOI: 10.1021/acs.chemrev.7b00776
Chem. Rev. 2018, 118, 4981−5079

(261) Dreier, T. A.; Wong, O. A.; Ackerson, C. J. Oxidative Decomposition of $Au_{25}(SR)_{18}$ Clusters in a Catalytic Context. *Chem. Commun.* **2015**, *51*, 1240−1243.
(262) Crampton, A. S.; Rotzer, M. D.; Ridge, C. J.; Schweinberger, F. F.; Heiz, U.; Yoon, B.; Landman, U. Structure Sensitivity in the Nonscalable Regime Explored via Catalysed Ethylene Hydrogenation on Supported Platinum Clusters. *Nat. Commun.* **2016**, *7*, 10389.
(263) Bond, G. C. Supported Metal Catalysts: Some Unsolved Problems. *Chem. Soc. Rev.* **1991**, *20*, 441−475.
(264) Godbey, D.; Zaera, F.; Yeates, R.; Somorjai, G. A. Hydrogenation of Chemisorbed Ethylene on Clean, Hydrogen, and Ethylidyne Covered Platinum(111) Crystal Surfaces. *Surf. Sci.* **1986**, *167*, 150−166.
(265) Crampton, A. S.; Rötzer, M. D.; Ridge, C. J.; Yoon, B.; Schweinberger, F. F.; Landman, U.; Heiz, U. Assessing the Concept of Structure Sensitivity or Insensitivity for Sub-Nanometer Catalyst Materials. *Surf. Sci.* **2016**, *652*, 7−19.
(266) Crampton, A. S.; Rotzer, M. D.; Schweinberger, F. F.; Yoon, B.; Landman, U.; Heiz, U. Controlling Ethylene Hydrogenation Reactivity on Pt_{13} Clusters by Varying the Stoichiometry of the Amorphous Silica Support. *Angew. Chem., Int. Ed.* **2016**, *55*, 8953−8957.
(267) Takahashi, M.; Imaoka, T.; Hongo, Y.; Yamamoto, K. Formation of a Pt_{12} Cluster by Single-Atom Control that Leads to Enhanced Reactivity: Hydrogenation of Unreactive Olefins. *Angew. Chem., Int. Ed.* **2013**, *52*, 7419−7421.
(268) Takahashi, M.; Imaoka, T.; Hongo, Y.; Yamamoto, K. A Highly-Active and Poison-Tolerant Pt12 Sub-Nanocluster Catalyst for the Reductive Amination of Aldehydes with Amines. *Dalton Trans.* **2013**, *42*, 15919−15921.
(269) Maeno, Z.; Kibata, T.; Mitsudome, T.; Mizugaki, T.; Jitsukawa, K.; Kaneda, K. Subnanoscale Size Effect of Dendrimer-encapsulated Pd Clusters on Catalytic Hydrogenation of Olefin. *Chem. Lett.* **2011**, *40*, 180−181.
(270) Nakamula, I.; Yamanoi, Y.; Imaoka, T.; Yamamoto, K.; Nishihara, H. A Uniform Bimetallic Rhodium/Iron Nanoparticle Catalyst for the Hydrogenation of Olefins and Nitroarenes. *Angew. Chem., Int. Ed.* **2011**, *50*, 5830−5833.
(271) Nakamula, I.; Yamanoi, Y.; Yonezawa, T.; Imaoka, T.; Yamamoto, K.; Nishihara, H. Nanocage Catalysts-Rhodium Clusters Encapsulated with Dendrimers as Accessible and Stable Catalysts for Olefin and Nitroarene Hydrogenations. *Chem. Commun.* **2008**, *44*, 5716−5718.
(272) Zhu, Y.; Qian, H.; Drake, B. A.; Jin, R. Atomically Precise $Au_{25}(SR)_{18}$ Nanoparticles as Catalysts for the Selective Hydrogenation of α,β-Unsaturated Ketones and Aldehydes. *Angew. Chem., Int. Ed.* **2010**, *49*, 1295−1298.
(273) Li, G.; Jiang, D.-e.; Kumar, S.; Chen, Y.; Jin, R. Size Dependence of Atomically Precise Gold Clusters in Chemoselective Hydrogenation and Active Site Structure. *ACS Catal.* **2014**, *4*, 2463−2469.
(274) Li, G.; Jin, R. Gold Nanocluster-Catalyzed Semihydrogenation: a Unique Activation Pathway for Terminal Alkynes. *J. Am. Chem. Soc.* **2014**, *136*, 11347−11354.
(275) Wan, X.-K.; Wang, J.-Q.; Nan, Z.-A.; Wang, Q.-M. Ligand Effects in Catalysis by Atomically Precise Gold Clusters. *Sci. Adv.* **2017**, *3*, e1701823.
(276) Maity, P.; Yamazoe, S.; Tsukuda, T. Dendrimer-Encapsulated Copper Cluster as a Chemoselective and Regenerable Hydrogenation Catalyst. *ACS Catal.* **2013**, *3*, 182−185.
(277) Fernández, E.; Boronat, M.; Corma, A. Trends in the Reactivity of Molecular O_2 with Copper Clusters: Influence of Size and Shape. *J. Phys. Chem. C* **2015**, *119*, 19832−19846.
(278) Argo, A. M.; Odzak, J. F.; Lai, F. S.; Gates, B. C. Observation of Ligand Effects During Alkene Hydrogenation Catalysed by Supported Metal Clusters. *Nature* **2002**, *415*, 623−626.
(279) Lu, J.; Serna, P.; Aydin, C.; Browning, N. D.; Gates, B. C. Supported Molecular Iridium Catalysts: Resolving Effects of Metal Nuclearity and Supports as Ligands. *J. Am. Chem. Soc.* **2011**, *133*, 16186−16195.
(280) Okrut, A.; Runnebaum, R. C.; Ouyang, X.; Lu, J.; Aydin, C.; Hwang, S. J.; Zhang, S.; Olatunji-Ojo, O. A.; Durkin, K. A.; Dixon, D. A.; et al. Selective Molecular Recognition by Nanoscale Environments in a Supported Iridium Cluster Catalyst. *Nat. Nanotechnol.* **2014**, *9*, 459−465.
(281) Corma, A. Cluster Catalysis: a Subtle Form of Recognition. *Nat. Nanotechnol.* **2014**, *9*, 412−413.
(282) Liu, L.; Díaz, U.; Arenal, R.; Agostini, G.; Concepción, P.; Corma, A. Generation of Subnanometric Platinum with High Stability During Transformation of a 2D Zeolite into 3D. *Nat. Mater.* **2017**, *16*, 132−138.
(283) Thomas, J. M.; Johnson, B. F.; Raja, R.; Sankar, G.; Midgley, P. A. High-Performance Nanocatalysts for Single-Step Hydrogenations. *Acc. Chem. Res.* **2003**, *36*, 20−30.
(284) Hungria, A. B.; Raja, R.; Adams, R. D.; Captain, B.; Thomas, J. M.; Midgley, P. A.; Golovko, V.; Johnson, B. F. Single-Step Conversion of Dimethyl Terephthalate into Cyclohexanedimethanol with Ru_5PtSn, a Trimetallic Nanoparticle Catalyst. *Angew. Chem., Int. Ed.* **2006**, *45*, 4782−4785.
(285) Raja, R.; Khimyak, T.; Thomas, J. M.; Hermans, S.; Johnson, B. F. G. Single-Step, Highly Active, and Highly Selective Nanoparticle Catalysts for the Hydrogenation of Key Organic Compounds. *Angew. Chem., Int. Ed.* **2001**, *40*, 4638−4642.
(286) Olah, G. A. Beyond Oil and Gas: the Methanol Economy. *Angew. Chem., Int. Ed.* **2005**, *44*, 2636−2639.
(287) Jadhav, S. G.; Vaidya, P. D.; Bhanage, B. M.; Joshi, J. B. Catalytic Carbon Dioxide Hydrogenation to Methanol: A Review of Recent Studies. *Chem. Eng. Res. Des.* **2014**, *92*, 2557−2567.
(288) Studt, F.; Sharafutdinov, I.; Abild-Pedersen, F.; Elkjaer, C. F.; Hummelshoj, J. S.; Dahl, S.; Chorkendorff, I.; Norskov, J. K. Discovery of a Ni-Ga Catalyst for Carbon Dioxide Reduction to Methanol. *Nat. Chem.* **2014**, *6*, 320−324.
(289) Liu, C.; Yang, B.; Tyo, E.; Seifert, S.; DeBartolo, J.; von Issendorff, B.; Zapol, P.; Vajda, S.; Curtiss, L. A. Carbon Dioxide Conversion to Methanol over Size-Selected Cu_4 Clusters at Low Pressures. *J. Am. Chem. Soc.* **2015**, *137*, 8676−8679.
(290) Iglesia, E.; Reyes, S. C.; Madon, R. J.; Soled, S. L. Selectivity Control and Catalyst Design in the Fischer−Tropsch Synthesis: Sites, Pellets, and Reactors. *Adv. Catal.* **1993**, *39*, 221−302.
(291) Lee, S.; Lee, B.; Seifert, S.; Winans, R. E.; Vajda, S. Fischer−Tropsch Synthesis at a Low Pressure on Subnanometer Cobalt Oxide Clusters: The Effect of Cluster Size and Support on Activity and Selectivity. *J. Phys. Chem. C* **2015**, *119*, 11210−11216.
(292) Yang, Q.; Fu, X.-P.; Jia, C.-J.; Ma, C.; Wang, X.; Zeng, J.; Si, R.; Zhang, Y.-W.; Yan, C.-H. Structural Determination of Catalytically Active Subnanometer Iron Oxide Clusters. *ACS Catal.* **2016**, *6*, 3072−3082.
(293) Chirik, P. J. Iron- and Cobalt-Catalyzed Alkene Hydrogenation: Catalysis with Both Redox-Active and Strong Field Ligands. *Acc. Chem. Res.* **2015**, *48*, 1687−1695.
(294) Hoyt, J. M.; Shevlin, M.; Margulieux, G. W.; Krska, S. W.; Tudge, M. T.; Chirik, P. J. Synthesis and Hydrogenation Activity of Iron Dialkyl Complexes with Chiral Bidentate Phosphines. *Organometallics* **2014**, *33*, 5781−5790.
(295) Gieshoff, T. N.; Chakraborty, U.; Villa, M.; Jacobi von Wangelin, A. Alkene Hydrogenations by Soluble Iron Nanocluster Catalysts. *Angew. Chem., Int. Ed.* **2017**, *56*, 3585−3589.
(296) Zhang, G.; Scott, B. L.; Hanson, S. K. Mild and Homogeneous Cobalt-Catalyzed Hydrogenation of C = C, C = O, and C = N Bonds. *Angew. Chem., Int. Ed.* **2012**, *51*, 12102−12106.
(297) Chakraborty, S.; Bhattacharya, P.; Dai, H.; Guan, H. Nickel and Iron Pincer Complexes as Catalysts for the Reduction of Carbonyl Compounds. *Acc. Chem. Res.* **2015**, *48*, 1995−2003.
(298) Elangovan, S.; Topf, C.; Fischer, S.; Jiao, H.; Spannenberg, A.; Baumann, W.; Ludwig, R.; Junge, K.; Beller, M. Selective Catalytic Hydrogenations of Nitriles, Ketones, and Aldehydes by Well-Defined Manganese Pincer Complexes. *J. Am. Chem. Soc.* **2016**, *138*, 8809−8814.
(299) Sattler, J. J.; Ruiz-Martinez, J.; Santillan-Jimenez, E.; Weckhuysen, B. M. Catalytic Dehydrogenation of Light Alkanes on Metals and Metal oxides. *Chem. Rev.* **2014**, *114*, 10613−10653.

DOI: 10.1021/acs.chemrev.7b00776
Chem. Rev. 2018, 118, 4981−5079

(300) Vajda, S.; Pellin, M. J.; Greeley, J. P.; Marshall, C. L.; Curtiss, L. A.; Ballentine, G. A.; Elam, J. W.; Catillon-Mucherie, S.; Redfern, P. C.; Mehmood, F.; et al. Subnanometre Platinum Clusters as Highly Active and Selective Catalysts for the Oxidative Dehydrogenation of Propane. *Nat. Mater.* **2009**, *8*, 213−216.
(301) Baxter, E. T.; Ha, M.-A.; Cass, A. C.; Alexandrova, A. N.; Anderson, S. L. Ethylene Dehydrogenation on $Pt_{4,7,8}$ Clusters on Al_2O_3: Strong Cluster Size Dependence Linked to Preferred Catalyst Morphologies. *ACS Catal.* **2017**, *7*, 3322−3335.
(302) Lee, S.; Di Vece, M.; Lee, B.; Seifert, S.; Winans, R. E.; Vajda, S. Oxidative Dehydrogenation of Cyclohexene on Size Selected Subnanometer Cobalt Clusters: Improved Catalytic Performance via Evolution of Cluster-Assembled Nanostructures. *Phys. Chem. Chem. Phys.* **2012**, *14*, 9336−9342.
(303) Lee, S.; Di Vece, M.; Lee, B.; Seifert, S.; Winans, R. E.; Vajda, S. Support-Dependent Performance of Size-selected Subnanometer Cobalt Cluster-based Catalysts in the Dehydrogenation of Cyclohexene. *ChemCatChem* **2012**, *4*, 1632−1637.
(304) Judai, K.; Abbet, S.; Worz, A. S.; Heiz, U.; Henry, C. R. Low-Temperature Cluster Catalysis. *J. Am. Chem. Soc.* **2004**, *126*, 2732−2737.
(305) Worz, A. S.; Judai, K.; Abbet, S.; Heiz, U. Cluster Size-Dependent Mechanisms of the CO+NO Reaction on Small Pdn (n≤ 30) Clusters on Oxide Surfaces. *J. Am. Chem. Soc.* **2003**, *125*, 7964−7970.
(306) Ahmed, F.; Nagumo, R.; Miura, R.; Suzuki, A.; Tsuboi, H.; Hatakeyama, N.; Takaba, H.; Miyamoto, A. CO Oxidation and NO Reduction on a MgO(100) Supported Pd Cluster: A Quantum Chemical Molecular Dynamics Study. *J. Phys. Chem. C* **2011**, *115*, 24123−24132.
(307) Liu, X.; Tian, D.; Ren, S.; Meng, C. Structure Sensitivity of NO Adsorption−Dissociation on Pdn (n = 8, 13, 19, 25) Clusters. *J. Phys. Chem. C* **2015**, *119*, 12941−12948.
(308) Shimizu, K.-i.; Satsuma, A.; Hattori, T. Catalytic Performance of Ag-Al_2O_3 Catalyst for the Selective Catalytic Reduction of NO by Higher Hydrocarbons. *Appl. Catal., B* **2000**, *25*, 239−247.
(309) Shibata, J. Ag Cluster as Active Species for SCR of NO by Propane in the Presence of Hydrogen over Ag-MFI. *J. Catal.* **2004**, *222*, 368−376.
(310) Satsuma, A.; Shibata, J.; Shimizu, K.-i.; Hattori, T. Ag Clusters as Active Species for HC-SCR Over Ag-Zeolites. *Catal. Surv. Asia* **2005**, *9*, 75−85.
(311) Murdoch, M.; Waterhouse, G. I.; Nadeem, M. A.; Metson, J. B.; Keane, M. A.; Howe, R. F.; Llorca, J.; Idriss, H. The Effect of Gold Loading and Particle Size on Photocatalytic Hydrogen Production from Ethanol over Au/TiO_2 Nanoparticles. *Nat. Chem.* **2011**, *3*, 489−492.
(312) Wang, W. N.; An, W. J.; Ramalingam, B.; Mukherjee, S.; Niedzwiedzki, D. M.; Gangopadhyay, S.; Biswas, P. Size and Structure Matter: Enhanced CO_2 Photoreduction Efficiency by Size-Resolved Ultrafine Pt Nanoparticles on TiO_2 Single Crystals. *J. Am. Chem. Soc.* **2012**, *134*, 11276−11281.
(313) Berr, M. J.; Schweinberger, F. F.; Doblinger, M.; Sanwald, K. E.; Wolff, C.; Breimeier, J.; Crampton, A. S.; Ridge, C. J.; Tschurl, M.; Heiz, U.; et al. Size-Selected Subnanometer Cluster Catalysts on Semiconductor Nanocrystal Films for Atomic Scale Insight into Photocatalysis. *Nano Lett.* **2012**, *12*, 5903−5906.
(314) Schweinberger, F. F.; Berr, M. J.; Doblinger, M.; Wolff, C.; Sanwald, K. E.; Crampton, A. S.; Ridge, C. J.; Jackel, F.; Feldmann, J.; Tschurl, M.; et al. Cluster Size Effects in the Photocatalytic Hydrogen Evolution Reaction. *J. Am. Chem. Soc.* **2013**, *135*, 13262−13265.
(315) Negishi, Y.; Matsuura, Y.; Tomizawa, R.; Kurashige, W.; Niihori, Y.; Takayama, T.; Iwase, A.; Kudo, A. Controlled Loading of Small Au_n Clusters (n = 10−39) onto $BaLa_4Ti_4O_{15}$ Photocatalysts: Toward an Understanding of Size Effect of Cocatalyst on Water-Splitting Photocatalytic Activity. *J. Phys. Chem. C* **2015**, *119*, 11224−11232.
(316) Li, Y. H.; Xing, J.; Chen, Z. J.; Li, Z.; Tian, F.; Zheng, L. R.; Wang, H. F.; Hu, P.; Zhao, H. J.; Yang, H. G. Unidirectional Suppression of Hydrogen Oxidation on Oxidized Platinum Clusters. *Nat. Commun.* **2013**, *4*, 2500.
(317) Xing, J.; Li, Y. H.; Jiang, H. B.; Wang, Y.; Yang, H. G. The Size and Valence State Effect of Pt on Photocatalytic H_2 Evolution over Platinized TiO_2 Photocatalyst. *Int. J. Hydrogen Energy* **2014**, *39*, 1237−1242.
(318) Li, Z.; Liu, C.; Abroshan, H.; Kauffman, D. R.; Li, G. $Au_{38}S_2(SAdm)_{20}$ Photocatalyst for One-Step Selective Aerobic Oxidations. *ACS Catal.* **2017**, *7*, 3368−3374.
(319) von Weber, A.; Anderson, S. L. Electrocatalysis by Mass-Selected Pt_n Clusters. *Acc. Chem. Res.* **2016**, *49*, 2632−2639.
(320) von Weber, A.; Baxter, E. T.; Proch, S.; Kane, M. D.; Rosenfelder, M.; White, H. S.; Anderson, S. L. Size-Dependent Electronic Structure Controls Activity for Ethanol Electro-Oxidation at Pt_n/Indium Tin Oxide (n = 1 to 14). *Phys. Chem. Chem. Phys.* **2015**, *17*, 17601−17610.
(321) Proch, S.; Wirth, M.; White, H. S.; Anderson, S. L. Strong Effects of Cluster Size and Air Exposure on Oxygen Reduction and Carbon Oxidation Electrocatalysis by Size-Selected Pt_n ($n \leq 11$) on Glassy Carbon Electrodes. *J. Am. Chem. Soc.* **2013**, *135*, 3073−3086.
(322) von Weber, A.; Baxter, E. T.; White, H. S.; Anderson, S. L. Cluster Size Controls Branching between Water and Hydrogen Peroxide Production in Electrochemical Oxygen Reduction at Pt_n/ITO. *J. Phys. Chem. C* **2015**, *119*, 11160−11170.
(323) Nesselberger, M.; Roefzaad, M.; Hamou, R. F.; Biedermann, P. U.; Schweinberger, F. F.; Kunz, S.; Schloegl, K.; Wiberg, G. K.; Ashton, S.; Heiz, U.; et al. The Effect of Particle Proximity on the Oxygen Reduction Rate of Size-Selected Platinum Clusters. *Nat. Mater.* **2013**, *12*, 919−924.
(324) Kwon, G.; Ferguson, G. A.; Heard, C. J.; Tyo, E. C.; Yin, C.; DeBartolo, J.; Seifert, S.; Winans, R. E.; Kropf, A. J.; Greeley, J.; et al. Size-Dependent Subnanometer Pd Cluster (Pd_4, Pd_6, and Pd_{17}) Water Oxidation Electrocatalysis. *ACS Nano* **2013**, *7*, 5808−5817.
(325) Yamamoto, K.; Imaoka, T.; Chun, W. J.; Enoki, O.; Katoh, H.; Takenaga, M.; Sonoi, A. Size-Specific Catalytic Activity of Platinum Clusters Enhances Oxygen Reduction Reactions. *Nat. Chem.* **2009**, *1*, 397−402.
(326) Imaoka, T.; Kitazawa, H.; Chun, W. J.; Yamamoto, K. Finding the Most Catalytically Active Platinum Clusters With Low Atomicity. *Angew. Chem., Int. Ed.* **2015**, *54*, 9810−9815.
(327) Imaoka, T.; Kitazawa, H.; Chun, W. J.; Omura, S.; Albrecht, K.; Yamamoto, K. Magic Number Pt_{13} and Misshapen Pt_{12} Clusters: Which One is the Better Catalyst? *J. Am. Chem. Soc.* **2013**, *135*, 13089−13095.
(328) Yang, X.; Gan, L.; Zhu, C.; Lou, B.; Han, L.; Wang, J.; Wang, E. A Dramatic Platform for Oxygen Reduction Reaction based on Silver Clusters. *Chem. Commun.* **2014**, *50*, 234−236.
(329) Antonello, S.; Hesari, M.; Polo, F.; Maran, F. Electron Transfer Catalysis with Monolayer Protected Au_{25} Clusters. *Nanoscale* **2012**, *4*, 5333−5342.
(330) Chen, W.; Chen, S. Oxygen Electroreduction Catalyzed by gold Clusters: Strong Core Size Effects. *Angew. Chem., Int. Ed.* **2009**, *48*, 4386−4389.
(331) Lu, Y.; Jiang, Y.; Gao, X.; Chen, W. Charge State-Dependent Catalytic Activity of $[Au_{25}(SC_{12}H_{25})_{18}]$ Clusters for the Two-Electron Reduction of Dioxygen to Hydrogen Peroxide. *Chem. Commun.* **2014**, *50*, 8464−8467.
(332) Kauffman, D. R.; Alfonso, D.; Matranga, C.; Ohodnicki, P.; Deng, X.; Siva, R. C.; Zeng, C.; Jin, R. Probing Active Site Chemistry with Differently Charged Au_{25}^q Clusters (q = − 1, 0, + 1). *Chem. Sci.* **2014**, *5*, 3151.
(333) Pellin, M. J.; Riha, S. C.; Tyo, E. C.; Kwon, G.; Libera, J. A.; Elam, J. W.; Seifert, S.; Lee, S.; Vajda, S. Water Oxidation by Size-Selected Co_{27} Clusters Supported on Fe_2O_3. *ChemSusChem* **2016**, *9*, 3005−3011.
(334) Yin, L.; Liebscher, J. Carbon-Carbon Coupling Reactions Catalyzed by Heterogeneous Palladium Catalysts. *Chem. Rev.* **2007**, *107*, 133−173.
(335) Molnar, A. Efficient, Selective, and Recyclable Palladium Catalysts in Carbon-Carbon Coupling Reactions. *Chem. Rev.* **2011**, *111*, 2251−2320.
(336) Fihri, A.; Bouhrara, M.; Nekoueishahraki, B.; Basset, J. M.; Polshettiwar, V. Nanocatalysts for Suzuki Cross-Coupling Reactions. *Chem. Soc. Rev.* **2011**, *40*, 5181−5203.

DOI: 10.1021/acs.chemrev.7b00776
Chem. Rev. 2018, 118, 4981−5079

(337) Fang, P. P.; Jutand, A.; Tian, Z. Q.; Amatore, C. Au-Pd Core-Shell Nanoparticles Catalyze Suzuki-Miyaura Reactions in Water Through Pd Leaching. *Angew. Chem., Int. Ed.* **2011**, *50*, 12184−12188.
(338) Niu, Z.; Peng, Q.; Zhuang, Z.; He, W.; Li, Y. Evidence of an Oxidative-Addition-Promoted Pd-Leaching Mechanism in the Suzuki Reaction by Using a Pd-Nanostructure Design. *Chem. - Eur. J.* **2012**, *18*, 9813−9817.
(339) Phan, N. T. S.; Van Der Sluys, M.; Jones, C. W. On the Nature of the Active Species in Palladium Catalyzed Mizoroki−Heck and Suzuki−Miyaura Couplings-Homogeneous or Heterogeneous Catalysis, A Critical Review. *Adv. Synth. Catal.* **2006**, *348*, 609−679.
(340) Briggs, B. D.; Bedford, N. M.; Seifert, S.; Koerner, H.; Ramezani-Dakhel, H.; Heinz, H.; Naik, R. R.; Frenkel, A. I.; Knecht, M. R. Atomic-Scale Identification of Pd Leaching in Nanoparticle Catalyzed C−C Coupling: Effects of Particle Surface Disorder. *Chem. Sci.* **2015**, *6*, 6413−6419.
(341) Thathagar, M. B.; ten Elshof, J. E.; Rothenberg, G. Pd Clusters in C-C Coupling Reactions: Proof of Leaching. *Angew. Chem., Int. Ed.* **2006**, *45*, 2886−2890.
(342) de Vries, A. H.; Mulders, J. M.; Mommers, J. H.; Henderickx, H. J.; de Vries, J. G. Homeopathic Ligand-Free Palladium as a Catalyst in the Heck Reaction. A Comparison with a Palladacycle. *Org. Lett.* **2003**, *5*, 3285−3288.
(343) de Vries, J. G. A. Unifying Mechanism for all High-Temperature Heck Reactions. The Role of Palladium Colloids and Anionic Species. *Dalton Trans.* **2006**, 421−429.
(344) Leyva-Perez, A.; Oliver-Meseguer, J.; Rubio-Marques, P.; Corma, A. Water-Stabilized Three- and Four-Atom Palladium Clusters as Highly Active Catalytic Species in Ligand-Free C-C Cross-Coupling Reactions. *Angew. Chem., Int. Ed.* **2013**, *52*, 11554−11559.
(345) Bruno, N. C.; Tudge, M. T.; Buchwald, S. L. Design and Preparation of New Palladium Precatalysts for C-C and C-N Cross-Coupling Reactions. *Chem. Sci.* **2013**, *4*, 916−920.
(346) Fu, F.; Xiang, J.; Cheng, H.; Cheng, L.; Chong, H.; Wang, S.; Li, P.; Wei, S.; Zhu, M.; Li, Y. A Robust and Efficient Pd_3 Cluster Catalyst for the Suzuki Reaction and Its Odd Mechanism. *ACS Catal.* **2017**, *7*, 1860−1867.
(347) Kashin, A. S.; Ananikov, V. P. Catalytic C-C and C-heteroatom bond formation reactions: in situ generated or preformed catalysts? Complicated mechanistic picture behind well-known experimental procedures. *J. Org. Chem.* **2013**, *78*, 11117−11125.
(348) Ananikov, V. P.; Beletskaya, I. P. Toward the Ideal Catalyst: From Atomic Centers to a "Cocktail" of Catalysts. *Organometallics* **2012**, *31*, 1595−1604.
(349) Jiang, X. F.; Huang, H.; Chai, Y. F.; Lohr, T. L.; Yu, S. Y.; Lai, W.; Pan, Y. J.; Delferro, M.; Marks, T. J. Hydrolytic Cleavage of Both CS_2 Carbon-Sulfur Bonds by Multinuclear Pd(II) Complexes at Room Temperature. *Nat. Chem.* **2017**, *9*, 188−193.
(350) Oliver-Meseguer, J.; Cabrero-Antonino, J. R.; Dominguez, I.; Leyva-Perez, A.; Corma, A. Small Gold Clusters Formed in Solution Give Reaction Turnover Numbers of 10^7 at Room Temperature. *Science* **2012**, *338*, 1452−1455.
(351) Oliver-Meseguer, J.; Dominguez, I.; Gavara, R.; Domenech-Carbo, A.; Gonzalez-Calbet, J. M.; Leyva-Perez, A.; Corma, A. The Wet Synthesis and Quantification of Ligand-Free Sub-Nanometric Au Clusters in Solid Matrices. *Chem. Commun.* **2017**, *53*, 1116−1119.
(352) Oliver-Meseguer, J.; Leyva-Pérez, A.; Corma, A. Very Small (3−6 Atoms) Gold Cluster Catalyzed Carbon-Carbon and Carbon-Heteroatom Bond-Forming Reactions in Solution. *ChemCatChem* **2013**, *5*, 3509−3515.
(353) Oliver-Meseguer, J.; Leyva-Perez, A.; Al-Resayes, S. I.; Corma, A. Formation and Stability of 3−5 Atom Gold Clusters from Gold Complexes during the Catalytic Reaction: Dependence on Ligands and Counteranions. *Chem. Commun.* **2013**, *49*, 7782−7784.
(354) Hughes, M. D.; Xu, Y. J.; Jenkins, P.; McMorn, P.; Landon, P.; Enache, D. I.; Carley, A. F.; Attard, G. A.; Hutchings, G. J.; King, F.; et al. Tunable Gold Catalysts for Selective Hydrocarbon Oxidation under Mild Conditions. *Nature* **2005**, *437*, 1132−1135.
(355) Turner, M.; Golovko, V. B.; Vaughan, O. P.; Abdulkin, P.; Berenguer-Murcia, A.; Tikhov, M. S.; Johnson, B. F.; Lambert, R. M. Selective Oxidation with Dioxygen by Gold Nanoparticle Catalysts Derived from 55-Atom Clusters. *Nature* **2008**, *454*, 981−983.
(356) Qian, L.; Wang, Z.; Beletskiy, E. V.; Liu, J.; Dos Santos, H. J.; Li, T.; Rangel, M. D.; Kung, M. C.; Kung, H. H. Stable and Solubilized Active Au Atom Clusters for Selective Epoxidation of Cis-Cyclooctene with Molecular Oxygen. *Nat. Commun.* **2017**, *8*, 14881.
(357) He, C.; Zhang, G.; Ke, J.; Zhang, H.; Miller, J. T.; Kropf, A. J.; Lei, A. Labile Cu(I) Catalyst/Spectator Cu(II) Species in Copper-Catalyzed C-C Coupling Reaction: Operando IR, In Situ XANES/EXAFS Evidence and Kinetic Investigations. *J. Am. Chem. Soc.* **2013**, *135*, 488−493.
(358) Schoch, R.; Desens, W.; Werner, T.; Bauer, M. X-ray Spectroscopic Verification of the Active Species in Iron-Catalyzed Cross-Coupling Reactions. *Chem. - Eur. J.* **2013**, *19*, 15816−15821.
(359) Das, R. K.; Saha, B.; Rahaman, S. M.; Bera, J. K. Bimetallic Catalysis Involving Dipalladium(I) and Diruthenium(I) Complexes. *Chem. - Eur. J.* **2010**, *16*, 14459−14468.
(360) Sarkar, M.; Doucet, H.; Bera, J. K. Room temperature C-H bond activation on a [Pd(I)-Pd(I)] platform. *Chem. Commun.* **2013**, *49*, 9764−9766.
(361) Oliver-Meseguer, J.; Liu, L.; Garcia-Garcia, S.; Canos-Gimenez, C.; Dominguez, I.; Gavara, R.; Domenech-Carbo, A.; Concepcion, P.; Leyva-Perez, A.; Corma, A. Stabilized Naked Sub-Nanometric Cu Clusters Within a Polymeric Film Catalyze C-N, C-C, C-O, C-S, and C-P Bond-Forming Reactions. *J. Am. Chem. Soc.* **2015**, *137*, 3894−3900.
(362) Rivero-Crespo, M. A.; Leyva-Perez, A.; Corma, A. A Ligand-Free Pt_3 Cluster Catalyzes the Markovnikov Hydrosilylation of Alkynes with up to 10^6 Turnover Frequencies. *Chem. - Eur. J.* **2017**, *23*, 1702−1708.
(363) Schlogl, R.; Abd Hamid, S. B. Nanocatalysis: Mature Science Revisited or Something Really New? *Angew. Chem., Int. Ed.* **2004**, *43*, 1628−1637.
(364) Roldan Cuenya, B.; Behafarid, F. Nanocatalysis: Size- and Shape-Dependent Chemisorption and Catalytic Reactivity. *Surf. Sci. Rep.* **2015**, *70*, 135−187.
(365) Takei, T.; Akita, T.; Nakamura, I.; Fujitani, T.; Okumura, M.; Okazaki, K.; Huang, J.; Ishida, T.; Haruta, M. Heterogeneous Catalysis by Gold. *Adv. Catal.* **2012**, *55*, 1−126.
(366) Sankar, M.; Dimitratos, N.; Miedziak, P. J.; Wells, P. P.; Kiely, C. J.; Hutchings, G. J. Designing Bimetallic Catalysts for a Green and Sustainable Future. *Chem. Soc. Rev.* **2012**, *41*, 8099−8139.
(367) Chen, M.; Goodman, D. W. Catalytically Active Gold: from Nanoparticles to Ultrathin Films. *Acc. Chem. Res.* **2006**, *39*, 739−746.
(368) Chen, M. S.; Goodman, D. W. Structure-Activity Relationships in Supported Au Catalysts. *Catal. Today* **2006**, *111*, 22−33.
(369) Valden, M.; Lai, X.; Goodman, D. W. Onset of Catalytic Activity of Gold Clusters on Titania with the Appearance of Nonmetallic Properties. *Science* **1998**, *281*, 1647−1650.
(370) Chen, M.; Cai, Y.; Yan, Z.; Goodman, D. W. On the Origin of the Unique Properties of Supported Au Nanoparticles. *J. Am. Chem. Soc.* **2006**, *128*, 6341−6346.
(371) Chen, M. S.; Goodman, D. W. The Structure of Catalytically Active Gold on Titania. *Science* **2004**, *306*, 252−255.
(372) Haruta, M. Low-Temperature Oxidation of CO over Gold Supported on TiO_2, α-Fe_2O_3, and Co_3O_4. *J. Catal.* **1993**, *144*, 175−192.
(373) Haruta, M. Size- and Support-Dependency in the Catalysis of Gold. *Catal. Today* **1997**, *36*, 153−166.
(374) Liu, Y.; Jia, C. J.; Yamasaki, J.; Terasaki, O.; Schuth, F. Highly Active Iron Oxide Supported Gold Catalysts for CO Oxidation: How Small Must the Gold Nanoparticles be? *Angew. Chem., Int. Ed.* **2010**, *49*, 5771−5775.
(375) Widmann, D.; Behm, R. J. Activation of Molecular Oxygen and the Nature of the Active Oxygen Species for CO Oxidation on Oxide Supported Au Catalysts. *Acc. Chem. Res.* **2014**, *47*, 740−749.
(376) Green, I. X.; Tang, W.; Neurock, M.; Yates, J. T., Jr Spectroscopic Observation of Dual Catalytic Sites during Oxidation of CO on a Au/TiO_2 Catalyst. *Science* **2011**, *333*, 736−739.

DOI: 10.1021/acs.chemrev.7b00776
Chem. Rev. 2018, 118, 4981−5079

(377) An, N.; Li, S.; Duchesne, P. N.; Wu, P.; Zhang, W.; Lee, J.-F.; Cheng, S.; Zhang, P.; Jia, M.; Zhang, W. Size Effects of Platinum Colloid Particles on the Structure and CO Oxidation Properties of Supported Pt/Fe_2O_3 Catalysts. *J. Phys. Chem. C* **2013**, *117*, 21254−21262.
(378) Joo, S. H.; Park, J. Y.; Renzas, J. R.; Butcher, D. R.; Huang, W.; Somorjai, G. A. Size Effect of Ruthenium Nanoparticles in Catalytic Carbon Monoxide Oxidation. *Nano Lett.* **2010**, *10*, 2709−2713.
(379) Qadir, K.; Joo, S. H.; Mun, B. S.; Butcher, D. R.; Renzas, J. R.; Aksoy, F.; Liu, Z.; Somorjai, G. A.; Park, J. Y. Intrinsic Relation between Catalytic Activity of CO Oxidation on Ru Nanoparticles and Ru Oxides Uncovered with Ambient Pressure XPS. *Nano Lett.* **2012**, *12*, 5761−5768.
(380) An, K.; Alayoglu, S.; Musselwhite, N.; Plamthottam, S.; Melaet, G.; Lindeman, A. E.; Somorjai, G. A. Enhanced CO Oxidation Rates at the Interface of Mesoporous Oxides and Pt Nanoparticles. *J. Am. Chem. Soc.* **2013**, *135*, 16689−16696.
(381) Cargnello, M.; Doan-Nguyen, V. V.; Gordon, T. R.; Diaz, R. E.; Stach, E. A.; Gorte, R. J.; Fornasiero, P.; Murray, C. B. Control of Metal Nanocrystal Size Reveals Metal-Support Interface Role for Ceria Catalysts. *Science* **2013**, *341*, 771−773.
(382) Fu, Q.; Yang, F.; Bao, X. Interface-Confined Oxide Nanostructures for Catalytic Oxidation Reactions. *Acc. Chem. Res.* **2013**, *46*, 1692−1701.
(383) Fu, Q.; Li, W. X.; Yao, Y.; Liu, H.; Su, H. Y.; Ma, D.; Gu, X. K.; Chen, L.; Wang, Z.; Zhang, H.; et al. Interface-Confined Ferrous Centers for Catalytic Oxidation. *Science* **2010**, *328*, 1141−1144.
(384) Chen, G.; Zhao, Y.; Fu, G.; Duchesne, P. N.; Gu, L.; Zheng, Y.; Weng, X.; Chen, M.; Zhang, P.; Pao, C. W.; et al. Interfacial Effects in Iron-Nickel Hydroxide-Platinum Nanoparticles Enhance Catalytic Oxidation. *Science* **2014**, *344*, 495−499.
(385) Ramirez, A.; Hueso, J. L.; Suarez, H.; Mallada, R.; Ibarra, A.; Irusta, S.; Santamaria, J. A Nanoarchitecture Based on Silver and Copper Oxide with an Exceptional Response in the Chlorine-Promoted Epoxidation of Ethylene. *Angew. Chem., Int. Ed.* **2016**, *55*, 11158−11161.
(386) Linic, S.; Barteau, M. A. Formation of a Stable Surface Oxametallacycle that Produces Ethylene Oxide. *J. Am. Chem. Soc.* **2002**, *124*, 310−317.
(387) Christopher, P.; Linic, S. Engineering Selectivity in Heterogeneous Catalysis: Ag Nanowires as Selective Ethylene Epoxidation Catalysts. *J. Am. Chem. Soc.* **2008**, *130*, 11264−11265.
(388) Christopher, P.; Linic, S. Shape- and Size-Specific Chemistry of Ag Nanostructures in Catalytic Ethylene Epoxidation. *ChemCatChem* **2010**, *2*, 78−83.
(389) Pulido, A.; Concepción, P.; Boronat, M.; Corma, A. Aerobic Epoxidation of Propene over Silver (111) and (100) Facet Catalysts. *J. Catal.* **2012**, *292*, 138−147.
(390) Vinod, C. P.; Wilson, K.; Lee, A. F. Recent Advances in the Heterogeneously Catalysed Aerobic Selective Oxidation of Alcohols. *J. Chem. Technol. Biotechnol.* **2011**, *86*, 161−171.
(391) Zhang, Q.; Deng, W.; Wang, Y. Effect of Size of Catalytically Active Phases in the Dehydrogenation of Alcohols and the Challenging Selective Oxidation of Hydrocarbons. *Chem. Commun.* **2011**, *47*, 9275−9292.
(392) Mallat, T.; Baiker, A. Oxidation of Alcohols with Molecular Oxygen on Solid Catalysts. *Chem. Rev.* **2004**, *104*, 3037−3058.
(393) Abad, A.; Corma, A.; Garcia, H. Catalyst Parameters Determining Activity and Selectivity of Supported Gold Nanoparticles for the Aerobic Oxidation of Alcohols: the Molecular Reaction Mechanism. *Chem. - Eur. J.* **2008**, *14*, 212−222.
(394) Roldan Cuenya, B. Metal Nanoparticle Catalysts Beginning to Shape-up. *Acc. Chem. Res.* **2013**, *46*, 1682−1691.
(395) Mostafa, S.; Behafarid, F.; Croy, J. R.; Ono, L. K.; Li, L.; Yang, J. C.; Frenkel, A. I.; Cuenya, B. R. Shape-Dependent Catalytic Properties of Pt Nanoparticles. *J. Am. Chem. Soc.* **2010**, *132*, 15714−15719.
(396) Mistry, H.; Behafarid, F.; Zhou, E.; Ono, L. K.; Zhang, L.; Roldan Cuenya, B. Shape-Dependent Catalytic Oxidation of 2-Butanol over Pt Nanoparticles Supported on γ-Al_2O_3. *ACS Catal.* **2014**, *4*, 109−115.
(397) Bond, G. C. Strategy of Research on Supported Metal Catalysts. Problems of Structure-Sensitive Reactions in the Gas Phase. *Acc. Chem. Res.* **1993**, *26*, 490−495.
(398) Che, M.; Bennett, C. O. The Influence of Particle Size on the Catalytic Properties of Supported Metals. *Adv. Catal.* **1989**, *36*, 55−172.
(399) Van Santen, R. A. Complementary Structure Sensitive and Insensitive Catalytic Relationships. *Acc. Chem. Res.* **2009**, *42*, 57−66.
(400) Strongin, D. The Importance of C7 Sites and Surface Roughness in the Ammonia Synthesis Reaction over Iron. *J. Catal.* **1987**, *103*, 213−215.
(401) Dumesic, J. Surface, Catalytic and Magnetic Properties of Small Iron Particles II. Structure Sensitivity of Ammonia Synthesis. *J. Catal.* **1975**, *37*, 503−512.
(402) Iglesia, E. Design, Synthesis, and Use of Cobalt-Based Fischer−Tropsch Synthesis Catalysts. *Appl. Catal., A* **1997**, *161*, 59−78.
(403) Bezemer, G. L.; Bitter, J. H.; Kuipers, H. P.; Oosterbeek, H.; Holewijn, J. E.; Xu, X.; Kapteijn, F.; van Dillen, A. J.; de Jong, K. P. Cobalt Particle Size Effects in the Fischer−Tropsch Reaction Studied with Carbon Nanofiber Supported Catalysts. *J. Am. Chem. Soc.* **2006**, *128*, 3956−3964.
(404) den Breejen, J. P.; Radstake, P. B.; Bezemer, G. L.; Bitter, J. H.; Froseth, V.; Holmen, A.; de Jong, K. P. On the Origin of the Cobalt Particle Size Effects in Fischer−Tropsch Catalysis. *J. Am. Chem. Soc.* **2009**, *131*, 7197−7203.
(405) Song, H.; Rioux, R. M.; Hoefelmeyer, J. D.; Komor, R.; Niesz, K.; Grass, M.; Yang, P.; Somorjai, G. A. Hydrothermal Growth of Mesoporous SBA-15 Silica in the Presence of PVP-Stabilized Pt Nanoparticles: Synthesis, Characterization, and Catalytic Properties. *J. Am. Chem. Soc.* **2006**, *128*, 3027−3037.
(406) Pushkarev, V. V.; An, K.; Alayoglu, S.; Beaumont, S. K.; Somorjai, G. A. Hydrogenation of benzene and toluene over size controlled Pt/SBA-15 catalysts: Elucidation of the Pt particle size effect on reaction kinetics. *J. Catal.* **2012**, *292*, 64−72.
(407) Somorjai, G. A.; Park, J. Y. Colloid Science of Metal Nanoparticle Catalysts in 2D and 3D Structures. Challenges of Nucleation, Growth, Composition, Particle Shape, Size Control and Their Influence on Activity and Selectivity. *Top. Catal.* **2008**, *49*, 126−135.
(408) Kuhn, J. N.; Huang, W.; Tsung, C. K.; Zhang, Y.; Somorjai, G. A. Structure Sensitivity of Carbon-Nitrogen Ring Opening: Impact of Platinum Particle Size from below 1 to 5 nm upon Pyrrole Hydrogenation Product Selectivity over Monodisperse Platinum Nanoparticles Loaded onto Mesoporous Silica. *J. Am. Chem. Soc.* **2008**, *130*, 14026−14027.
(409) Michalak, W. D.; Krier, J. M.; Komvopoulos, K.; Somorjai, G. A. Structure Sensitivity in Pt Nanoparticle Catalysts for Hydrogenation of 1,3-Butadiene: In Situ Study of Reaction Intermediates Using SFG Vibrational Spectroscopy. *J. Phys. Chem. C* **2013**, *117*, 1809−1817.
(410) Kliewer, C. J.; Aliaga, C.; Bieri, M.; Huang, W.; Tsung, C. K.; Wood, J. B.; Komvopoulos, K.; Somorjai, G. A. Furan Hydrogenation over Pt(111) and Pt(100) Single-Crystal Surfaces and Pt Nanoparticles from 1 to 7 nm: a Kinetic and Sum Frequency Heneration Vibrational Spectroscopy Study. *J. Am. Chem. Soc.* **2010**, *132*, 13088−13095.
(411) Pushkarev, V. V.; Musselwhite, N.; An, K.; Alayoglu, S.; Somorjai, G. A. High Structure Sensitivity of Vapor-Phase Furfural Decarbonylation/Hydrogenation Reaction Network as a Function of Size and Shape of Pt Nanoparticles. *Nano Lett.* **2012**, *12*, 5196−5201.
(412) Zang, W.; Li, G.; Wang, L.; Zhang, X. Catalytic Hydrogenation by Noble-Metal Nanocrystals with Well-Defined Facets: a Review. *Catal. Sci. Technol.* **2015**, *5*, 2532−2553.
(413) Bratlie, K. M.; Lee, H.; Komvopoulos, K.; Yang, P.; Somorjai, G. A. Platinum Nanoparticle Shape Effects on Benzene Hydrogenation Selectivity. *Nano Lett.* **2007**, *7*, 3097−3101.
(414) Schoenbaum, C. A.; Schwartz, D. K.; Medlin, J. W. Controlling the Surface Environment of Heterogeneous Catalysts Using Self-Assembled Monolayers. *Acc. Chem. Res.* **2014**, *47*, 1438−1445.
(415) Liu, P.; Qin, R.; Fu, G.; Zheng, N. Surface Coordination Chemistry of Metal Nanomaterials. *J. Am. Chem. Soc.* **2017**, *139*, 2122−2131.

DOI: 10.1021/acs.chemrev.7b00776
Chem. Rev. 2018, 118, 4981−5079

(416) Baiker, A. Crucial Aspects in the Design of Chirally Modified Noble Metal Catalysts for Asymmetric Hydrogenation of Activated Ketones. *Chem. Soc. Rev.* **2015**, *44*, 7449−7464.
(417) Schmidt, E.; Vargas, A.; Mallat, T.; Baiker, A. Shape-Selective Enantioselective Hydrogenation on Pt Nanoparticles. *J. Am. Chem. Soc.* **2009**, *131*, 12358−12367.
(418) Marshall, S. T.; O'Brien, M.; Oetter, B.; Corpuz, A.; Richards, R. M.; Schwartz, D. K.; Medlin, J. W. Controlled Selectivity for Palladium Catalysts Using Self-Assembled Monolayers. *Nat. Mater.* **2010**, *9*, 853−858.
(419) Wu, B.; Huang, H.; Yang, J.; Zheng, N.; Fu, G. Selective Hydrogenation of α,β-Unsaturated Aldehydes Catalyzed by Amine-Capped Platinum-Cobalt Nanocrystals. *Angew. Chem., Int. Ed.* **2012**, *51*, 3440−3443.
(420) Lee, I.; Zaera, F. Thermal Chemistry of C4 Hydrocarbons on Pt(111): Mechanism for Double-Bond Isomerization. *J. Phys. Chem. B* **2005**, *109*, 2745−2753.
(421) Lee, I.; Zaera, F. Selectivity in Platinum-Catalyzed Cis-Trans Carbon-Carbon Double-Bond Isomerization. *J. Am. Chem. Soc.* **2005**, *127*, 12174−12175.
(422) Lee, I.; Delbecq, F.; Morales, R.; Albiter, M. A.; Zaera, F. Tuning Selectivity in Catalysis by Controlling Particle Shape. *Nat. Mater.* **2009**, *8*, 132−138.
(423) Lee, I.; Morales, R.; Albiter, M. A.; Zaera, F. Synthesis of Heterogeneous Catalysts with Well Shaped Platinum Particles to Control Reaction Selectivity. *Proc. Natl. Acad. Sci. U. S. A.* **2008**, *105*, 15241−15246.
(424) Mistry, H.; Varela, A. S.; Kühl, S.; Strasser, P.; Cuenya, B. R. Nanostructured Electrocatalysts with Tunable Activity and Selectivity. *Nat. Rev. Mater.* **2016**, *1*, 16009.
(425) Seh, Z. W.; Kibsgaard, J.; Dickens, C. F.; Chorkendorff, I.; Norskov, J. K.; Jaramillo, T. F. Combining Theory and Experiment in Electrocatalysis: Insights into Materials Design. *Science* **2017**, *355*, eaad4998.
(426) Stamenkovic, V.; Mun, B. S.; Mayrhofer, K. J.; Ross, P. N.; Markovic, N. M.; Rossmeisl, J.; Greeley, J.; Norskov, J. K. Changing the Activity of Electrocatalysts for Oxygen Reduction by Tuning the Surface Electronic Structure. *Angew. Chem., Int. Ed.* **2006**, *45*, 2897−2901.
(427) Stamenkovic, V. R.; Mun, B. S.; Arenz, M.; Mayrhofer, K. J.; Lucas, C. A.; Wang, G.; Ross, P. N.; Markovic, N. M. Trends in Electrocatalysis on Extended and Nanoscale Pt-Bimetallic Alloy Surfaces. *Nat. Mater.* **2007**, *6*, 241−247.
(428) Greeley, J.; Stephens, I. E.; Bondarenko, A. S.; Johansson, T. P.; Hansen, H. A.; Jaramillo, T. F.; Rossmeisl, J.; Chorkendorff, I.; Norskov, J. K. Alloys of Platinum and Early Transition Metals as Oxygen Reduction Electrocatalysts. *Nat. Chem.* **2009**, *1*, 552−556.
(429) Stamenkovic, V. R.; Fowler, B.; Mun, B. S.; Wang, G.; Ross, P. N.; Lucas, C. A.; Markovic, N. M. Improved Oxygen Reduction Activity on $Pt_3Ni(111)$ via Increased Surface Site Availability. *Science* **2007**, *315*, 493−497.
(430) Cui, C.; Gan, L.; Li, H. H.; Yu, S. H.; Heggen, M.; Strasser, P. Octahedral PtNi Nanoparticle Catalysts: Exceptional Oxygen Reduction Activity by Tuning the Alloy Particle Surface Composition. *Nano Lett.* **2012**, *12*, 5885−5889.
(431) Wu, J.; Qi, L.; You, H.; Gross, A.; Li, J.; Yang, H. Icosahedral Platinum Alloy Nanocrystals with Enhanced Electrocatalytic Activities. *J. Am. Chem. Soc.* **2012**, *134*, 11880−11883.
(432) Bu, L.; Zhang, N.; Guo, S.; Zhang, X.; Li, J.; Yao, J.; Wu, T.; Lu, G.; Ma, J. Y.; Su, D.; et al. Biaxially Strained PtPb/Pt Core/Shell Nanoplate Boosts Oxygen Reduction Catalysis. *Science* **2016**, *354*, 1410−1414.
(433) Koh, S.; Strasser, P. Electrocatalysis on Bimetallic Surfaces: Modifying Catalytic Reactivity for Oxygen Reduction by Voltammetric Surface Dealloying. *J. Am. Chem. Soc.* **2007**, *129*, 12624−12625.
(434) Strasser, P.; Koh, S.; Anniyev, T.; Greeley, J.; More, K.; Yu, C.; Liu, Z.; Kaya, S.; Nordlund, D.; Ogasawara, H.; et al. Lattice-Strain Control of the Activity in Dealloyed Core-Shell Fuel Cell Catalysts. *Nat. Chem.* **2010**, *2*, 454−460.
(435) Wang, D.; Xin, H. L.; Hovden, R.; Wang, H.; Yu, Y.; Muller, D. A.; DiSalvo, F. J.; Abruna, H. D. Structurally Ordered Intermetallic Platinum-Cobalt Core-Shell Nanoparticles with Enhanced Activity and Stability as Oxygen Reduction Electrocatalysts. *Nat. Mater.* **2013**, *12*, 81−87.
(436) Chen, C.; Kang, Y.; Huo, Z.; Zhu, Z.; Huang, W.; Xin, H. L.; Snyder, J. D.; Li, D.; Herron, J. A.; Mavrikakis, M.; et al. Highly Crystalline Multimetallic Nanoframes with Three-Dimensional Electrocatalytic Surfaces. *Science* **2014**, *343*, 1339−1343.
(437) Li, M.; Zhao, Z.; Cheng, T.; Fortunelli, A.; Chen, C. Y.; Yu, R.; Zhang, Q.; Gu, L.; Merinov, B. V.; Lin, Z.; et al. Ultrafine Jagged Platinum Nanowires Enable Ultrahigh Mass Activity for the Oxygen Reduction Reaction. *Science* **2016**, *354*, 1414−1419.
(438) Mistry, H.; Reske, R.; Zeng, Z.; Zhao, Z. J.; Greeley, J.; Strasser, P.; Cuenya, B. R. Exceptional Size-Dependent Activity Enhancement in the Electroreduction of CO_2 over Au Nanoparticles. *J. Am. Chem. Soc.* **2014**, *136*, 16473−16476.
(439) Reske, R.; Mistry, H.; Behafarid, F.; Roldan Cuenya, B.; Strasser, P. Particle Size Effects in the Catalytic Electroreduction of CO_2 on Cu Nanoparticles. *J. Am. Chem. Soc.* **2014**, *136*, 6978−6986.
(440) Feng, X.; Jiang, K.; Fan, S.; Kanan, M. W. Grain-Boundary-Dependent CO_2 Electroreduction Activity. *J. Am. Chem. Soc.* **2015**, *137*, 4606−4609.
(441) Liu, S.; Tao, H.; Zeng, L.; Liu, Q.; Xu, Z.; Liu, Q.; Luo, J. L. Shape-Dependent Electrocatalytic Reduction of CO_2 to CO on Triangular Silver Nanoplates. *J. Am. Chem. Soc.* **2017**, *139*, 2160−2163.
(442) Li, Y.; Cui, F.; Ross, M. B.; Kim, D.; Sun, Y.; Yang, P. Structure-Sensitive CO_2 Electroreduction to Hydrocarbons on Ultrathin 5-fold Twinned Copper Nanowires. *Nano Lett.* **2017**, *17*, 1312−1317.
(443) Gao, S.; Lin, Y.; Jiao, X.; Sun, Y.; Luo, Q.; Zhang, W.; Li, D.; Yang, J.; Xie, Y. Partially Oxidized Atomic Cobalt Layers for Carbon Dioxide Electroreduction to Liquid Fuel. *Nature* **2016**, *529*, 68−71.
(444) Sen, S.; Liu, D.; Palmore, G. T. R. Electrochemical Reduction of CO_2 at Copper Nanofoams. *ACS Catal.* **2014**, *4*, 3091−3095.
(445) Ren, D.; Deng, Y.; Handoko, A. D.; Chen, C. S.; Malkhandi, S.; Yeo, B. S. Selective Electrochemical Reduction of Carbon Dioxide to Ethylene and Ethanol on Copper(I) Oxide Catalysts. *ACS Catal.* **2015**, *5*, 2814−2821.
(446) Dutta, A.; Rahaman, M.; Luedi, N. C.; Mohos, M.; Broekmann, P. Morphology Matters: Tuning the Product Distribution of CO_2 Electroreduction on Oxide-Derived Cu Foam Catalysts. *ACS Catal.* **2016**, *6*, 3804−3814.
(447) Kim, D.; Kley, C. S.; Li, Y.; Yang, P. Copper Nanoparticle Ensembles for Selective Electroreduction of CO_2 to C2-C3 Products. *Proc. Natl. Acad. Sci. U. S. A.* **2017**, *114*, 10560−10565.
(448) Santoro, S.; Kozhushkov, S. I.; Ackermann, L.; Vaccaro, L. Heterogeneous Catalytic Approaches in C−H Activation Reactions. *Green Chem.* **2016**, *18*, 3471−3493.
(449) Pla, D.; Gómez, M. Metal and Metal Oxide Nanoparticles: A Lever for C−H Functionalization. *ACS Catal.* **2016**, *6*, 3537−3552.
(450) Yasukawa, T.; Miyamura, H.; Kobayashi, S. Chiral Ligand-Modified Metal Nanoparticles as Unique Catalysts for Asymmetric C−C Bond-Forming Reactions: How Are Active Species Generated? *ACS Catal.* **2016**, *6*, 7979−7988.
(451) Izawa, Y.; Pun, D.; Stahl, S. S. Palladium-Catalyzed Aerobic Dehydrogenation of Substituted Cyclohexanones to Phenols. *Science* **2011**, *333*, 209−213.
(452) Iosub, A. V.; Stahl, S. S. Palladium-Catalyzed Aerobic Dehydrogenation of Cyclic Hydrocarbons for the Synthesis of Substituted Aromatics and Other Unsaturated Products. *ACS Catal.* **2016**, *6*, 8201−8213.
(453) Diao, T.; Pun, D.; Stahl, S. S. Aerobic Dehydrogenation of Cyclohexanone to Cyclohexenone Catalyzed by $Pd(DMSO)_2(TFA)_2$: Evidence for Ligand-Controlled Chemoselectivity. *J. Am. Chem. Soc.* **2013**, *135*, 8205−8212.
(454) Pun, D.; Diao, T.; Stahl, S. S. Aerobic Dehydrogenation of Cyclohexanone to Phenol Catalyzed by $Pd(TFA)_2$/2-dimethylamino-pyridine: Evidence for the Role of Pd Nanoparticles. *J. Am. Chem. Soc.* **2013**, *135*, 8213−8221.

DOI: 10.1021/acs.chemrev.7b00776
Chem. Rev. 2018, 118, 4981−5079

(455) Xue, T.; Lin, Z.; Chiu, C. Y.; Li, Y.; Ruan, L.; Wang, G.; Zhao, Z.; Lee, C.; Duan, X.; Huang, Y. Molecular Ligand Modulation of Palladium Nanocatalysts for Highly Efficient and Robust Heterogeneous Oxidation of Cyclohexenone to Phenol. *Sci. Adv.* **2017**, *3*, e1600615.
(456) Tang, D. T.; Collins, K. D.; Glorius, F. Completely Regioselective Direct C-H Functionalization of Benzo[b]thiophenes Using a Simple Heterogeneous Catalyst. *J. Am. Chem. Soc.* **2013**, *135*, 7450−7453.
(457) Tang, D. T.; Collins, K. D.; Ernst, J. B.; Glorius, F. Pd/C as a Catalyst for Completely Regioselective C-H Functionalization of Thiophenes under Mild Conditions. *Angew. Chem., Int. Ed.* **2014**, *53*, 1809−1813.
(458) Vasquez-Cespedes, S.; Ferry, A.; Candish, L.; Glorius, F. Heterogeneously Catalyzed Direct C-H Thiolation of Heteroarenes. *Angew. Chem., Int. Ed.* **2015**, *54*, 5772−5776.
(459) Matsumoto, K.; Yoshida, M.; Shindo, M. Heterogeneous Rhodium-Catalyzed Aerobic Oxidative Dehydrogenative Cross-Coupling: Nonsymmetrical Biaryl Amines. *Angew. Chem., Int. Ed.* **2016**, *55*, 5272−5276.
(460) Warratz, S.; Burns, D. J.; Zhu, C.; Korvorapun, K.; Rogge, T.; Scholz, J.; Jooss, C.; Gelman, D.; Ackermann, L. meta-C-H Bromination on Purine Bases by Heterogeneous Ruthenium Catalysis. *Angew. Chem., Int. Ed.* **2017**, *56*, 1557−1560.
(461) Sankar, M.; Dimitratos, N.; Miedziak, P. J.; Wells, P. P.; Kiely, C. J.; Hutchings, G. J. Designing Bimetallic Catalysts for a Green and Sustainable Future. *Chem. Soc. Rev.* **2012**, *41*, 8099−8139.
(462) Ferrando, R.; Jellinek, J.; Johnston, R. L. Nanoalloys: from Theory to Applications of Alloy Clusters and Nanoparticles. *Chem. Rev.* **2008**, *108*, 845−910.
(463) Kim, D.; Resasco, J.; Yu, Y.; Asiri, A. M.; Yang, P. Synergistic Geometric and Electronic Effects for Electrochemical Reduction of Carbon Dioxide Using Gold-Copper Bimetallic Nanoparticles. *Nat. Commun.* **2014**, *5*, 4948.
(464) Furukawa, S.; Komatsu, T. Intermetallic Compounds: Promising Inorganic Materials for Well-Structured and Electronically Modified Reaction Environments for Efficient Catalysis. *ACS Catal.* **2017**, *7*, 735−765.
(465) Penner, S.; Armbrüster, M. Formation of Intermetallic Compounds by Reactive Metal-Support Interaction: A Frequently Encountered Phenomenon in Catalysis. *ChemCatChem* **2015**, *7*, 374−392.
(466) Yan, Y.; Du, J. S.; Gilroy, K. D.; Yang, D.; Xia, Y.; Zhang, H. Intermetallic Nanocrystals: Syntheses and Catalytic Applications. *Adv. Mater.* **2017**, *29*, 1605997.
(467) Furukawa, S.; Ochi, K.; Luo, H.; Miyazaki, M.; Komatsu, T. Selective Stereochemical Catalysis Controlled by Specific Atomic Arrangement of Ordered Alloys. *ChemCatChem* **2015**, *7*, 3472−3479.
(468) Wowsnick, G.; Teschner, D.; Kasatkin, I.; Girgsdies, F.; Armbrüster, M.; Zhang, A.; Grin, Y.; Schlögl, R.; Behrens, M. Surface Dynamics of the Intermetallic Catalyst Pd_2Ga, Part I − Structural Stability in UHV and Different Gas Atmospheres. *J. Catal.* **2014**, *309*, 209−220.
(469) Wowsnick, G.; Teschner, D.; Armbrüster, M.; Kasatkin, I.; Girgsdies, F.; Grin, Y.; Schlögl, R.; Behrens, M. Surface Dynamics of the Intermetallic Catalyst Pd_2Ga, Part II − Reactivity and Stability in Liquid-Phase Hydrogenation of Phenylacetylene. *J. Catal.* **2014**, *309*, 221−230.
(470) Enache, D. I.; Edwards, J. K.; Landon, P.; Solsona-Espriu, B.; Carley, A. F.; Herzing, A. A.; Watanabe, M.; Kiely, C. J.; Knight, D. W.; Hutchings, G. J. Solvent-Free Oxidation of Primary Alcohols to Aldehydes Using Au-Pd/TiO_2 Catalysts. *Science* **2006**, *311*, 362−365.
(471) Kesavan, L.; Tiruvalam, R.; Ab Rahim, M. H.; bin Saiman, M. I.; Enache, D. I.; Jenkins, R. L.; Dimitratos, N.; Lopez-Sanchez, J. A.; Taylor, S. H.; Knight, D. W.; et al. Solvent-Free Oxidation of Primary Carbon-Hydrogen Bonds in Toluene Using Au-Pd Alloy Nanoparticles. *Science* **2011**, *331*, 195−199.
(472) Luo, W.; Sankar, M.; Beale, A. M.; He, Q.; Kiely, C. J.; Bruijnincx, P. C.; Weckhuysen, B. M. High Performing and Stable Supported Nano-Alloys for the Catalytic Hydrogenation of Levulinic Acid to γ-Valerolactone. *Nat. Commun.* **2015**, *6*, 6540.
(473) Carter, J. H.; Althahban, S.; Nowicka, E.; Freakley, S. J.; Morgan, D. J.; Shah, P. M.; Golunski, S.; Kiely, C. J.; Hutchings, G. J. Synergy and Anti-Synergy between Palladium and Gold in Nanoparticles Dispersed on a Reducible Support. *ACS Catal.* **2016**, *6*, 6623−6633.
(474) Zhang, Z.; Yates, J. T., Jr Band Bending in Semiconductors: Chemical and Physical Consequences at Surfaces and Interfaces. *Chem. Rev.* **2012**, *112*, 5520−5551.
(475) Humbert, M.; Chen, J. Correlating Hydrogenation Activity with Binding Energies of Hydrogen and Cyclohexene on M/Pt(111) (M = Fe, Co, Ni, Cu) Bimetallic Surfaces. *J. Catal.* **2008**, *257*, 297−306.
(476) Bai, S.; Wang, C.; Deng, M.; Gong, M.; Bai, Y.; Jiang, J.; Xiong, Y. Surface Polarization Matters: Enhancing the Hydrogen-Evolution Reaction by Shrinking Pt Shells in Pt-Pd-Graphene Stack Structures. *Angew. Chem., Int. Ed.* **2014**, *53*, 12120−12124.
(477) Bai, S.; Yang, L.; Wang, C.; Lin, Y.; Lu, J.; Jiang, J.; Xiong, Y. Boosting Photocatalytic Water Splitting: Interfacial Charge Polarization in Atomically Controlled Core-Shell Cocatalysts. *Angew. Chem., Int. Ed.* **2015**, *54*, 14810−14814.
(478) Erlebacher, J.; Aziz, M. J.; Karma, A.; Dimitrov, N.; Sieradzki, K. Evolution of Nanoporosity in Dealloying. *Nature* **2001**, *410*, 450−453.
(479) Xu, C.; Su, J.; Xu, X.; Liu, P.; Zhao, H.; Tian, F.; Ding, Y. Low Temperature CO Oxidation over Unsupported Nanoporous Gold. *J. Am. Chem. Soc.* **2007**, *129*, 42−43.
(480) Wittstock, A.; Neumann, B. r.; Schaefer, A.; Dumbuya, K.; Kübel, C.; Biener, M. M.; Zielasek, V.; Steinrück, H.-P.; Gottfried, J. M.; Biener, J. r.; et al. Nanoporous Au: An Unsupported Pure Gold Catalyst? *J. Phys. Chem. C* **2009**, *113*, 5593−5600.
(481) Fujita, T.; Guan, P.; McKenna, K.; Lang, X.; Hirata, A.; Zhang, L.; Tokunaga, T.; Arai, S.; Yamamoto, Y.; Tanaka, N.; et al. Atomic Origins of the High Catalytic Activity of Nanoporous Gold. *Nat. Mater.* **2012**, *11*, 775−780.
(482) Fujita, T.; Tokunaga, T.; Zhang, L.; Li, D.; Chen, L.; Arai, S.; Yamamoto, Y.; Hirata, A.; Tanaka, N.; Ding, Y.; et al. Atomic Observation of Catalysis-Induced Nanopore Coarsening of Nanoporous Gold. *Nano Lett.* **2014**, *14*, 1172−1177.
(483) Wittstock, A.; Zielasek, V.; Biener, J.; Friend, C. M.; Baumer, M. Nanoporous Gold Catalysts for Selective Gas-Phase Oxidative Coupling of Methanol at Low Temperature. *Science* **2010**, *327*, 319−322.
(484) Personick, M. L.; Madix, R. J.; Friend, C. M. Selective Oxygen-Assisted Reactions of Alcohols and Amines Catalyzed by Metallic Gold: Paradigms for the Design of Catalytic Processes. *ACS Catal.* **2017**, *7*, 965−985.
(485) Wang, L.-C.; Personick, M. L.; Karakalos, S.; Fushimi, R.; Friend, C. M.; Madix, R. J. Active sites for methanol partial oxidation on nanoporous gold catalysts. *J. Catal.* **2016**, *344*, 778−783.
(486) Biener, J.; Wittstock, A.; Zepeda-Ruiz, L. A.; Biener, M. M.; Zielasek, V.; Kramer, D.; Viswanath, R. N.; Weissmuller, J.; Baumer, M.; Hamza, A. V. Surface-Chemistry-Driven Actuation in Nanoporous gold. *Nat. Mater.* **2009**, *8*, 47−51.
(487) Zugic, B.; Wang, L.; Heine, C.; Zakharov, D. N.; Lechner, B. A. J.; Stach, E. A.; Biener, J.; Salmeron, M.; Madix, R. J.; Friend, C. M. Dynamic Restructuring Drives Catalytic Activity on Nanoporous Gold-Silver Alloy Catalysts. *Nat. Mater.* **2016**, *16*, 558−564.
(488) Tao, F. F.; Salmeron, M. In Situ Studies of Chemistry and Structure of Materials in Reactive Environments. *Science* **2011**, *331*, 171−174.
(489) Tao, F.; Dag, S.; Wang, L. W.; Liu, Z.; Butcher, D. R.; Bluhm, H.; Salmeron, M.; Somorjai, G. A. Break-up of Stepped Platinum Catalyst Surfaces by High CO Coverage. *Science* **2010**, *327*, 850−853.
(490) Eren, B.; Zherebetskyy, D.; Patera, L. L.; Wu, C. H.; Bluhm, H.; Africh, C.; Wang, L. W.; Somorjai, G. A.; Salmeron, M. Activation of Cu(111) Surface by Decomposition into Clusters Driven by CO Adsorption. *Science* **2016**, *351*, 475−478.
(491) Imbihl, R.; Ertl, G. Oscillatory Kinetics in Heterogeneous Catalysis. *Chem. Rev.* **1995**, *95*, 697−733.
(492) Imbihl, R. Nonlinear Dynamics on Catalytic Surfaces. *Catal. Today* **2005**, *105*, 206−222.
(493) Beusch, H.; Fieguth, D.; Wicke, E. *Chem. Ing. Tech.* **1972**, *15*, 445.

DOI: 10.1021/acs.chemrev.7b00776
Chem. Rev. 2018, 118, 4981−5079

(494) Eiswirth, M.; Ertl, G. Kinetic Oscillations in the Catalytic CO Oxidation on a Pt(110) Surface. *Surf. Sci.* **1986**, *177*, 90−100.
(495) Nicolis, G.; Prigogine, I. *Self-Organization in Non-Equilibrium Systems*; Wiley: New York, 1977.
(496) Kim, M.; Bertram, M.; Pollmann, M.; von Oertzen, A.; Mikhailov, A. S.; Rotermund, H. H.; Ertl, G. Controlling Chemical Turbulence by Global Delayed Feedback: Pattern Formation in Catalytic CO Oxidation on Pt(110). *Science* **2001**, *292*, 1357−1360.
(497) Hendriksen, B. L. M.; Bobaru, S. C.; Frenken, J. W. M. Oscillatory CO Oxidation on Pd(100) Studied with in situ Scanning Tunneling Microscopy. *Surf. Sci.* **2004**, *552*, 229−242.
(498) Vendelbo, S. B.; Elkjaer, C. F.; Falsig, H.; Puspitasari, I.; Dona, P.; Mele, L.; Morana, B.; Nelissen, B. J.; van Rijn, R.; Creemer, J. F.; et al. Visualization of Oscillatory Behaviour of Pt Nanoparticles Catalysing CO Oxidation. *Nat. Mater.* **2014**, *13*, 884−890.
(499) Ertl, G. Reactions at Surfaces: from Atoms to Complexity. *Angew. Chem., Int. Ed.* **2008**, *47*, 3524−3535.
(500) Zhdanov, V. P. Impact of Surface Science on the Understanding of Kinetics of Heterogeneous Catalytic Reactions. *Surf. Sci.* **2002**, *500*, 966−985.
(501) Stötzel, J.; Frahm, R.; Kimmerle, B.; Nachtegaal, M.; Grunwaldt, J.-D. Oscillatory Behavior during the Catalytic Partial Oxidation of Methane: Following Dynamic Structural Changes of Palladium Using the QEXAFS Technique. *J. Phys. Chem. C* **2012**, *116*, 599−609.
(502) Zhou, Z. Y.; Tian, N.; Li, J. T.; Broadwell, I.; Sun, S. G. Nanomaterials of High Surface Energy with Exceptional Properties in Catalysis and Energy Storage. *Chem. Soc. Rev.* **2011**, *40*, 4167−4185.
(503) Ruditskiy, A.; Peng, H. C.; Xia, Y. Shape-Controlled Metal Nanocrystals for Heterogeneous Catalysis. *Annu. Rev. Chem. Biomol. Eng.* **2016**, *7*, 327−348.
(504) Cui, C.; Gan, L.; Heggen, M.; Rudi, S.; Strasser, P. Compositional Segregation in Shaped Pt Alloy Nanoparticles and Their Structural Behaviour during Electrocatalysis. *Nat. Mater.* **2013**, *12*, 765−771.
(505) Tian, N.; Zhou, Z.-Y.; Sun, S.-G. Platinum Metal Catalysts of High-Index Surfaces: From Single-Crystal Planes to Electrochemically Shape-Controlled Nanoparticles. *J. Phys. Chem. C* **2008**, *112*, 19801−19817.
(506) Chen, Q.; Jia, Y.; Xie, S.; Xie, Z. Well-Faceted Noble-Metal Nanocrystals with Nonconvex Polyhedral Shapes. *Chem. Soc. Rev.* **2016**, *45*, 3207−3220.
(507) Zhang, H.; Jin, M.; Xia, Y. Noble-Metal Nanocrystals with Concave Surfaces: Synthesis and Applications. *Angew. Chem., Int. Ed.* **2012**, *51*, 7656−7673.
(508) Qiao, B.; Lin, J.; Li, L.; Wang, A.; Liu, J.; Zhang, T. Highly Active Small Palladium Clusters Supported on Ferric Hydroxide for Carbon Monoxide-Tolerant Hydrogen Oxidation. *ChemCatChem* **2014**, *6*, 547−554.
(509) Yang, F.; Deng, D.; Pan, X.; Fu, Q.; Bao, X. Understanding nano effects in catalysis. *Natl. Sci. Rev.* **2015**, *2*, 183−201.
(510) An, K.; Somorjai, G. A. Nanocatalysis I: Synthesis of Metal and Bimetallic Nanoparticles and Porous Oxides and Their Catalytic Reaction Studies. *Catal. Lett.* **2015**, *145*, 233−248.
(511) Alayoglu, S.; Somorjai, G. A. Nanocatalysis II: In Situ Surface Probes of Nano-Catalysts and Correlative Structure−Reactivity Studies. *Catal. Lett.* **2015**, *145*, 249−271.
(512) Wang, J.; Tan, H.; Yu, S.; Zhou, K. Morphological Effects of Gold Clusters on the Reactivity of Ceria Surface Oxygen. *ACS Catal.* **2015**, *5*, 2873−2881.
(513) Guo, L. W.; Du, P. P.; Fu, X. P.; Ma, C.; Zeng, J.; Si, R.; Huang, Y. Y.; Jia, C. J.; Zhang, Y. W.; Yan, C. H. Contributions of Distinct Gold Species to Catalytic Reactivity for Carbon Monoxide Oxidation. *Nat. Commun.* **2016**, *7*, 13481.
(514) Liu, L.; Zakharov, D.; Arenal, R.; Concepcion, P.; Stach, E. A.; Corma, A. Evolution and Stabilization of Subnanometric Metal Species in Confined Space During Catalytic Reactions by in situ TEM. *Nat. Commun.* **2018**, *9*, 574.
(515) Yang, M.; Flytzani-Stephanopoulos, M. Design of Single-Atom Metal Catalysts on Various Supports for the Low-Temperature Water-Gas Shift Reaction. *Catal. Today* **2017**, *298*, 216−225.
(516) Yao, S.; Zhang, X.; Zhou, W.; Gao, R.; Xu, W.; Ye, Y.; Lin, L.; Wen, X.; Liu, P.; Chen, B.; et al. Atomic-Layered Au Clusters on α-MoC as Catalysts for the Low-Temperature Water-Gas Shift Reaction. *Science* **2017**, *357*, 389−393.
(517) Carter, J. H.; Liu, X.; He, Q.; Althahban, S.; Nowicka, E.; Freakley, S. J.; Niu, L.; Morgan, D. J.; Li, Y.; Niemantsverdriet, J. W. H.; et al. Activation and Deactivation of Gold/Ceria-Zirconia in the Low-Temperature Water-Gas Shift Reaction. *Angew. Chem., Int. Ed.* **2017**, *56*, 16037−16041.
(518) Alvaro, M.; Aprile, C.; Corma, A.; Ferrer, B.; Garcia, H. Influence of Radical Initiators in Gold Catalysis: Evidence Supporting Trapping of Radicals Derived from Azobis(isobutyronitrile) by Gold Halides. *J. Catal.* **2007**, *245*, 249−252.
(519) Donoeva, B. G.; Ovoshchnikov, D. S.; Golovko, V. B. Establishing a Au Nanoparticle Size Effect in the Oxidation of Cyclohexene Using Gradually Changing Au Catalysts. *ACS Catal.* **2013**, *3*, 2986−2991.
(520) Ovoshchnikov, D. S.; Donoeva, B. G.; Williamson, B. E.; Golovko, V. B. Tuning the Selectivity of a Supported Gold Catalyst in Solvent- and Radical Initiator-Free Aerobic Oxidation of Cyclohexene. *Catal. Sci. Technol.* **2014**, *4*, 752−757.
(521) Serna, P.; Corma, A. Towards a Zero-Waste Oxidative Coupling of Nonactivated Aromatics by Supported Gold Nanoparticles. *ChemSusChem* **2014**, *7*, 2136−2139.
(522) Ishida, T.; Aikawa, S.; Mise, Y.; Akebi, R.; Hamasaki, A.; Honma, T.; Ohashi, H.; Tsuji, T.; Yamamoto, Y.; Miyasaka, M.; et al. Direct C-H Arene Homocoupling Over Gold Nanoparticles Supported on Metal Oxides. *ChemSusChem* **2015**, *8*, 695−701.
(523) Serna, P.; Corma, A. A Residue-Free Production of Biaryls Using Supported Gold Nanoparticles. *J. Catal.* **2014**, *315*, 41−47.
(524) Liu, L.; Matsushita, T.; Concepción, P.; Leyva-Pérez, A.; Corma, A. Facile Synthesis of Surface-Clean Monodispersed CuOx Nanoparticles and Their Catalytic Properties for Oxidative Coupling of Alkynes. *ACS Catal.* **2016**, *6*, 2211−2221.
(525) Corma, A.; Concepcion, P.; Boronat, M.; Sabater, M. J.; Navas, J.; Yacaman, M. J.; Larios, E.; Posadas, A.; Lopez-Quintela, M. A.; Buceta, D.; et al. Exceptional Oxidation Activity with Size-Controlled Supported Gold Clusters of Low Atomicity. *Nat. Chem.* **2013**, *5*, 775−781.
(526) Yang, D.; Xu, P.; Browning, N. D.; Gates, B. C. Tracking Rh Atoms in Zeolite HY: First Steps of Metal Cluster Formation and Influence of Metal Nuclearity on Catalysis of Ethylene Hydrogenation and Ethylene Dimerization. *J. Phys. Chem. Lett.* **2016**, *7*, 2537−2543.
(527) Guan, E.; Gates, B. C. Stable Rhodium Pair-Sites on MgO: Influence of Ligands and Rhodium Nuclearity on Catalysis of Ethylene Hydrogenation and H-D Exchange in the Reaction of H_2 with D_2. *ACS Catal.* **2018**, *8* (1), 482−487.
(528) Rondelli, M.; Zwaschka, G.; Krause, M.; Rötzer, M. D.; Hedhili, M. N.; Högerl, M. P.; D'Elia, V.; Schweinberger, F. F.; Basset, J.-M.; Heiz, U. Exploring the Potential of Different-Sized Supported Subnanometer Pt Clusters as Catalysts for Wet Chemical Applications. *ACS Catal.* **2017**, *7*, 4152−4162.
(529) Lu, J.; Serna, P.; Gates, B. C. Zeolite- and MgO-Supported Molecular Iridium Complexes: Support and Ligand Effects in Catalysis of Ethene Hydrogenation and H−D Exchange in the Conversion of H_2+D_2. *ACS Catal.* **2011**, *1*, 1549−1561.
(530) Crampton, A. S.; Rötzer, M. D.; Landman, U.; Heiz, U. Can Support Acidity Predict Sub-Nanometer Catalyst Activity Trends? *ACS Catal.* **2017**, *7*, 6738−6744.
(531) Somorjai, G. A.; Park, J. Y. Colloid Science of Metal Nanoparticle Catalysts in 2D and 3D Structures. Challenges of Nucleation, Growth, Composition, Particle Shape, Size Control and Their Influence on Activity and Selectivity. *Top. Catal.* **2008**, *49*, 126−135.
(532) Zhu, J.; Yang, M.-L.; Yu, Y.; Zhu, Y.-A.; Sui, Z.-J.; Zhou, X.-G.; Holmen, A.; Chen, D. Size-Dependent Reaction Mechanism and

DOI: 10.1021/acs.chemrev.7b00776
Chem. Rev. 2018, 118, 4981−5079

Kinetics for Propane Dehydrogenation over Pt Catalysts. *ACS Catal.* **2015**, *5*, 6310−6319.
(533) Cybulskis, V. J.; Pradhan, S. U.; Lovón-Quintana, J. J.; Hock, A. S.; Hu, B.; Zhang, G.; Delgass, W. N.; Ribeiro, F. H.; Miller, J. T. The Nature of the Isolated Gallium Active Center for Propane Dehydrogenation on Ga/SiO_2. *Catal. Lett.* **2017**, *147*, 1252−1262.
(534) Searles, K.; Siddiqi, G.; Safonova, O. V.; Copéret, C. Silica-Supported Isolated Gallium Sites as Highly Active, Selective and Stable Propane Dehydrogenation Catalysts. *Chem. Sci.* **2017**, *8*, 2661−2666.
(535) Gonzalez-Arellano, C.; Abad, A.; Corma, A.; Garcia, H.; Iglesias, M.; Sanchez, F. Catalysis by Gold(I) and Gold(III): a Parallelism between Homo- and Heterogeneous Catalysts for Copper-free Sonogashira Cross-Coupling Reactions. *Angew. Chem., Int. Ed.* **2007**, *46*, 1536−1538.
(536) Corma, A.; Juarez, R.; Boronat, M.; Sanchez, F.; Iglesias, M.; Garcia, H. Gold Catalyzes the Sonogashira Coupling Reaction without the Requirement of Palladium Impurities. *Chem. Commun.* **2011**, *47*, 1446−1448.
(537) Boronat, M.; Combita, D.; Concepción, P.; Corma, A.; García, H.; Juárez, R.; Laursen, S.; de Dios López-Castro, J. Making C−C Bonds with Gold: Identification of Selective Gold Sites for Homo- and Cross-Coupling Reactions between Iodobenzene and Alkynes. *J. Phys. Chem. C* **2012**, *116*, 24855−24867.
(538) Boronat, M.; López-Ausens, T.; Corma, A. Making C−C Bonds with Gold Catalysts: A Theoretical Study of the Influence of Gold Particle Size on the Dissociation of the C−X Bond in Aryl Halides. *J. Phys. Chem. C* **2014**, *118*, 9018−9029.
(539) Beaumont, S. K.; Kyriakou, G.; Lambert, R. M. Identity of the Active Site in Gold Nanoparticle-Catalyzed Sonogashira Coupling of Phenylacetylene and Iodobenzene. *J. Am. Chem. Soc.* **2010**, *132*, 12246−12248.
(540) Kyriakou, G.; Beaumont, S. K.; Humphrey, S. M.; Antonetti, C.; Lambert, R. M. Sonogashira Coupling Catalyzed by Gold Nanoparticles: Does Homogeneous or Heterogeneous Catalysis Dominate? *ChemCatChem* **2010**, *2*, 1444−1449.
(541) Oliver-Meseguer, J.; Dominguez, I.; Gavara, R.; Leyva-Pérez, A.; Corma, A. Disassembling Metal Nanocrystallites into Sub-nanometric Clusters and Low-faceted Nanoparticles for Multisite Catalytic Reactions. *ChemCatChem* **2017**, *9*, 1429−1435.
(542) Oliver-Meseguer, J.; Domenech-Carbo, A.; Boronat, M.; Leyva-Perez, A.; Corma, A. Partial Reduction and Selective Transfer of Hydrogen Chloride on Catalytic Gold Nanoparticles. *Angew. Chem., Int. Ed.* **2017**, *56*, 6435−6439.
(543) Corma, A.; Leyva-Perez, A.; Sabater, M. J. Gold-Catalyzed Carbon-Heteroatom Bond-Forming Reactions. *Chem. Rev.* **2011**, *111*, 1657−1712.
(544) Leyva-Perez, A.; Corma, A. Similarities and Differences between the "Relativistic" Triad Gold, Platinum, and Mercury in Catalysis. *Angew. Chem., Int. Ed.* **2012**, *51*, 614−635.
(545) Furstner, A. From Understanding to Prediction: Gold- and Platinum-Based π-Acid Catalysis for Target Oriented Synthesis. *Acc. Chem. Res.* **2014**, *47*, 925−938.
(546) Muller, T. E.; Hultzsch, K. C.; Yus, M.; Foubelo, F.; Tada, M. Hydroamination: Direct Addition of Amines to Alkenes and Alkynes. *Chem. Rev.* **2008**, *108*, 3795−3892.
(547) Rubio-Marques, P.; Rivero-Crespo, M. A.; Leyva-Perez, A.; Corma, A. Well-Defined Noble Metal Single Sites in Zeolites as an Alternative to Catalysis by Insoluble Metal Salts. *J. Am. Chem. Soc.* **2015**, *137*, 11832−11837.
(548) Witham, C. A.; Huang, W.; Tsung, C. K.; Kuhn, J. N.; Somorjai, G. A.; Toste, F. D. Converting Homogeneous to Heterogeneous in Electrophilic Catalysis Using Monodisperse Metal Nanoparticles. *Nat. Chem.* **2010**, *2*, 36−41.
(549) Huang, W.; Liu, J. H.; Alayoglu, P.; Li, Y.; Witham, C. A.; Tsung, C. K.; Toste, F. D.; Somorjai, G. A. Highly Active Heterogeneous Palladium Nanoparticle Catalysts for Homogeneous Electrophilic Reactions in Solution and the Utilization of a Continuous Flow Reactor. *J. Am. Chem. Soc.* **2010**, *132*, 16771−16773.
(550) Gross, E.; Liu, J. H.; Toste, F. D.; Somorjai, G. A. Control of Selectivity in Heterogeneous Catalysis by Tuning Nanoparticle Properties and Reactor Residence Time. *Nat. Chem.* **2012**, *4*, 947−952.
(551) Gross, E.; Krier, J. M.; Heinke, L.; Somorjai, G. A. Building Bridges in Catalysis Science. Monodispersed Metallic Nanoparticles for Homogeneous Catalysis and Atomic Scale Characterization of Catalysts Under Reaction Conditions. *Top. Catal.* **2012**, *55*, 13−23.
(552) Gross, E.; Liu, J. H.; Alayoglu, S.; Marcus, M. A.; Fakra, S. C.; Toste, F. D.; Somorjai, G. A. Asymmetric Catalysis at the Mesoscale: Gold Clusters Embedded in Chiral Self-Assembled Monolayer as Heterogeneous Catalyst for Asymmetric Reactions. *J. Am. Chem. Soc.* **2013**, *135*, 3881−3886.
(553) Fortea-Perez, F. R.; Mon, M.; Ferrando-Soria, J.; Boronat, M.; Leyva-Perez, A.; Corma, A.; Herrera, J. M.; Osadchii, D.; Gascon, J.; Armentano, D.; et al. The MOF-Driven Synthesis of Supported Palladium Clusters with Catalytic Activity for Carbene-Mediated Chemistry. *Nat. Mater.* **2017**, *16*, 760−766.
(554) Meemken, F.; Baiker, A. Recent Progress in Heterogeneous Asymmetric Hydrogenation of C = O and C = C Bonds on Supported Noble Metal Catalysts. *Chem. Rev.* **2017**, *117*, 11522−11569.
(555) Vazquez-Vazquez, C.; Banobre-Lopez, M.; Mitra, A.; Lopez-Quintela, M. A.; Rivas, J. Synthesis of Small Atomic Copper Clusters in Microemulsions. *Langmuir* **2009**, *25*, 8208−8216.
(556) Murdoch, M.; Waterhouse, G. I.; Nadeem, M. A.; Metson, J. B.; Keane, M. A.; Howe, R. F.; Llorca, J.; Idriss, H. The Effect of Gold Loading and Particle Size on Photocatalytic Hydrogen Production from Ethanol over Au/TiO_2 Nanoparticles. *Nat. Chem.* **2011**, *3*, 489−492.
(557) Ben-Shahar, Y.; Scotognella, F.; Kriegel, I.; Moretti, L.; Cerullo, G.; Rabani, E.; Banin, U. Optimal Metal Domain Size for Photocatalysis with Hybrid Semiconductor-Metal Nanorods. *Nat. Commun.* **2016**, *7*, 10413.
(558) Prier, C. K.; Rankic, D. A.; MacMillan, D. W. Visible Light Photoredox Catalysis with Transition Metal Complexes: Applications in Organic Synthesis. *Chem. Rev.* **2013**, *113*, 5322−5363.
(559) Narayanam, J. M.; Stephenson, C. R. Visible Light Photoredox Catalysis: Applications in Organic Synthesis. *Chem. Soc. Rev.* **2011**, *40*, 102−113.
(560) Mubeen, S.; Lee, J.; Singh, N.; Kramer, S.; Stucky, G. D.; Moskovits, M. An Autonomous Photosynthetic Device in Which All Charge Carriers Derive from Surface Plasmons. *Nat. Nanotechnol.* **2013**, *8*, 247−251.
(561) Kumar, D.; Lee, A.; Lee, T.; Lim, M.; Lim, D. K. Ultrafast and Efficient Transport of Hot Plasmonic Electrons by Graphene for Pt Free, Highly Efficient Visible-Light Responsive Photocatalyst. *Nano Lett.* **2016**, *16*, 1760−1767.
(562) Christopher, P.; Xin, H.; Linic, S. Visible-Light-Enhanced Catalytic Oxidation Reactions on Plasmonic Silver Nanostructures. *Nat. Chem.* **2011**, *3*, 467−472.
(563) Christopher, P.; Xin, H.; Marimuthu, A.; Linic, S. Singular Characteristics and Unique Chemical Bond Activation Mechanisms of Photocatalytic Reactions on Plasmonic Nanostructures. *Nat. Mater.* **2012**, *11*, 1044−1050.
(564) Marimuthu, A.; Zhang, J.; Linic, S. Tuning Selectivity in Propylene Epoxidation by Plasmon Mediated Photo-Switching of Cu Oxidation State. *Science* **2013**, *339*, 1590−1593.
(565) Kale, M. J.; Avanesian, T.; Xin, H.; Yan, J.; Christopher, P. Controlling Catalytic Selectivity on Metal Nanoparticles by Direct Photoexcitation of Adsorbate-Metal Bonds. *Nano Lett.* **2014**, *14*, 5405−5412.
(566) Swearer, D. F.; Zhao, H.; Zhou, L.; Zhang, C.; Robatjazi, H.; Martirez, J. M.; Krauter, C. M.; Yazdi, S.; McClain, M. J.; Ringe, E.; et al. Heterometallic Antenna-Reactor Complexes for Photocatalysis. Heterometallic Antenna-Reactor Complexes for Photocatalysis. *Proc. Natl. Acad. Sci. U. S. A.* **2016**, *113*, 8916−8920.
(567) Vilar-Vidal, N.; Rey, J. R.; Lopez Quintela, M. A. Green Emitter Copper Clusters as Highly Efficient and Reusable Visible Degradation Photocatalysts. *Small* **2014**, *10*, 3632−3636.

DOI: 10.1021/acs.chemrev.7b00776
Chem. Rev. 2018, 118, 4981−5079

(568) Zhou, S.; Duan, Y.; Wang, F.; Wang, C. Fluorescent Au Clusters Stabilized by Silane: Facile Synthesis, Color-Tunability and Photocatalytic Properties. *Nanoscale* **2017**, *9*, 4981−4988.
(569) Wang, Z. J.; Ghasimi, S.; Landfester, K.; Zhang, K. A. I. Photocatalytic Suzuki Coupling Reaction Using Conjugated Microporous Polymer with Immobilized Palladium Nanoparticles under Visible Light. *Chem. Mater.* **2015**, *27*, 1921−1924.
(570) Jiao, Z.; Zhai, Z.; Guo, X.; Guo, X.-Y. Visible-Light-Driven Photocatalytic Suzuki−Miyaura Coupling Reaction on Mott−Schottky-type Pd/SiC Catalyst. *J. Phys. Chem. C* **2015**, *119*, 3238−3243.
(571) Zhang, S.; Chang, C.; Huang, Z.; Ma, Y.; Gao, W.; Li, J.; Qu, Y. Visible-Light-Activated Suzuki−Miyaura Coupling Reactions of Aryl Chlorides over the Multifunctional Pd/Au/Porous Nanorods of CeO_2 Catalysts. *ACS Catal.* **2015**, *5*, 6481−6488.
(572) Choi, C. H.; Kim, M.; Kwon, H. C.; Cho, S. J.; Yun, S.; Kim, H. T.; Mayrhofer, K. J.; Kim, H.; Choi, M. Tuning Selectivity of Electrochemical Reactions by Atomically Dispersed Platinum Catalyst. *Nat. Commun.* **2016**, *7*, 10922.
(573) Yang, S.; Kim, J.; Tak, Y. J.; Soon, A.; Lee, H. Single-Atom Catalyst of Platinum Supported on Titanium Nitride for Selective Electrochemical Reactions. *Angew. Chem., Int. Ed.* **2016**, *55*, 2058−2062.
(574) Zhu, C.; Fu, S.; Shi, Q.; Du, D.; Lin, Y. Single-Atom Electrocatalysts. *Angew. Chem., Int. Ed.* **2017**, *56*, 13944−13960.
(575) Wang, J.; Huang, Z.; Liu, W.; Chang, C.; Tang, H.; Li, Z.; Chen, W.; Jia, C.; Yao, T.; Wei, S.; et al. Design of N-Coordinated Dual-Metal Sites: A Stable and Active Pt-Free Catalyst for Acidic Oxygen Reduction Reaction. *J. Am. Chem. Soc.* **2017**, *139*, 17281−17284.
(576) Pidko, E. A. Toward the Balance between the Reductionist and Systems Approaches in Computational Catalysis: Model versus Method Accuracy for the Description of Catalytic Systems. *ACS Catal.* **2017**, *7*, 4230−4234.

DOI: 10.1021/acs.chemrev.7b00776
Chem. Rev. 2018, 118, 4981−5079